Technical Report of Modeling Result Analysis for Setback Distance of Onsite Sewage Treatment and Disposal Systems (OSTDS)

Draft Completed: July 11, 2023

Prepared by

Ming Ye[1], Wei Mao[1], and Michael Core[1,2]

[1]Department of Earth, Ocean, and Atmospheric Science, Florida State University, Tallahassee, FL 32306 (mye@fsu.edu and wm23a@fsu.edu)

[2]Florida Resources and Environmental Analysis Center, Florida State University, Tallahassee, FL 32306 (mcore@fsu.edu)

Prepared for

Florida Department of Environmental Protection, Tallahassee, FL

Grant Manager: Julia Danyuk (Julia.Danyuk@FloridaDEP.gov)

Agreement Number: AT013

Executive Summary

This project was funded by the Department of Environmental Protection (DEP) to investigate the setback distance of Onsite Sewage Treatment and Disposal Systems (OSTDS). We considered two different setback distances as follows:

(1) The vertical setback distance from an OSTDS drainfield to the water table beneath the drainfield: Within this distance, the nitrification process transforms ammonium into nitrate, which is transformed into nitrogen gas by the denitrification process.
(2) The horizontal setback distance from the water table beneath the drainfield to a surface water body (e.g., canals and lakes) where septic effluent flows through groundwater flow: Within this distance, while nitrification may still occur, denitrification dominates over nitrification to remove nitrogen.

The two distances are illustrated in Fig. 1. The figure shows two horizontal distances. One is the linear distance from OSTDS to surface water body, and it is denoted as HD_L. The other is the distance along a flow path from OSTDS to surface water body, and it is denoted as HD_F. Since HD_F is unknown in practice until a groundwater flow model is conducted, this project only considers HD_L.

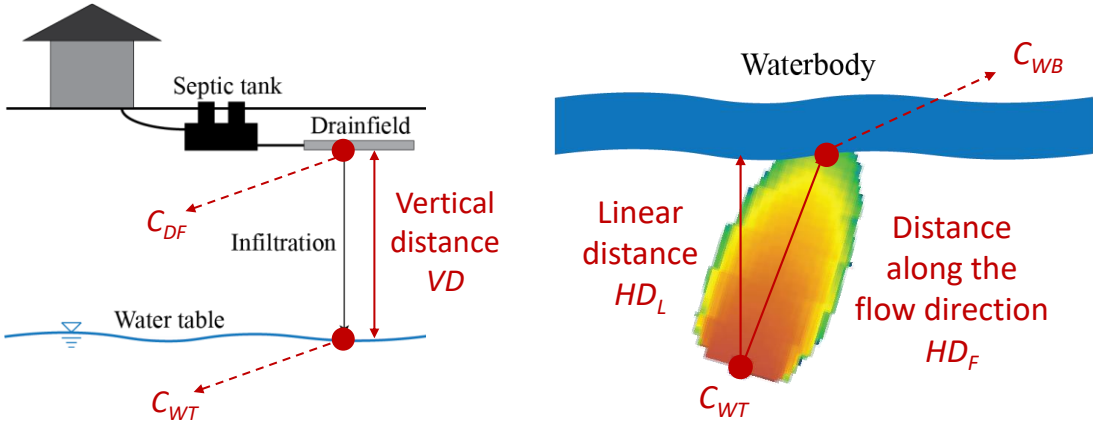

Fig 1. Illustration of (left) OSTDS vertical distance from drainfield to water table and (right) OSTDS linear horizontal distance from OSTDS to surface water body.

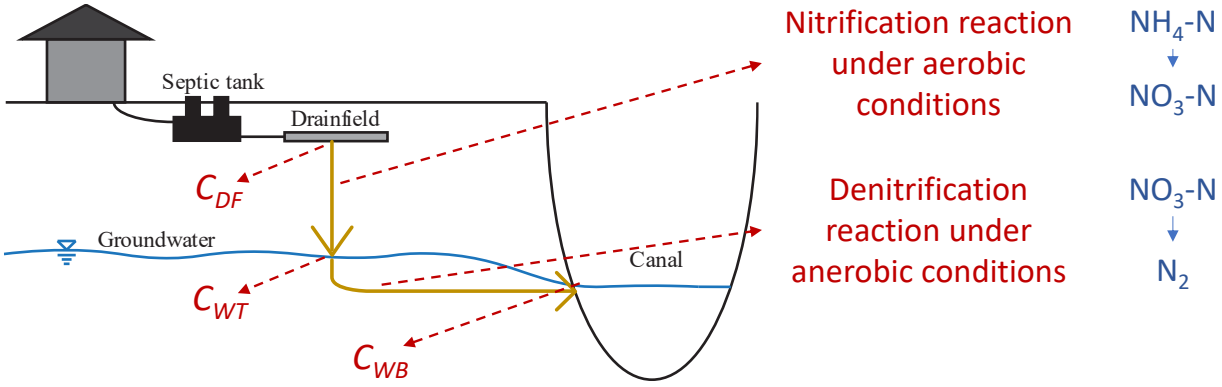

Fig. 2. Illustration of the importance of simultaneously considering both vertical and horizontal setback distances.

While the current OSTDS regulation mainly focuses on the horizontal setback distance, the vertical setback distance is also important. If the vertical distance is small, then ammonium may not adequately transform into nitrate and thus flows with groundwater into surface water bodies. To our knowledge, this project is the first attempt in Florida to investigate both vertical and horizontal setback distances quantitatively. The importance of simultaneously considering the vertical and horizontal distances is illustrated in Fig. 2.

We used three nitrogen attenuation rates (*AR*s) defined below to investigate the vertical and horizontal setback distances:

(1) Vertical attenuation rate (AR_V): This is calculated as $AR_V = (C_{DF} - C_{WT})/C_{DF} = 1 - C_{WT}/C_{DF}$ to quantify the percentage of attenuated nitrogen along the vertical distance from the drainfield to the water table, where C_{DF} and C_{WT} are nitrogen concentration at drainfield and water table, respectively.
(2) Horizontal attenuation rate (AR_H): This is calculated as $AR_H = (C_{WT} - C_{WB})/C_{WT} = 1 - C_{WB}/C_{WT}$ to quantify the percentage of attenuated nitrogen along the horizontal distance from the water table to a water body, where C_{WB} is nitrogen concentration at the water body.
(3) Total attenuation rate (AR_T): This is calculated as $AR_T = (C_{DF} - C_{WB})/C_{DF} = 1 - C_{WB}/C_{DF}$ to quantify the percentage of attenuated nitrogen along the distance from the drainfield to the water body; the distance includes both the vertical distance and the horizontal distances.

Using the three attenuation rates, we can investigate the vertical and horizontal setback distances separately and simultaneously investigate the two setback distances.

Overarching Research Question

This project intends to address the following overarching research question: *what should the vertical and/or horizontal setback distance be if an X% nitrogen attenuation rate is needed*? The attenuation rate may vary in different areas, depending on various natural and anthropogenic factors involved in OSTDS environmental management. Accordingly, the vertical and horizontal setback distances are not expected to be fixed but can vary in different areas. In other words, this project did not produce fixed values of setback distances but provided a tool for DEP to regulate the setback distances in a flexible but science-informed manner. We used two methods to address this question, which are discussed below.

Model-Driven Method Using ArcNLET

The model-drive method uses the process-based ArcGIS-based Nitrogen Load Estimation Toolkit (ArcNLET) to simulate nitrogen reactive transport from drainfields to surface water bodies. The reliability of the model-driven method depends on to what extent ArcNLET can simulate real-world data (e.g., hydraulic heads and nitrogen concentrations). This method was implemented in the following procedure in this project:

(1) Select multiple (five in this project) study areas where field observations of hydraulic head and nitrogen concentrations are available. Other researchers obtained the data used in this project at multiple locations in the backyards of individual homes.
(2) For each study area, develop an ArcNLET model, and calibrate the ArcNLET model against the field observations from multiple homes (maximum four in this project) by adjusting ArcNLET model parameters such as smoothing factor, dispersivity, and nitrification and denitrification rates.

(3) For each study area, use the calibrated ArcNLET model to simulate nitrogen reactive transport from a large number (several thousand in this project) of OSTDS. Based on the model simulations, investigate the relationship between the vertical nitrogen attenuation rate, the vertical setback distance, and the relation between the horizontal nitrogen attenuation rate and the horizontal setback distance.
(4) For each study area, use the calibrated ArcNLET model to conduct a sensitivity analysis for a single OSTDS with a large number (about one thousand in this project) of combinations of factors (e.g., hydraulic gradient and hydraulic conductivity) that influence nitrogen reactive transport. Based on the sensitivity analysis, investigate the relationship between the total nitrogen attenuation rate and the vertical and horizontal setback distances simultaneously.

The findings suggest that the relations examined in steps (3) and (4) above are similar, indicating that the model-driven method is generalizable for multiple areas and potentially across the states. Based on our modeling results, it is also possible to determine generalized vertical and horizontal setback distances for multiple areas, which, however, is empirical and should be examined further for more study areas.

The ArcNLET-based model-driven method has an inherent limitation: it entirely relies on ArcNLET, and we cannot gain more insights than the model can offer. For example, the current version of ArcNLET only simulates the reactive transport of nitrogen, not phosphorus. Phosphorus concentrations are available at each study area, and this information should be used. This inability to incorporate random variables motivates us to conduct parallel research using a data-driven method.

Data-Driven Method Using Bayesian Network

The data-driven method uses a Bayesian network (BN) to organize data and make statistical inferences on the probability of a range of nitrogen attenuation rates. The ranges considered in this project are 0% - 25%, 25% - 50%, 50% - 75%, 75% - 95%, and 95% - 100%. These ranges can be refined or adjusted if needed. The BN considers nitrogen and phosphorus attenuation and can be expanded to consider other water quality variables if needed. The BN is flexible in considering any factors that determine the attenuation rates. Theoretically speaking, the BN can utilize all information and data available. The method was implemented in the following procedure in this project:

(1) Select multiple (five in this project) study areas with sufficient data to support developing and training a BN. Note that the five study areas of BN modeling are not the same as those of ArcNLET modeling, and more details are given below. The BN modeling can use any random variables representing more data types for the same area than the ArcNLET modeling. For example, a BN can use dissolved oxygen data and phosphorate concentrations that ArcNLET does not use.
(2) For each study area, develop a BN's structure, and estimate probability distributions for variables used in the BN as nodes (e.g., nodes of vertical and horizontal distances and nodes of attenuation rates). The BN structure may vary at different areas, depending on data availability. For example, if water use data are unavailable, the BN does not have a node for water use. For this project, every BN has the nodes of the vertical distance between the drainfield and water, the horizontal distance between OSTDS and the water body, and the attenuation rates of nitrogen and phosphorus. The BN is built using the software Netica (Norsys Software Corp. - Bayes Net Software), which has a free version with limited nodes.

(3) For each study area, train the BN to develop conditional probabilities between the nodes, e.g., the probabilities of nitrogen attenuation rates conditioned on probabilities of the vertical and horizontal distances. The training used a Netica built-in function based on an Expectation Maximization (EM) algorithm.
(4) For each study area, use the trained BN to make statistical inferences on vertical and horizontal setback distances. The BN can also investigate the two distances separately or simultaneously but in a manner different from that of ArcNLET.
(5) For all study areas, use all the data of the areas to repeat steps (2) – (5). The BN for all the areas performs better than the BN for the individual areas, which is unsurprising because BN is essentially a data-driven method. When the data from all of the study areas were combined, the EM algorithm was used to estimate missing data points, i.e., if water use data were unavailable, then the most likely values were estimated based on the conditional probabilities between nodes and the training data derived from DEP-provided literature and reports.

Developing and training a BN model is computationally more efficient than developing and calibrating an ArcNLET model. Expanding a BN to include more input and output variables is straightforward and can be done by adding more BN nodes. Iteratively expanding the network is an advantage of BN modeling over ArcNLET modeling. For example, investigating phosphorus attenuation in BN only requires adding a node and developing its related conditional probabilities. Investigating phosphorus attenuation in ArcNLET requires writing many lines of code for phosphorus reactive transport modeling.

Despite the advantages of the BN-based data-driven method discussed above, we still prefer the ArcNLET-based model-driven method for several reasons. First, the data available at the study areas is insufficient to train BNs. For example, hydraulic conductivity and gradient data are unavailable at each area. While we can use data from ArcNLET modeling, this may not be appropriate because the resulting BN is not purely data-driven but a hybrid of data- and model-driven. In addition, since BN results are probabilities based, interpreting the results is not as straightforward as interpreting ArcNLET results because ArcNLET is a process-based model. We have more experience in ArcNLET modeling than in BN modeling. Nonetheless, we still believe that BN has more potential than ArcNLET if more data can be compiled and more experience in BN modeling can be acquired.

Study Areas

Based on our literature review and a presentation to DEP scientists, we selected a total of seven study areas, and their locations are shown in Fig. 3. Among the seven areas, five of them were used for ArcNLET modeling, and five for BN modeling, as shown in Table 1. Due to limited project time, the St. George Island and St. Johns areas were not used for ArcNLET modeling. The St. Lucie and Eggleston Height areas were not used for the BN modeling because data at the two areas are insufficient to support developing and training a BN. Although the Turkey Creek, Julington Creek, and Lakeshore areas were used for ArcNLET and BN modeling, the modeling results differ. Thus, we present their results separately, but comparing and comprehending them are warranted in future studies.

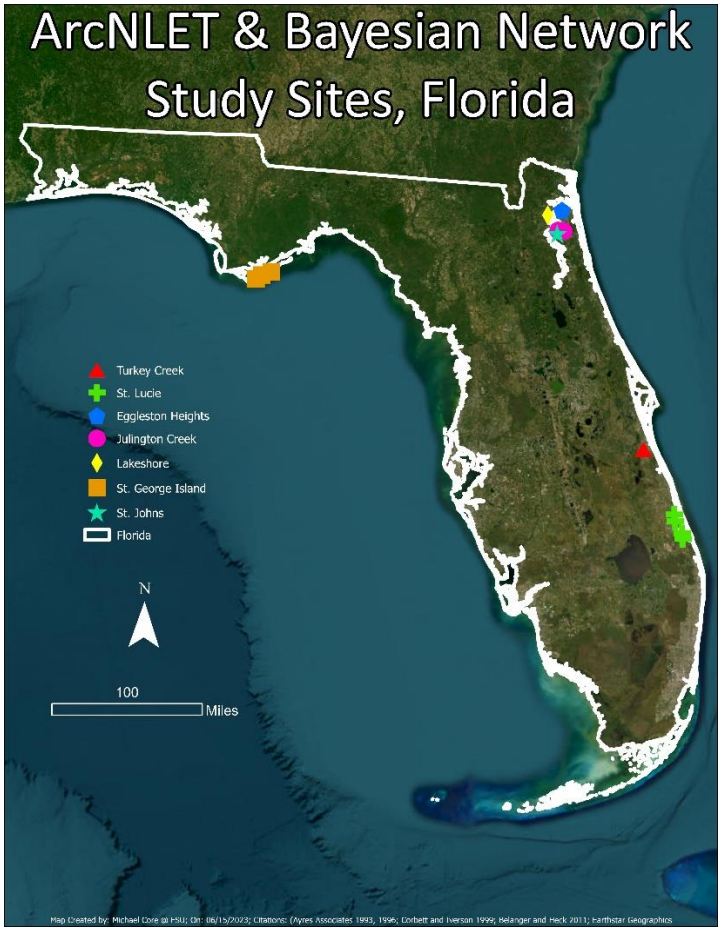

Fig. 3. Locations of study areas of this project for ArcNLET and BN modeling.

Area Name	County	ArcNLET	BN
Turkey Creek	Brevard	X	X
St. Lucie	St. Lucie and Martin	X	
Eggleston Height	Duval	X	
Julington Creek	Duval	X	X
Lakeshore	Duval	X	X
St. George Island	Franklin		X
St. Johns	St. Johns		X

Table 1. Lists of study areas for ArcNLET and BN modeling.

ArcNLET Modeling Results for Turkey Creek Study Area

The executive summary only presents the most important modeling results; more results are discussed in the report text. We first present the detailed modeling results for the Turkey Creek area, and then present summary results for the five study areas of the ArcNLET modeling. An ArcNLET model was developed and calibrated against field observations. Fig. 4 plots the ArcNLET-smoothed DEM (digital elevation model) with observed water levels at monitoring wells at Jones and Groseclose homes in the Turkey Creek area. The meaning of smoothed DEM and the details of the observations are explained in the report text to avoid having a lengthy executive summary. The figure indicates that ArcNLET can simulate the observations reasonably

well except at four locations, and the reason is discussed in the report text. Fig. 5 plots the ArcNLET-simulated NH_4-N and NO_3-N concentrations with their corresponding observations at the same monitoring wells of groundwater levels. The figure indicates that the calibrated ArcNLET can simulate the observations reasonably well.

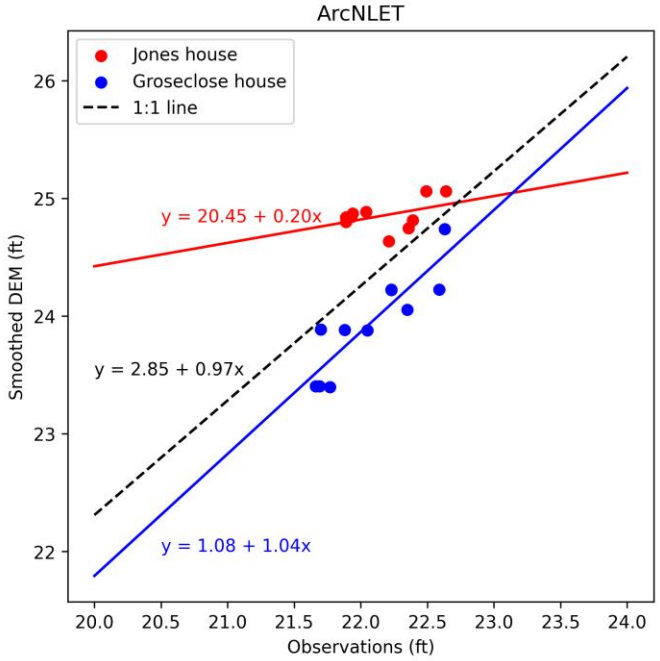

Fig. 4. Comparison of smoothed DEM and observed groundwater levels at monitoring wells located at Jones and Groseclose homes in the Turkey Creek area.

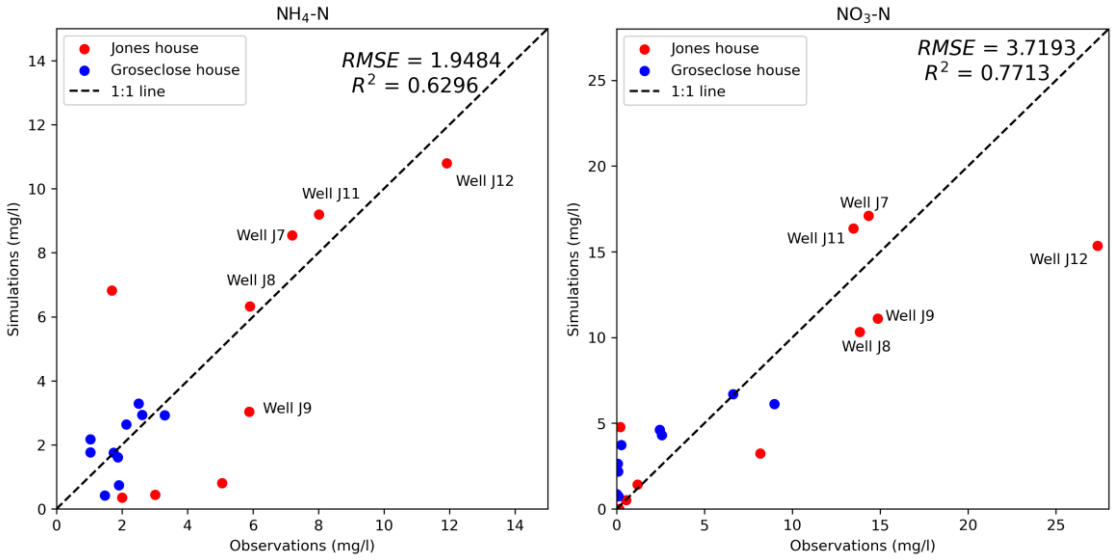

Fig. 5. Comparison of (left) simulated NH_4-N concentrations and (right) simulated NO_3-N concentrations with their corresponding observations at monitoring wells located at Jones and Groseclose homes in the Turkey Creek area.

The calibrated ArcNLET simulated 6,095 OSTDS at an area in the Turkey Creek area, including the Jones and Groseclose homes. Based on the simulation results, Fig. 6 plots the relationship between the vertical attenuation rate ($1 - C_{WT}/C_{DF}$) and the vertical distance, *VD*, from the drainfield to the water table for four soil types in the study area, where the concentration, *C*, is for both ammonium-N (NH_4-N) and nitrate-N (NO_3-N). The figure shows that the vertical attenuation rate increases with the vertical distance. This is expected considering nitrification and nitrification processes in the vadose zone. The figure also shows that the vertical nitrogen attenuation rate increases rapidly for all four soil types when the vertical distance increases from zero to 2 ft. At the vertical distance of 2 ft, the vertical attenuation rate ranges approximately between 65% and 85%. When the vertical distance is larger than 2 ft, the vertical attenuation rate increases at a small rate. At the vertical distance of 3 ft, the vertical attenuation rate ranges approximately between 68% and 95%. Soil types play an important role in the variation of the vertical attenuation rate. The rate is lower for sand and loamy sand than for sandy loam and sandy clay loam. The latter two soil types' rate can be 100% if the vertical distance is large enough. However, it is not the case for the former two soil types.

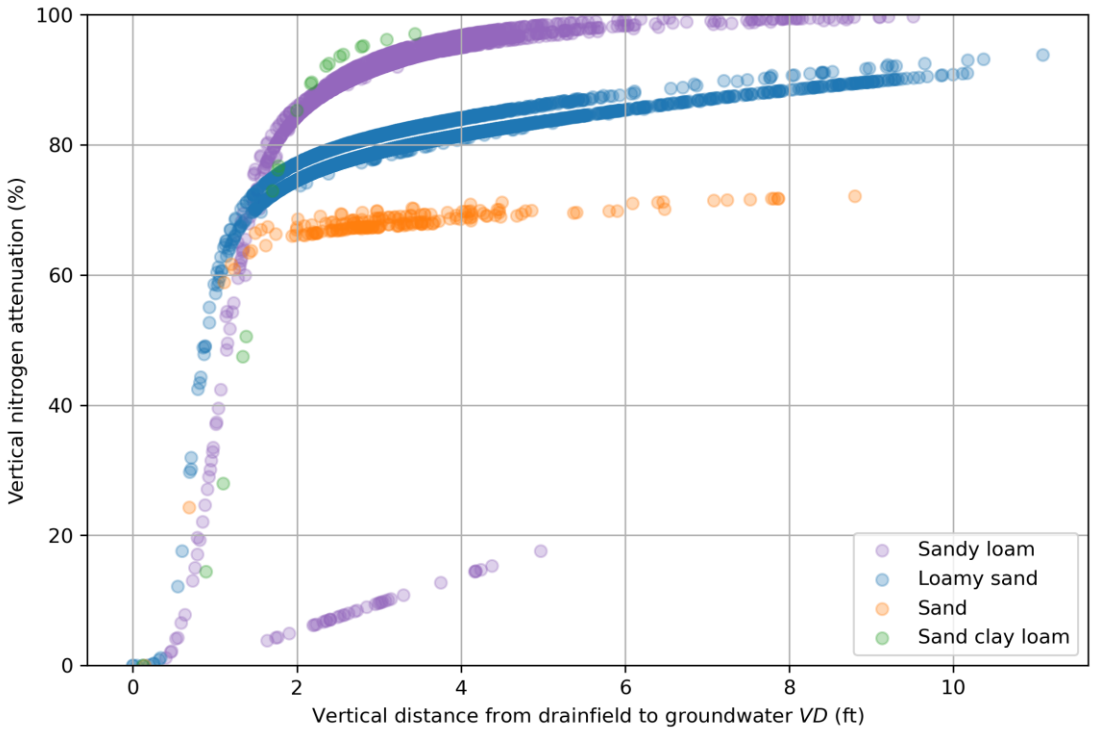

Fig. 6. Relations between vertical nitrogen attenuation rate ($1 - C_{WT}/C_{DF}$), and the vertical distance, *VD*, from drainfield to water table for four soil types at the Turkey Creek area.

Fig. 7 plots the relations between averaged horizontal nitrogen attenuation rate ($1 - C_{WB}/C_{WT}$) and the linear horizontal distance, HD_L, between OSTDS and receiving water bodies for the four soil types. The attenuation rate was calculated for NH_4-N and NO_3-N separately. The reason for using averaged attenuation rate and the procedure for estimating the average is discussed in Chapter 2 of the report. The figure shows that the attenuation rate increases with the horizontal distance, which is attributed again to nitrification and denitrification. The dashed line in the figure is for the distance of 75 ft, the currently used setback distance. For this distance, the attenuation rate can be 80% (for sand and loamy sand) and larger (for sandy load and sandy clay loam).

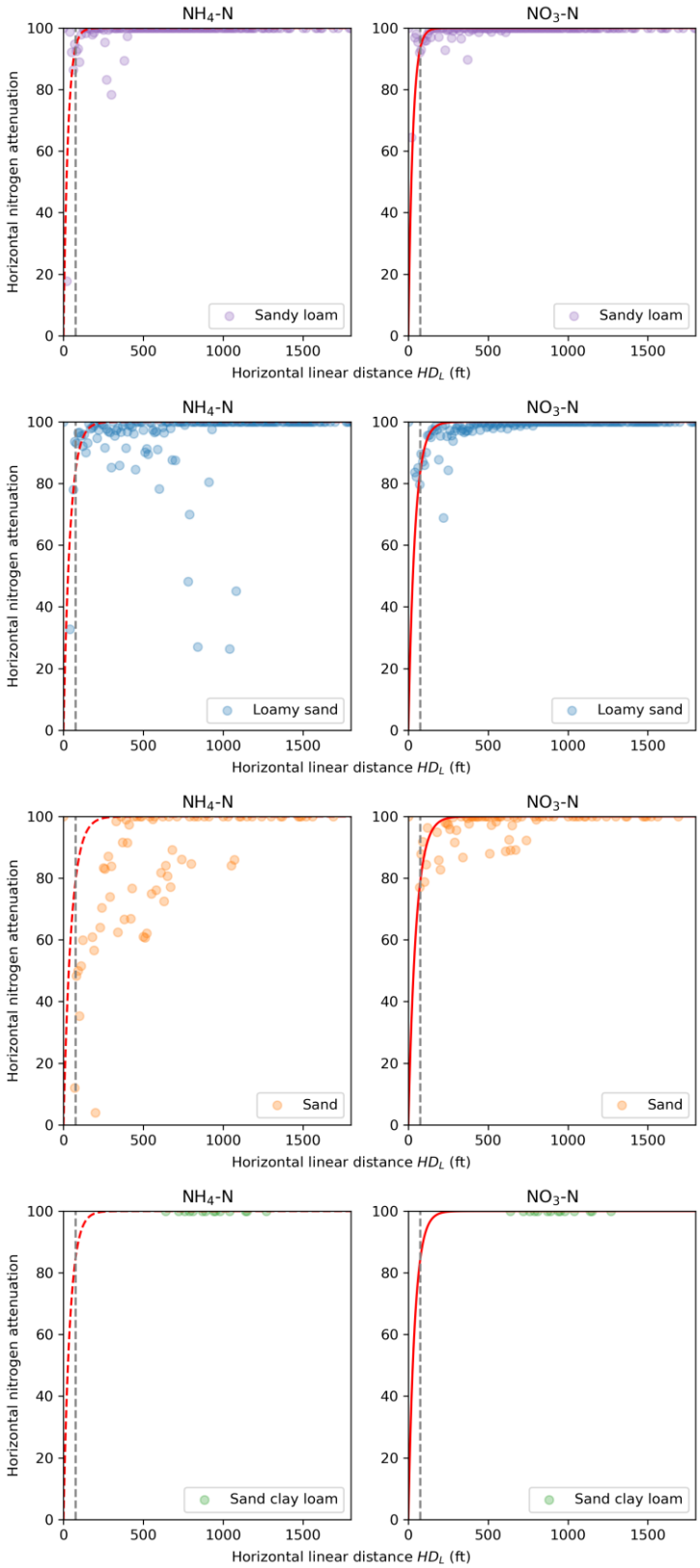

Fig. 7. Relations between averaged horizontal nitrogen attenuation rate ($1 - C_{WB}/C_{WT}$) and the linear horizontal distance, HD_L, between OSTDS and receiving water bodies.

Based on the data in Fig. 7, we developed an empirical function below to describe the relationship between the horizontal nitrogen attenuation rate and the linear horizontal distance (HD_L)

$$AR_H = 1 - C/C_{WT} = 100 \times AF \times (1 - e^{((-HD_L)/(4\times K_s+20))}) \quad (1)$$

Where *AF* (between 0 and 1) is an adjustment factor for different soil types, and K_s is the hydraulic conductivity of a soil type. The equation is shown in Fig. 7 and fits the data reasonably well. Note that it is a monotonically increasing function and reaches the maximum of 100 × AF (e.g., 80% and 100%) when the linear horizontal distance is large enough. This equation is practically applicable because it only requires knowing hydraulic conductivity values readily available in the SURRGO database. The report shows that the empirical equation is applicable at other study areas considered in this study, and it is promising that it may be applicable across the state. However, a more thorough evaluation is needed at more study areas.

In order to simultaneously investigate the vertical and horizontal setback distances, a sensitivity analysis was conducted by running ArcNLET for one septic tank with a total of 1,320 simulations corresponding to combinations of 11 linear horizontal distances/hydraulic gradients (the minimum linear horizontal distance was set as 75 ft), 30 vertical distances, and four soil types. Fig. 8 plots the total nitrogen attenuation rate contours for each soil type with horizontal and vertical distances. Similarly, the figure also plots the contours of the concentrations of NH_4-N and NO_3-N entering surface water bodies (i.e., at the end of the groundwater flow paths terminating at surface water bodies). The figure shows that increasing either the linear horizontal distance or the vertical distance can increase the total nitrogen attenuation rate. The vertical distance is more influential than the linear horizontal distance because the attenuation rate changes more quickly with the vertical distance than with the linear horizontal distance.

Fig. 8 shows that the attenuation rate is affected by soil types. When the horizontal linear distance is greater than 75 ft, and the vertical distance is greater than 2 ft, a total nitrogen attenuation rate of 90% can be achieved for sandy loam and sandy clay loam. This, however, is not the case for loamy sand and sand, for which achieving a 90% attenuation rate requires a large vertical and/or horizontal setback distance. If the linear horizontal distance is set at 75 ft, the vertical distance needs to be about 2.5 ft for loamy sand and unrealistically more than 10 ft for sand. Based on our limited experience with OSTDS management, we believe that Fig. 8 is the most useful result produced by this project.

We imagine a possible application of Fig. 8 for determining setback distances based on Fig. 8, illustrated in Table 2 for the Turkey Creek area. For each soil type at an area of interest, one needs to determine a total nitrogen attenuation rate by considering various factors involved in environmental management (determining the rate is beyond the scope of this study). A constant rate for all soil types is possible. Subsequently, one can use Fig. 8 to determine a set of possible combinations of vertical and horizontal distances. Afterward, a realistic set of vertical and horizontal distances can be determined for the area of interest. For example, if the area has many canals (e.g., in South Florida), having a large horizontal setback distance may not be possible, and a large vertical setback distance may be needed. The final setback distances may vary at different areas, and we do not recommend using constant setback distances across the state until more studies are conducted for more study areas that can represent OSTDS-related natural and anthropogenic conditions across the state.

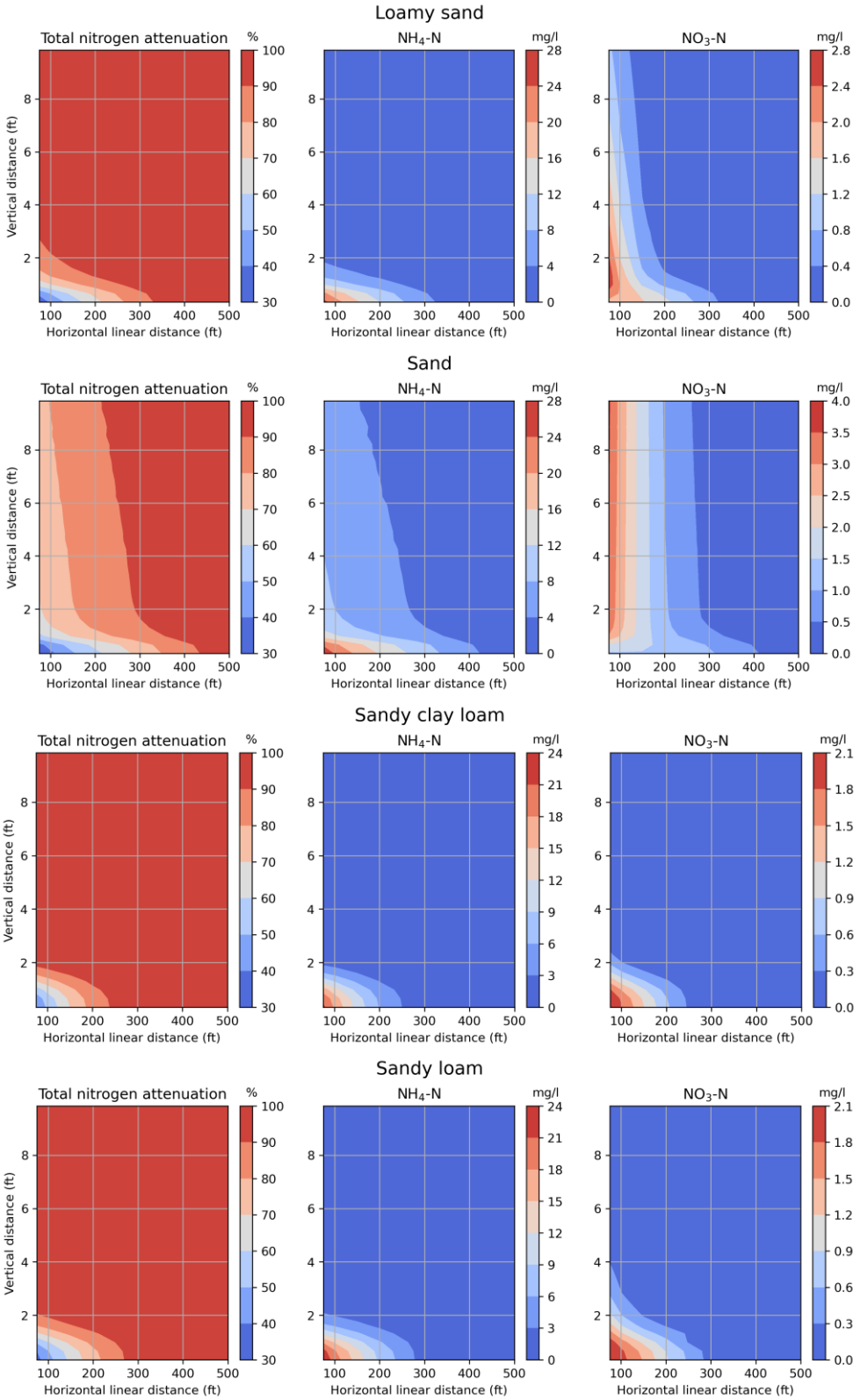

Fig. 8. Contours of total nitrogen attenuation and concentrations of NH_4-N and NO_3-N entering water bodies as a function of linear horizontal distance and vertical distance for four soil types. The smallest linear horizontal distance is 75 ft, the currently used OSTDS setback distance.

Study Area	Soil Type	OSTDS Number	Attenuation Rate	Horizontal Distance	Vertical Distance
Turkey Creek	Loamy sand	4,381	90%	H_1	V_1
	Sand	185	80%	H_2	V_2
	Sandy clay loam	19	100%	H_3	V_3
	Sandy loam	1,510	100%	H_4	V_4
Another Area					
Another Area					

Table 2. Possible use of Fig. 8 for OSTDS environmental management related to setback distances.

ArcNLET Modeling Results for Six ArcNLET Study Areas

ArcNLET modeling was conducted for the five study areas listed in Table 1, and the flow and transport modules of ArcNLET were also calibrated. Fig. 9 plots the mean and standard deviation of the observed and simulated NH_4-N and NO_3-N concentrations. The figure indicates that the mean values of the simulations are close to the mean of the observations. Generally speaking, the standard deviations of observed concentrations are larger than those of simulated concentrations, which is expected given that model results represent smoothed reality. Fig. 9 indicates that the calibrated models are acceptable for investigating the vertical and horizontal OSTDS setback distances in the give study areas.

Fig. 10 plots the vertical attenuation rate (AR_V) with vertical distance (*VD*) for the soil types in the five study areas of ArcNLET modeling. The same patterns are observed for the five study areas. First, AR_V increases with *VR*, and this is expected because of the denitrification in the vadose zone. For each area, the variation of AR_V with *VD* depends on soil types, which determine the vertical profile of water saturation. Water saturation in turn determines the actual values of nitrification and denitrification rates. Table 3 lists AR_V at the *VD* of 2 feet for the soil types in the five study areas of ArcNLET. The table indicates that at least 75% of nitrogen is attenuated at the 2 feet vertical distance. Whether the 75% attenuation is adequate for environmental protection is beyond the scope of this project.

Fig. 11 plots the horizontal attenuation rate (AR_H) with horizontal distance (*HD*) for the sand soil in the five study areas of ArcNLET modeling. The same patterns are observed for the five study areas that AR_H increases with *HD*, and this is expected because of the denitrification in the groundwater aquifer. For each area, the variation of AR_H with *HD* also depends on soil types, and the variation for other soil types are given in the report text. Fig. 11 indicates that equation (1) is applicable for all the five study areas, which is an important finding of this study. Table 4 lists AR_H at the *HD* of 75 feet for the soil types in the five study areas of ArcNLET. The table indicates that at least 75% of nitrogen is attenuated at the 75 feet horizontal distance. Whether the 75% attenuation is adequate for environmental protection is beyond the scope of this project.

Fig. 12 plots the contours of total attenuation rate (AR_T) as a function of linear horizontal distance and vertical distance for sand soil in the five study areas of ArcNLET modeling. The smallest linear horizontal distance is 75 ft, the currently used OSTDS setback distance. The figure shows that, while the general variation patterns are similar for the five study areas, there are differences at different study areas. This is the case for other soil types, and the contours of other soil types are given in the report text.

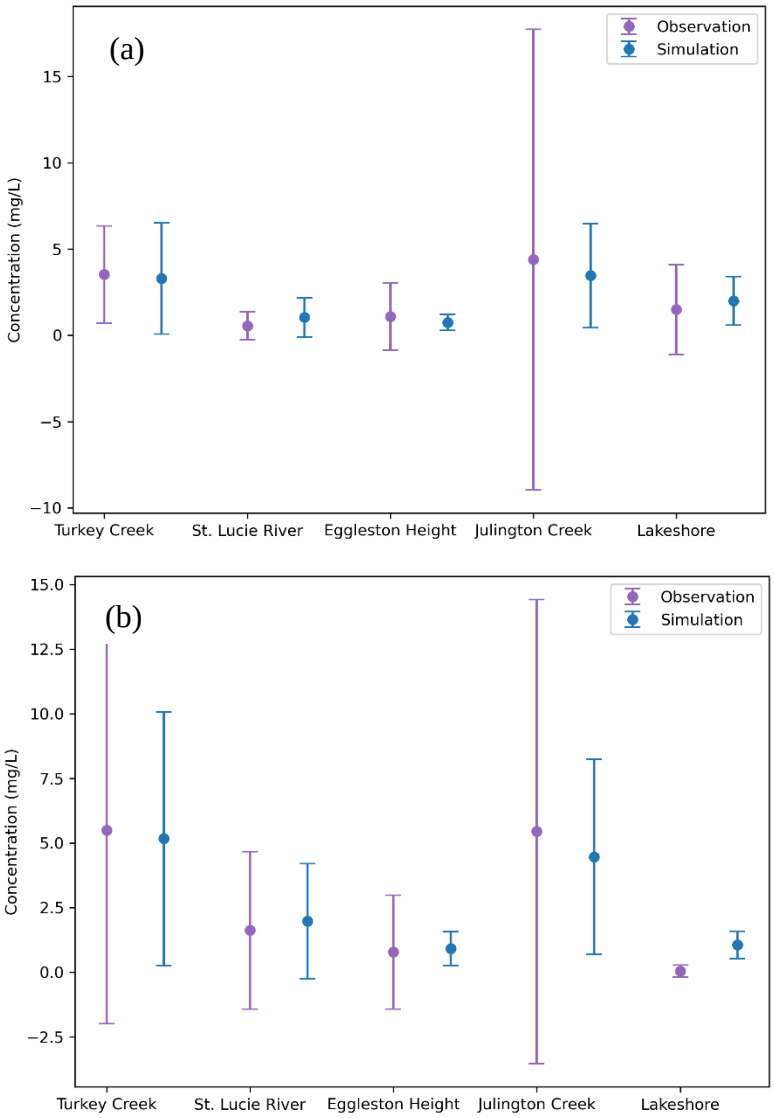

Fig. 9. (a) Mean and standard deviation of observations and simulaton of NH_4-N concentrations, and (b) mean and standard deviation of observations and simulaton of NO_3-N concentrations at five study areas of ArcNLET modeling.

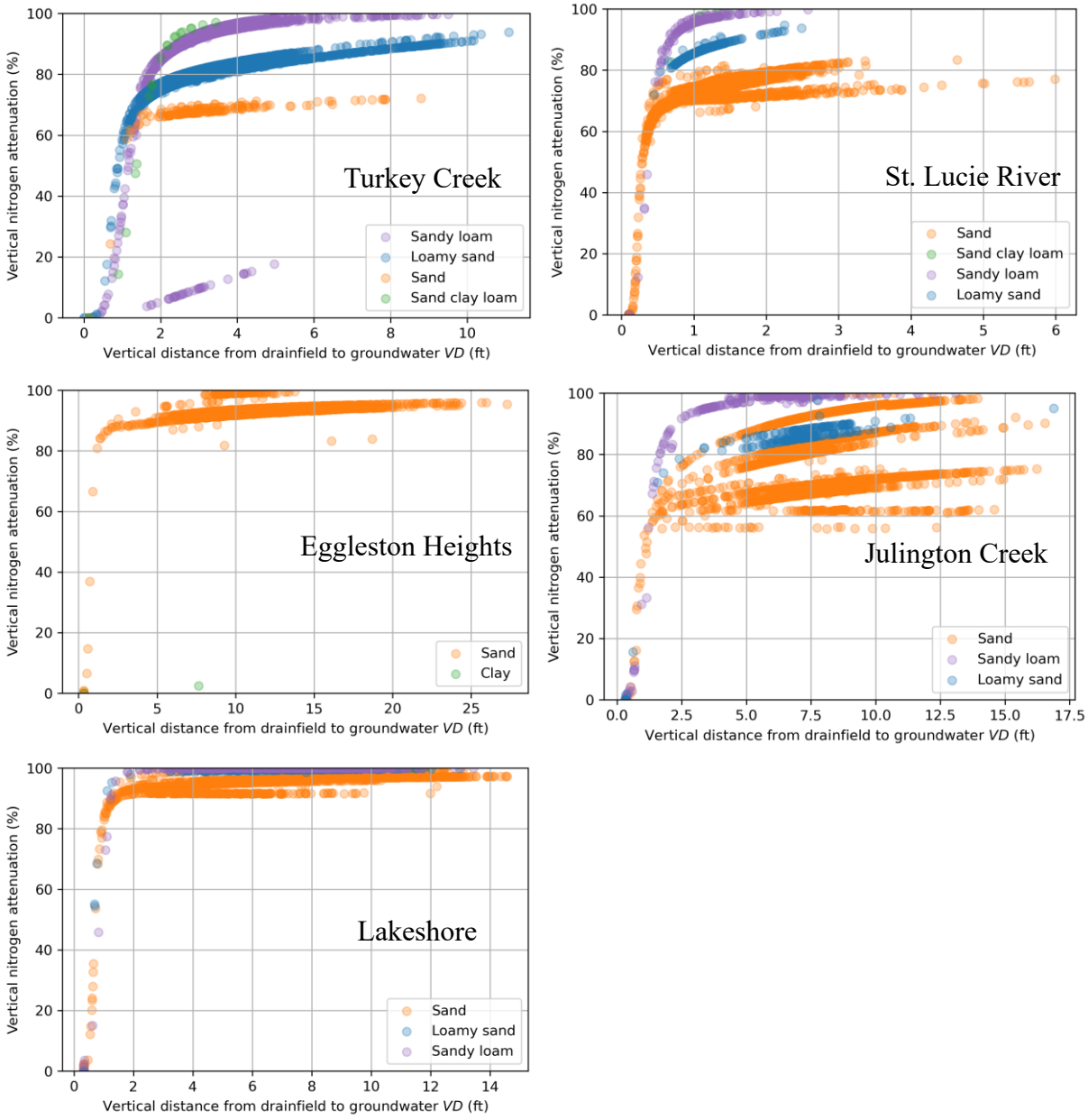

Fig. 10. Variation of vertical attenuation rate (AR_V) with vertical distance (VD) for the soil types in the five study areas of ArcNLET modeling.

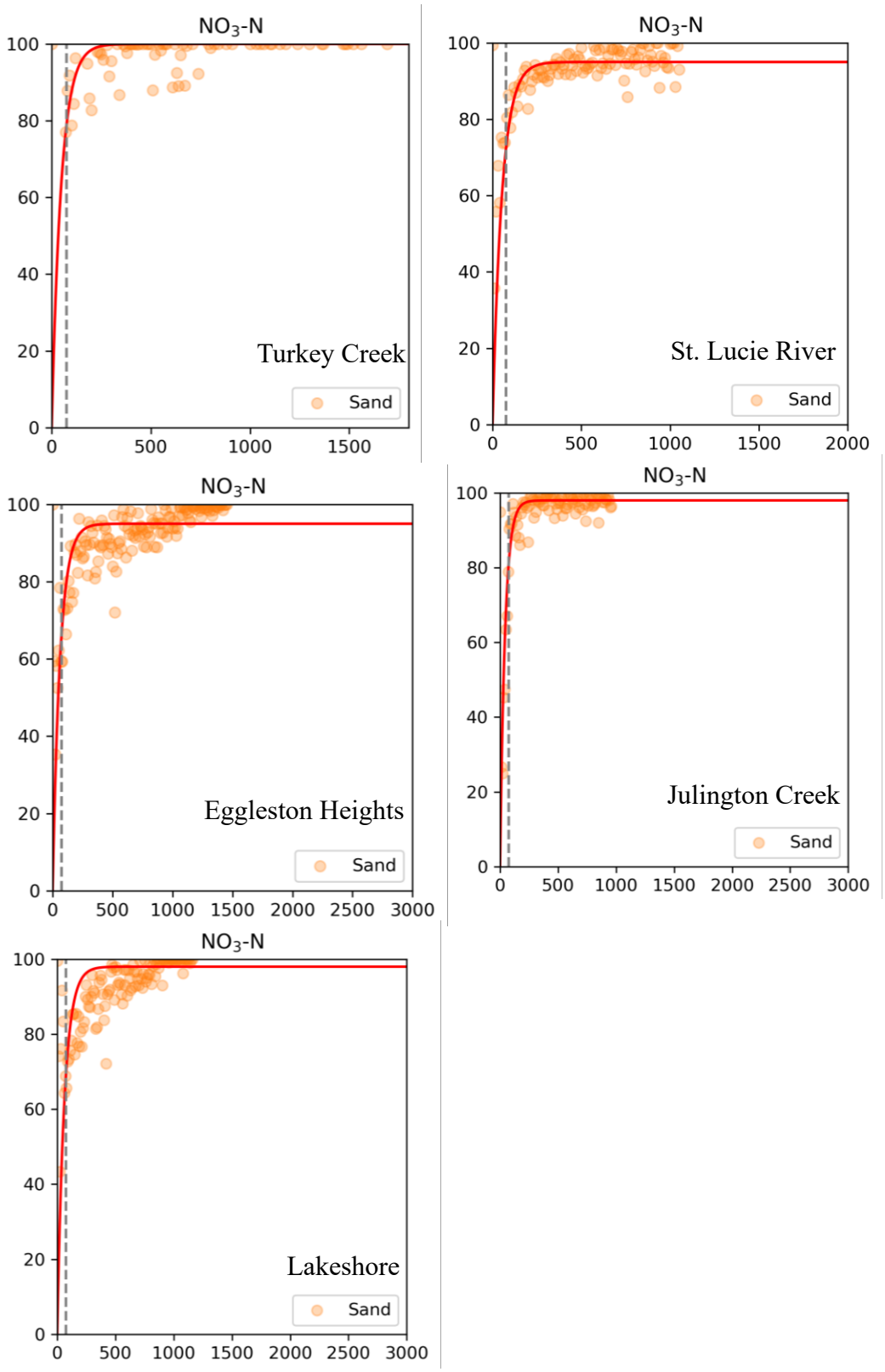

Fig. 11. Variation of horizontal attenuation rate (AR_H) with horizontal distance (HD) for sand soil in the five study areas of ArcNLET modeling.

Soil Type	Turkey Creek	St. Lucie River	Eggleston Heights	Julington Creek	Lakeshore	Average
Sand	67%	70%	86%	65%	90%	75.6%
Loamy sand	75%	81%	-	75%	95%	81.5%
Sandy loam	85%	91%	-	91%	95%	90.5%
Sandy clay loam	85%	91%	-	-	-	88%

Table 3. Vertical attenuation rate (AR_V) at the vertical distance (VD) of 2 feet for the soil types in the five study areas of ArcNLET modeling.

Soil Type	Turkey Creek	St. Lucie River	Eggleston Heights	Julington Creek	Lakeshore	Average
Sand	80%	72%	67%	81%	70%	75%
Loamy sand	84%	87%	-	77%	76%	81%
Sandy loam	93%	89%	-	80%	76%	84.5%
Sandy clay loam	85%	97%	-	-	-	91%

Table 4. Horizontal attenuation rate (AR_H) at the horizontal distance (HD) of 75 feet for the soil types in the five study areas of ArcNLET modeling.

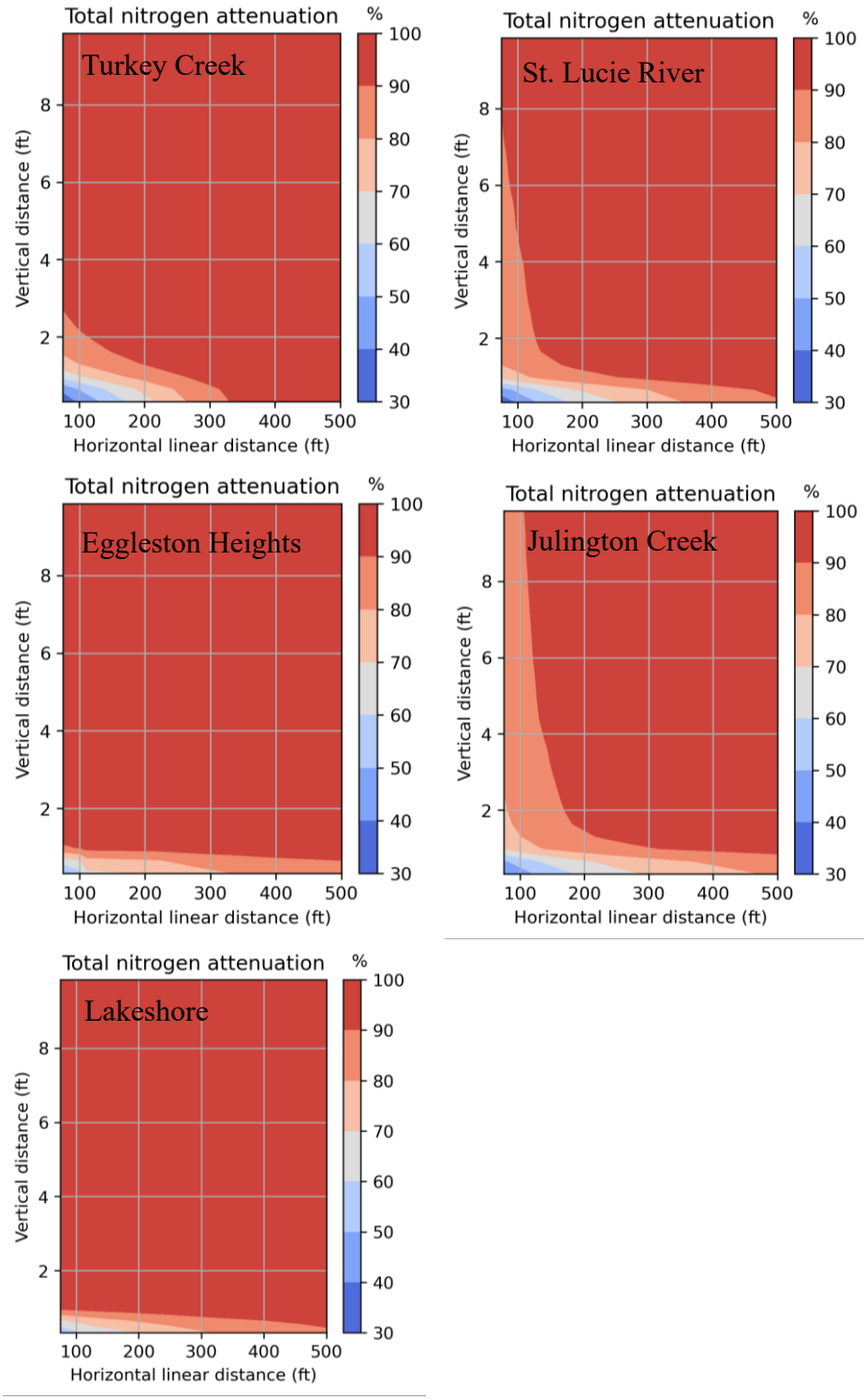

Fig. 12. Contours of total attenuation rate as a function of linear horizontal distance and vertical distance for sand soil in the five study areas of ArcNLET modeling. The smallest linear horizontal distance is 75 ft, the currently used OSTDS setback distance.

BN Modeling Results

As discussed above, we first developed a BN for each study area based on its data and then developed a BN for all the areas based on all their data. The latter BN outperforms the former BN, which is unsurprising because BN is a data-driven statistical method. We here only present the BN developed for the Turkey Creek area. Note that the BN results have not been compared with the ArcNLET results to gain more insights on the setback distances.

Fig. 13 shows the BN developed for the Turkey Creek area, including the Groseclose and Jones sites in the area. The BN's structure (e.g., nodes of environmental variables and connections between the nodes) was based on our understanding of the physical, chemical, and microbial processes related to nitrogen reactive transport in the vadose zone and surficial aquifer. The nodes are grouped and colored based on the same process. For example, the nodes in gray are variables (e.g., water use per capita and household occupancy) related to concentrations of TKN, NO_3, and TP in septic tanks. The nodes in blue are variables (e.g., hydraulic conductivity and hydraulic gradient) related to groundwater flow. The four nodes between the gray and the blue nodes are related to the vertical distance between the drainfield and water table and the horizontal distance between OSTDS and surface water bodies that receive septic effluent. The ultimate outputs of the BN are the three nodes in orange at the bottom of the BN, which are attenuation rates of TKN, NO_3, and TP. These are child nodes of all the nodes above them, which are parent nodes in BN terminology.

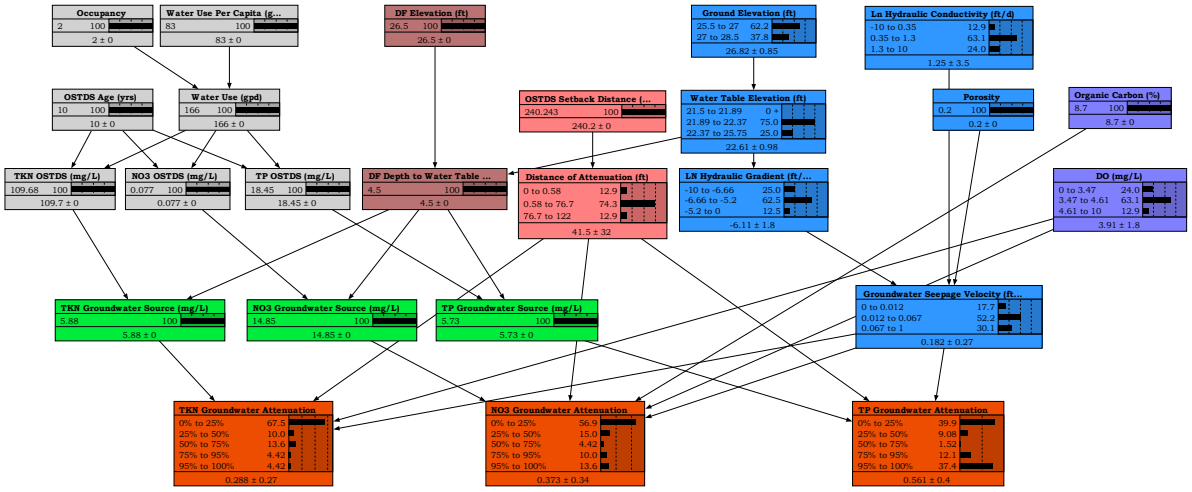

Fig. 13. BN developed for the Turkey Creek area.

For each BN node, the probability density function (in the form of a histogram) of the node's variable was estimated either based on data given by Ayres Associates (1993) or estimates using data from Ayres Associates (1993). Fig. 14 shows the histogram of log hydraulic conductivity (ft/d) given in Ayres Associates (1993), and the histogram indicates a normal distribution of log hydraulic conductivity commonly used in hydrogeology. Fig. 15 plots the histogram of the log hydraulic gradient, and a normal distribution was assumed. The hydraulic gradients were estimated using the Darcy law based on data pairs shown in Fig. 16.

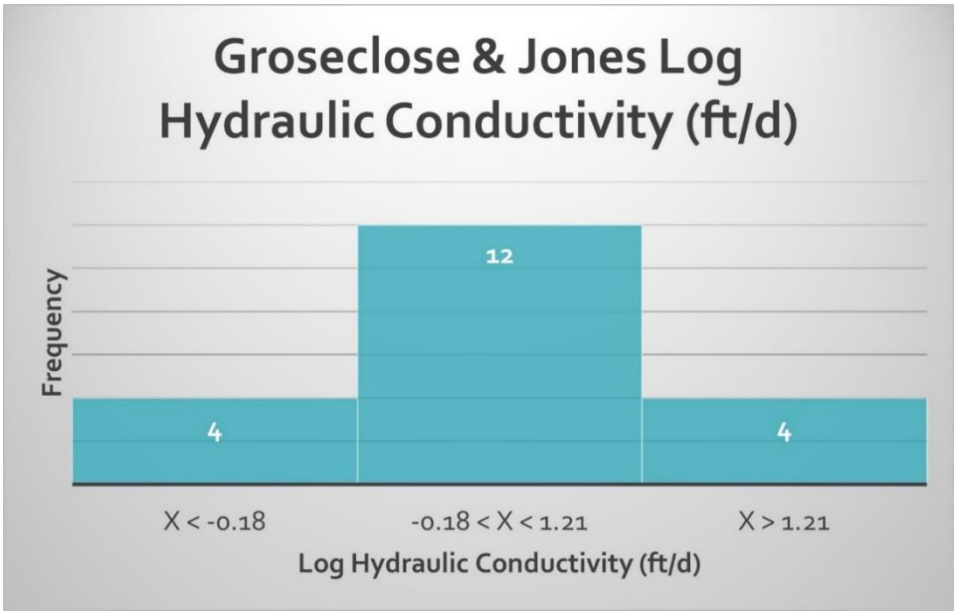

Fig. 14. Histogram of log hydraulic conductivity (ft/day) based on data given in Ayres Associates (1993).

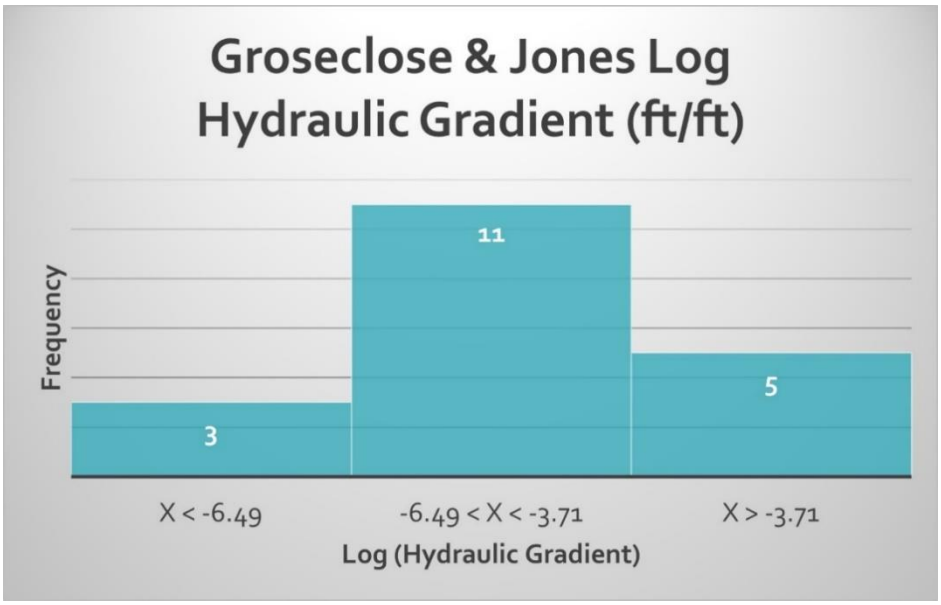

Fig. 15. Histogram of log hydraulic gradient (ft/day). Hydraulic gradients were estimated based on hydraulic head data given by Ayres Associates (1993).

Fig. 16. Diagram shows the pairs of hydraulic heads used for estimating hydraulic gradients. Hydraulic heads and a survey of the Groseclose house and its drainfield locations were given by Ayres Associates (1993).

Area	Well ID	BN-Estimated Attenuation			Data-based Attenuation		
		TNK	NO3	TP	TKN	NO3	TP
Groseclose	G7	0% to 25%	95% to 100%	75% to 95%	0%	72.6%	66.4%
Groseclose	G11	0% to 25%	95% to 100%	95% to 100%	41%	98.8%	58.8%
Jones	J8	0% to 25%	0% to 25%	95% to 100%	0%	6.9%	95.3%
Jones	J14	0% to 25%	0% to 25%	95% to 100%	48.8%	92%	97%

Table 5. Evaluation of the trained BN developed for the Turkey Creek area with Groseclose and Jones areas.

The BN of the Turkey Creek area was trained using the EM algorithm implemented in Netica, a BN software used in this project. This training develops the probability of a child node conditioned on its parent nodes based on the node connection specified for the BN. The success of the training heavily depends on the amount of data. If there are no data for a child node and its parent node, equal probability is used for the child node. A trained BN should be tested before it is used for statistical inference in investigating setback distances. We used a cross-validation method to test the trained BN, and the results are listed in Table 5. We excluded wells G7 and G11

of the Groseclose area and wells J8 and J14 of the Jones area from the BN training and used the trained BN to estimate attenuation rates at the four wells. Table 5 indicates that, among the 12 attenuation rates (three rates at four wells), only six attenuation rates were correctly estimated. The 50% success rate of the BN is not high enough for using the BN to make statistical inferences on setback distances.

The relations between the attenuation rates and the horizontal distance were also investigated based on report data. Since the reports did not have data for the vadose zone, the relation for vertical distance was not studied. The attenuation rates were estimated based on data reported by Ayres Associates (1993). Estimating the attenuation rates is empirical based on determining the location, magnitude, flow direction, and OSTDS-related nitrogen and phosphorus plums. The plumes were identified by georeferencing monitoring well and piezometer location data from report figures, charts, and text to identify the groundwater contamination source near the OSTDS and associated contaminant plume in the downgradient direction towards a surface waterbody. Figs. 17 – 19 show the results of the attenuation rate calculations and distances of attenuation for the Jones and Groseclose datasets for total Kjeldahl nitrogen (TKN), nitrate (NO_3), and total phosphorus (TP). The plots show a maximum attenuation distance was observed at approximately 125 ft for the study areas at well J-5 at the Jones area. Although the aforementioned monitoring location was 125 ft from the blackwater tank, which was in the backyard at the Jones area, J-5 was near a greywater tank in the front yard of the Jones site. The monitoring wells at the Groseclose site had a maximum distance of approximately 65 ft from the groundwater source well (J5) between the blackwater and graywater tanks.

Fig 17 suggests that TKN needs greater distances than 75 feet to achieve 90% to 100% attenuation rates. For example, the highest attenuation rate for TKN was observed at well J-13 at the Jones site, with approximately 72% TKN attenuation at a distance of 66 ft (northerly from the groundwater source well) and a concentration of 1.7 mg/L. The following monitoring location confounds these results, well J-5, with a TKN attenuation rate of 67% at a distance of 121 ft (easterly from the groundwater source well) and a concentration of 2 mg/L. As previously stated, location J-5 is near a greywater holding tank that could impact the analyte concentrations. More information is needed to model the maximum TKN attenuation at the Jones and Groseclose areas.

On the other hand, Figs. 18 and 19 suggest that within 75 ft, NO_3 and TP should attenuate by 90% to 100% of the concentration of the groundwater source well of the analyte originating from the OSTDS for the Jones and Groseclose sites. These findings suggest that the current OSTDS setback from surface waterbodies of 75 ft is adequate for NO_3 and TP attenuation distances for the Jones and Groseclose sites. These findings are corroborated by Ayres Associates (1993), who reported that nitrogen attenuated to or below the background level within 40 ft of the OSTDS.

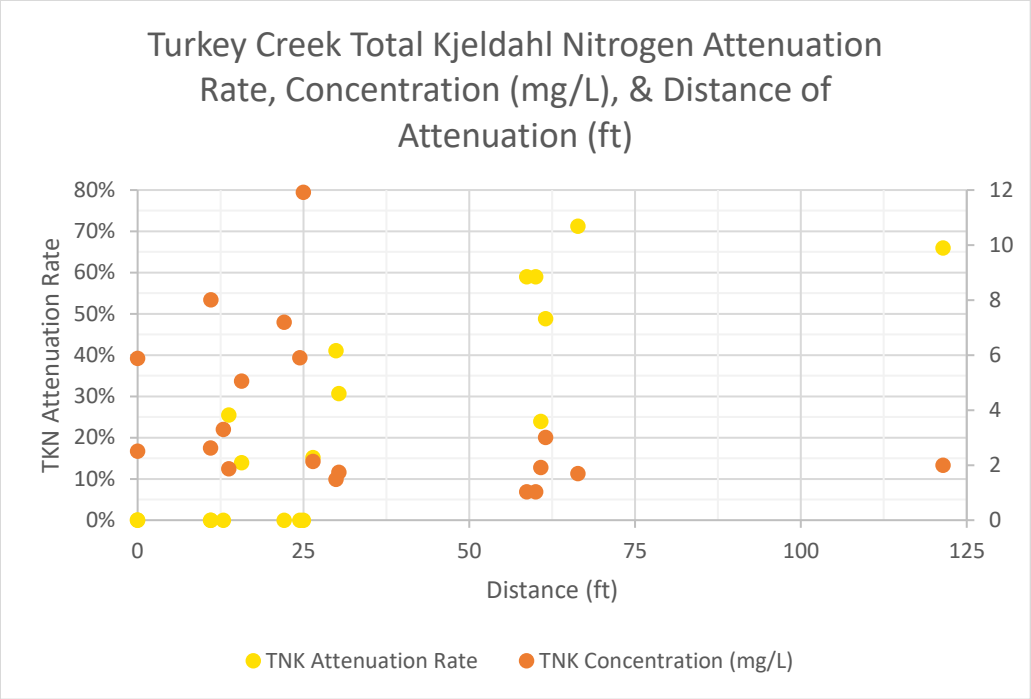

Fig. 17. Plot of TKN attenuation rates, TKN concentrations (mg/L), and the attenuation distances (ft) for the Jones and Groseclose sites in Turkey Creek. The attenuation rates were calculated with data from Ayres Associates (1993), and the distances were estimated in the GIS.

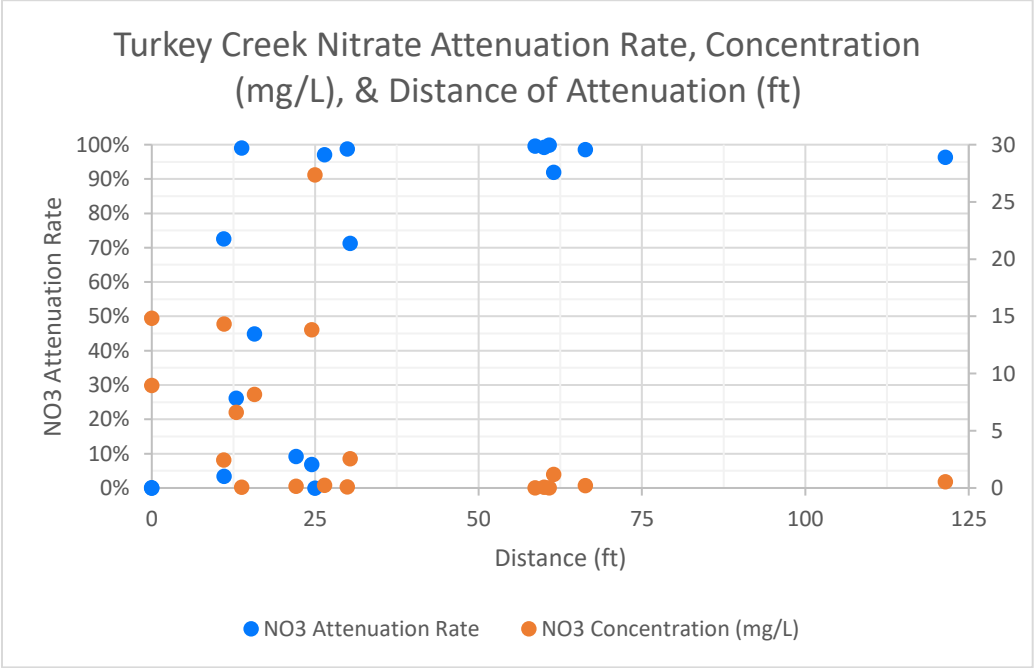

Fig. 18. Plot of NO_3 attenuation rates, NO_3 concentrations (mg/L), and the attenuation distances (ft) for the Jones and Groseclose areas in Turkey Creek. The attenuation rates were calculated with data from Ayres Associates (1993), and the distances were estimated in the GIS.

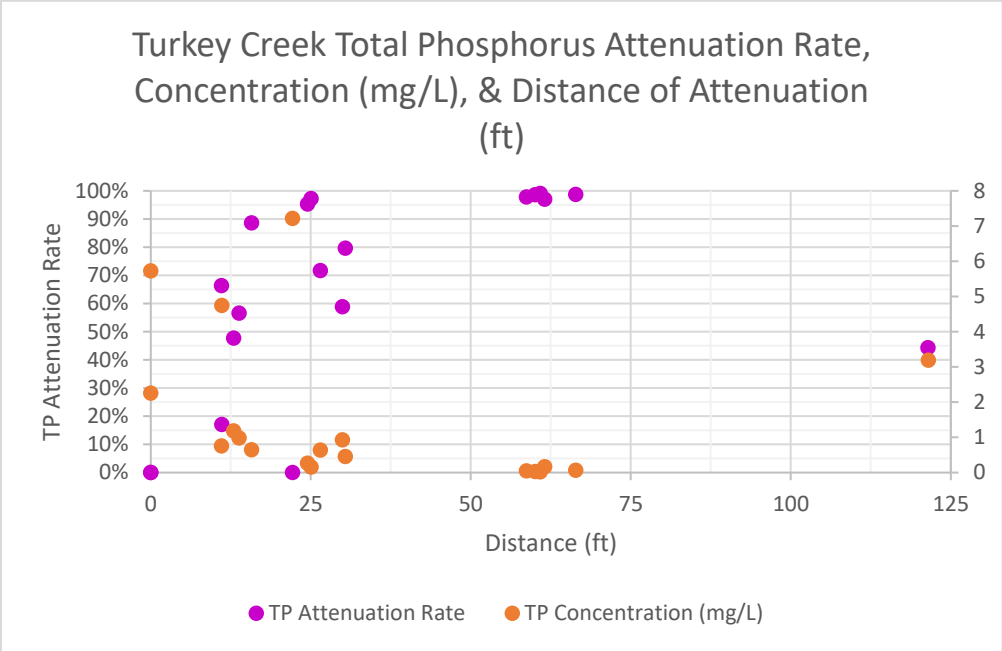

Fig. 19. Plot of TP attenuation rates, TP concentrations (mg/L), and the attenuation distances (ft) for the Jones and Groseclose areas in Turkey Creek. The attenuation rates were calculated with data from Ayres Associates (1993), and the distances were estimated in the GIS.

More analysis of the report data (e.g., the attenuation rates, distances of attenuation, and analyte concentrations) and the BNs developed in this project were given in Chapter 5. The attenuation rates, distance of attenuation, and analyte concentrations were all derived from georeferencing data from figures, charts, and text from FDEP-provided literature. The information is presented separately for Turkey Creek, Lakeshore, Julington Heights, St. George Island, and St. Johns, and then the datasets were combined, and plots were created to represent data for analytes that were measured in multiple studies. For example, total phosphorus was measured at 79 of the 89 monitoring locations used in the BN analysis. Likewise, a BN based on data from all the areas was developed and trained for making statistical inferences. The BN was based on all available data from each area and had improved error rates during cross-validation. The improved error rates and statistical inferences are also discussed in Chapter 5 of the report.

Conclusions

This report presents our ArcNLET and BN modeling results for investigating OSTDS horizontal and vertical distances. Our ArcNLET modeling provides a systematic way of investigating the horizontal and vertical distances either separately or simultaneously. The ArcNLET modeling results at the five study areas showed consistent patterns for the horizontal and vertical attenuation rates. For the horizontal attenuation rate, we developed an empirical equation that was applicable to the five study areas. The equation uses hydraulic conductivity and horizontal distance as inputs, and are thus practically applicable, since hydraulic conductivity can be estimated using SSURGO data. Soil type plays an important role to determine both horizontal and vertical attenuation rates. The report provides the attenuation rates for the vertical distance of 2 feet and horizontal distance of 75 feet. At these distances, at least 75% attenuation rates can be achieved. Our ArcNLET modeling results should be ready to be used for OSTDS environmental

management. A meaningful management strategy is possible by closely collaborating with DEP scientists and policy makers.

Our BN modeling results are not as substantial or practically useful as ArcNLET modeling results. While our study demonstrated that it is feasible to develop a BN for individual study areas for multiple areas together, reliability of the BN was still unknown, and it may depend on the amount of data and the node arrangement within the model. The data in the reports of the study areas do not appear to be sufficient to develop a reliable BN for making statistical inferences on OSTDS setback distances. More work on the BN modeling is warranted in a future study.

Contents

Chapter 1. Introduction

Since the executive summary of this report already includes the scope, overarching question, and the model-driven and data-driven methods used in this project, this chapter does not repeat them, but provide a brief description of the ArcNLET and BN models used in this project.

1.1. A Brief Introduction of ArcNLET

ArcNLET is based on a simplified conceptual model of groundwater flow and nitrate transport. The model has three sub-models: groundwater flow model, nitrate transport model, and nitrate load estimation model. The results from the flow model are used by the transport model, whose results are in turn utilized by the nitrate load estimation model. By invoking assumptions and simplifications to the system being modeled, computational cost is significantly reduced, which enables ArcNLET to provide quick estimates of nitrate loads from septic systems to surface water bodies. The three submodels are briefly described here; more details of them can be found in Rios (2010) and Rios et al. (2013a). Ammonium is not explicitly simulated in ArcNLET. Instead, it is assumed in this study that ammonium transport is the same as nitrate transport so that ArcNLET can simulate nitrogen transport and estimate nitrogen load, not merely nitrate load, from septic systems to surface water bodies. This assumption however may overestimate nitrogen loads.

The groundwater flow model of ArcNLET is simplified by assuming that the water table is a subdued replica of the topography in the surficial aquifer. According to Haitjema and Mitchell-Bruker (2005), the assumption is valid if

$$\frac{RL^2}{mKHd} > 1, \tag{1.1}$$

where R [m/day] is recharge, L [m] is average distance between surface waters, m is a dimensionless factor accounting for the aquifer geometry, and is between 8 and 16 for aquifers that are strip-like or circular in shape, K [m/day] is hydraulic conductivity, H [m] is average aquifer thickness, and d [m] is the maximum distance between the average water level in surface water bodies and the elevation of the terrain. The criterion, as a rule of thumb, can be met in shallow aquifers in flat or gently rolling terrain. Based on the assumption, the shape of water table can be obtained by smoothing land surface topography given by DEM of the study area. In ArcNLET, the smoothing is accomplished using moving-window average via a averaging window, and the window size can be adjusted by users. The smoothing process needs to be repeated for multiple times, depending on discrepancy between the shapes of topography and water table. The number of the smoothing process, called smoothing factor, is specified by ArcNLET users as an input parameter of ArcNLET. This parameter needs to be calibrated against measured hydraulic heads in the study area, as explained in detail in Chapter 2.

With the assumption that smoothed DEM has the same shape (not the same elevation) of water table, hydraulic gradients can be estimated from the smoothed DEM. Subsequently, groundwater seepage velocity, v, can be obtained by applying Darcy's Law

$$\begin{aligned} v_x &= -\frac{K}{\phi}\frac{\partial h}{\partial x} \approx -\frac{K}{\phi}\frac{\partial z}{\partial x} \\ v_y &= -\frac{K}{\phi}\frac{\partial h}{\partial y} \approx -\frac{K}{\phi}\frac{\partial z}{\partial y} \end{aligned}, \tag{1.2}$$

where K is hydraulic conductivity [LT^{-1}], ϕ is porosity, h is hydraulic head, and hydraulic gradient ($\partial h/\partial x$ and $\partial h/\partial y$) is approximated by the gradient of the smoothed topography ($\partial z/\partial x$ and $\partial z/\partial y$). Implementing the groundwater flow model in the GIS environment yields the magnitude and direction of the flow velocity for every discrete cell of the modeling domain, which are used to estimate flow paths originating from individual septic systems and ending in surface water bodies. The calculation considers spatial variability of hydraulic conductivity, porosity, hydraulic head, and septic system locations. Because hydraulic gradients and water bodies are not hydraulically linked in the model, ArcNLET users need to evaluate whether the resulting shape of the water table is consistent with the drainage network associated the water bodies. The values of hydraulic conductivity and conductivity can be obtained from field measurements, literature data, and/or by calibration against measurements of hydraulic head and groundwater velocity.

Additional assumptions and approximations of the flow model are made as follows: (1) the Dupuit-Forchheimer assumption is used so that the vertical flow can be ignored and only two-dimensional (2-D) isotropic horizontal flow is simulated; (2) the steady-state flow condition is assumed, since this software is used for the purpose of long-term environmental planning; (3) the surficial aquifer does not include karsts or conduits so that Darcy's Law can be used; (4) mounding on water table due to recharge from septic systems and rainfall is not explicitly considered (but assumed to be reflected by the steady-state water table); (5) the flow field is obtained from the water table without explicit consideration of a water balance; (6) groundwater recharge from the estuary is disregarded. While these assumptions may not be ideal, especially the assumption of steady-state, they are needed to make model complexity compatible with available data and information and to make the model run efficient in the GIS modeling environment.

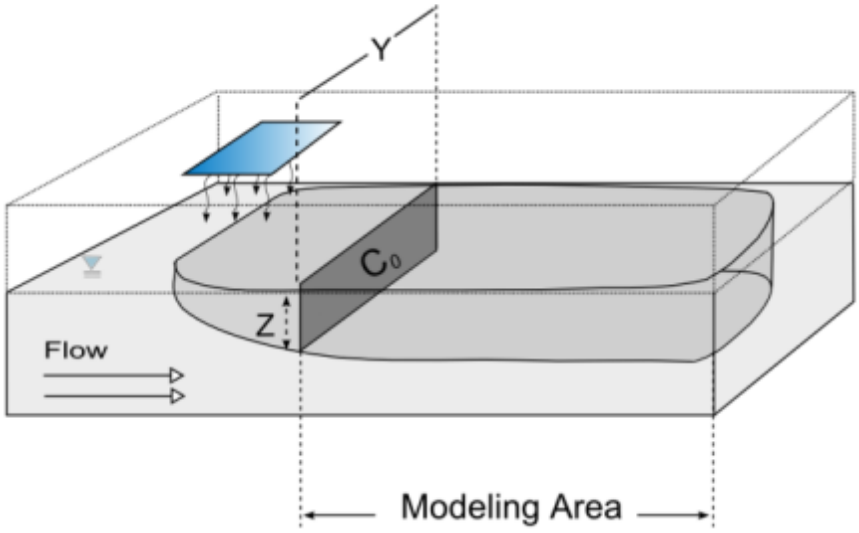

Fig. 1.1. Conceptual model of nitrate transport in groundwater adapted from Aziz et al. (2000). The unsaturated zone is bounded by the rectangular box delineated by the dotted lines; the groundwater zone is bounded by the box delineated by the solid lines

Fig. 1.1 shows the conceptual model of nitrate transport in ArcNLET, which is similar to that of BIOSCREEN (Newell et al. 1996) and BIOCHLOR (Aziz et al. 2000) developed by the U.S. EPA. In the conceptual model, nitrate enters the groundwater zone with a uniform and steady flow in the direction indicated. The Y−Z plane in Fig. 1.1 is considered as a source plane (with a constant concentration C_0 [ML^{-3}]) through which nitrate enters the groundwater system. Two-

dimensional (2-D) nitrate transport in groundwater is described using the advection-dispersion equation

$$\frac{\partial C}{\partial t} = D_x \frac{\partial^2 C}{\partial x^2} + D_y \frac{\partial^2 C}{\partial y^2} - v \frac{\partial C}{\partial x} - kC \tag{1.3}$$

where C is the nitrate concentration [M/L^3], t is time [T], D_x and D_y are the dispersion coefficients in the x and y directions, respectively [L^{2}T^{-1}], v is the constant seepage velocity in the longitudinal direction [L], and k is the first-order decay coefficient [T^{-1}]. This equation assumes homogeneity of parameters (e.g., dispersion coefficient) and uniform flow in the longitudinal direction. The last term in Eq. 3 is to simulate the denitrification, in which nitrate is transformed into nitrogen gas through a series of biogeochemical reactions. Following McCray et al. (2005) and Heinen (2006), the denitrification process is modeled using first-order kinetics and included as the decay term, which can also be used to take into account other loss processes. The steady-state form, semi-analytical solution of Eq. 1.3 is derived based on that of West et al. (2007), which is of 3-D, steady-state form and similar to the work of Domenico (1987). The analytical solution used in this study is (Rios, 2010; Rios et al., 2013a)

$$\begin{aligned} C(x,y) &= \frac{C_0}{2} F_1(x) F_2(y,x) \\ F_1 &= \exp\left[\frac{x}{2\alpha_x} \left(1 - \sqrt{1 + \frac{4k\alpha_x}{v}} \right) \right] \\ F_2 &= erf\left(\frac{y + Y/2}{2\sqrt{\alpha_y x}} \right) - erf\left(\frac{y - Y/2}{2\sqrt{\alpha_y x}} \right) \end{aligned} \tag{1.4}$$

where α_x and α_y [L] are longitudinal and horizontal transverse dispersivity, respectively, Y [L] is the width of the source plane, and C_0 [M/L^3] is the constant source concentration at the source plane. A review of analytical solutions of this kind and errors due to assumptions involved in their derivation is provided by Srinivasan et al. (2007).

The 2-D concentration plume is extended downwards to the depth Z of the source plane (Fig. 1); the pseudo three-dimensional (3-D) plume is the basis for estimating the amount of nitrate that enters into groundwater and loads to surface water bodies. While each individual septic system has its own source concentration, C_0, drainfield width, Y, and average plume thickness, Z, the information and data of these variables are always unavailable in a management project. Therefore, constant values are used for all septic systems in this study. ArcNLET allows using different C_0 values for different septic systems, if the data are available. Despite of the constant values used for all the septic systems, each individual septic system has its own concentration plume, because flow velocity varies between the septic systems. Since the flow velocity estimated in the groundwater flow model is not uniform but varies in space, in order to use the analytical solution with uniform velocity, the harmonic mean of velocity (averaged along the flow path of a plume) is used for evaluating each individual plume. The plumes either end at surface water bodies or are truncated at a threshold concentration value (usually very small, e.g., 10^{-6}). After the plumes for all septic systems are estimated, by virtue of linearity of the advection-dispersion equation with respect to concentration, the individual plumes are added together to obtain the spatial distribution of nitrate concentration in the modeling domain. The superposition however may result in higher and shallower concentrations than exist in the field unless the averaging depth is deep enough.

The nitrate load estimation model evaluates the amount of nitrate loaded to target surface water bodies. For the steady-state model, this is done using the mass balance equation, $M_{out} = M_{in} - M_{dn}$, where M_{out} [MT^{-1}] is mass load rate to surface water bodies, M_{in} [MT^{-1}] is mass inflow rate from septic systems to groundwater, and M_{dn} [MT^{-1}] is mass removal rate due to denitrification. The mass inflow rate, M_{in}, consists of inflow due to advection and dispersion, and is evaluated via

$$M_{in} = YZ\phi\left(vC_0 - \alpha_x v \left.\frac{\partial C}{\partial x}\right|_{x=0} \right) = YZ\phi v C_0 \frac{1+\sqrt{1+\frac{4ka_x}{v}}}{2} \quad . \tag{1.5}$$

The derivative, $\partial C/\partial x$, used for calculating the dispersive flux is evaluated using an analytical expression based on the analytical expression of concentration in Eq. 1.4. When the mass inflow rate is known, it can be specified within ArcNLET. Otherwise, the mass inflow rate is calculated by specifying the *Z* value. The mass removal rate due to denitrification, M_{dn}, is estimated via

$$M_{dn} = \sum_i kC_i V_i \phi_i \ , \tag{1.6}$$

where C_i and V_i are concentration and volume of the *i*-th cell of the modeling domain, and kC_i is denitrification rate assuming that denitrification is the first-order kinetic reaction (Heinen 2006). If a plume does not reach any surface water bodies, the corresponding nitrate load is theoretically zero.

The simplified groundwater flow and nitrate transport model is implemented as an extension of ArcGIS using the Visual Basic .NET programming language. In keeping with the object-oriented paradigm, the code project is structured in a modular fashion. Development of the graphical user interface (GUI) elements is separated from that of the model elements; further modularization is kept within the development of GUI and model sub-modules. The main panel of the model GUI is shown in Fig. 1.2; there are four tabs, each of which represents a separate modeling component. For example, the tab of Groundwater Flow is for estimating magnitude and direction of groundwater flow velocity, and the tab of Particle Tracking for estimating flow path from each septic system. Each tab is designed to be a self-contained module and can be executed individually within ArcGIS. Five ArcGIS layers are needed for running ArcNLET. They are DEM, hydraulic conductivity, and porosity in raster form, septic system locations in point form, and surface water bodies in polygon form. These ArcGIS files need to be prepared outside ArcNLET. The output files are also ArcGIS layers that can be readily post-processed and visualized within ArcGIS. More details of the software development, including verification and validation, are described in Rios (2010) and Rios et al. (2013a).

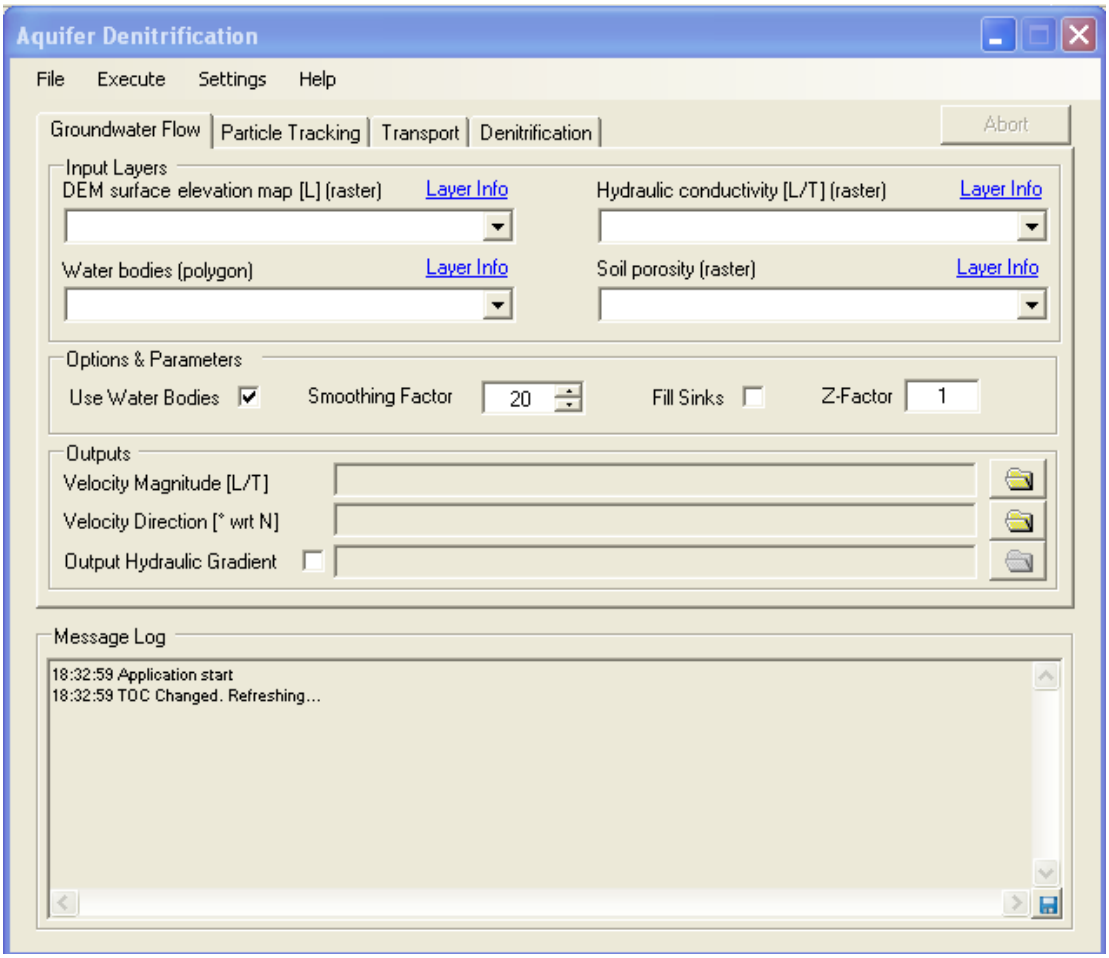

Fig. 1.2. Main Graphic User Interface (GUI) of ArcNLET with four modules of Groundwater Flow, Particle Tracking, Transport, and Denitrification

Before ArcNLET is used for estimating nitrogen load to surface water bodies, calibrating the model parameters is always needed to match model simulations to field observations. However, in many projects of nitrogen pollution management, field observations are scarce. This is the reason of developing ArcNLET whose complexity is compatible with available data. As shown in the next section, observation data is extremely limited in the modeling area, and the conceptual model based on the limited data should be simple. On the other hand, the calibrated ArcNLET model is able to reasonably match field observations, as shown in Chapter 2.

1.2. A Brief Introduction of Bayesian Network (BN)

According to the Wikipedia website at https://en.wikipedia.org/wiki/Bayesian_network, "A Bayesian network (also known as a Bayes network, Bayes net, belief network, or decision network) is a probabilistic graphical model that represents a set of variables and their conditional dependencies via a directed acyclic graph (DAG)." The website further explains that "… Bayesian networks are directed acyclic graphs (DAGs) whose nodes represent variables in the Bayesian sense: they may be observable quantities, latent variables, unknown parameters or hypotheses. Edges represent conditional dependencies; nodes that are not connected (no path connects one node to another) represent conditionally independent variables. Each node is associated with a probability function that takes, as input, a particular set of values for the

node's parent variables and gives (as output) the probability (or probability distribution, if applicable) of the variable represented by the node.

Fig. 1.3 illustrates a simple Bayesian network given on the Wikipedia website. Wikipedia explains the Bayesian network: "Two events can cause the grass to be wet: an active sprinkler or rain. Rain directly affects the use of the sprinkler (namely, when it rains, the sprinkler usually is not active). This situation can be modeled with a Bayesian network. Each variable has two possible values, T (for true) and F (for false). The rain probability is independent and is forecasted as 0.2 for rain and 0.8 for no rain. The sprinkler probability depends on the rain probability. If there is no rain (F for rain), there is a 0.4 probability that the sprinkler is on (T for sprinkler) and a 0.6 probability that the sprinkler is off (F for sprinkler). Otherwise, the corresponding probabilities are 0.01 and 0.99. In other words, the probability of a sprinkler depends on the probability of rain, and the conditional probabilities are either directly provided by a developer of the Bayesian network or indirectly trained by using data. The sprinkler node is the child node of the rain node. Both nodes are parent nodes of the node of grass wet, and the conditional probability of grass wet is given in Fig. 1.3. For example, if the sprinkler is off (F for sprinkler) and there is no rain (F for rain), the probability of wet grass is 0 (T for wet grass), and correspondingly, the probability of dry grass is 1 (F from wet grass). This probability is calculated based on the Bayesian theorem using the law of total probability and conditional probability.

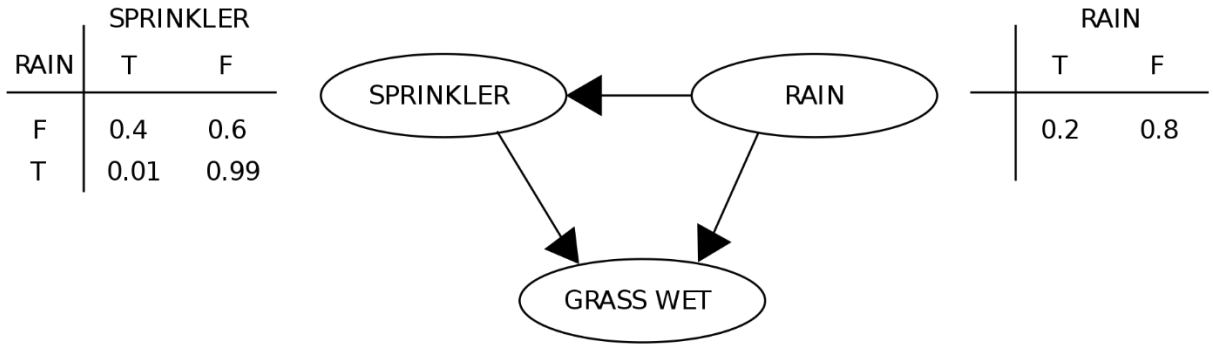

SPRINKLER	RAIN	GRASS WET T	GRASS WET F
F	F	0.0	1.0
F	T	0.8	0.2
T	F	0.9	0.1
T	T	0.99	0.01

Fig. 1.3. A simple Bayesian network with conditional probability tables. This example is adopted from Wikipedia at https://en.wikipedia.org/wiki/Bayesian_network.

Glendell et al. (2021) recently published a report that developed a Bayesian network to estimate phosphorus, nitrogen, and microbial pollution to water from septic tanks. This report addresses the following three research questions:

(1) What factors contribute to the risk of phosphorus (P) pollution from septic tank systems (STS)?

(2) Can a probabilistic risk model informed by expert knowledge be applied nationally, given available data?

(3) What factors would need to be considered to apply the model to nitrogen (N) and microbial (FIOs) pollution risk?

This study was expanded in Glendell et al. (2022) to simulate the probability of soluble reactive phosphorus concentration falls into the European Union Water Framework Directive high/good or moderate/poor status classifications and the effectiveness of three mitigation measures, including buffer strips, fertilizer input reduction, and septic tank management.

The Bayesian network developed by Glendell et al. (2021) is copied in Fig. 1.4 below. The figure quality is low, as it was taken as a snapshot from the report of Glendell et al. (2021). We could not find a figure of high resolution. To better illustrate the concept of the Bayesian network, we copied Fig. 1.5, the Bayesian network given in Glendell et al. (2022). The difference between Glendell et al. (2021) and Glendell et al. (2022) is that the former study was focused solely on OSTDS but the latter study considered other pollution sources such as fertilizer inputs. It should be noted that the studies of Glendell et al. (2021, 2022) are not for OSTDS setback distance.

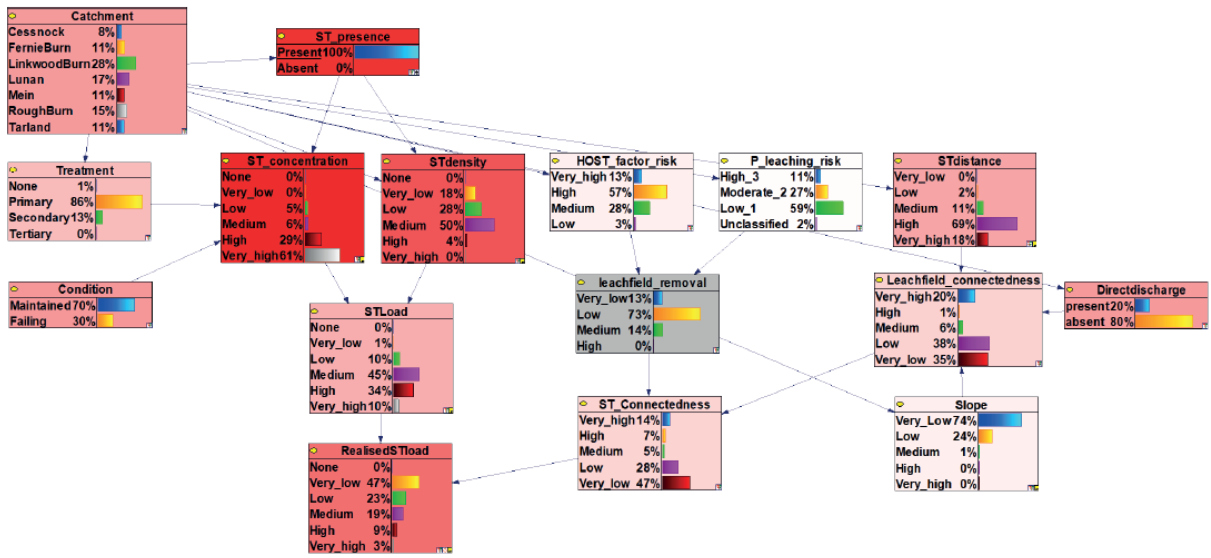

Fig. 1.4. The Bayesian network was developed by Glendell et al. (2021). The figure quality is low because it was taken as a snapshot from the report of Glendell et al. (2021). We could not find a figure with high resolution. Figures 1.3 and 1.4 from Glendell et al. (2022) illustrate the Bayesian network better.

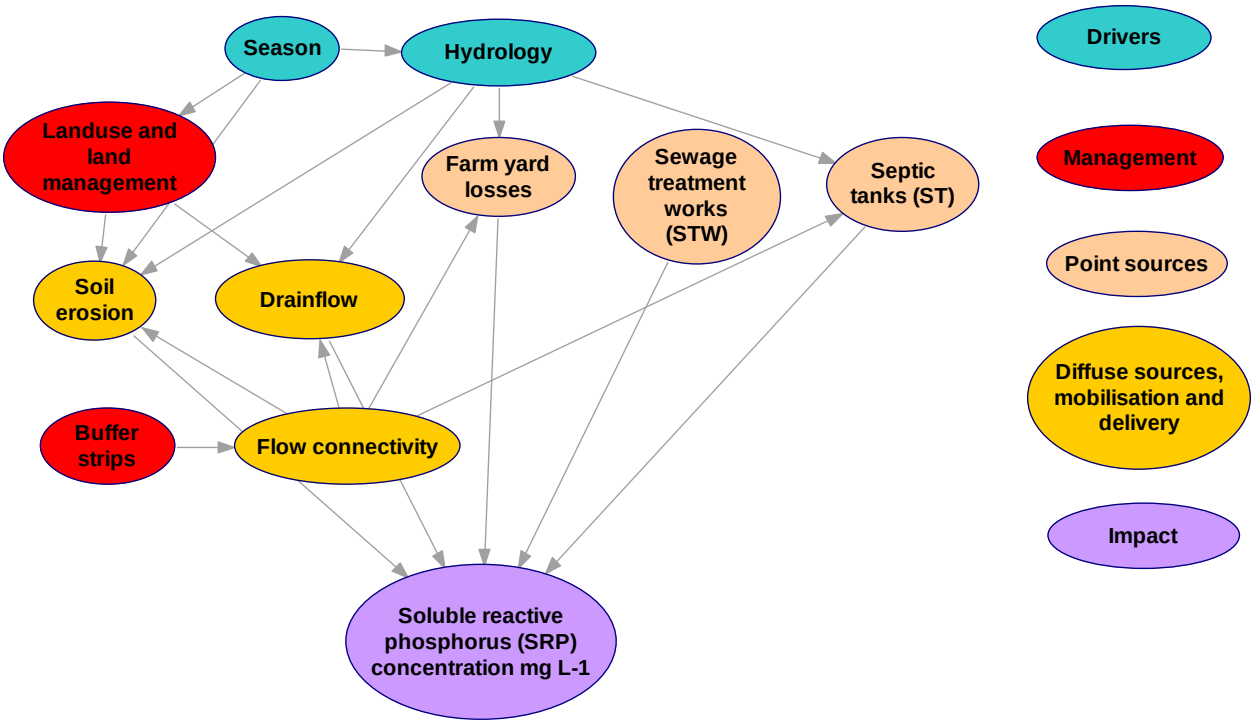

Fig. 1.5. Glendell et al. (2022) developed an example Bayesian network for an OSTDS-related study. The ultimate child node is soluble reactive phosphorus concentration, and the other nodes are its parent nodes. The edges are the grey arrows that represent the causal relationship between the nodes.

Fig. 1.5 above shows five kinds of nodes in different colors. The ultimate child node is for soluble reactive phosphorus concentration at the bottom of the Bayesian network, and the other four kinds of nodes are its parent nodes. Each node is associated with an environmental variable that can be either deterministic or random. A random node is characterized by the probability (or probability density) of the variable of the node. The probability propagates through the network, and the final product is the probability of child nodes conditioned on the probability of parent nodes. The Bayesian network with conditional probabilities is shown in Fig. 1.4. A better illustration of the conditional probabilities is given in Fig. 1.6, a portion of the Bayesian network developed by Glendell et al. (2022). The Bayesian network provides a flexible way of managing multiple factors and their interactions and explicitly considering the uncertainty of environmental variables.

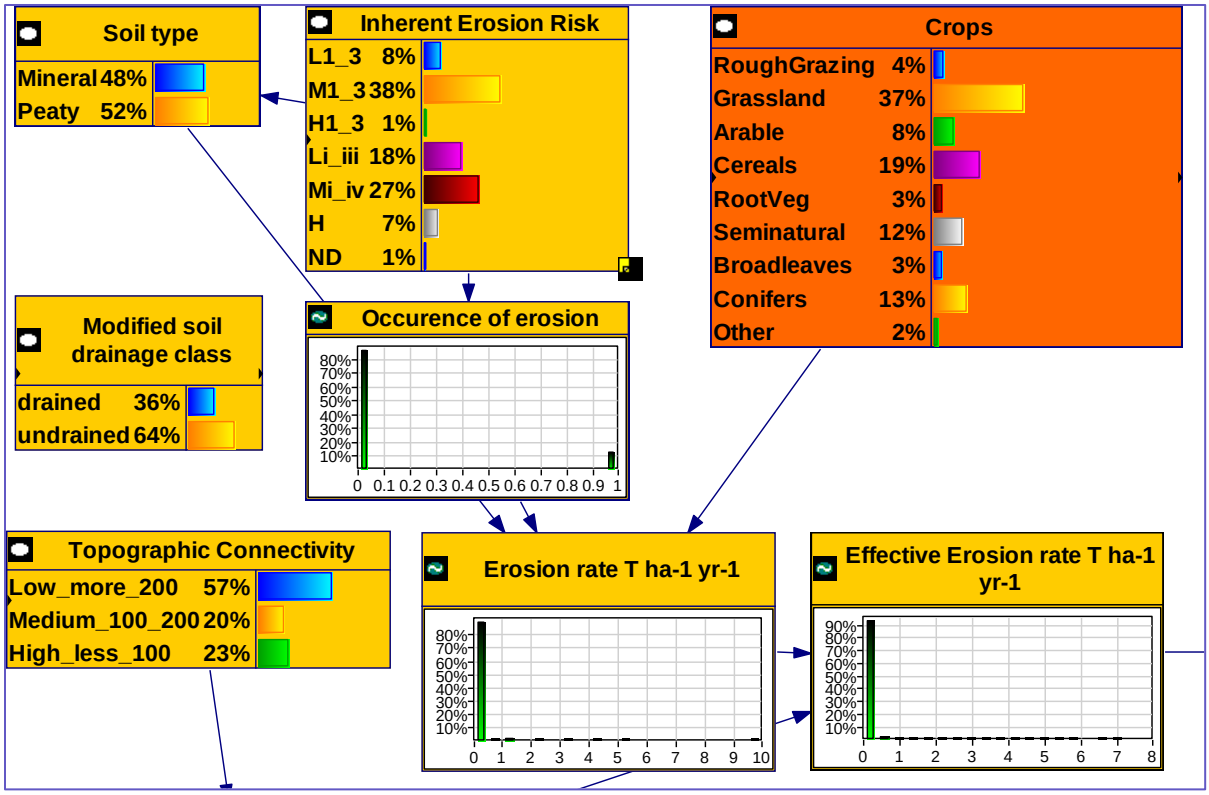

Fig. 1.6. A portion of the Bayesian network developed by Glendell et al. (2022). This sub-Bayesian network shows the relation between soil type, drainage class, crops, topographic connectivity, and soil erosion.

A general procedure for building a Bayesian network is as follows:

(1) Arrange the environmental factors discussed above as the nodes of the Bayesian network. These nodes will be parent nodes, and OSTDS setback distance will be the ultimate child node because it is the variable of ultimate interest in this project.

(2) Arrange the nodes in a hierarchical structure and link the nodes with edges in the manner shown in Fig. 1.3. The hierarchical structure and the node edges should reflect the casual relation between the nodes based on our understanding of the physical, chemical, and biological processes that control reactive nitrogen transport from OSTDS.

(3) Characterize the nodes in a probabilistic way based on literature data, and use the data to train the Bayesian network to develop the conditional probability from parent nodes to child nodes. The node characterization and Bayesian network training can be implemented using software such as Netica.

(4) Validate the trained Bayesian network by using independent data compiled from the literature. After the validation, the Bayesian network can investigate OSTDS setback distance.

1.2.1 An example BN and description of its nodes

Fig. 1.7 show a BN developed based on data at the Groseclose site in the Turkey Creek sub-basin. The BN is a probabilistic model examining the relationship between the OSTDS and adjacent surface water. Attenuation of TKN/NO3/TP is affected by several factors, such as soil,

groundwater, and OSTDS conditions (Glendell et al. 2021; Troldborg et al. 2022). These factors are included as nodes of the BN and are described below.

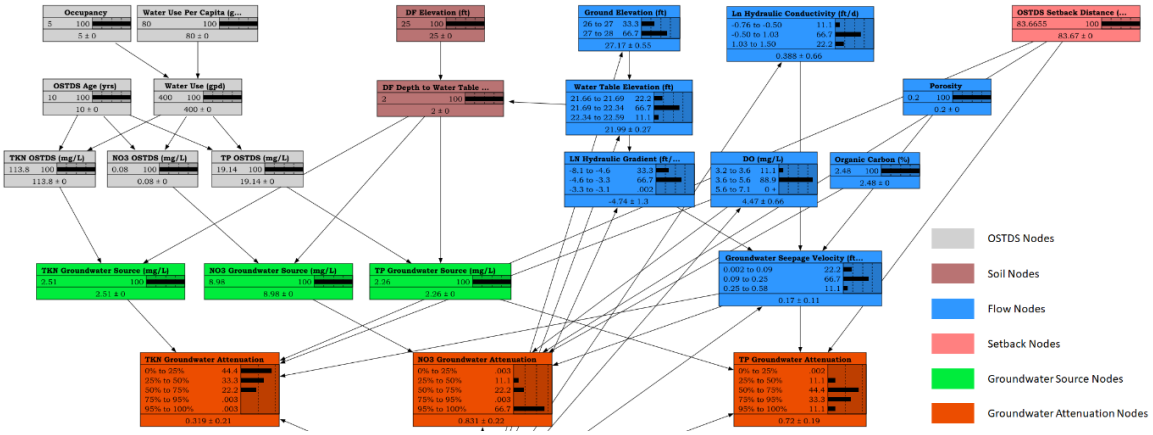

Fig. 1.7. An example Bayesian Network (BN) in the context of this project based on data of the Groseclose site in the Turkey Creek sub-basin. A landscape version of this figure is given as Figure A1 in the appendix, and it is easier to read. The nodes are colored and classified as follows: OSTDS nodes (grey), Soil nodes (brown), Groundwater nodes (blue), the OSTDS Setback node (pink), Groundwater Source nodes (green), and Groundwater Attenuation nodes (orange).

OSTDS nodes in grey color

The OSTDS nodes and their structure are shown in Fig. 1.8. For example, the "Occupancy" of the household and the "Water Use Per Capita" are the parent nodes of the "Water Use". Likewise, the "OSTDS Age" and "Water Use" are the parent nodes of the nodes of "TKN OSTDS", "NO3 OSTDS", and "OSTDS TP". More OSTDS nodes (i.e., OSTDS type) can be added later if the information for the nodes is available.

Soil nodes in brown color

As shown in Fig. 1.8, the soil nodes in the BN represent the vertical setback distance between the OSTDS drainfield and the water table. The "DF Elevation" is the average water table elevation reported by Ayres Associates (1993), and it is used to calculate the "DF Depth to Water Table" node for the Groseclose site. There are only soil nodes because the report of Ayres Associates (1993) only contains data on drainfield elevation and drainfield depth to the water table. More nodes may be added if more soil data (i.e., DO in soils) are available in reports of other sites.

Groundwater source nodes in green color

The groundwater source nodes (Fig. 1.8) represent TKN, NO3, and TP concentrations at the water table. They are the child nodes of OSTDS and soil nodes because septic effluent flows through the vadose zone to enter groundwater.

The nodes shown in Fig. 1.8 are deterministic because there is only one OSTDS at the Groseclose site. When more OSTDS are considered for multiple sites, the nodes will be characterized by probabilities of the node variables. For example, the Jones site has an occupancy of 2. Adding this information into the Occupancy node gives a 50% probability for occupancy of

2 and a 50% probability for occupancy of 5. The probability can be further updated by using literature data on occupancy.

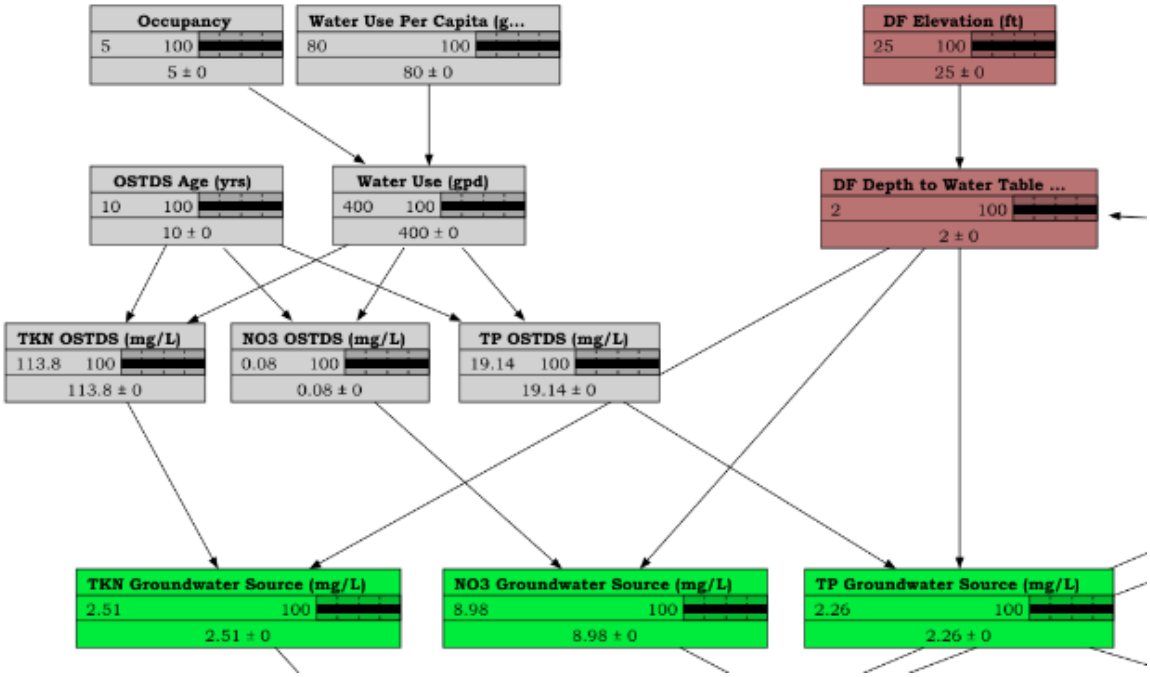

Fig. 1.8. OSTDS, soil, and groundwater source nodes in the BN developed for the Groseclose site.

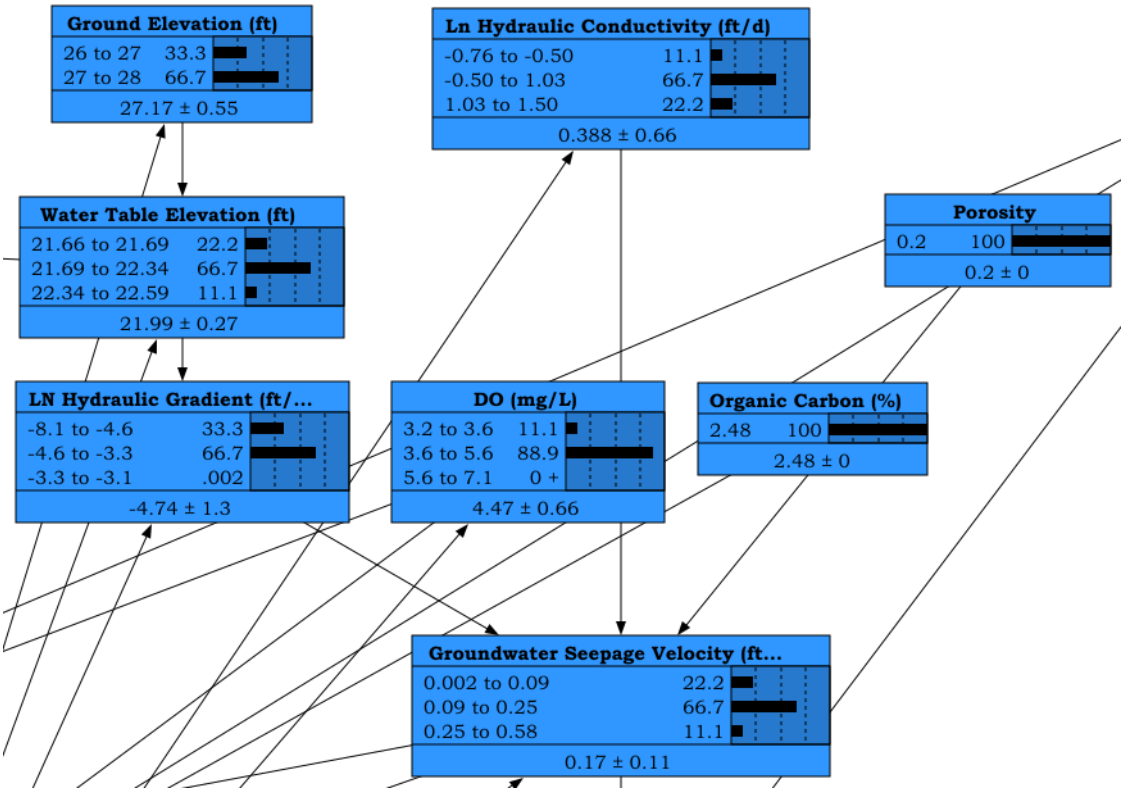

Fig. 1.9. Groundwater Nodes in the BN developed for the Groseclose site.

Groundwater nodes in blue color

The TKN/NO3/TP Groundwater Source nodes shown in Fig. 1.8 and the groundwater nodes shown in Fig. 1.9 are parent nodes of the groundwater attenuation nodes shown below, reflecting the understanding that the TKN/NO3/TP concentrations at the water table may be attenuated during nutrient transport in surficial aquifers. The number of groundwater nodes is relatively large because the report of Ayres Associates (1993) includes many groundwater data at multiple piezometers and monitoring wells.

Based on the reported data, we can characterize the groundwater nodes (except the nodes "Porosity" and "Organic Carbon") in a probabilistic way. For example, slug tests were conducted for hydraulic conductivity at ten monitoring wells, and as reported in Ayres Associates (1993), ten hydraulic conductivity values were listed. The histogram of the data is shown in Fig. 1.10, and the data range -0.5 – 1.03 represent the range of μ-σ – μ+σ, where μ and σ are the mean and standard deviation of the ten data. Therefore, the histogram indicates that log hydraulic conductivity follows the normal distribution of $N(\mu,\sigma)$. This procedure was applied to the nodes of "Water Table Elevation", "Log Hydraulic Gradient", "Groundwater Seepage Velocity", and "DO" to determine the probabilities of their ranges.

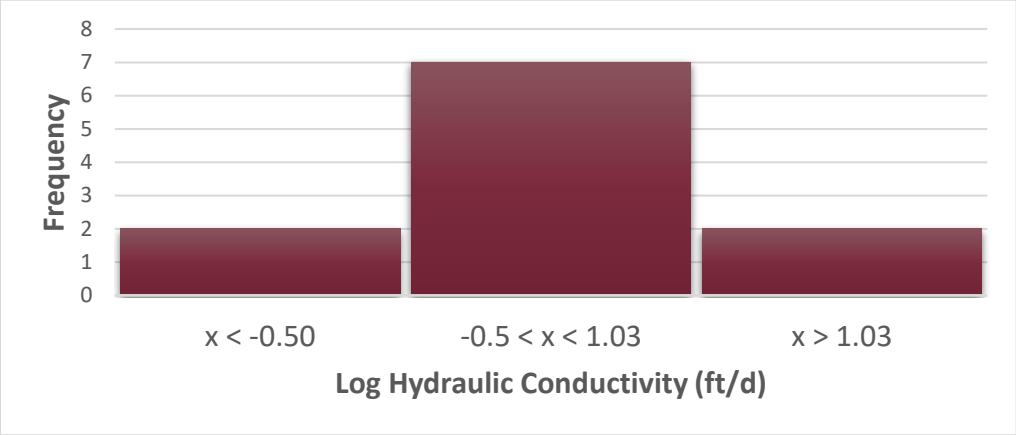

Fig. 1.10. Histogram of log hydraulic conductivity for ten values of hydraulic conductivity measured at the Groseclose site.

OSTDS setback node in pink color

The setback node is special. Although it can be a groundwater node, it is listed as a separate node (Fig. 1.11) because the OSTDS setback distance is the final product of this project. The distance of 83.6655, shown in Fig. 1.11, is the distance between the drainfield and the canal at the Groseclose site. There is only one distance value in the BN developed for the Groseclose site, and multiple distance values will be used when more OSTDS are considered for developing the final BN of this project.

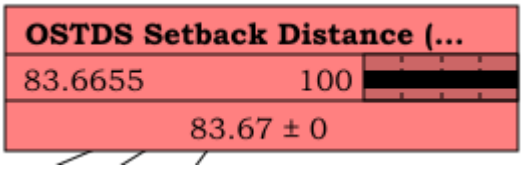

Fig. 1.11. OSTDS Setback Distance node in the BN developed for the Groseclose site.

Groundwater attenuation nodes in orange color

The three groundwater attenuation nodes (Fig. 1.9) are the child nodes of the groundwater source nodes, groundwater nodes, and the OSTDS setback distance node, reflecting the understanding that TKN/NO3/TP concentrations are attenuated when nutrient transport in surficial aquifers over the setback distance. The attenuation rates were calculated by dividing the contaminant concentrations at monitoring wells by the concentrations at well G5. Monitoring well G5 was between the drainfields of black water and grey water. Therefore, TKN/NO3/TP concentrations at well G5 are considered the groundwater source concentrations.

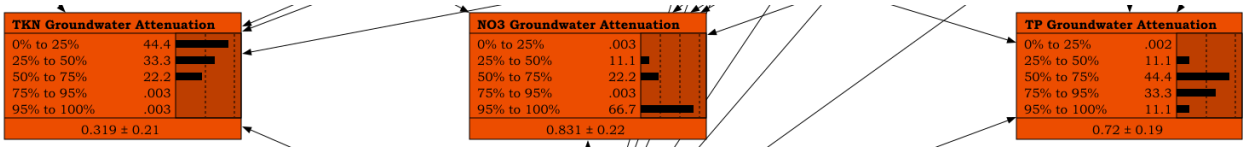

Fig. 1.12. Groundwater attenuation nodes in the BN developed for the Groseclose site. The groundwater attenuation nodes (orange) represent the percent of TKN, NO3, and TP attenuation from the OSTDS.

BN development and training

ArcGIS Pro version 3.1.0 software suite was used to organize, visually analyze, and present geospatial data (Esri 2023) for the Groseclose site. Furthermore, the hydraulic gradients were calculated between each pair of adjacent monitoring wells for the Groseclose site within the GIS. The site surveys from Ayres Associates (1993) were georeferenced to obtain the specific location of the groundwater monitoring wells, the monitoring well distances from the drainfield, the monitoring well pair distances (for calculating hydraulic gradients), and the OSTDS distance from the nearest surface water. Afterward, the Microsoft Excel for Microsoft 365 MSO (Version 2302 Build 16.0.16130.20298) 64-bit (Microsoft Corporation 2023) software suite was used to calculate data, organize information for the BN learning process, create histograms, and categorize and discretize variables. Furthermore, the Bayesian network software Norsys Netica version 6.09, 64 Bit for MS Windows 7 to 10 (Netica) (Norsys 2020) was used to build the network probability tables based on existing data in the report of Ayres Associates (1993).

The node-link relationships in the network describe the causal relationship between parent and child nodes. In addition, the links determine the structure and probability distributions within the network's conditional probability tables (CPTs) (Neil et al. 2000, Fenton and Neil 2018). The CPTs were obtained using the expectation-maximization (EM) algorithm, which was developed by Dempster et al. (1977) and adapted for BNs by Lauritzen (1995). Netica provides the function for applying the EM algorithm (Norsys 2020).

BN analysis can be conducted based on cell-by-cell map algebra, which is a spatial analysis and GIS modeling standard (Morgan et al. 2012). Explicitly including spatial data within a BN at the resolution of pixels allows for the opportunity to perform probabilistic map algebra (Ames and Anselmo 2008). For example, within the Groseclose BN, the location of the georeferenced groundwater monitoring wells from Ayres Associates (1993) serves as the pixel to transfer the conditional probabilities from the BN to the GIS. A unique benefit of Bayesian statistics is that posterior distributions contain the information needed to make inferences. Moving analysis results from a BN to a GIS allows for creating probabilistic maps based on Bayesian inference findings. This feature, however, has not been explored.

1.2.2 Evaluating the BN and using it for studying the OSTDS setback distance

For the BN shown in Fig. 1.7, the three final output nodes are those in orange and labeled as "TKN Groundwater Attenuation", "NO3 Groundwater Attenuation", and "TP Groundwater Attenuation". The attenuation rates (%) were calculated by dividing TKN/NO3/TP concentrations at monitoring wells by the corresponding concentrations at a well between the black water and gray water septic tanks at the Groseclose site. In the BN terminology, the three attenuation nodes are the child nodes, and their parent nodes are those above the child nodes (Fenton and Neil 2018). The BN can be used in the following two ways:

(1) Forward inference: based on data (i.e., conditional probability) of the parent nodes, the BN can estimate the probabilities of the child nodes for attenuation rates. These results can be used for evaluating the BN; an example is given below.

(2) Backward inference: for a given attenuation rate, the BN can estimate the probabilities of the parent nodes. They include the two nodes labeled "DF Depth to Water Table" and "OSTDS Setback Distance", which are the vertical setback distance and the horizontal setback distance, respectively.

One way to evaluate the BN is to investigate whether the BN can estimate known data and/or information with a high probability. For this kind of evaluation, we used the groundwater seepage velocity of 0.24 ft/d given in the report of Ayres Associates (1993). This value is estimated based on a tracer test and is not used for developing the BN. The forward inference of the BN gives:

$$P(0.09 \leq \text{Groundwater Seepage Velocity} \leq 0.25) = 66.7\% \quad (1.7)$$

The probability is relatively high, indicating that the BN is reasonable.

Another way of evaluating the BN is to run the forward inference of the BN developed for the Groseclose site to estimate the probabilities of data at the Jones site. For example, we can replace the probabilities of groundwater seepage rates of the Groseclose site with those of the Jones site, which will lead to new probabilities of TKN/NO3/TP groundwater attenuating. We can evaluate the probabilities using data-based attenuation rates. For example, if the BN estimates a 90% probability for the attenuation rate range of 95 – 100%, we expect that the attenuation rate within the range of 95 – 100% should occur at a relatively large number of monitoring wells. This type of evaluation is ongoing.

Below is an example of backward inference. If a 90% NO3 groundwater attenuation rate is desired, we can condition the NO3 Groundwater Attenuation node to the probability of 100% for the range of 75 – 95%. This conditioning is shown in Fig. 1.13. The conditioning of the child node changes the probabilities of the parent nodes, which is expected for a BN (Neil et al. 2000, Fenton and Neil 2018). For the 90% NO3 groundwater attenuation rate, the probability of "Groundwater Seepage Velocity" changes from 66.7% to 43.9% for the range 0.09 – 0.25 (ft/d) and from 22.2% to 29.8% for the range 0.002 – 0.09 (ft/d). These changes indicate that slower groundwater velocity is needed for a large volume of nitrate attenuation in groundwater. This relationship is physically reasonable because slower groundwater seepage velocity leads to more denitrification and, thus, a larger groundwater attenuation rate.

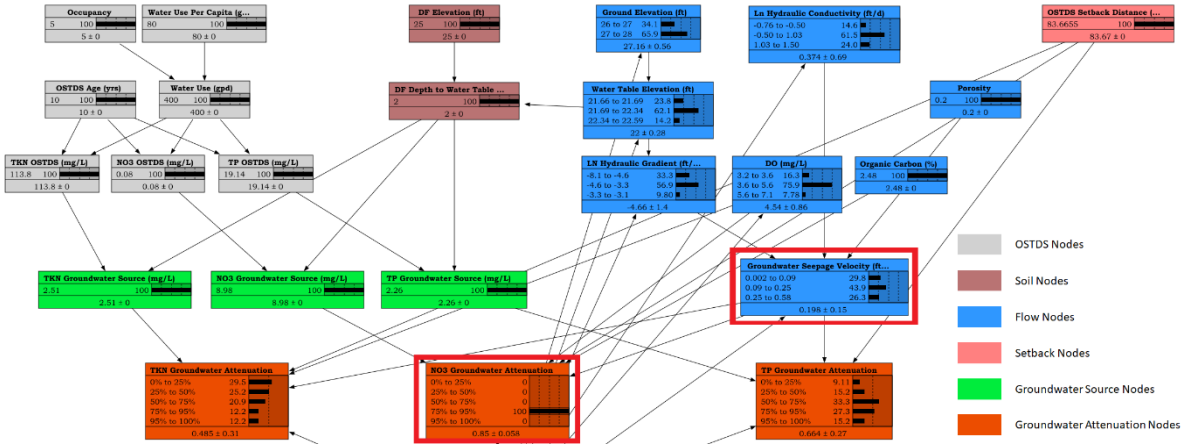

Fig. 1.13. BN was developed for the Groseclose site for backward inference by conditioning the NO3 Groundwater Attenuation rate with 100% probability.

References

Ayres Associates (1993) An Investigation of the Surface Water contamination Potential from

Onsite Sewage Disposal Systems (OSDS) in the Turkey Creek Sub-Basin of the Indian River Lagoon Basin. Florida Department of Health and Rehabilitative Services (HRS)

Aziz, C.E., Newell, C.J., Gonzales, J.R., Haas, P., Clement, T.P., Sun, Y. (2000) BIOCHLOR natural attenuation decision support system user's manual version 1.0. U.S. Environmental Protection Agency, Washington, DC.

Domenico, P.A. (1987) An analytical model for multidimensional transport of a decaying contaminant species. J Hydrol 91:49–58.

Glendell, M., Gagkas, Z., Richards, S., Halliday, S. (2021) Developing a probabilistic model to estimate phosphorus, nitrogen and microbial pollution to water from septic tanks. CRW2018_12. Scotland's Centre of Expertise for Waters (CREW). Available online at: crew.ac.uk/publications

Glendell M, Gagkas Z, Stutter M, et al (2022) A systems approach to modeling phosphorus pollution risk in Scottish rivers using a spatial Bayesian Belief Network helps targeting effective mitigation measures. Front Environ Sci 10:976933. https://doi.org/10.3389/fenvs.2022.976933

Heinen, M (2006) Simplified denitrification models: Overview and properties. Geoderma 133(3-4):444–463.

McCray, JE, Kirkland SL, Siegrist RL, Thyne GD (2005) Model parameters for simulating fate and transport of on-site wastewater nutrients. Ground Water 43(4):628–639.

McNeillie JI, Anderson DL, Belanger TV (1994) Investigation of the surface water contamination potential from on-site wastewater treatment systems (OWTS) in the Indian River Lagoon Basin. In On-site Wastewater Treatment: Proceedings of the Seventh National Symposium on Individual and Small Community Sewage Systems.

Rios, J.F. (2010), A GIS-Based Model for Estimating Nitrate Fate and Transport from Septic Systems in Surfacial Aquifers, Master Thesis, Florida State University, Tallahassee, FL.

Rios, J.F., M. Ye, and L. Wang (2011a), uWATER-PA: Ubiquitous WebGIS Analysis Toolkit for Extensive Resources - Pumping Assessment, Ground Water, 49(6), 776-780, DOI: 10.1111/j.1745-6584.2011.00872.x.

Rios, J.F., M. Ye, L. Wang, and P. Lee (2011b), ArcNLET: An ArcGIS-Based Nitrate Load Estimation Toolkit, User's Manual, Florida State University, Tallahassee, FL., available online at http://people.sc.fsu.edu/~mye/ArcNLET/users_manual.pdf.

Rios, J.F., M. Ye, L. Wang, P.Z. Lee, H. Davis, and R.W. Hicks (2013a), ArcNLET: A GIS-based software to simulate groundwater nitrate load from septic systems to surface water bodies, Computers and Geosciences, 52, 108-116, 10.1016/j.cageo.2012.10.003.

Rios, J.F., M. Ye, and H. Sun (2013b), ArcNLET 2.0: New ArcNLET Function of Monte Carlo Simulation for Uncertainty Quantification, Florida State University, Tallahassee, FL.

Srinivasan V, Clement TP, Lee KK (2007) Domenico solution – is it valid? Ground Water 45(2):136–146.

Troldborg M, Gagkas Z, Vinten A, et al (2022) Probabilistic modeling of the inherent field-level

pesticide pollution risk in a small drinking water catchment using spatial Bayesian belief networks. Hydrology and Earth System Sciences 26:1261–1293. https://doi.org/10.5194/hess-26-1261-2022.

West, MR, Kueper, BH, Ungs, MJ (2007) On the use and error of approximation in the Domenico (1987) solution. Ground Water 45(2): 126–135.

Chapter 2. Numerical Investigation of OSTDS Setback Distances in the Turkey Creek Sub-basin of Indian River Lagoon

The numerical investigation presented in this chapter was based on the data presented in the technical report of Ayres Association (1993) for two homes located in the Turkey Creek sub-basin of India River Lagoon. The homes are in the Port Malabar Subdivision of the City of Palm Bay in Brevard County, Florida. The two study sites corresponding to the two homes were referred to as **Groseclose Site and Jones Site** in the report of Ayres Associates (1993), where Groseclose and Jones are last names of the homeowners at the time when the study was conducted. The report includes measurements of groundwater level and nitrogen concentrations, and they were used in this study to calibrate ArcNLET. The calibrated ArcNLET was subsequently used for investigating OSTDS setback distances.

Based on information (e.g., Fig. 2.1) in the report and information in the county appraiser's office, we located the two homes on Google Map and Google Earth (Fig. 2.2). The property record cards for the Groseclose and Jones homes are at https://www.bcpao.us/PropertySearch/#/account/2806200 and https://www.bcpao.us/PropertySearch/#/account/2806183, respectively. The specific locations of the Groseclose and Jones homes are shown in Fig 2.3.

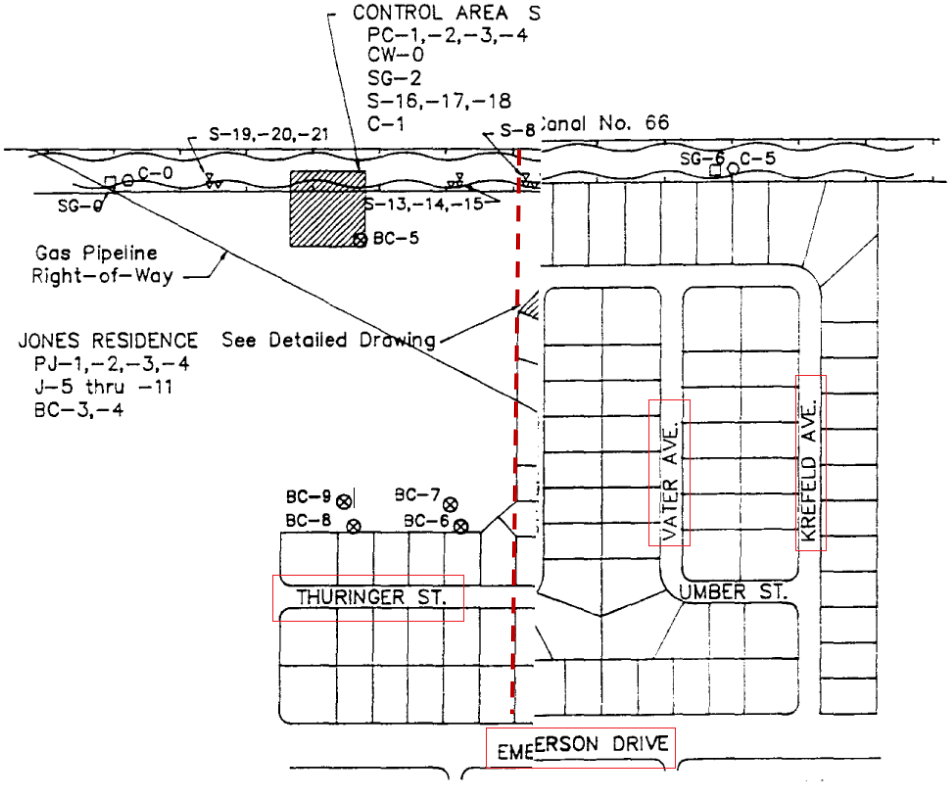

Fig. 2.1. The location of Groseclose home and Jones home illustrated in the report of Ayres Associates (1993). The figure is copied from Figure 3 of the report.

(a) Google map

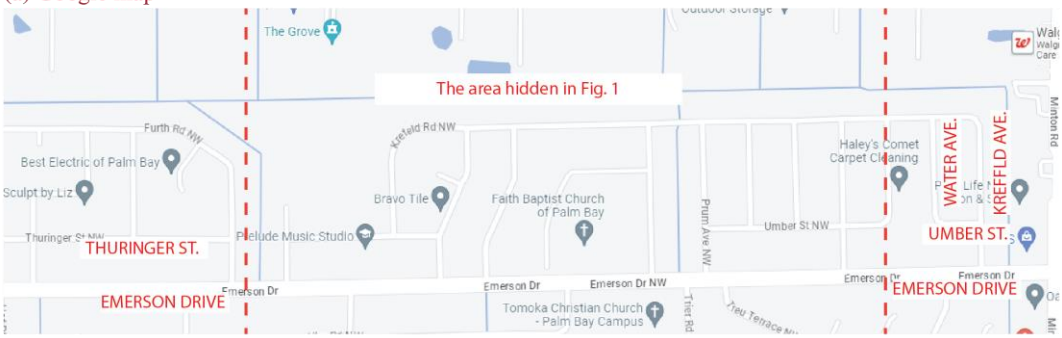

(b) Google Earth

Fig. 2.2. Screenshots of Google Map and Google Earth for the study area.

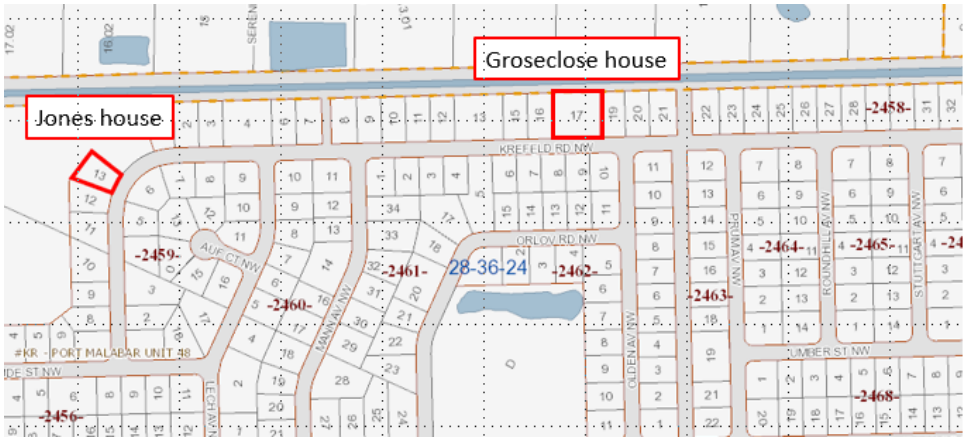

Fig. 2.3. Specific locations of Groseclose house and Jones house.

2.1 Procedure of Numerical Investigation

The ArcNLET-based numerical investigation was conducted in the following procedure:

(1) Develop an ArcNLET-3.0 model (including VZMOD) using public domain data of OSTDS locations, DEM, water body locations, hydraulic conductivity, and porosity. The modeling domain (shown below) contains a total of 6,095 OSTDS, and is substantially larger than the area shown in Figs 2.2 and 2.3.

(2) Run ArcNLET-3.0 for the Groseclose and Jones sites (by setting nitrogen concentrations as zero for other OSTDS), and adjust ArcNLET model parameters (e.g., smoothing factor, dispersivity, and nitrification and denitrification rates) to match model simulations to corresponding field observations of water level and nitrogen concentration to the extent possible. This ArcNLET model is referred to as the calibrated ArcNLET model.

(3) Run the calibrated ArcNLET-3.0 model for all the 6,095 OSTDS to investigate the impacts of OSTDS **vertical** setback distance on nitrogen attenuation from OSTDS drainfields to water table, and nitrogen concentrations at drainfields and water table are used for calculating the attenuation.

(4) Run the calibrated ArcNLET-3.0 model for all the 6,095 OSTDS to investigate the impacts of OSTDS **horizontal** setback distance on nitrogen attenuation from water table to surface water bodies, and nitrogen concentrations at water table and locations immediately adjacent to water bodies are used for calculating the attenuation.

(5) Run the calibrated ArcNLET for a sensitivity analysis to evaluate the impacts of **both vertical and horizontal** setback distance on nitrogen attenuation from drainfields to surface waterbodies, and nitrogen concentrations at drainfields and locations immediately adjacent to water bodies are used for calculating the attenuation.

Every step of the modeling procedure is described in detail below.

2.2 Data for ArcNLET Modeling

This section describes preparation of OSTDS locations, DEM, water body locations, hydraulic conductivity, and porosity data for ArcNLET modeling.

2.2.1 Septic tank data

The modeling domain contains a total of 6,095 OSTDS, and OSTDS data were obtained from the Florida Water Management Inventory (FLWMI) project available at https://ww10.doh.state.fl.us/pub/bos/Inventory/FloridaWaterManagementInventory/. The shapefile data were found in the [brevard-public] folder at the link. The polygons in the shape file represent the parcels of household, and the attribute table of the shape file includes a column labeled as “WW”. This column describes the method by which domestic wastewater is disposed for each parcel, as shown in Fig. 2.4. To generate the OSTDS file for ArcNLET modeling, we selected the parcels that are identified as known as onsite septic systems, likely onsite septic systems, and somewhat likely onsite septic systems. The geometric centers of the polygons were found using ArcToolbox in ArcGIS, and a portion of the parcels and parcel centers are shown in Fig. 2.5. It should be noted that the center points are assumed OSTDS locations, not their actual locations. ArcNLET can handle actual OSTDS locations if they are known. For the Groseclose and Jones sites, Ayres Associates (1993) provided the actual locations, and they were used in ArcNLET modeling.

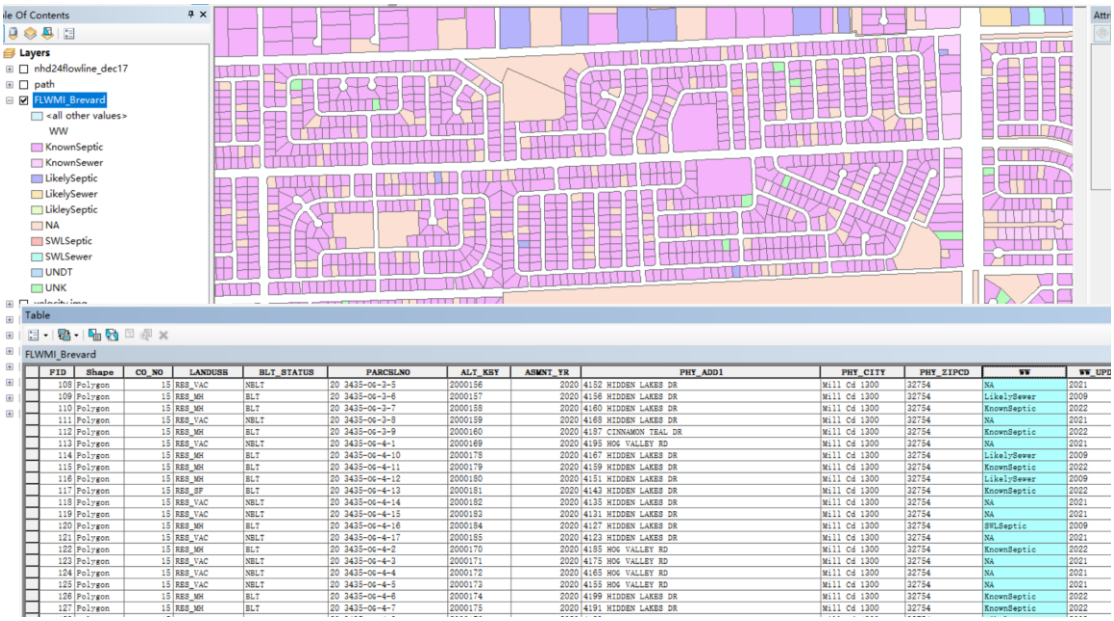

Fig. 2.4. Polygons and associated attribute table of raw data downloaded from FLWMI.

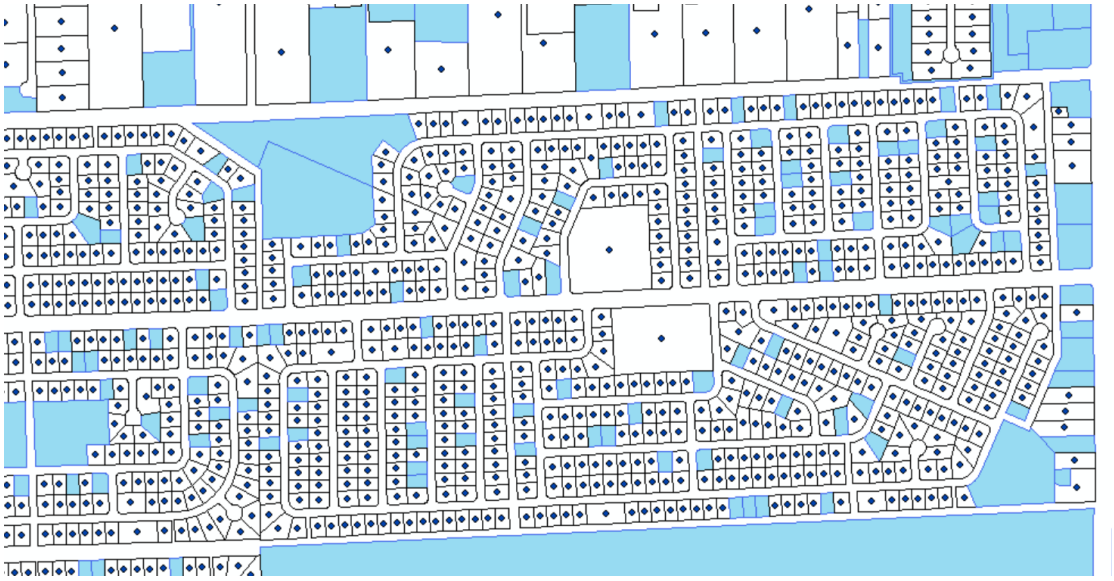

Fig. 2.5. An example of spatial distribution of parcels and parcel centers. The centers are assumed OSTDS locations.

2.2.2 DEM data

The DEM data were downloaded from the NOAA website at https://coast.noaa.gov/dataviewer/#/, and the DEM resolution is 9.84 ft × 9.84 ft. The NAD_1983_UTM_Zone_17N projected coordinate system was selected as the projected coordinate system for this study. The DEM data are shown in Fig. 2.6.

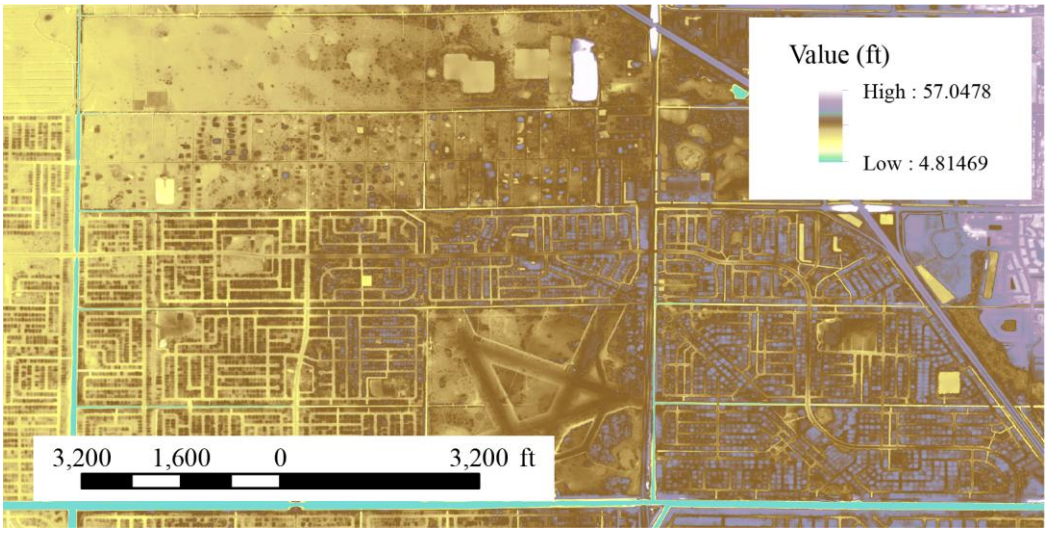

Fig. 2.6. DEM data of the ArcNLET modeling domain. The blue lines represent canals in the domain.

2.2.3 Water body data

The water body data were download from the Florida Geographic Data Library (FGDL) at https://fgdl.org/fgdlmap/. The water body data of this website is actually based on the data from the USGS National Map Downloader (https://apps.nationalmap.gov/downloader/#/, but the data are specifically for Florida. We downloaded the National Hydrography Dataset (NHD) (24K) with the scale of 1:24K. The data has three layers as follows: NHD(24K) Linear Surface Water Drainage Network to represent canals, NHD(24K) Water Bodies to represent the water bodies (e.g., lakes and ponds), and NHD(24K) Hydrographic Landmark Areas to represent streams and rivers.

It has been long known that the NHD data are not accurate enough to represent all surface water bodies, especially canals. For example, Google Earth revealed canals on the east side of Minton Road (Fig. 2.7), and this is confirmed by the DEM data in that the elevations at these locations are lower than their surrounding areas. Such canals were manually added into the NHD data, and canal elevations were also manually corrected based on DEM data.

While the canals are represented as flow lines in the NHD data, ArcNLET needs to represent the canals as polygons. We thus converted the flow lines (polylines) to polygons with canal width measured on Google Earth. The general canal width is 10.5 ft, but several canals have larger width. The resulting shape file for canals was merged with the NHD polygon shape file for water bodies, and the final water body data are shown in Fig. 2.8.

Fig. 2.7. Canals on the east side of Minton Road shown on Google Earth but not in NHD data downloaded from FGDL website.

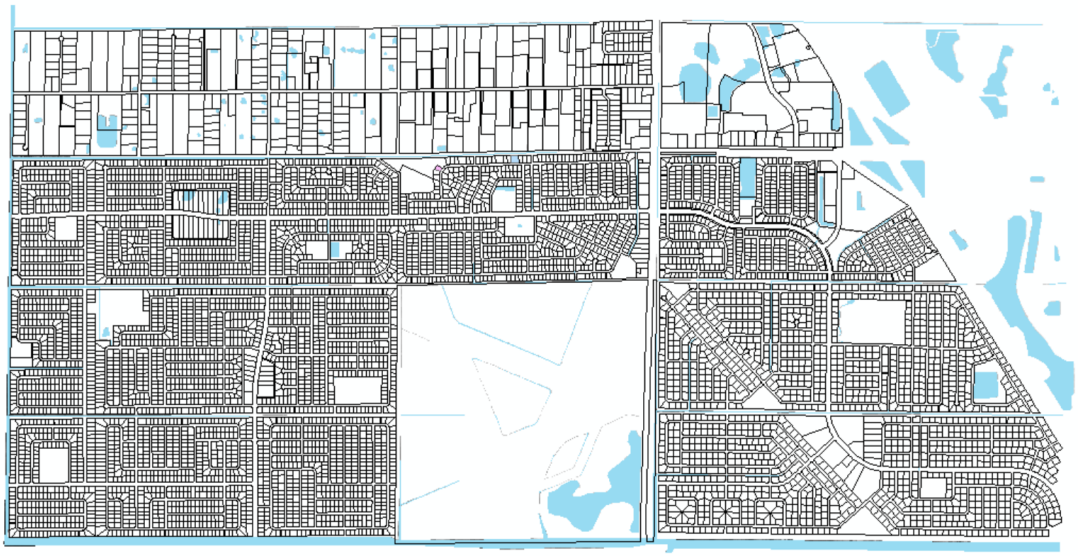

Fig. 2.8. Illustration of adjusted water body data.

2.2.4 SURRGO data of hydraulic conductivity and porosity

The hydraulic conductivity and porosity of the modeling domain were obtained from the SSURGO database by using the USDA soilDB package developed in the R programming language. SSURGO divided the soil of the nation into soil zones, and the zone indices are available at https://casoilresource.lawr.ucdavis.edu/gmap/. For our modeling domain, its soil zone index is fl009.

SoilDB is an easy-to-use tool for downloading soil data. The downloaded data are contained in two folders. The folder called "spatial" includes shape files representing spatial distribution of soil units. The other folder called "tabular" includes detailed soil data of various types (e.g., saturated hydraulic conductivity, porosity, bulk density and organic

matter). We wrote a R code to extract from the "tabular" folder the following data: saturated hydraulic conductivity, bulk density, porosity, and texture (percentages of sand, silt, and clay) for the depth of 2.6 ft to 6.6 ft, which is the depth of water samples were collected according to Ayres Associates (1993). Our R code used the SoilDB option of "weighted average" to estimate the weighted average of each data type, and the weights are the percentage of components. For example, if a soil column has the length of 50cm, with a horizon of 20cm and the other horizon of 30cm. The component percentages are 20/50 = 40% and 30/50 = 60%. The data of saturated hydraulic conductivity were readily available in the downloaded data for the entire modeling domain. Porosity data were missing at certain locations, and porosity was then estimated as $1 - (D_B/D_P)$, where D_B and D_P are bulk density and particle density, respectively. The bulk density were available in the downloaded data, and particle density was assumed as 2.65 g/cm^3. Our R code wrote the data of hydraulic conductivity and porosity into the shape file in tge "spatial" folder based on mukey of the shape file and the data file. Subsequently, the shape file was converted into two raster files for hydraulic conductivity and porosity.

2.3 Calibration of ArcNLET Groundwater Flow Module

The goal of the flow module calibration is to match, to the extent possible, ArcNLET-smoothed DEM with corresponding observed water levels. An ideal calibration result is that the smoothed DEM and observed water level fall into a line with slope 1. The calibration involves adjusting smoothing factor, number of smoothing cells (called smoothing cell in ArcNLET, which is the size of the smoothing window), and saturated hydraulic conductivity. Since hydraulic conductivity data are from SSURGO database and thus should be relatively reliable, we started the calibration by adjusting smoothing factors and smoothing cell.

2.3.1 DEM smoothing with canal elevation

ArcNLET does not solve a flow equation for hydraulic heads, but smooths DEM to obtain the shape of water table based on the Dupuit assumption. A common problem of smoothing DEM is that, after smoothing the DEM for multiple times, the elevation difference between water bodies and their surrounding areas becomes negligible. An extreme case is that, for a large smoothing factor, the smooth DEM is flat. This always lead to unreasonable flow paths. An illustration is given in Fig. 2.9 that displays the ArcNLET-simulated flow paths calculated after 20 times of smoothing the DEM (smoothing cell is 7, the default value in ArcNLET), with the blue and pink squares representing the Groseclose and Jones homes, respectively. This figure shows that many flow paths unreasonably converge to local low elevations. For the Groseclose home, water from its OSTDS even does not flow into the canal located north to the home. Fig. 2.10 shows the DEM and smoothed DEM along the A-A' profile (Fig. 2.9) across the Groseclose home. After the smoothing, the low elevations at the canal and the road disappear, leading to a southward flow path; a physically reasonable flow path should be northward to the canal.

An empirical solution to the problem described above is to first include the DEM of water bodies in the smoothed DEM, and then smooth the new DEM with a small smoothing factor. In this study, the elevation of water bodies (e.g., canals and ponds) were extracted from the original DEM using the "Extract by Mask" function in the ArcGIS Toolbox's Spatial Analysis tools. The extracted elevations were merged into the smoothed DEM using

either the “Mosaic” function or “Mosaic to New Raster” function in the Data Management Tools of ArcGIS Toolbox. Finally, another round of smoothing in ArcNLET was performed until satisfactory results of flow path are obtained.

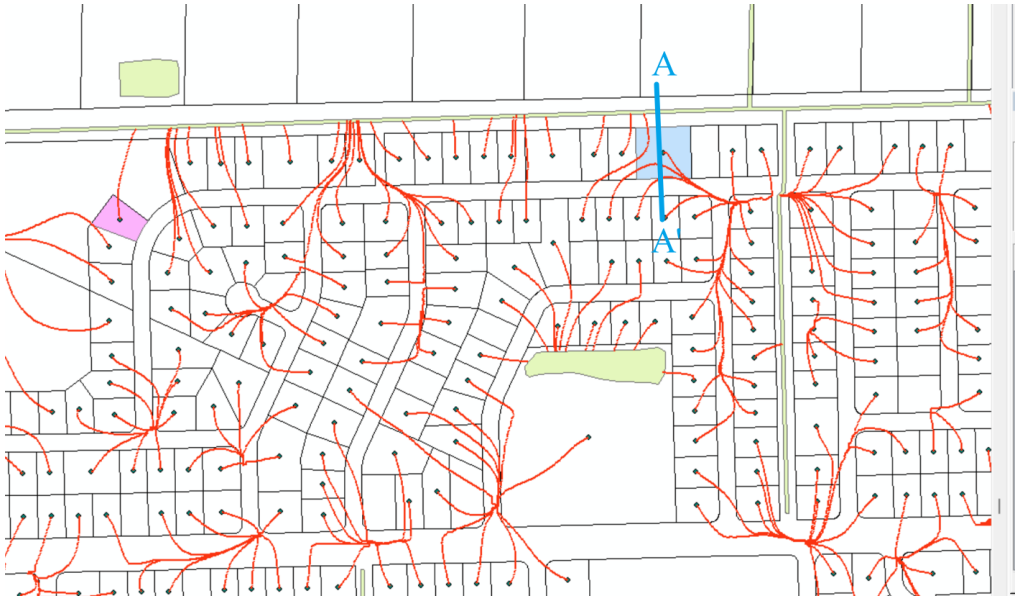

Fig. 2.9. ArcNLET-simulated flow paths with a smoothing factor of 20. The blue square represents the Groseclose home, and the pink square the Jones home.

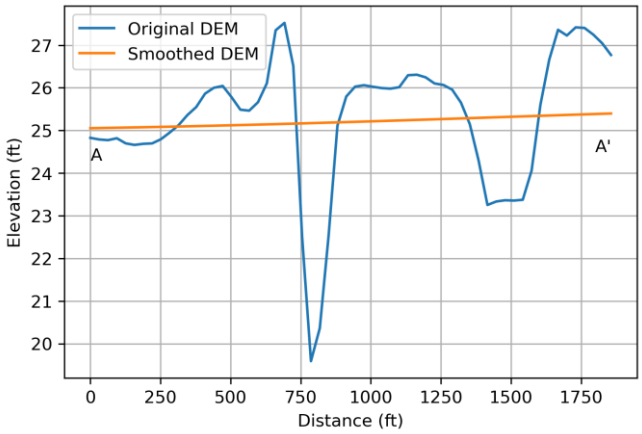

Fig. 2.10. Comparison of DEM and smoothed DEM along the A-A’ profile shown in Fig. 2.9.

Fig. 11 illustrates the smoothing procedure along the A-A’ profile shown in Fig. 2.9. Fig. 2.11(a) shows the original DEM, and the locations of the canal and the road along the profile are observed. Fig. 2.11(b) shows that the two area of low elevations disapper after 20 times of smoothing with the smoothing cell of 31, which corresponds to a smoothing window with the size of about 300 ft^2, given that each cell is about 10 ft × 10 ft. The result of merging the canal DEM with the smoothed DEM is shown in Fig. 2.11(c). Figure 2.11(d)

shows the result of the new smoothed DEM with smoothing factor of 10 and smoothing cell of 27. The canal DEM is added back to the smoothed DEM, as shown in Fig. 2.11(e), and Fig. 2.11(f) shows the smoothed DEM with smoothing factor of 1 and smoothing cell of 23. A final smoothing was conducted with smoothing factor of 2 and smoothing cell of 7. We gradually decreased the smoothing cell to limit the smoothing effects to a smaller range in space, so that the areas away from the canal were not affected by the added canal elevation.

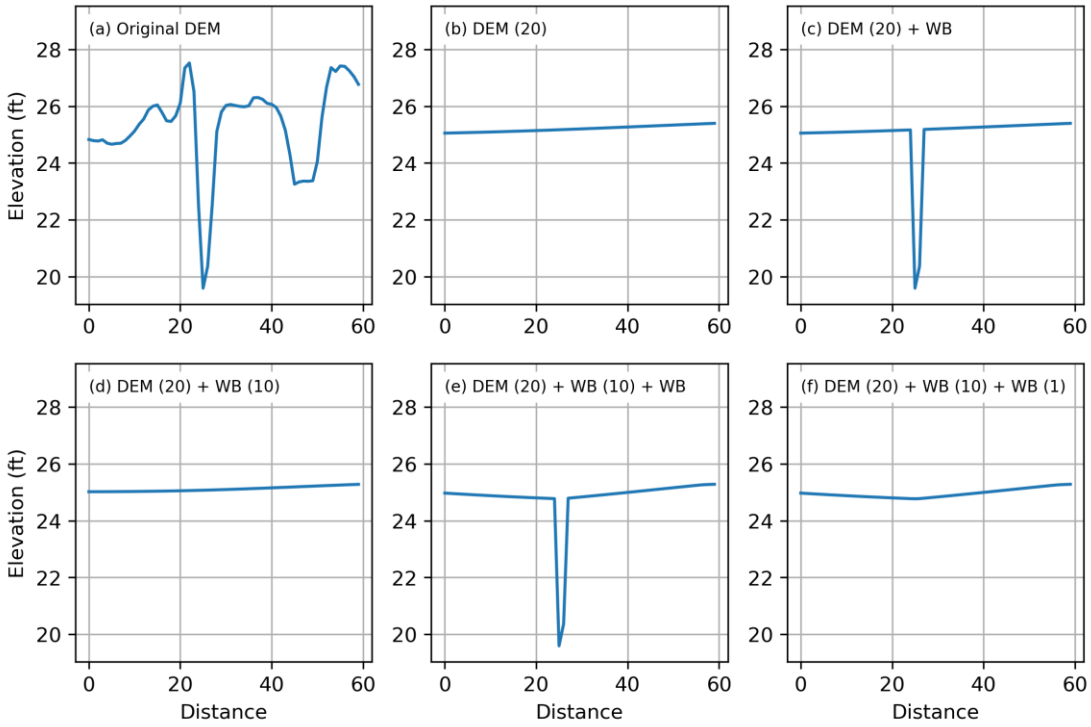

Fig. 2.11 Illustration of original DEM and smoothed DEM along the A-A' profile shown in Fig. 2.9.

2.3.2 Results of flow module calibration

The final calibration results for the ArcNLET groundwater module are shown in Fig. 2.12. The blue dots are for measured water level and corresponding smoothed DEM at the Groseclose site, and the red dots are for the Jones site. The blue and red lines are fitted to the data at Groseclose and Jones sites, respectively. The dashed line is fitted to all the data. For the blue and dashed lines, their slopes are 1.04 and 0.97, respectively, indicating a good fit.

For the red line, the slope is only 0.2, indicating a poor fit. The poor fit was caused mainly by data at monitoring wells J8, J9, J10, and J11, whose locations are shown in Fig. 2.13. The surface elevations of the four wells range from 26.2 to 27.1 (Table 1 of Ayres Associates, 1993), which are relatively higher than those of other wells are. As a result, their smoothed DEM values are larger. However, water level elevations at the four wells are lower than those of other wells, resulting in poor fit shown in Fig. 2.12. It is beyond the scope of the study to examine why water level at the four wells are lower than those at other wells.

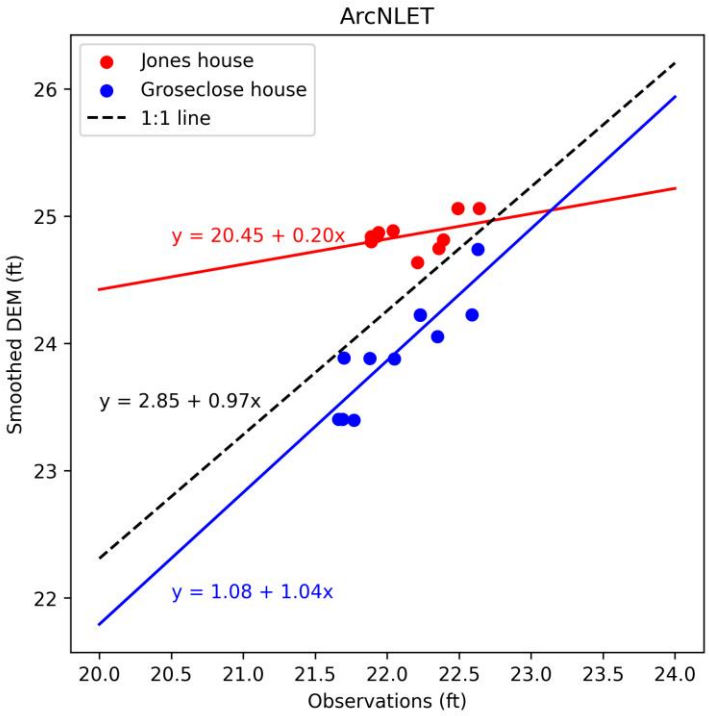

Fig. 2.12. Comparison of smoothed DEM and observations of groundwater level.

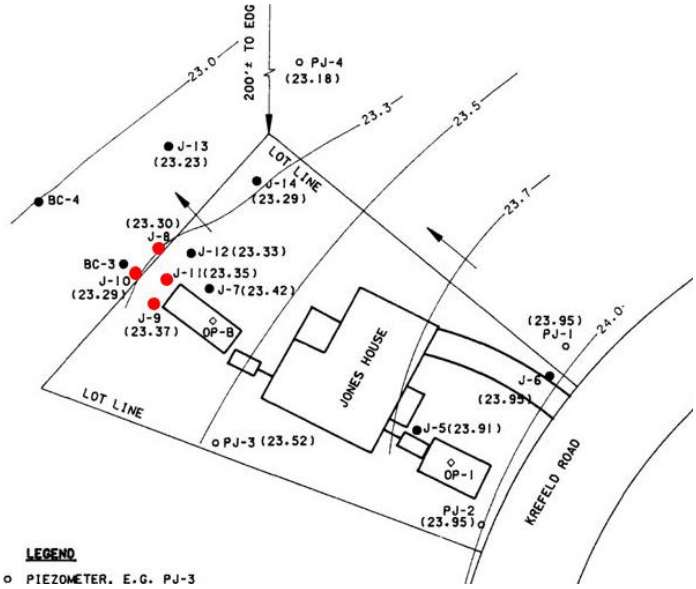

Fig. 2.13. Location of monitoring wells J8, J9, J10, and J11, where the smooth DEM does not agree with measured water level.

2.4 MODFLOW Simulation

A steady state MODFLOW model was developed to simulate hydraulic heads at the study site, and the model results were used as a reference to evaluate the results of

ArcNLET modeling. The flopy package (Bakker et al., 2016) was used to develop the MODFLOW model. The modeling domain was the same as that of ArcNLET model. The surface elevation was based on DEM, and the elevation of model bottom was set as 0 ft. Due to the close distance between the groundwater wells, a fine mesh of 1,000 rows and 2,000 columns was used in the MODFLOW model. The areas of water bodies were set as a constant head boundary, and hydraulic heads on the boundary were assigned based the values reported in Ayres Associates (1993) or based on Google Earth. The recharge of the MODFLOW model was estimated based on precipitation. The rainfall data was downloaded from the website of the Florida Climate Center (https://climatecenter.fsu.edu/climate-data-access-tools/downloadable-data). The annual average rainfall in the study area is 4.54 ft, which was multiplied by a recharge coefficient of 0.03 to estimate recharge of 0.0045 in/d. A MODFLOW simulation using the SSURGO data of hydraulic conductivity did not yield satisfactory results, in that the simulated heads were almost constant at the observation wells but the observed heads varied between the wells. This may be due to large values of hydraulic conductivity. Ayres Associates (1993) listed hydraulic conductivity values estimated using slug tests, and the average values for the two sites are listed in Table 2.1. The table shows that the SSURGO values are about ten times as large as the report values. The adjusted values of hydraulic conductivity are listed in Table 2.1.

Table 2.1. Saturated hydraulic conductivity values in the study area.

	SSURGO	Ayres Associates (1993)	Adjusted values
Groseclose house	16.85 m/d	1.40 ft/d	1.88 ft/d
Jones house	18.05 m/d	2.46 ft/d	2.03 ft/d

Fig. 2.14 compares MODFLOW-simulated water level and the measured water level. The blue and red dots are for the Groseclose and Jones sites, respectively. The closer the dstribution of points in Fig. 2.12 is to the 1:1 line, the better the result. For the Jones site, the water levels at the four wells of J8, J9, J10, and J11 were also overestimated, which is the same problem that occurred to the ArcNLET model. While the water levels at other wells of the Jones were well simulated (they fall on the line with 1:1 slope), the water levels at the Groseclose site were not well simulated. The MODFLOW simulation results are actually worse than the ArcNLET results.

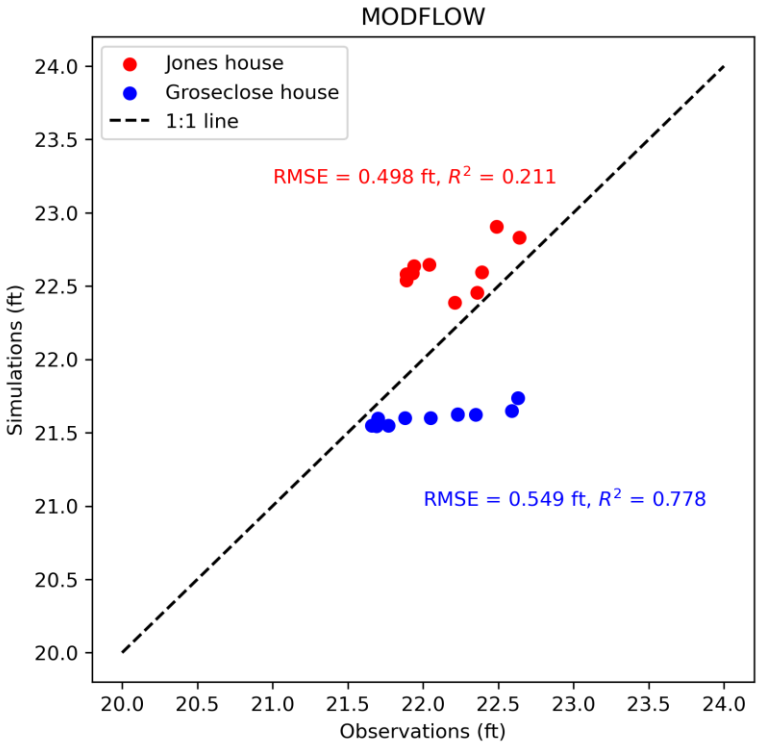

Fig. 2.14. Comparison of MODFLOW-simulated water levels and measured water level. The blue and red dots are for the Groseclose and Jones sites, respectively.

2.5. Calibration of VZMOD Solute Transport Module

ArcNLET modeling requires specifying ammonium and nitrate concentrations at a hypothetical source plane. If the VZMOD module is used for simulating soil processes related to nitrogen reactive transport, ammonium and nitrate concentrations at the drainfield are needed. Table 2.2 lists the measured concentrations of NO_3-N and TKN (ammonium and organic nitrogen) in the septic tanks of the Groseclose home; these values were given in Table 8 of Ayres Associates (1993). The home has two septic tanks for graywater and blackwater separately. At groundwater monitoring well G5 located between the drainfields for graywater and Blackwater, the concentration is 8.98 mg/l for of NO_3-N and 2.51 mg/l for TKN. TKN includes both NH_4-N and organic nitrogen. In a septic tank, NH_4-N accounts for approximately 70% to 90% of the TKN, and organic nitrogen for about 10% to 30% (Lusk et al., 2017; McCray et al., 2005), as shown in Fig. 2.15. The highest NH_4-N concentration can be observed adjacent to the drainfield inlets. In groundwater, TKN is primarily composed of NH_4-N and generally does not contain organic nitrogen.

Table 2.2. Measured nitrogen concentrations ((mg/l)) in the graywater and blackwater septic tanks of Groseclose home

	Graywater	Blackwater
NO_3-N	0.06	<0.02
TKN	3.8	110

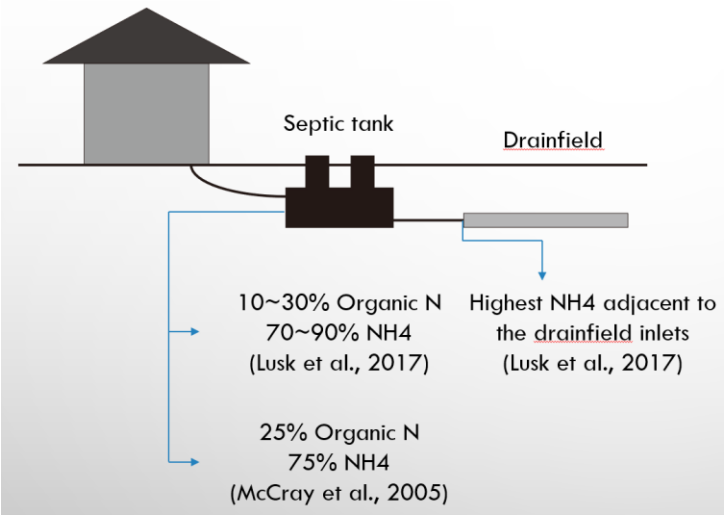

Fig. 2.15. Transformation of nitrogen in OSTDS (adopted from (Lusk et al., 2017).

VZMOD simulates the transport and transformation processes of NH_4-N and NO_3-N from the drainfield to groundwater. To accomplish this, it is necessary to estimate the concentration of NH_4-N and NO_3-N of the infiltrated water in the drainfield. For blackwater, it is assumed that 27% and 73% of the TKN in the septic tank is in the form of organic nitrogen and NH_4-N, respectively, and this leads to a NH_4-N concentration of 80 mg/L for blackwater and 2.76 mg/L for graywater. In addition, the septic tank contains a significant number of oils and grease, which belongs to organic nitrogen and may cause oil deposition and floating. It is assumed that this nitrogen will remain in the septic tank and be removed during septic tank maintenance. The highest concentration of NH_4-N is expected at the inlet of the drainfield, where ammonification reactions occur mainly in the septic tank to convert organic nitrogen into NH_4-N. Therefore, it is assumed that there will be no significant change in NO_3-N concentration from septic tanks to drainfields. The concentrations of NH_4-N and NO_3-N in the infiltration water at the drainfield of the Groseclose home are listed in Table 2.3.

Table 2.3. Concentrations (mg/l) of NH_4-N and NO_3-N in the infiltration water at the drainfield of the Groseclose home.

	Graywater	Blackwater
NO_3-N	0.06	0.02
NH_4-N	2.76	80

The parameters of VZMOD were calibrated to match VZMOD-simulated nitrogen concentrations with the observed concentrations at well G5. The VZMOD simulation results for the graywater drainfield and the blackwater drainfield are shown in Fig. 2.16. VZMOD model parameters used for the blackwater drainfield are shown in Fig. 2.17. The ammonia concentrations at well G5 indicate that the nitrification process in the unsaturated zone did not completely convert ammonium into nitrate. On the other hand, because the total nitrogen concentration at well G5 is around 10 mg/l, substantially smaller than the total nitrogen concentration of 82.76 mg/l at the drainfield, a strong denitrification process is expected. These physical understanding of the vadose zone processes of nitrogen reactive transport is the basis of adjusting the VZMOD parameters.

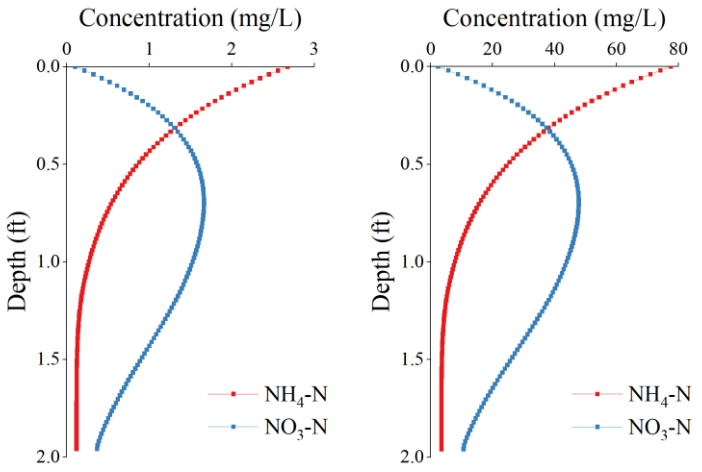

Fig. 2.16. VZMOD simulation results for the graywater drainfield and the blackwater drainfield at the Groseclose home.

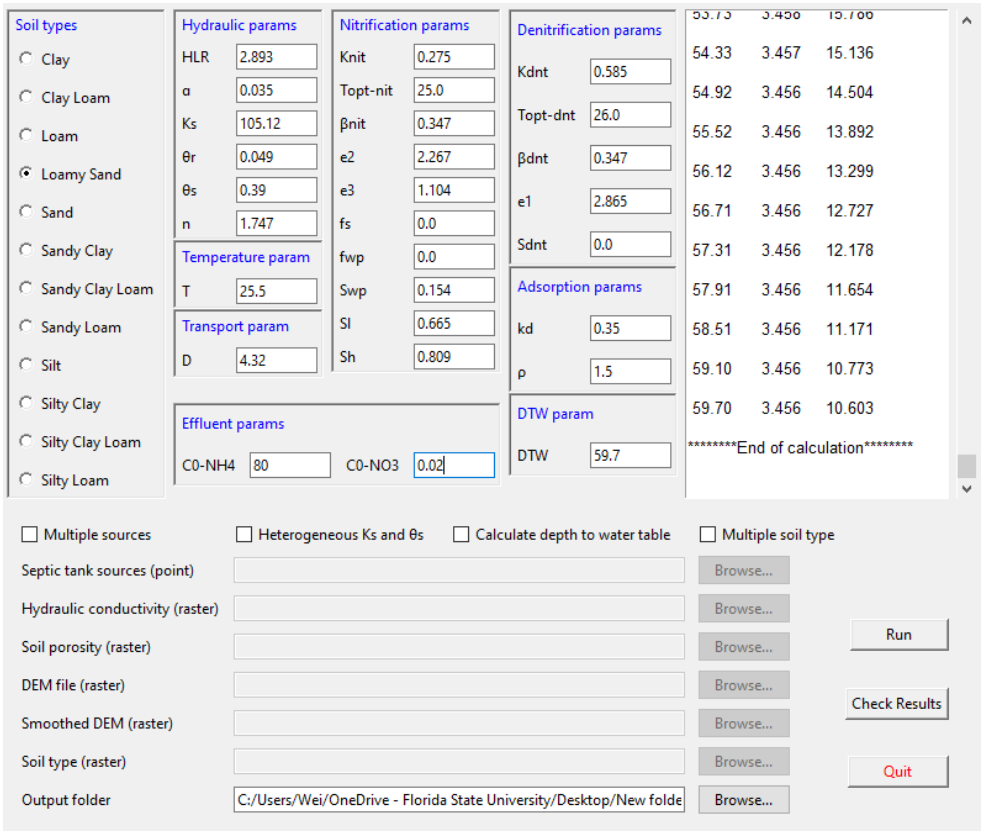

Fig. 2.17. VZMOD parameters used for the blackwater field at the Groseclose home.

Based on the nitrogen concentrations in the septic tanks at the Groseclose home, the nitrogen concentrations at the Jones home were estimated with the assumption of equal nitrogen production per person per day in the two homes. Table 9 of Ayres Associates (1993) shows an average of 400 gallons of water use per day, with an average of 80 gallons of

water use per person per day at the Groseclose home. At the Jones home, the average water use was 166 gallons per day, and the average water use per person per day was 83 gallons. Based on these data, the concentrations of TKN and NO_3-N in the septic tank of Jones home were estimated, and they are listed in Table 2.4. For example, the blackwater TKN concentration was estimated as 106.02 = 110 × (80/83). Based on the nitrogen reduction ratio used for the Groseclose home, the NH_4-N and NO_3-N concentrations at the drainfield of the Jones home are listed in Table 2.5.

Table 2.4. Estimated TKN and NO_3-N concentrations (mg/l) in the septic tank of the Jones home.

	Graywater	Blackwater
NO_3-N	0.058	0.019
TKN	3.66	106.02

Table 2.5. Concentrations (mg/l) of NH_4-N and NO_3-N in the infiltration water at the drainfield of the Jones home.

	Graywater	Blackwater
NO_3-N	0.058	0.019
NH_4-N	2.66	77.1

VZMOD parameters were calibrated to match nitrogen concentrations near the black water drainfield at the Jones home. The calculation results of VZMOD for graywater drainfield and blackwater drainfield are shown in Fig. 2.18. The VZMOD for blackwater in Jones house is shown in Fig. 2.19. For the Jones site, the concentrations of both ammonium and nitrate nitrogen in groundwater are relatively larger than those at the Groseclose site, indicating that both nitrification and denitrification reactions at the Jones site were weaker than those at the Groseclose site.

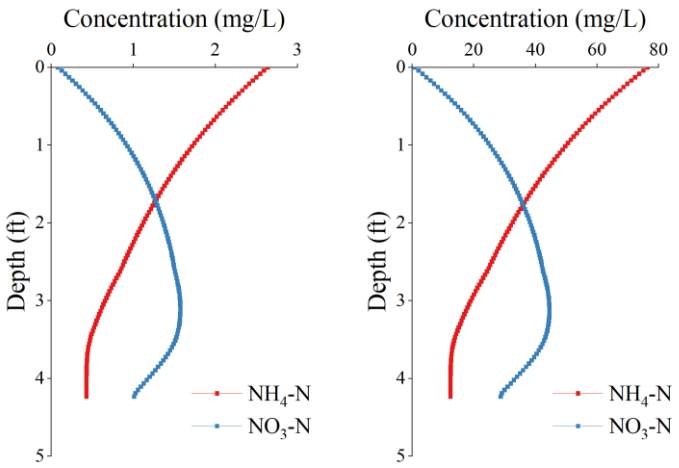

Fig. 2.18. VZMOD simulation results for the graywater drainfield and the blackwater drainfield at the Jones home.

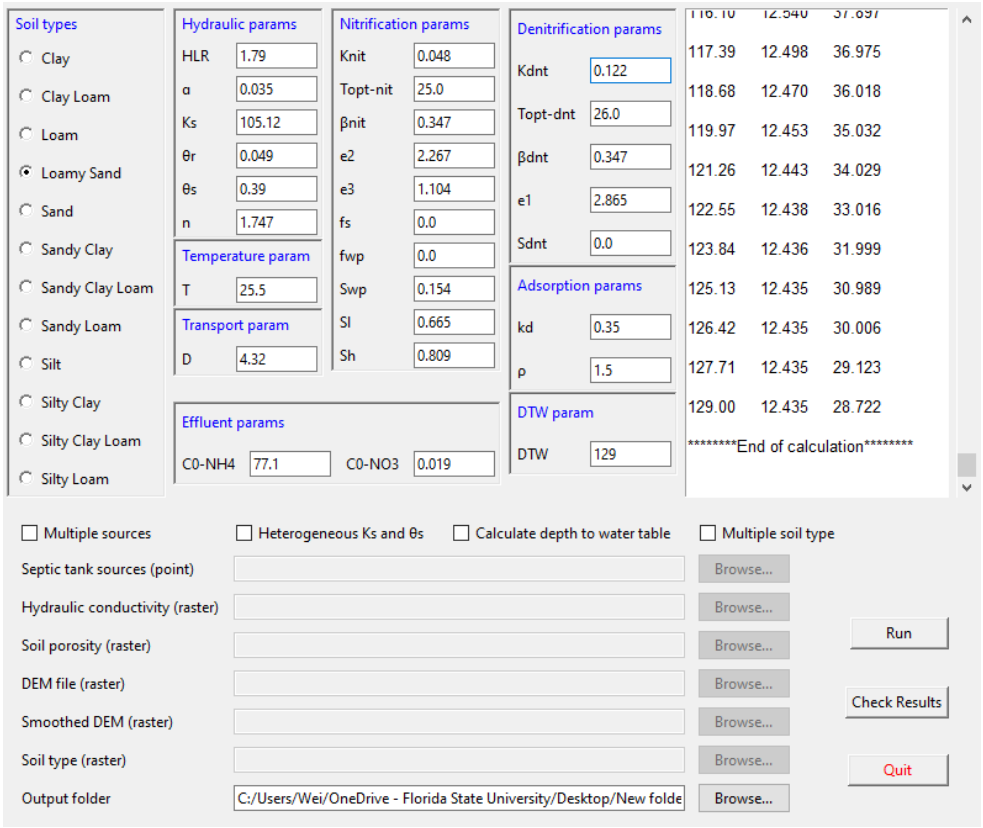

Fig. 2.19. VZMOD parameters used for the blackwater septic tank at the Jones home.

The comparison of parameters used by Groseclose and Jones house, and the parameter ranges given in McCray et al. (2005) are shown in Table 2.6. The parameter ranges given in the reference are wide, and the parameters used in VZMOD calculations are within the range given in the reference. Since both the groundwater in Groseclose and Jones houses contain a certain concentration of NH_4-N, the calibration process reduced the value of K_{nit} comparing with the initial parameter values before calibration. Additionally, due to the high initial input of nitrogen (NH_4-N and NO_3-N), the value of K_{dnt} was increased, causing excessive nitrogen to leave the calculation profile through denitrification. K_d remained the same as the initial value of the model.

Table 2.6. VZMOD default and calibrated parameter values for the Groseclose and Jones sites, and the parameter ranges given in McCray et al. (2005).

	VZMOD Default	Groseclose	Jones	McCray et al., 2005
K_{nit} (1/d)	2.9	0.275	0.048	0.0768~211.2
K_{dnt} (1/d)	0.025	0.585	0.122	0.004~2.27

Fig. 2.20 shows the VZMOD-simulated concentrations of NH_4-N and NO_3-N at water table and measured concentrations at monitoring wells at the Groseclose site. Fig. 2.21 does the same for the Jones site. The concentrations beneath the graywater septic tank are lower than those at groundwater monitoring wells, but the concentrations beneath the backwater septic tank are higher. This is expected. It is also expected that the nitrogen concentrations at water table beneath the blackwater septic tank are larger than those in groundwater wells (e.g., well G5 in Fig. 2.20) to account for possible denitrification

between the septic tank to monitoring wells.

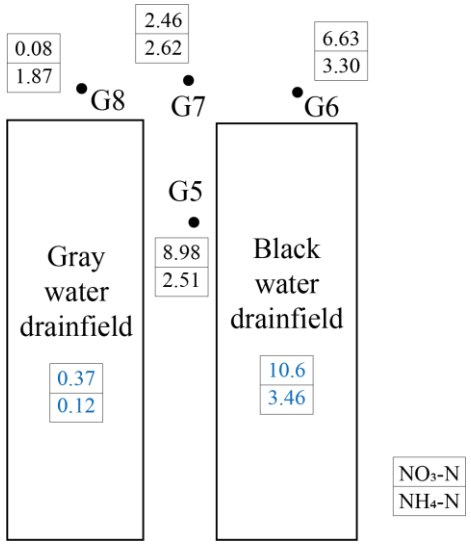

Fig. 2.20. VZMOD-simulated concentrations (in blue) of NH_4-N and NO_3-N and water table and measured concentrations (black) in groundwater monitoring wells at the Groseclose site.

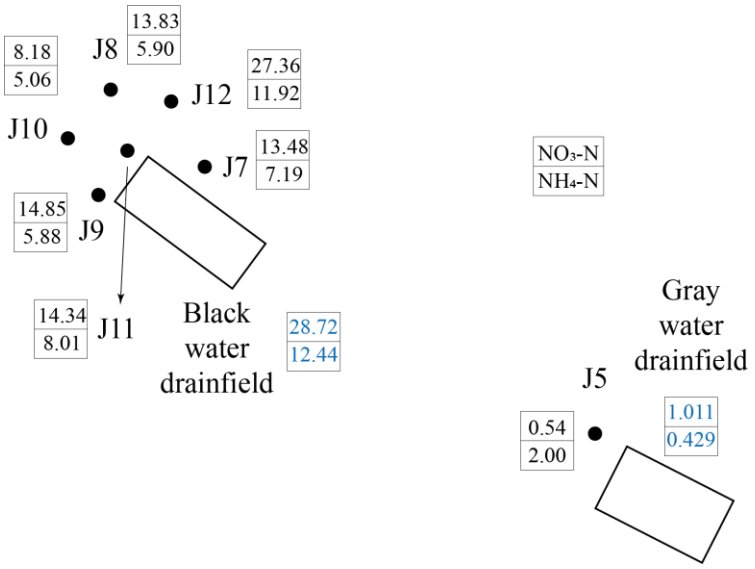

Fig. 2.21. VZMOD-simulated concentrations (in blue) of NH_4-N and NO_3-N and water table and measured concentrations (black) in groundwater monitoring wells at the Jones site.

2.6. Calibration of ArcNLET Solute Transport Module

Fig. 2.22 shows the ArcNLET interface for simulating NH_4-N and NO_3-N concentrations in groundwater. The concentrations (C_0) of NH_4-N and NO_3-N at a source plane of ArcNLET are those simulated by VZMOD at water table. Three ArcNLET parameters, and their default values in ArcNLET and calibrated values are listed in Table 2.7. Several other parameters were also calibrated, but it did not improve model fit. Therefore, default values of these parameters given in ArcNLET were used in the

ArcNLET simulations.

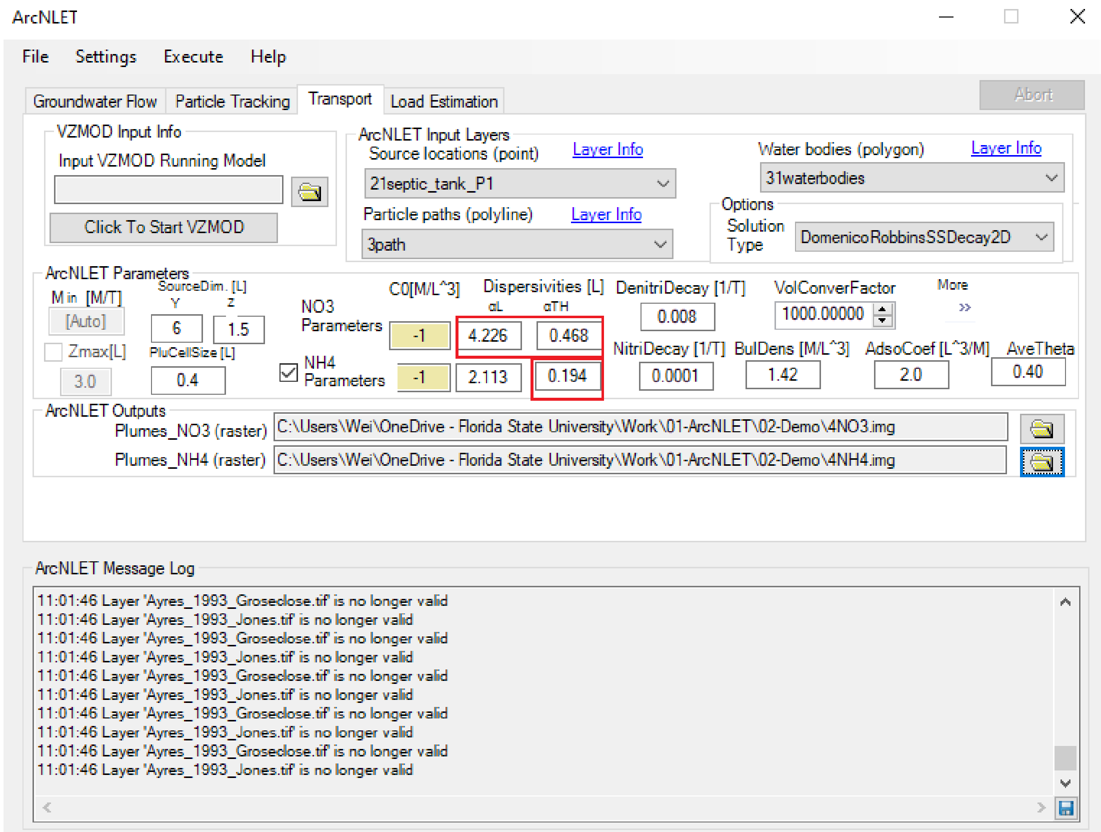

Fig. 2.22. ArcNLET interface for simulating ammonium and nitrate concentrations in groundwater.

Table 2.7. Calibrated ArcNLET parameter values.

	Before calibration	After calibration
Longitudinal dispersivity of NO_3-N	2.113	4.226
Horizontal transverse dispersivity of NO_3-N	0.234	0.468
Horizontal transverse dispersivity of NH_4-N	0.234	0.194

The comparison between the simulated and measured concentrations of NH_4-N is shown in Fig. 2.22, and the similar comparison between the simulated and measured concentrations of NO_3-N is shown in Fig. 2.23. The blue dots in the figures are for the Groseclose site, and the red dots for the Jones site. The R^2 value is 0.6296 for NH_4-N and 0.7713 for NO_3-N. The *RMSE* value is 1.9484 mg/L for NH_4-N and 3.7193 mg/L for NO_3-N. The larger *RMSE* of NO_3-N is mainly due to the larger measured concentration at well J12 in the Jones site. While the measured NO_3-N and NH_4-N concentrations at well J12 are larger than at other wells, well J12 is not the closest well to the drainfield. Investigating why nitrogen concentrations at well J12 was beyond the scope of this project. Figs. 2.24 and 2.25 indicate that the ArcNLET-simulated nitrogen concentrations are acceptable for using the calibrated model to investigate vertical and horizontal OSTDS setback distances.

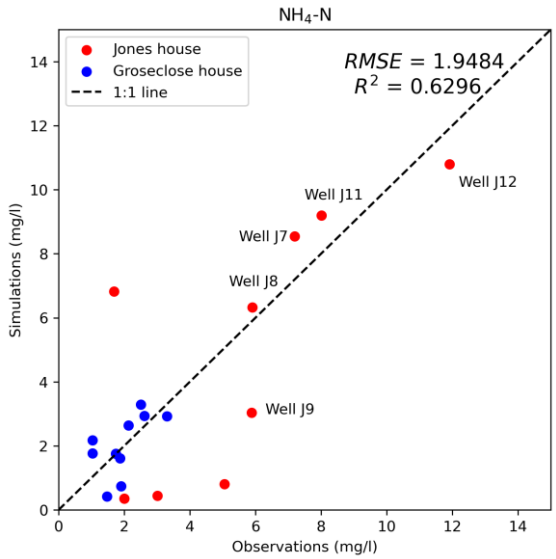

Fig. 2.24. Comparison of simulated NH_4-N concentration in groundwater and measured values.

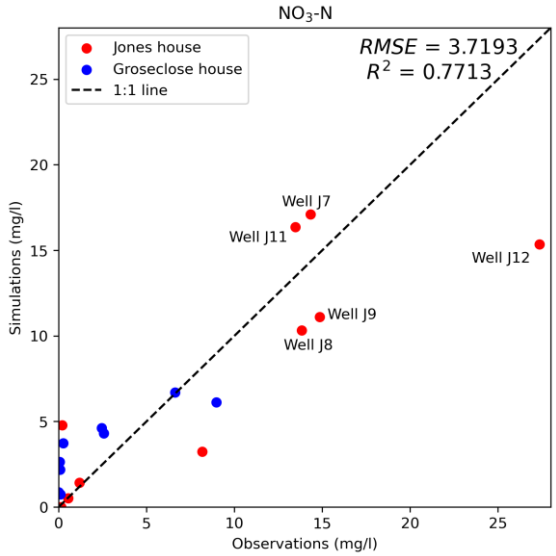

Fig. 2.25. Comparison of simulated NO_3-N concentration in groundwater and measured values.

ArcNLET-simulated NH_4-N plumes at the Groseclose and Jones sites are plotted in Fig. 2.26, while the plumes of NO3-N in Fig. 2.27. Note that the graywater and blackwater septic tanks were simulated separately. At the Jones site, the graywater septic tank was at the front yard, while the blackwater septic tank was in the backyard.

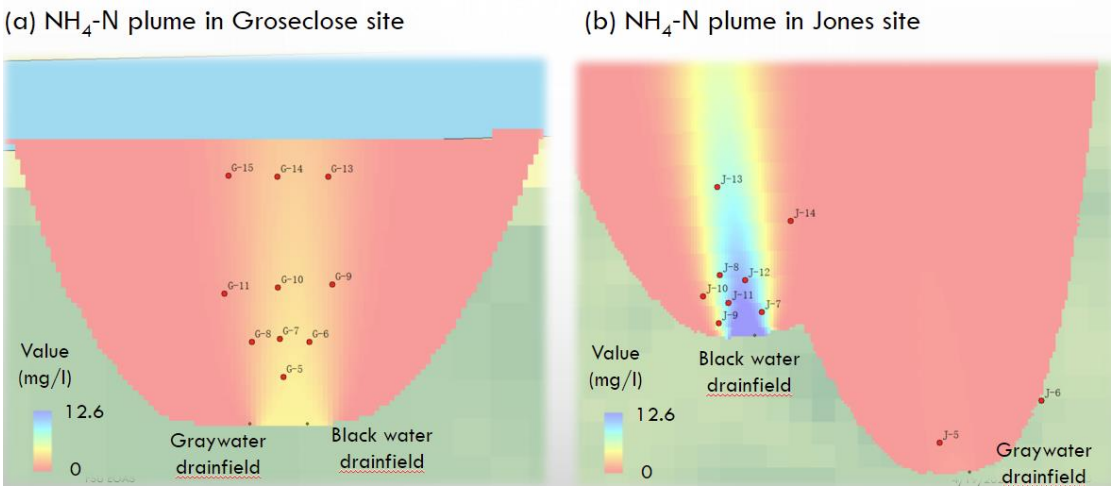

Fig. 2.26 NH_4-N plume in Groseclose and Jones houses calculated by ArcNLET.

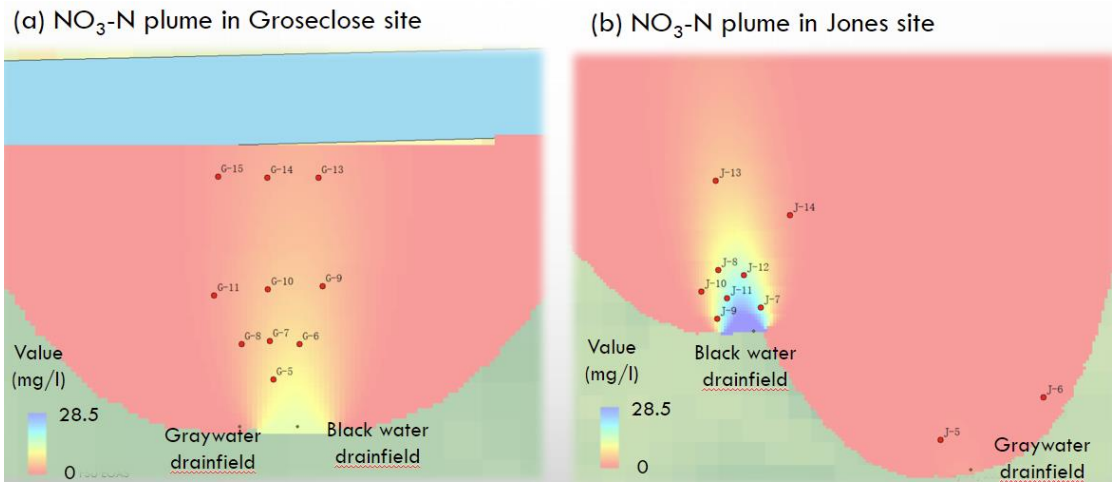

Fig. 2.27 NO_3-N plume in Groseclose and Jones houses calculated by ArcNLET.

We also used the ArcNLET simulation results to estimate nitrogen reduction ratio in the vadose zone based on nitrogen mass load to groundwater and nitrogen mass in septic tanks. The nitrogen load from septic tanks to groundwater is called inflow mass rate (M_{in}) in ArcNLET. The analytical expression of M_{in} is given as (Wang et al., 2013)

$$\mathrm{M}_{in} = YZ\theta v C_0 \frac{1+\sqrt{1+\frac{4k\alpha_x}{v}}}{Z}, \qquad (2.1)$$

where Y and Z are the dimensions of the source plane [L]; v is the seepage velocity [L/T]; θ is the porosity [-]; C_0 is the concentration of the source plane; k is the decay constant [1/T]; α_x is the medium's dispersivity in the x-direction [L]. The values of these variables and the resulting M_{in} are listed in Table 2.8. The estimated M_{in} values were used to estimate nitrogen reduction ratio in vadose zone by comparing with the nitrogen load to septic tanks. Based on water use and nitrogen concentrations in septic tanks at the Groseclose and Jones homes, the nitrogen load (for both TKN and NO_3-N) to the septic tank were calculated, and the results are listed in Table 2.9. The table indicates that the reduction ratio in the vadose

zone varies between 87% and 97%, suggesting importance of the vadose zone on nitrogen removal. The reduction ratios however were model estimation, and they were not evaluated using field data.

Table 2.8. The calculated parameters and results of NH_4-N and NO_3-N flowing into the groundwater for Groseclose and Jones.

	Groseclose				Jones			
	Blackwater		Graywater		Blackwater		Graywater	
	NO_3-N	NH_4-N	NO_3-N	NH_4-N	NO_3-N	NH_4-N	NO_3-N	NH_4-N
Y (ft)	19.7		19.7		19.7		19.7	
Z (ft)	4.9		4.9		4.9		4.9	
θ (-)	0.42		0.38		0.38		0.38	
v (ft/d)	0.222		0.268		0.145		0.092	
C_0 (mg/L)	10.6	3.5	0.37	0.12	28.72	12.55	1.005	0.433
k (1/d)	0.008	0.001	0.008	0.001	0.008	0.001	0.008	0.001
α_x (ft)	13.86	6.93	13.86	6.93	13.86	6.93	13.86	6.93
M_{in} (mg/d)	3658.1	900.6	137.7	34.8	6625.8	1990.7	167.2	44.5

Table 2.9. Nitrogen (TKN and NO_3-N) loads to septic tanks and groundwater at the Groseclose and Jones sites.

		Nitrogen load to septic tanks (mg/d)	Nitrogen load to groundwater (mg/d)	Reduction Ratio
Groseclose	Blackwater	166588.4	4558.7	97.26%
	Graywater	5844.7	172.5	97.05%
Jones	Blackwater	66632.6	8616.5	87.07%
	Graywater	2336.3	211.6	90.94%

2.7. VZMOD Simulation for the entire study area

The calibrated VZMOD was used to simulate ammonium and nitrate concentrations at water table due to 6,095 OSTDS at the study area discussed in Section 2.2. The simulation requires processing several VZMOD parameters, and they are discussed in detail below. Fig. 2.28 shows the interface of the VZMOD simulation with all parameter values shown in the figure.

2.7.1 Effluent parameters

While Ayres Associates (1993) provided sufficient details on locations of blackwater and graywater septic tanks and nitrogen concentrations in the septic tanks, such information was not available for other OSTDS. Therefore, it was assumed that each household has only one septic tank, and that the septic tank is located at the center of a parcel.

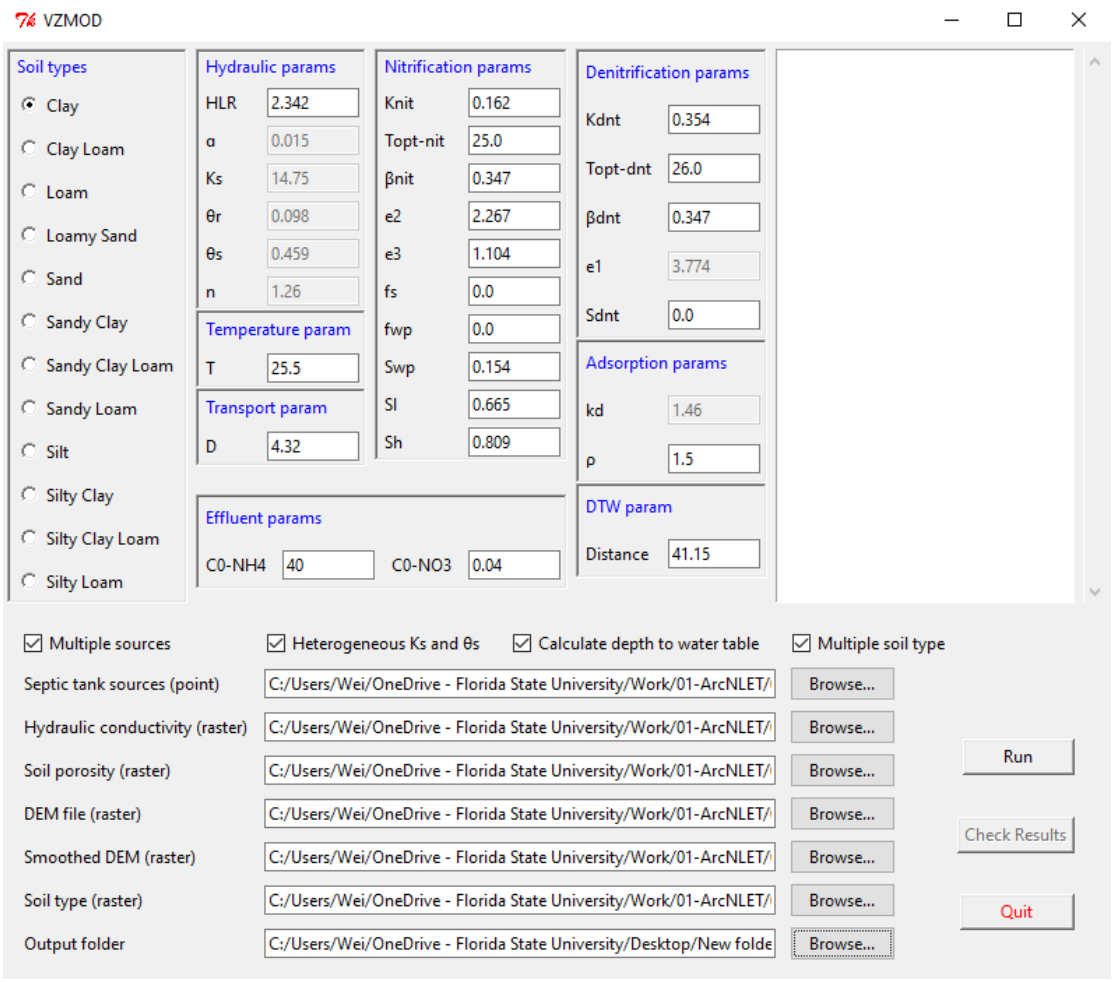

Fig. 2.28. Interface of VZMOD simulation with all parameter values shown.

VZMOD simulation requires specifying ammonium and nitrate concentrations at the infiltration surface of the drainfield. The concentrations at the Groseclose home were estimated based on the following data given in Ayres Associates (1993) and estimated in Section 2.5 for VZMOD calibration:

(1) The per capita daily wastewater discharge is 80 gallons at Groseclose home. It was assumed the amounts of blackwater and graywater are the same, i.e., 40 gallon.

(2) According to Table 2.3, at the infiltration surface of the drainfield, NO_3-N concentrations are 0.02 mg/L and 0.06 mg/L for blackwater and graywater, respectively. The NH_4-N concentrations are 80 mg/L and 2.76 mg/L for blackwater and graywater, respectively.

Therefore, the mass of NO_3-N per person per day at the drainfield of the Groseclose home is 12.11 mg = (0.02 + 0.06) mg/L × 40 gallon × 3.7854 L/gallon. Similarly, the mass of NH_4-N was estimated as 12,531.23 mg. For the Jones home, using the per capita daily wastewater discharge of 83 gallons and the concentrations of NO_3-N and NH_4-N listed in Table 2.5, the masses of NO_3-N and NH_4-N per person per day at the drainfield were

estimated as 8.80 mg and 12,529.86 mg, respectively. The average mass (over the two sites) of NO_3-N and NH_4-N per person per day is 10.5 mg and 12,530 mg, respectively. Dividing these values by 80 gallon gives NO_3-N and NH_4-N concentrations as 0.035 mg/L and 41.38 mg/L, respectively. They were rounded to 0.04 mg/l and 40 mg/l for the convenience of modeling. These values were assumed for all the OSTDS in the study area.

The hydraulic loading rate (HLR), a parameter of VZMOD, was estimated as 0.077 ft/d based on the population of each household, the daily wastewater discharge per capita, and the size of drainfield. This value was assumed for all the OSTDS in the study area.

The nitrification and denitrification rates calibrated for VZMOD are 0.162 1/d and 0.354 1/d, respectively, as listed in Table 2.6. These values were assumed for all the OSTDS in the study area.

The distance from the infiltrative surface to water table (DTW) is needed to calculate the elevation of water table. DTW was estimated using a formula A−B, where A is the distance between the smoothed DEM and the water table and B is the distance between the infiltration surface and the land surface. To determine the value of A, we conducted a linear regression analysis by plotting the measured water level and the smoothed DEM. The intercept of the resulting linear curve represents the value of A. The value of A is 2.85 ft as shown in Fig. 2.12. For B value, Ayres Associates (1993) indicated that at the Groseclose home the drainfield is approximately 3 feet below land surface. At the Jones home, this value is approximately 1 foot, which is substantially smaller than that of Groseclose home. To address the difference, we used the B value of 18 inches (1.5 feet) given in the VZMOD user manual. As a result, DTW value is 1.35 feet = 2.85 feet – 1.5 feet, which is 41.15 cm used in VZMOD.

2.7.2 VZMOD simulation results

Figs 2.29 and 2.30 illustrate the VZMOD-simulated concentrations of NH_4-N and NO_3-N, respectively, around the Groseclose and Jones homes. The NH_4-N concentrations range from 0.0001 to 38.77 mg/L, and the NO_3-N of concentration range from 0.79 to 12.71 mg/L. Fig. 2.29 shows one location with a large NH_4-N concentration of 38.77 mg/L, and the corresponding NO_3-N concentration is 0.79 mg/L (Fig. 2.30). The reason is that the vadose zone thickness at this location is only 0.34 ft, which means that nitrification reactions was not complete. This resulted in a large NH_4-N concentration and a small NO_3-N concentration. Excluding this point, the maximum NH_4-N concentration is 3.71 mg/L, which suggests the majority of the NH_4-N was converted to NO_3-N.

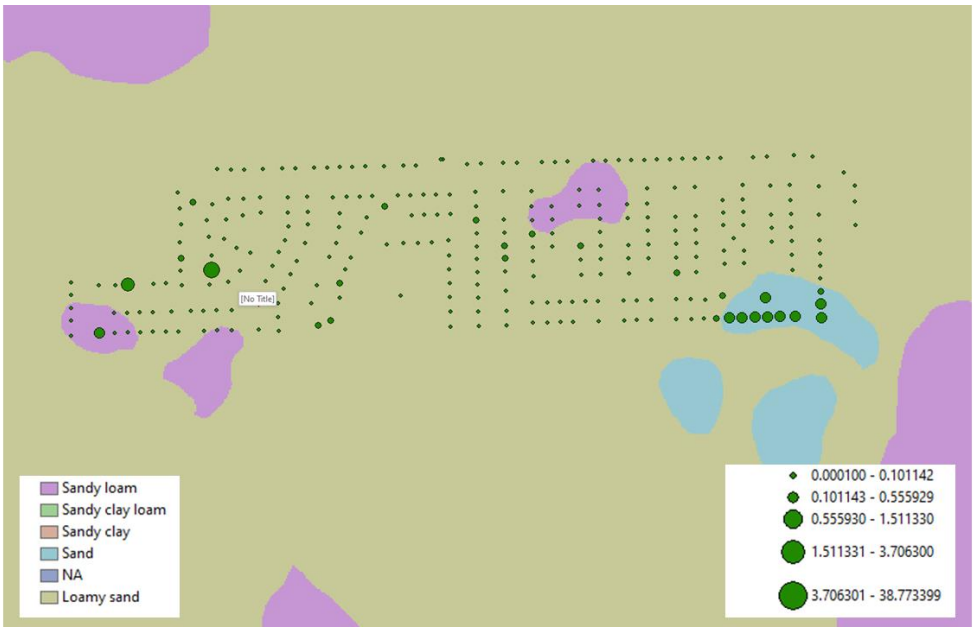

Fig. 2.29. VZMOD-simulated NH_4-N concentrations around the Groseclose and Jones homes.

Fig. 2.30. VZMOD-simulated NO_3-N concentrations around the Groseclose and Jones homes.

The spatial distribution of NO_3-N concentrations depends on soil types. Fig. 2.30 shows that the simulated NO_3-N concentrations are higher for the septic tanks in the sand than in other soil types. To understand the impacts of soil types on simulated nitrogen concentrations, Figs. 2.31 and 2.32 plot the vertical profiles of NH_4-N and NO_3-N concentrations, water content, and water content related factors of nitrification and denitrification at two septic tanks (OSTDS numbers 268 and 269 in the septic tank shape file) shown in Fig. 2.30. Although the two locations are next to each other and have a

similar vadose zone thickness, the nitrification and denitrification factors at the depth above 3.28 ft are larger at OSTDS 268 of sandy loam soil than at OSTDS 269 of sandy soil. For the sandy loam soil, the soil water content is higher, resulting in larger values of nitrification and denitrification factors.

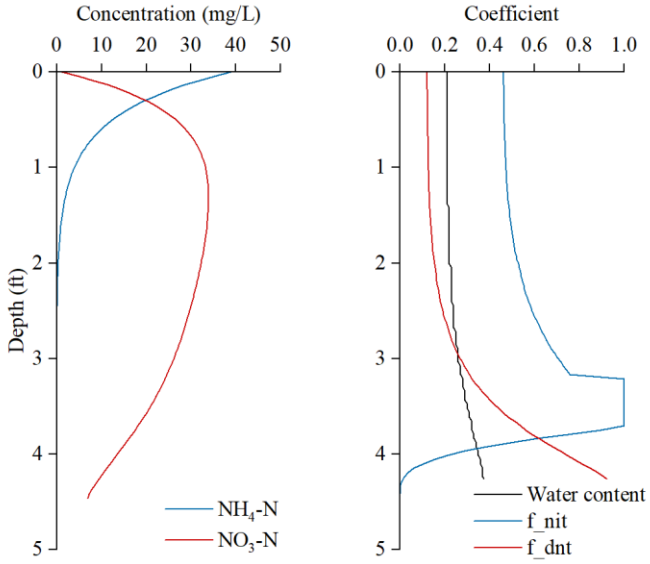

Fig. 2.31. Vertical profiles of NH_4-N and NO_3-N concentrations, water content, and water content related factors of nitrification and denitrification at OSTDS No. 268 shown in Fig. 2.30.

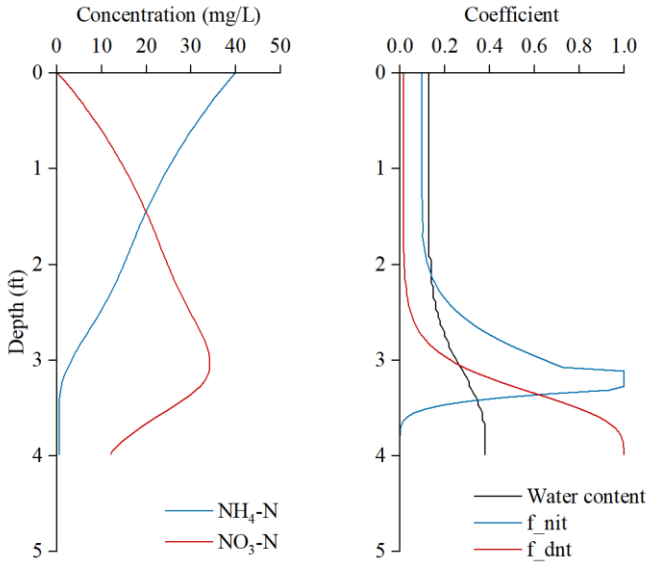

Fig. 2.32. Vertical profiles of NH_4-N and NO_3-N concentrations, water content, and water content related factors of nitrification and denitrification at OSTDS No. 269 shown in Fig. 2.30.

For the entire modeling domain, Figs. 2.33 and 2.34 plot the histograms of VZMOD-simulated concentrations of NH_4-N and NO_3-N at water table, respectively. Fig. 2.33 shows

that the NH_4-N concentrations are low for most of OSTDS, indicating that NH_4-N is converted to NO_3-N through nitrification reaction in the unsaturated zone. Fig. 2.34 shows that the NO_3-N concentrations cover a wide range from 1 to 12 mg/L, which is attributed to the four different soil types in the model domain. Fig. 2.35 plots the average NO_3-N and NH_4-N concentrations for each soil type. There are 4381, 185, 19, and 1510 OSTDS located in areas with loamy sand, sand, sandy clay loam, and sandy loam, respectively. For OSTDS in loamy sandy soil, the NH_4-N concentrations are close to 0 mg/L. Correspondingly, the NO_3-N concentrations are higher. Generally speaking, soils with higher clay content have higher NH_4-N concentrations but lower NO_3-N concentrations.

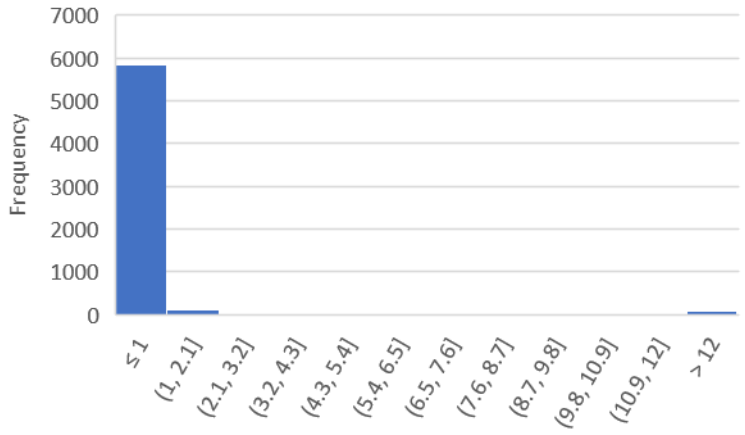

Fig. 2.33. Histogram of concentrations of NH_4-N at water table.

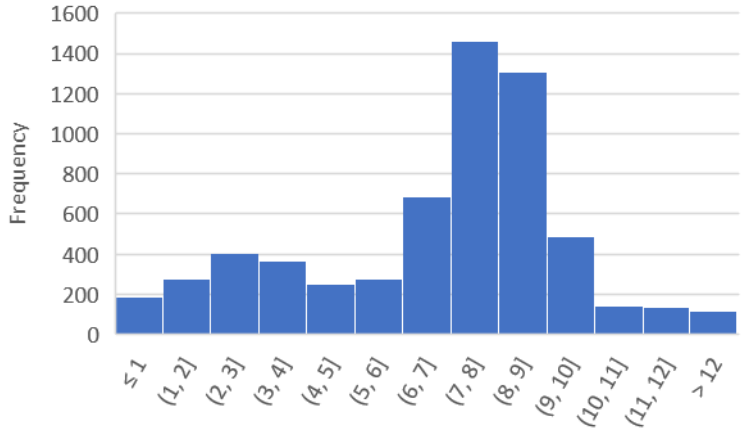

Fig. 2.34. Histogram of concentrations of NO_3-N at water table.

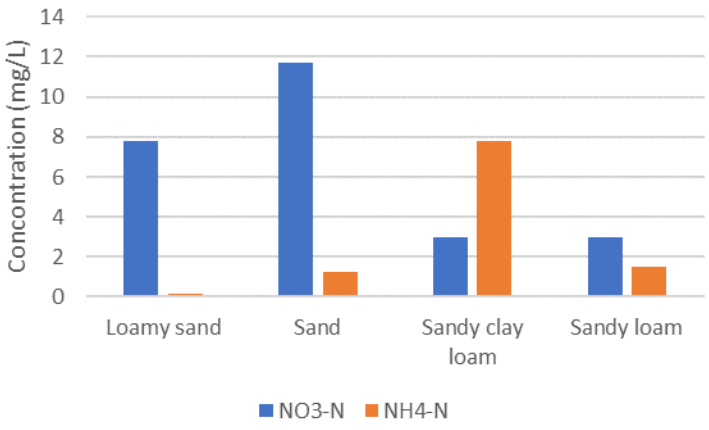

Fig. 2.35. Average NO_3-N and NH_4-N concentrations for different soil types.

We discussed above that high NH_4-N concentrations are attributed to small vertical distance from drainfield to water table. The spatial distribution of the vertical distance is shown in Fig. 2.36. This figure is only for illustrating that the distance varies in space, and was not used for VZMOD modeling. VZMOD modeling does not need use a raster file for the vertical distance, but only uses the vertical distance between the drainfields.

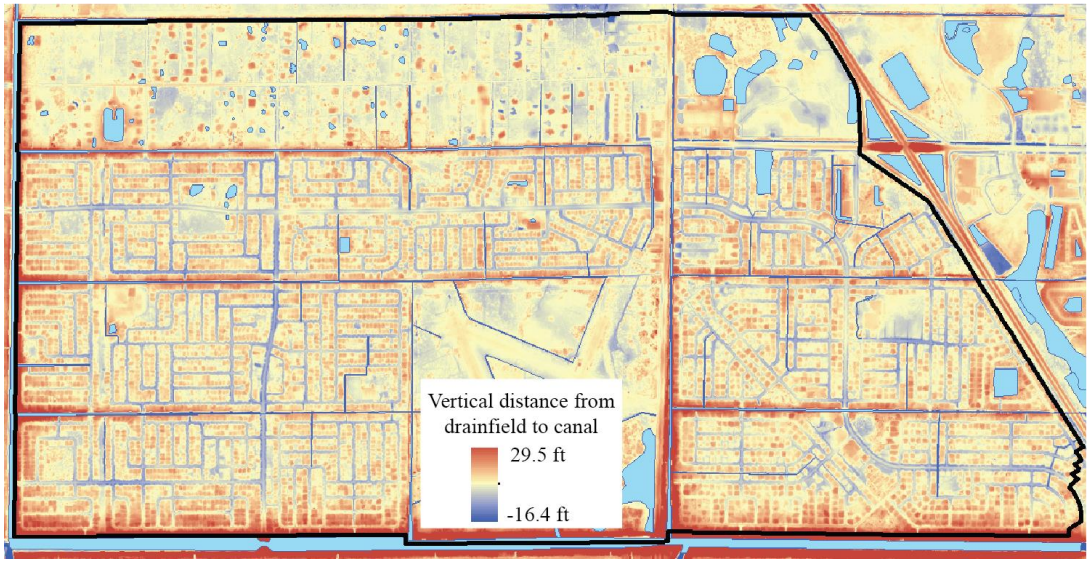

Fig. 2.36. Spatial distribution of vertical distance from drainfields to water table.

2.8. ArcNLET simulation for the entire study area

The ArcNLET simulation was relatively straightforward, and we only encountered one problem during the simulation related to post-processing simulated plumes. The post-processing is only for better illustrating modeling results, and does not affect nitrogen load estimation. ArcNLET has three post-processing options: None, Medium, and Full. The effects of these three options on the calculation can be observed in Fig. 2.37. When the None option is used (Fig. 2.37a), the pollution plumes are truncated with a straight line perpendicular to the flow direction. While this option is a simple and effective method, the truncation may not be along surface water bodies. The medium option is to make the

truncation more aligned with surface water bodies, and it is the default option of ArcNLET. However, its performance depends on the shape of water bodies and the distribution of OSTDS. Fig. 2.38 shows that, when OSTDS are located on both sides of a canal, the processes plumes may pass through the canal. If OSTDS are located on one side of the canal, the Medium option gives satisfactory post-processing results. The Full option is used is expected to give the best results, but it was found not the case, and the results shown in Fig. 2.37(c) are strange. We need to examine the source codes of ArcNLET to fix this problem, but it is beyond the scope of this project. To be on the safe side, we used the None option for post-processing.

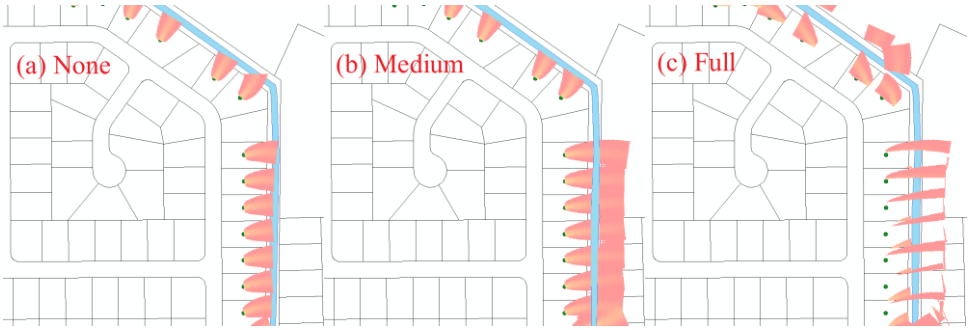

Fig. 2.37. Nitrogen plumes after post-processing options: (a) None, (b) Medium, and (c) Full.

Fig. 2.38. Nitrogen plumes for two situations: (a) OSTDS are located on both sides of canal, and (b) OSTDS on only one side of canal.

Due to a limitation on computer memory that ArcNLET can use (ArcGIS is a 32-bit software and the maximum memory available is 4GB), ArcNLET cannot simulate all the 6,095 OSTDS in one simulation. After several trials, we determined that the maximum number of OSTDS for one ArcNLET simulation is about 1,000. The study area was divided into a total of 13 sub-areas, and ArcNLET simulation was conducted for each sub-area. The simulated concentrations were merged into one raster file, and the simulated NH_4-N and concentrations are plotted in Figs. 2.39 and 2.40, respectively.

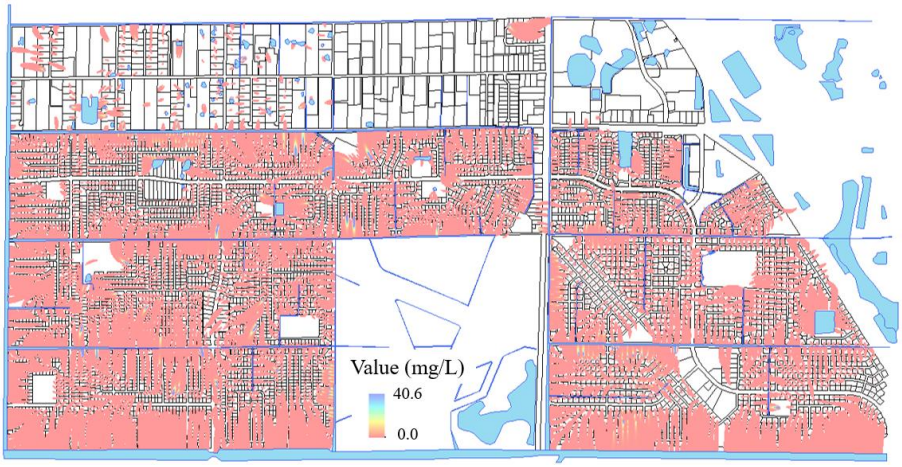

Fig. 2.39. Spatial distribution of NH_4-N concentrations.

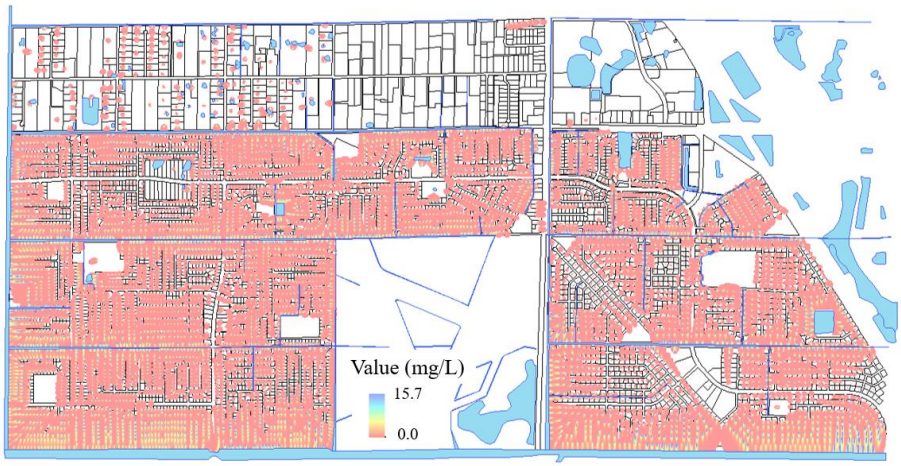

Fig. 2.40. Spatial distribution of NO_3-N concentrations.

2.9. Vertical setback distance and horizontal setback distance

Before discussing the setback distances, we first define several concentrations related to quantifying the distances. For each OSTDS, the concentration at its drainfield is denoted by C_{DF}, and the concentration reaching the water table is denoted by C_{WT}, as shown in Fig. 2.41(a). The distance between a drainfield and water table is denoted as VD. The three variables were used for exploring the vertical setback distance. For exploring the horizontal setback distance, we used C_{WB} to denote the concentration at the location where the central streamline of the contamination plume intersects with the waterbody, as shown in Fig. 2.41(b). C_{WB} and C_{WT} were used to explore the horizontal setback distance. The distance along the flow direction from the drainfield to water body is denoted as HD_F. Since HD_F is unknown in practice, the linear distance from a drainfield to a waterbody is used, and it is referred to HD_L.

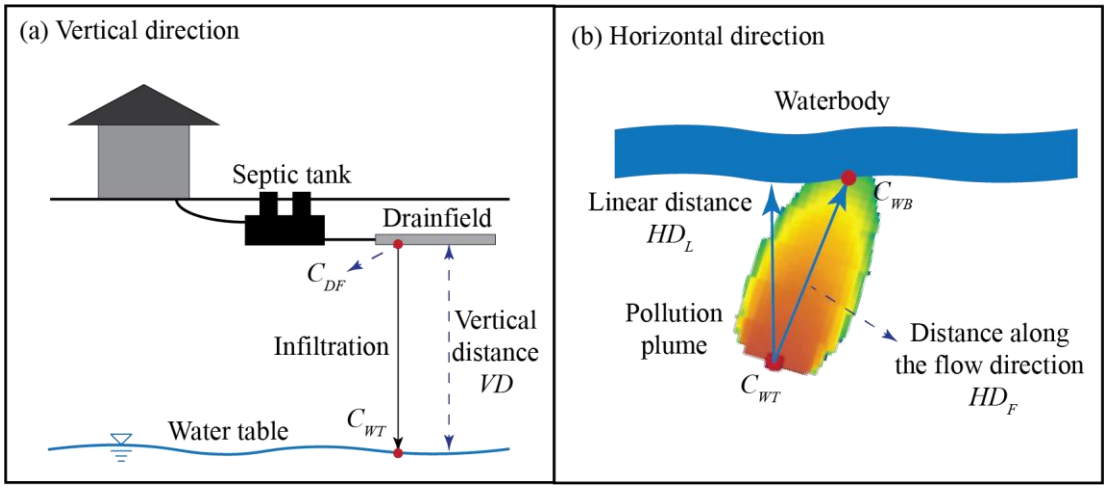

Fig. 2.41. (a) Illustration of the concentration at the drainfield (C_{DF}) and at water table (C_{WT}), and (b) illustration of concentration at the intersection between flow path and a waterbody (C_{WB}) and the horizontal distance along flow path (HD_F) and linear horizontal distance (HD_F) to the water body.

2.9.1 Vertical setback distance from drainfield to water table

Because the conversion from NH_4-N to NO_3-N due to nitrification, NH_4-N concentrations decrease from drainfield to water table, but NO_3-N concentrations increase. We thus considered NH_4-N and NO_3-N together, and calculated the vertical attenuation rate of nitrogen from drainfields to water table as $(1 - C_{WT}/C_{DF})$ along the vertical distance VD.

Fig. 2.42 plots the relation between the vertical attenuation rate and the vertical distance for four soil types in the study domain. The numbers of septic tanks corresponding to sandy loam, loamy sand, sand, and sandy clay loam are 1510, 4381, 185, and 19, respectively. Fig. 2.42 shows that the vertical attenuation rate increases with increasing *VD*. This is expected due to nitrification and nitrification processes in the vadose zone. It is noted in Fig. 2.42 that the purple points of sandy loam are separated into two parts with a substantially different attenuation rates. The reason is that hydraulic conductivities of sandy load is not a constant but vary at different locations. This is illustrated in Fig. 2.43. The figure shows two areas of sandy loam based on soil particle data in SSURGO, but hydraulic conductivity values of the two areas is 2.66 ft/d and 0.26 ft/d. For the area with small hydraulic conductivity, the soil is almost completely saturated, resulting small nitrification and subsequently small denitrification. As a result, the vertical attenuation rate is small in the area with small hydraulic conductivity. We did not examine why hydraulic conductivity of SURRGO varies substantially (e.g., from 2.66 to 0.26 ft/d), because it is beyond the scope of this project. The conclusions on the vertical attenuation rate are mainly based on the results corresponding to large hydraulic conductivity.

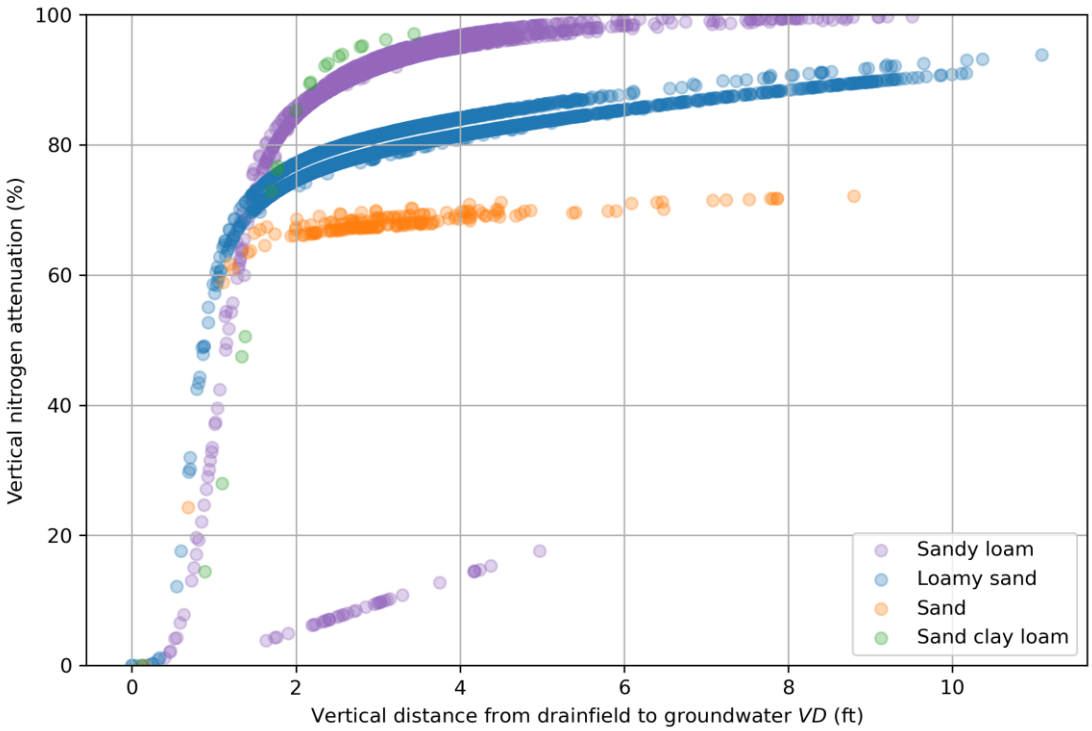

Fig. 2.42. Relation between vertical nitrogen attenuation rate ($1 - C_{WT}/C_{DF}$) and the vertical distance, VD, from drainfield to groundwater *VD* for four soil types.

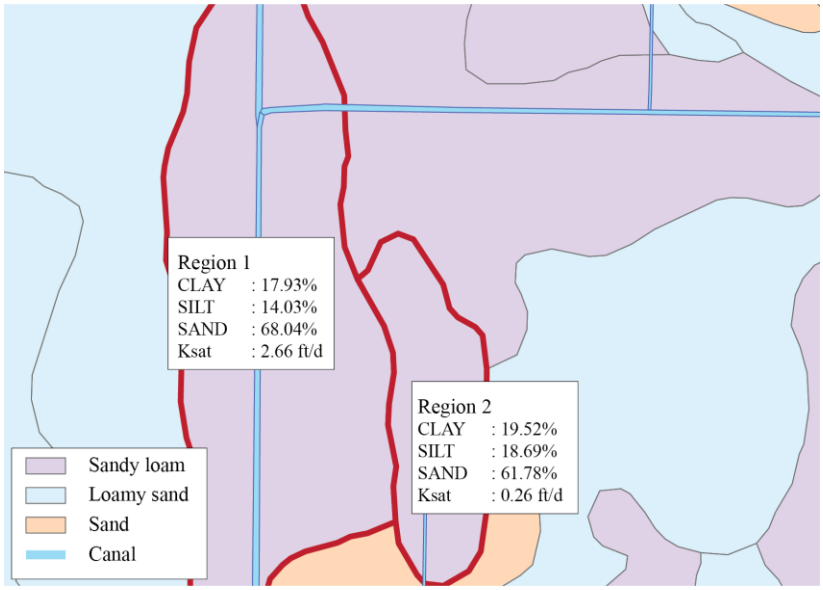

Fig. 2.43. Illustration of different hydraulic conductivity values for sandy loam.

Fig. 2.42 shows that, for all the four soil types, the vertical nitrogen attenuation rate ($1 - C_{WT}/C_{DF}$) increases very rapidly when the vertical distance increases from zero to 2 ft. At the vertical distance of 2 ft, the vertical attenuation rate ranges between 64.5% and 80.4%. When the vertical distance is larger than 2 ft, the vertical attenuation rate increase at a small rate. The rate ranges between 67.6% and 94.8% when the vertical distance is 3

ft. Soil type plays an important role in the variation of the vertical attenuation rate. For the sandy soil, a further increase in the vertical distance beyond 3 ft cannot lead to more increase in the vertical attenuation rate. For the other three soil types, the vertical attenuation rate still increases when the vertical distance is larger than 3 ft.

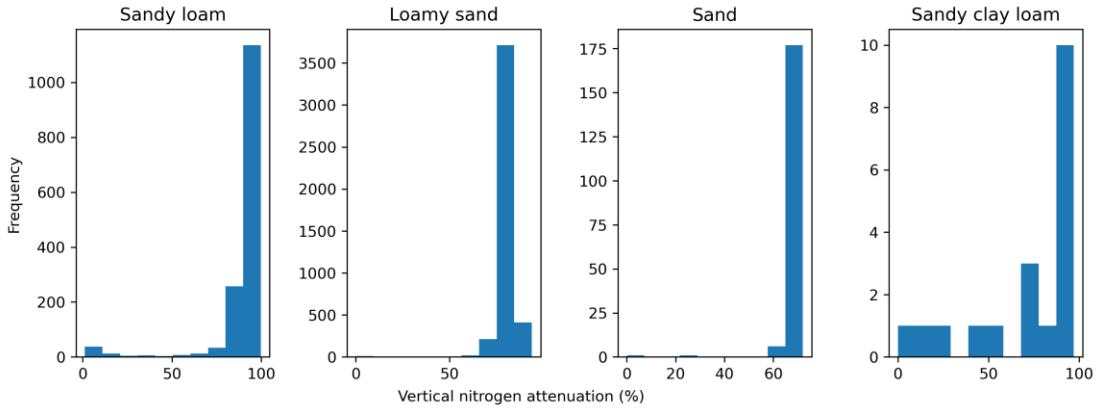

Fig. 2.44. Histograms of vertical nitrogen attenuation rate for four soil types.

Soil type is an important factor for the vertical attenuation rate, as indicated by Fig. 2.44 that plots the histograms of the vertical attenuation rate for four soil types. The effects of soil type are related to the relations between soil water saturation S and nitrification factor (f_{nit}) and denitrification factor (f_{dnt}). The relations are shown in Fig. 2.45, which is adopted from the VZMOD manual. For f_{nit}, its value is 1 within a range of water saturation, S. f_{nit} is an increasing function before S reaches the range, but a decreasing function after S passes the range. When S increases to 1, f_{nit} decreases to 0. f_{dnt} is a monotonically increasing function of S. When S reaches the maximum value 1, f_{dnt} also reaches its maximum value 1. These relations are assumed for all soil types.

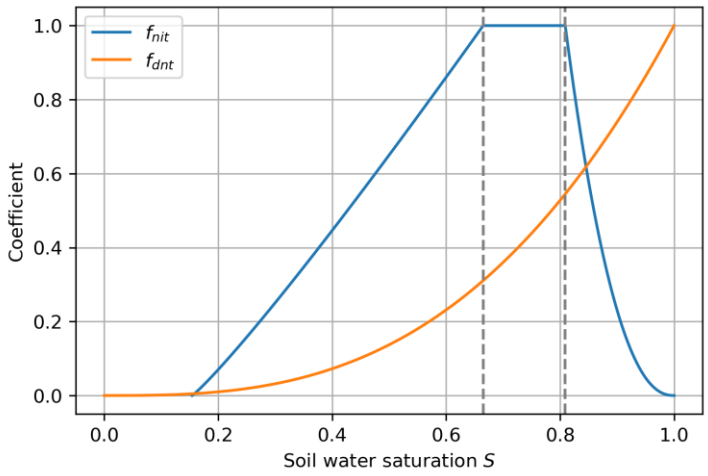

Fig. 2.45. Relations between soil water saturation S and nitrification factor (f_{nit}) and denitrification factor (f_{dnt}).

Soil types are important to the profiles of soil saturation, and this is illustrated in Fig. 2.46 for four locations with four different soil types. The top row of the figure shows the variation of NH_4-N and NO_3 -N concentrations, and the bottom row plots the variation of

soil water saturation S, nitrification factor (f_{nit}), and denitrification factor (f_{dnt}). In the area between the two vertical gray lines, f_{nit} takes its maximum value, as shown in Fig. 2.45. Fig. 2.46 shows that, because of the water saturation, for sandy loam and sandy clay loam, the maximum value of f_{nit} of one is achieved for certain vertical distance (e.g., less than 1.31 ft for sandy clay loam). Therefore, nitrification process of the two soil types is strong, and the concentration of NH_4-N decreases rapidly. The concentration becomes less than 1 mg/L at the depth of 0.75 ft for sandy clay loam. For loamy sand and sand, the soil saturation is not in the range of optimal nitrification factor, and the nitrification process is not as strong as for the other two soil types. The concentration of NH_4-N decreased to less than 1 mg/L for loamy sand and sand are at a depth of 1.44 and 2.82 ft, respectively.

The denitrification factor (f_{dnt}) is also a monotonically increasing function of water saturation. For sandy loam and sandy clay loam, both nitrification and denitrification are strong, leading to a rapid attenuation rate of nitrogen for the two soil types. This explains the rapid increase of attenuation rate in Fig. 2.42. For loamy sand and sand, while nitrification and denitrification occurs, they require a larger vertical distance to reach the same nitrogen attenuation rates.

The simulation results suggest that the vertical distance between drainfields and water table should be at least 2 ft, and that the vertical distance should be considered for different soil types.

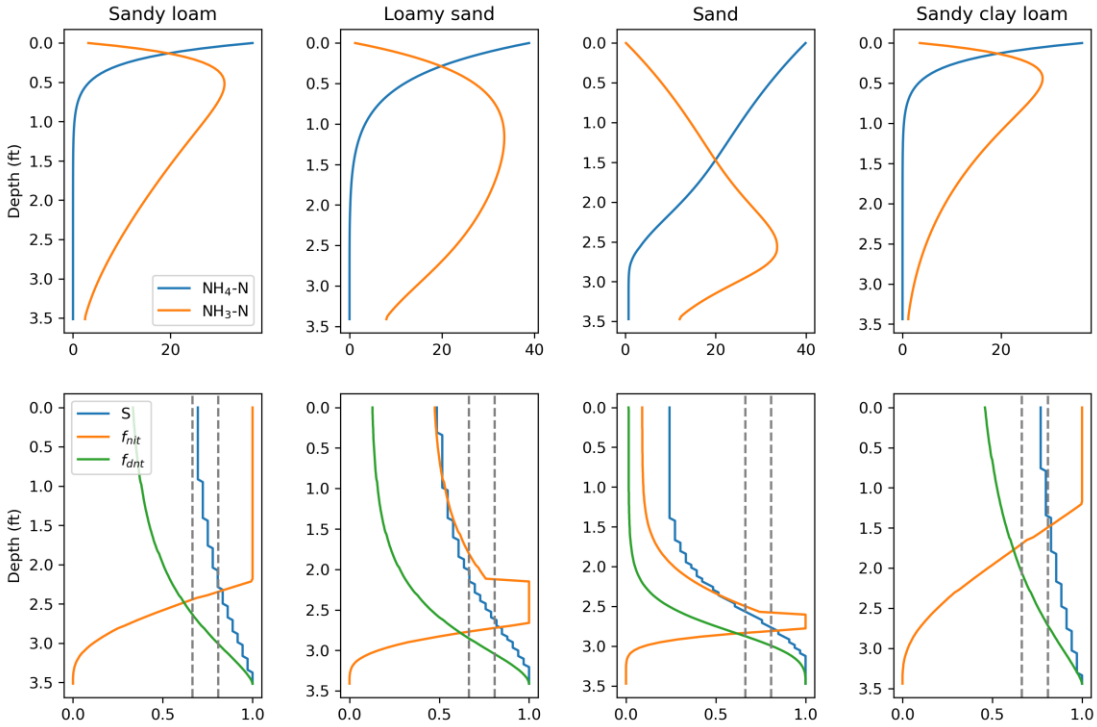

Fig. 2.46. (Top) Simulated nitrogen concentrations, and (bottom) simulated water saturation, nitrification factor, and denitrification factor for four different soil types.

2.9.2 Horizontal setback distance from water table to surface water body

Fig. 2.47 plot the histogram of the concentrations of NH_4-N and NO_3-N at water table (C_{WT}) for the four soil types in the modeling domain. Fig. 2.48 does the same for the concentrations at surface water body (C_{WB}). Fig. 2.47 shows that the C_{WT} of NH_4-N is negligible for all soil types due to nitrification. Several large values of C_{WT} of NH_4-N are mainly due to small vertical distance and/or small saturated hydraulic conductivity, as discussed above. For the C_{WT} of NO_3-N, Fig. 2.47 shows that the histograms of the two loamy soils have peaks around C_{WT} of 3 mg/L; the histograms of the two sandy soils have peaks around C_{WT} of 10 mg/L. The difference between soil types was explained above.

Fig. 2.48 plot the histogram of the concentrations of NH_4-N and NO_3-N at surface water body (C_{WB}) for the four soil types in the modeling domain. For sandy clay loam, almost all C_{WB} values are negligible for both NH_4-N and NO_3-N, indicating that neither NH_4-N nor NO_3-N reach surface water bodies. The reason is that ArcNLET allows nitrification of NH_4-N in groundwater and denitrification of NO_3-N. For the other three soil types, the histograms of C_{WB} have peaks near 0 mg/L. Fig. 2.48 indicates that, for all soil types, nitrogen concentrations near surface water bodies are low. The mean values of the ratio of C_{WB}/C_{WT} of NH_4 are 2.6%, 4.4%, 23.3%, and 0.0% for sandy loam, loamy sand, sand, and sandy clay loam, respectively. The mean values of C_{WB}/C_{WT} for NO_3-N are 1.6%, 4.1%, 4.4%, and 0.0% for sandy loam, loamy sand, sand, and sandy clay loam, respectively. These results suggest a small amount nitrogen load from OSTDS to surface water bodies.

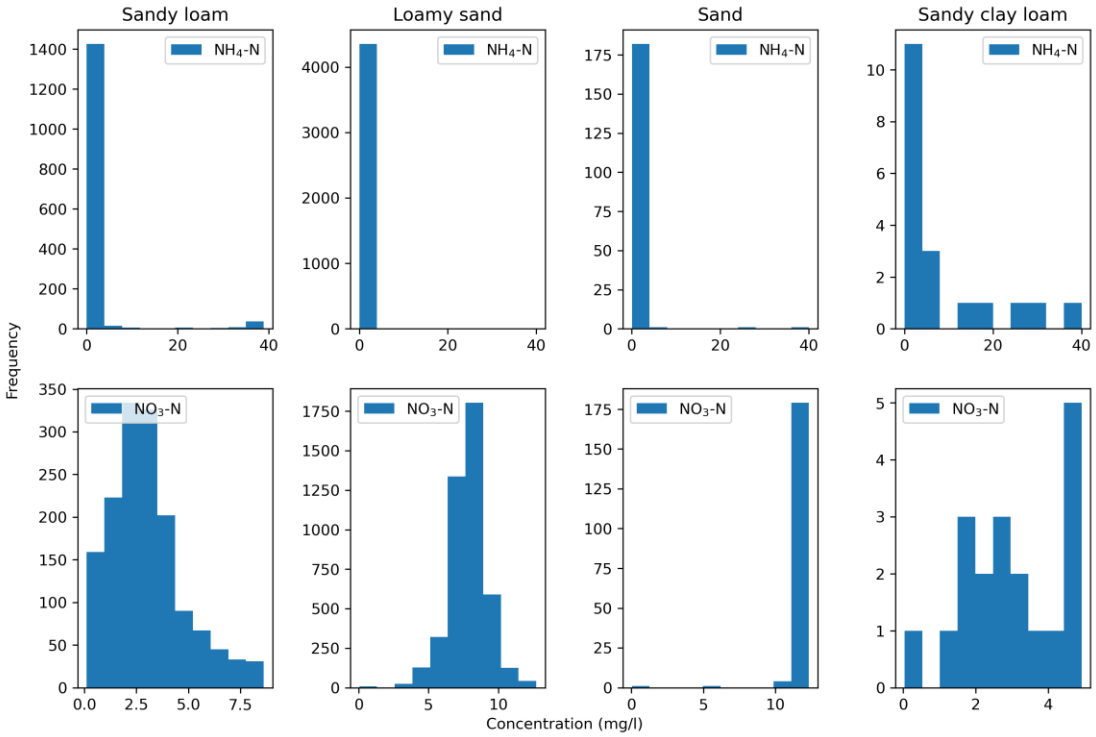

Fig. 2.47. Histograms of C_{WT} (NH_4-N and NO_3-N) for four soil types.

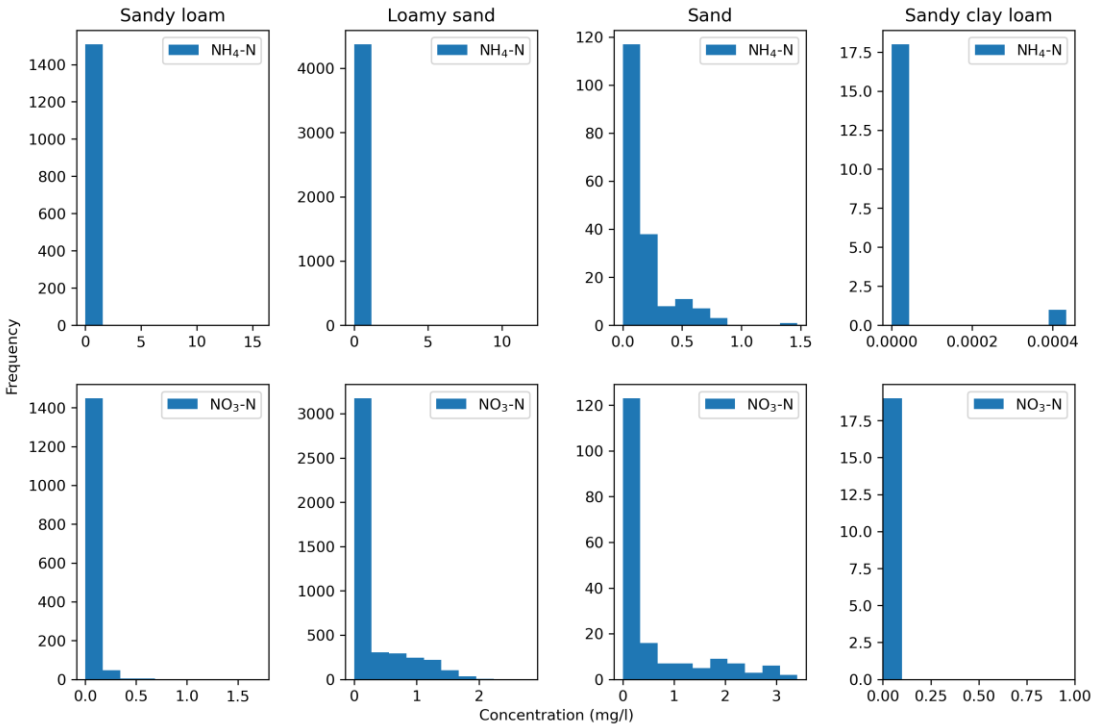

Fig. 2.48. Histograms of C_{WB} (NH_4-N and NO_3-N) for four soil types.

We noticed that for 59 out 6,095 OSTDS, the ratio of C_{WB}/C_{WT} exceeds 100%, meaning that the concentrations at surface waterbodies are larger than those at water table. This is caused by overlaps of simulated plumes. An example of this is shown in Fig. 2.49. In the figure, P1 and P2 are locations of two septic tanks, and P1 is closer to a waterbody than P2 is. Because the end of the flow path from P2 is close to the flow path of P1, a part of the plume of P2 overlaps the plume of P1. As a result, the C_{WB} value of P1 is affected by the plume of P2, and becomes larger than the C_{WT} value of P1, which leads to the value of C_{WB}/C_{WT} over 100%. Since C_{WB}/C_{WT} over 100% only occurred for 59 OSTDS, this should not affect the conclusions of this study.

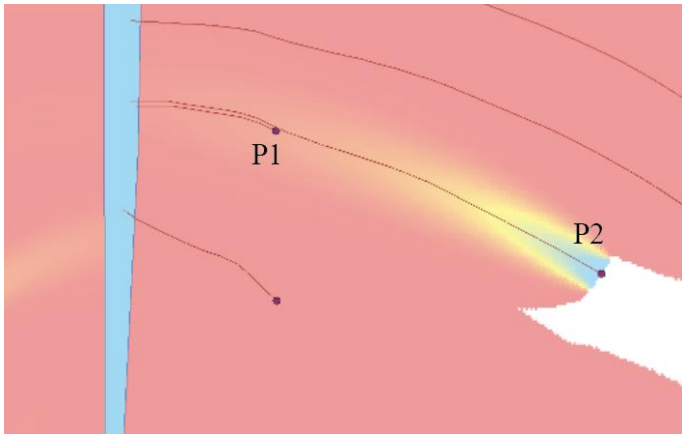

Fig. 2.49. Schematic diagram of the reasons of C_{WB}/C_{WT} values exceed 100%.

Since actual flow paths are unknown without modeling assistance, it is more practical

to use linear distance between a drainfield and a waterbody. The relation between the horizontal distances along flow paths and linear distances from drainfields to water bodies is shown in Fig. 2.50. The figure indicates that the linear horizontal distance can be used as a reasonable approximation of the horizontal distance along flow paths in the study area. Fig. 2.51 plots the relations between horizontal nitrogen attenuation rate ($1 - C_{WB}/C_{WT}$) and the distance along the flow direction from drainfield to waterbody for the four soil types, and Fig. 2.52 does the same for the linear distance between drainfields and water bodies. The two figures are visually similar, indicating again that it is reasonable to use the linear horizontal distance. Both Fig. 2.51 and Fig. 2.52 show that the relation between horizontal attenuation rate and the horizontal distance depends on soil types, and this were used to evaluate the relation for each soil type, as discussed below.

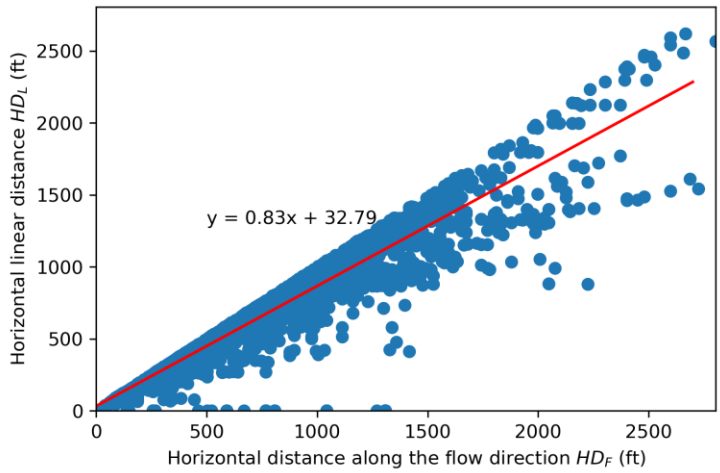

Fig. 2.50. The relationship between the horizontal distance along the flow direction and horizontal linear distance from drainfield to waterbody.

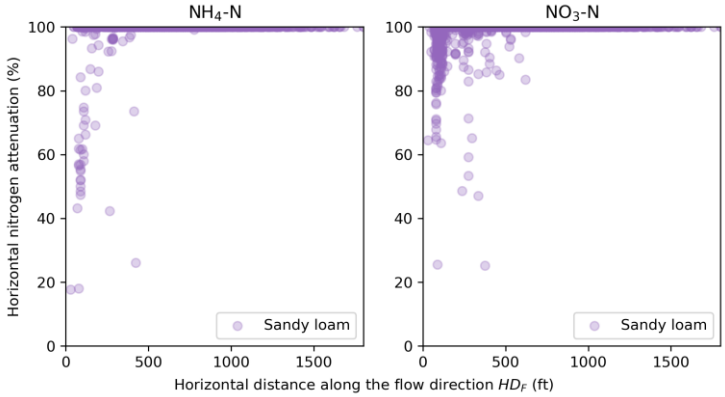

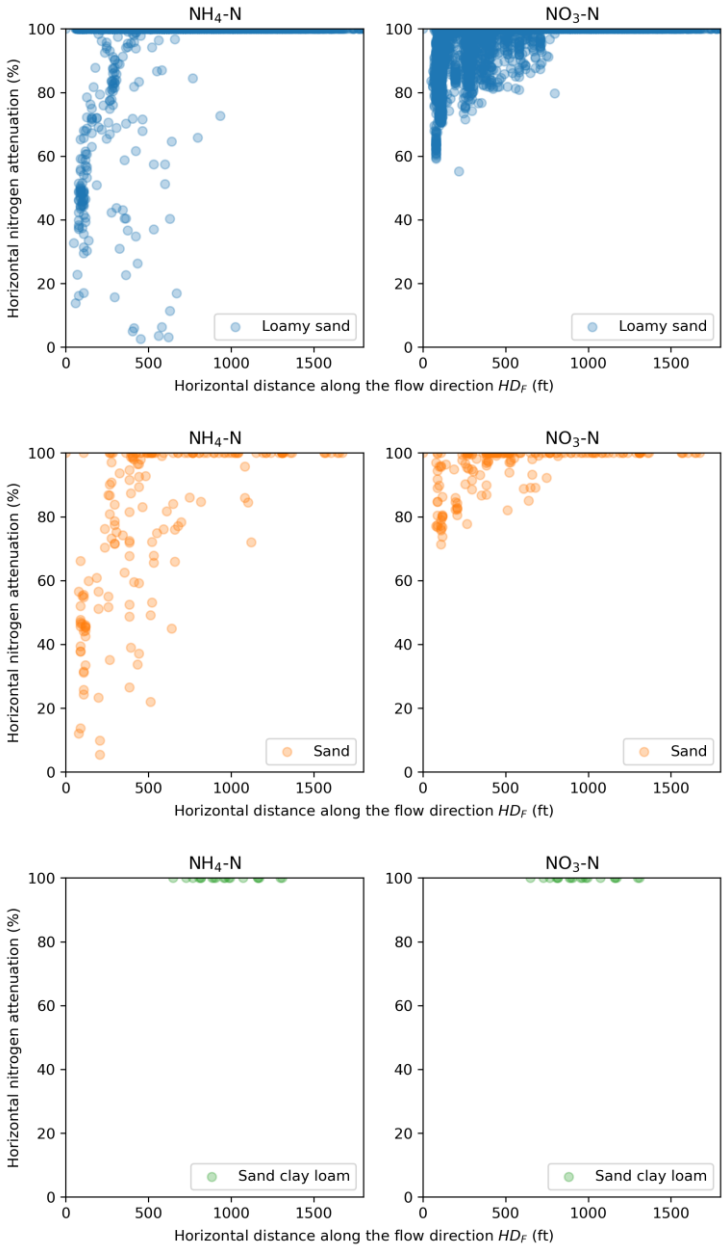

Fig. 2.51. Relations between horizontal nitrogen attenuation rate ($1 - C_{WB}/C_{WT}$) and the horizontal distance (HD_F) along flow paths from drainfield to waterbody for four soil types.

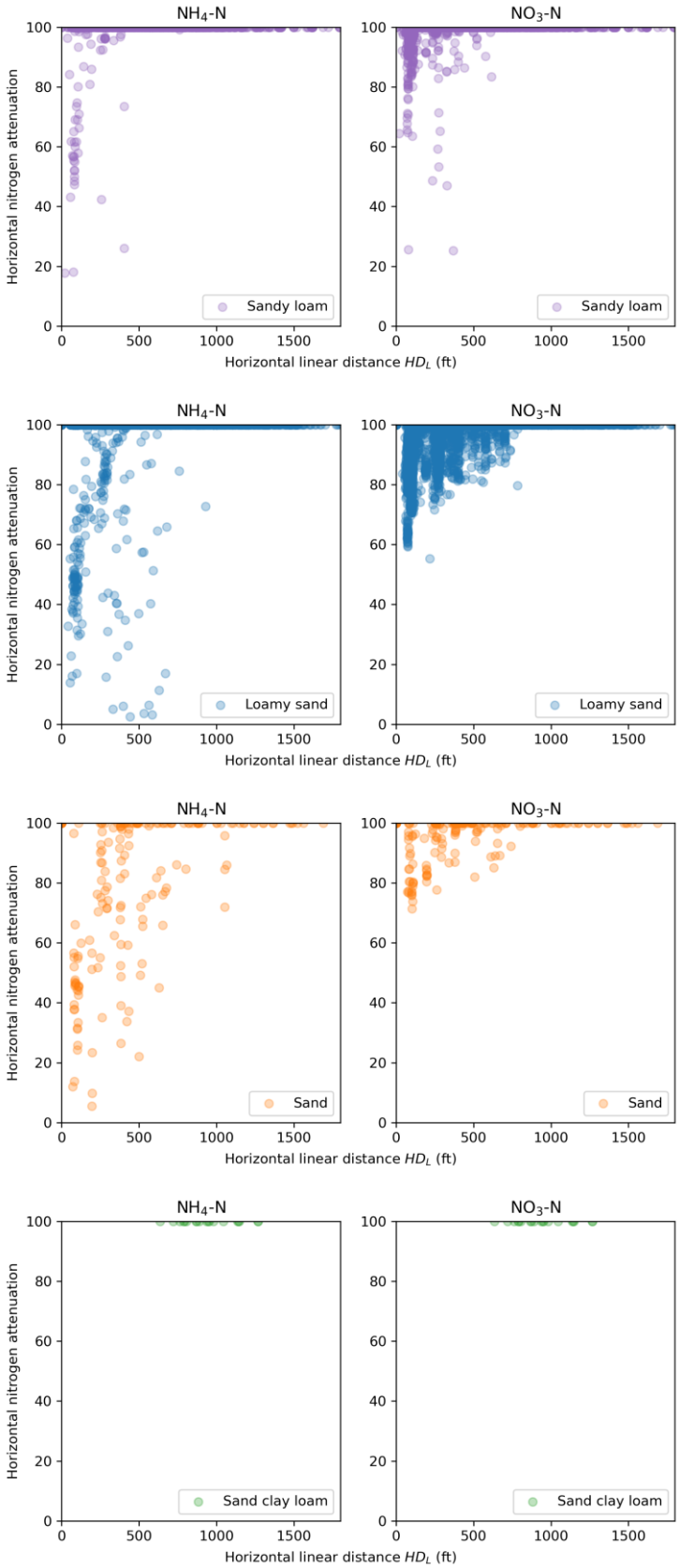
NH4-N
NO3-N
Horizontal nitrogen attenuation
Horizontal linear distance HDL (ft)
Sandy loam
Loamy sand
Sand
Sand clay loam
0
20
40
60
80
100
0
500
1000
1500

Fig. 2.52. Relations between horizontal nitrogen attenuation rate ($1 - C_{WB}/C_{WT}$) and linear horizontal distance (HD_L) from drainfield to waterbody for four soil types.

Fig. 2.53 plots the boxplots of horizontal nitrogen attenuation ($1 - C_{WB}/C_{WT}$) of NH_4-N and NO_3-N for the four soil types. The boxplots of sandy loam and loamy sand have more outliers than those of the other two soil types, because the numbers of OSTDS in sandy loam, loamy sand, sand, and sandy clay loam soils are 1510, 4381, 185, and 19, respectively. Figure 2.53 indicates that the attenuation rate of NH_4-N for sand is different from those for the other three soil types, and that the attenuation rate of NO_3-N for loamy sand and sand are different from those for the other two soil types.

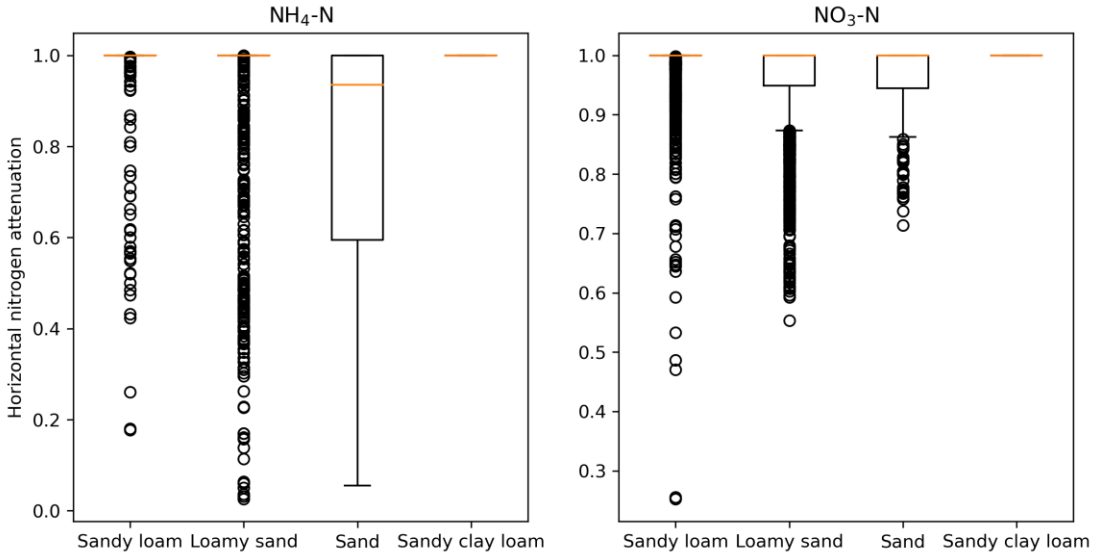

Fig. 2.53. Boxplots of horizontal nitrogen attenuation rate ($1 - C_{WB}/C_{WT}$) of NH_4-N and NO_3-N for four soil types.

Generally speaking and based on the conceptual model of VZMOD and ArcNLET, the horizontal nitrogen attenuation rate is a function of horizontal linear distance, saturated hydraulic conductivity, soil porosity, and groundwater gradient, i.e.,

$$1 - C_{WB}/C_{WT} = func(HD_L, \quad K_{sat}, \quad \phi, \quad \nabla h) \qquad (2.2)$$

We intended to obtain an empirical relation between the attenuation rate and the four factors, and the relation is first discussed qualitatively.

Groundwater gradient is an important factor affecting groundwater velocity that in turn affects nitrogen attenuation due to denitrification. Fig. 2.54 plots the relation between the attenuation rates and hydraulic grant for a short linear distance between 95 ft and 105 ft to canals. A linear trend is observed for both NH_4-N and NO_3-N. Generally speaking, larger groundwater gradients correspond to smaller horizontal nitrogen attenuation rate ($1 - C_{WB}/C_{WT}$). This is expected, because larger groundwater gradients lead to faster groundwater flow, less denitrification, and thus smaller nitrogen attenuation. Fig. 2.54 shows that the attenuation rate of NH_4-N is smaller than that of NO_3-N. The comparison

between NH_4-N and NO_3-N is not useful for understanding the attenuation rates, because the concentrations of NH_4-N are about one order of magnitude smaller than those of NO_3-N. The average concentrations at water table (C_{WT}) of NH_4-N and NO_3-N are 0.13 mg/L and 6.12 mg/L, respectively, and the average concentrations at water bodies (C_{WB}) of NH_4-N and NO_3-N are 0.01 mg/L and 0.77 mg/L, respectively. In addition, the C_{WB} value of one OSTDS can be affected by the C_{WB} of other OSTDS.

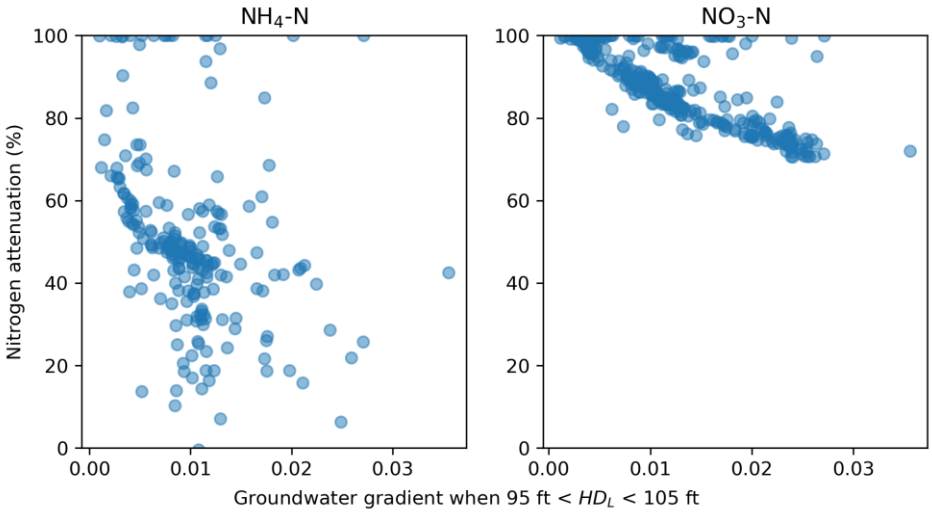

Fig. 2.54. Relations between horizontal nitrogen attenuation rate ($1 - C_{WB}/C_{WT}$) and groundwater gradient for .

The relation between linear horizontal distance (HD_L) and groundwater gradient ∇h is plotted in Fig. 2.55, and a negative relation is observed. Larger gradients occur at shorter horizontal distances. This is expected, because water table tends to be steep near water bodies. There is no a one-to-one relation between gradient and linear distance, because hydraulic gradient is affected by multiple factors such as hydraulic gradient.

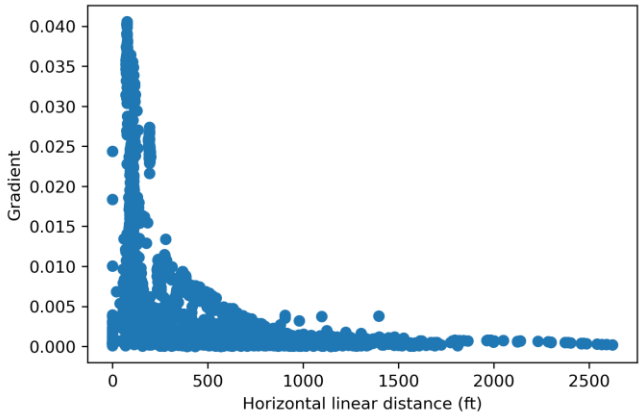

Fig. 2.55. Relation between horizontal linear distance and groundwater gradient

The values of porosity and hydraulic conductivity used in this research were from the SSURGO database. For the modeling domain, there are nine porosity values, ranging between 0.366 and 0.415. Therefore, porosity is not an important factor to the nitrogen attenuation rate. Fig. 2.56 plots the boxplots of horizontal nitrogen attenuation rate ($1 -$

C_{WB}/C_{WT}) for different values of hydraulic conductivity. The figure suggests that the attenuation rate is a function of hydraulic conductivity.

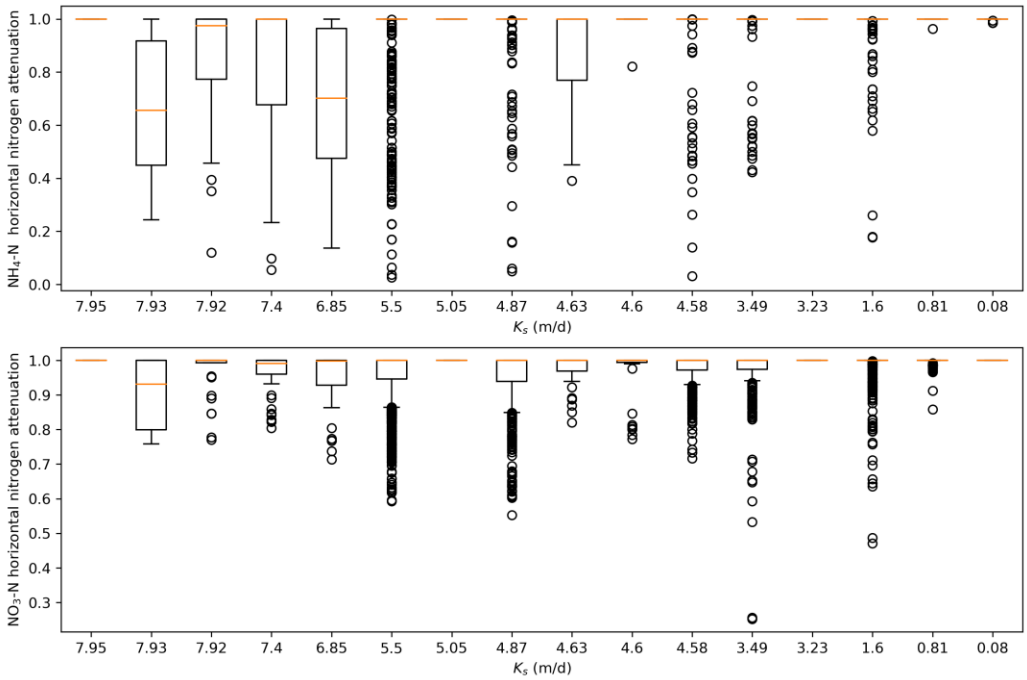

Fig. 2.56. Boxplots of horizontal nitrogen attenuation rate ($1 - C_{WB}/C_{WT}$) for different values of hydraulic conductivity. The top plot is for NH_4-N, and the bottom plot is for NO_3-N.

Since the linear distance HD_L, hydraulic gradient, and hydraulic conductivity K_s are important factors to horizontal nitrogen attenuation rate ($1 - C_{WB}/C_{WT}$). Fig. 2.57 shows the 3-D plot of linear horizontal distance HD_L, hydraulic conductivity K_s, and horizontal nitrogen attenuation ($1 - C_{WB}/C_{WT}$). Fig. 2.58 shows the 3-D plot of linear horizontal distance HD_L, groundwater gradient, and horizontal nitrogen attenuation rate ($1 - C_{WB}/C_{WT}$). While the 3-D plots show relations between the four variables, the relations are difficult to be quantified. We thus worked on 2-D plots.

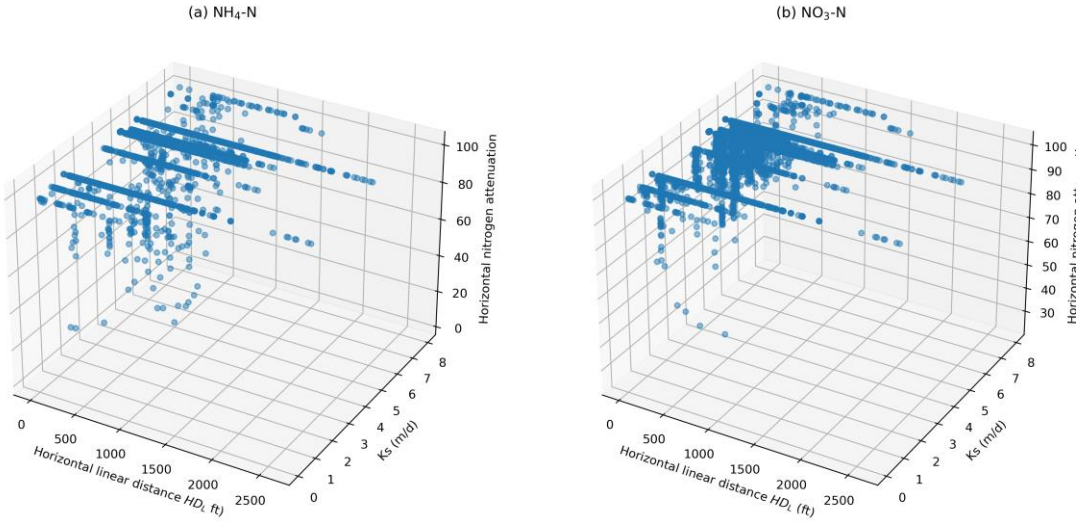

Fig. 2.56. 3-D plot of linear horizontal distance HD_L, hydraulic conductivity K_s, and horizontal nitrogen attenuation ($1 - C_{WB}/C_{WT}$).

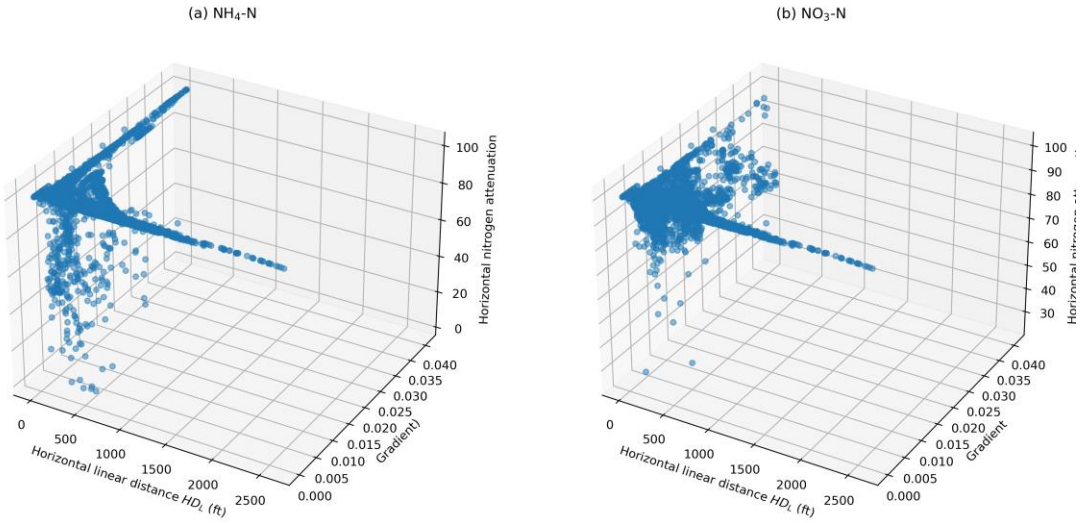

Fig. 2.57. 3-D diagram of the relationship between linear distance HD_L, groundwater gradient, and horizontal nitrogen attenuation ($1 - C_{WB}/C_{WT}$).

Based on the discussion above on the relations between horizontal nitrogen attenuation rate and the four factors (HD_L, K_{sat}, ϕ, ∇h), we decided to remove porosity ϕ from the relations, because it has small variation at the study site. For each horizontal linear distance HD_L value, we used the averaged value of horizontal attenuation rate so that we did not need to determine the relation between the attenuation rate and hydraulic gradient. This is a practical choice, because hydraulic gradient is unknown without a modeling assistance. The average attenuation rate was estimated for every 10 ft of the linear horizontal distance, and Fig. 2.58 plots the relations between the averaged horizontal attenuation rate and linear horizontal distance for the four soil types of the study site. The dashed line in the figure is for the distance of 75 ft, which is currently used OSTDS setback distance.

Based on the discussion above, the function of equation (2) can be simplified as,

$$1 - C_{WB}/C_{WT} = func(HD_L, \quad K_{sat}) \tag{2.3}$$

The empirical function is as follows

$$1 - C_{WB}/C_{WT} = 100 \times AF \times (1 - e^{((-HD_L)/(4\times K_s+20))}) \tag{2.4}$$

where AF is a adjust factor for the maximum nitrogen attenuation for large horizontal linear distance. This relation is practically applicable, because it only requires knowing hydraulic conductivity values of a site and the values are available in SURRGO. When determining the empirical relation, more attention was paid to the attenuation rate of NH_4-N than to that of NO_3-N, because the NH_4-N concentrations in groundwater are one order of magnitude smaller than those of NO_3-N, as discussed above.

The function given in equation (4) is plotted in Fig. 2.58. When the horizontal linear distance is 75 ft, the horizontal nitrogen attenuation based on the modified empirical expression for sandy loam, loamy sand, sand, and sandy clay loam are 93.5%, 83.9%, 79.0%, and 84.5%, respectively, indicating that most of the NO_3 can be removed. Equation (4) can be used for estimating the horizontal attenuation rate for a known value of hydraulic conductivity and a target value of linear horizontal distance.

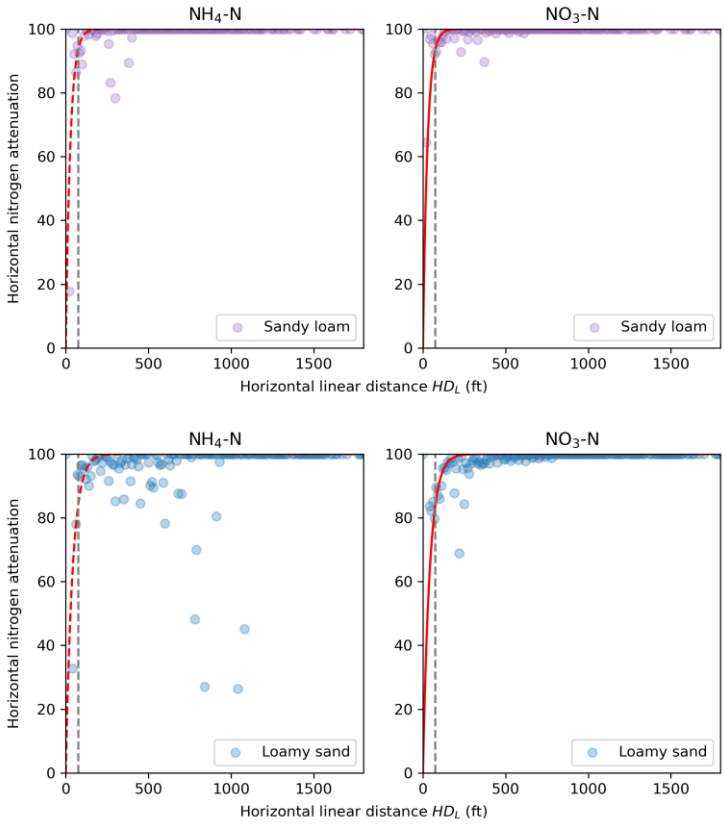

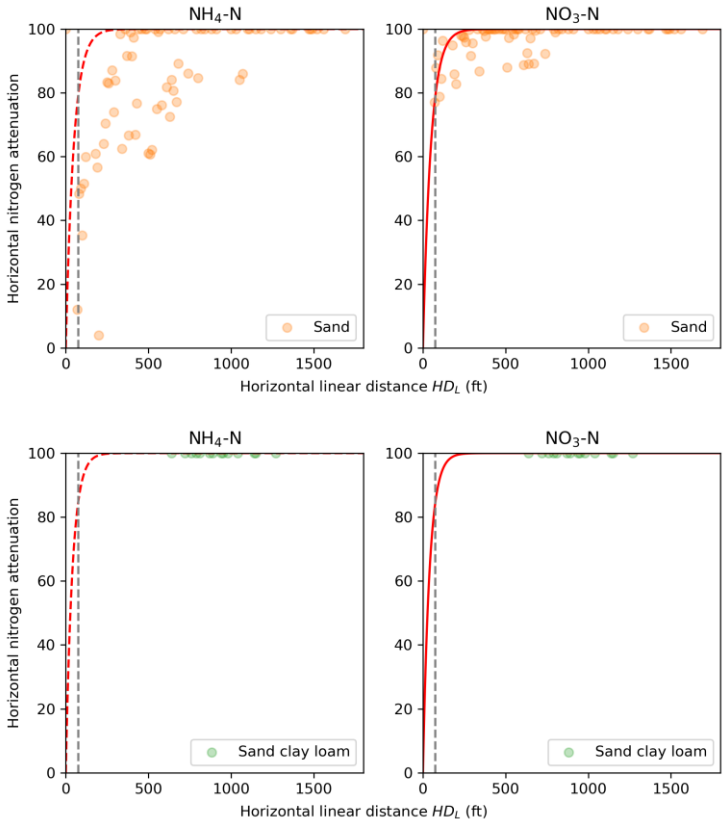

Fig. 2.58. Relations between horizontal nitrogen attenuation and the linear horizontal distance after averaging hydraulic gradient for every 10 feet of the distance.

2.9.3 Sensitivity analysis to simultaneously determine vertical and horizontal setback distances

While the last two sub-sections discussed the vertical and horizontal setback distances separately, the two distances cannot be separated in the real world. This subsection thus discusses how to simultaneously determine the vertical and horizontal setback distances. The determination is based on the total nitrogen attenuation rate from drainfields to waterbodies $(1-C_{WB}/C_{DF})\times 100\%$. Fig. 2.59 plots boxplots of the calculated rates for the four soil types in the modeling domain. The medians of sand and loamy sand are larger than those of sandy loam and sandy clay loam. An ANOVA test on the mean values yielded a p-value of 1.3×10^{-77}, which is much smaller than 0.05. This result indicates that the mean values of different soil types are not equal in the 5% statistical significance. Fig. 2.60 plots the boxplots of the total attenuation rate for different values of hydraulic conductivity. The figure shows that the boxplots are different for different values of hydraulic conductivity. Fig. 2.61 plots the relations between linear horizontal distance HD_L, vertical distance VD, and the total attenuation rate $(1-C_{WB}/C_{DF})$. While a relation between the three variables was observed, we could not obtain an empirical relation between the attenuation rate and the two setback distances.

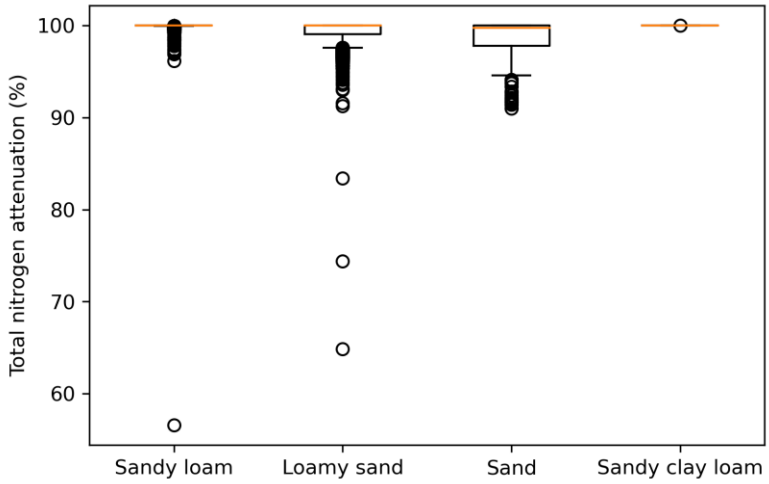

Fig. 2.59. Boxplots of $(1-C_{WB}/C_{DF})\times 100\%$ categorized by different soil types.

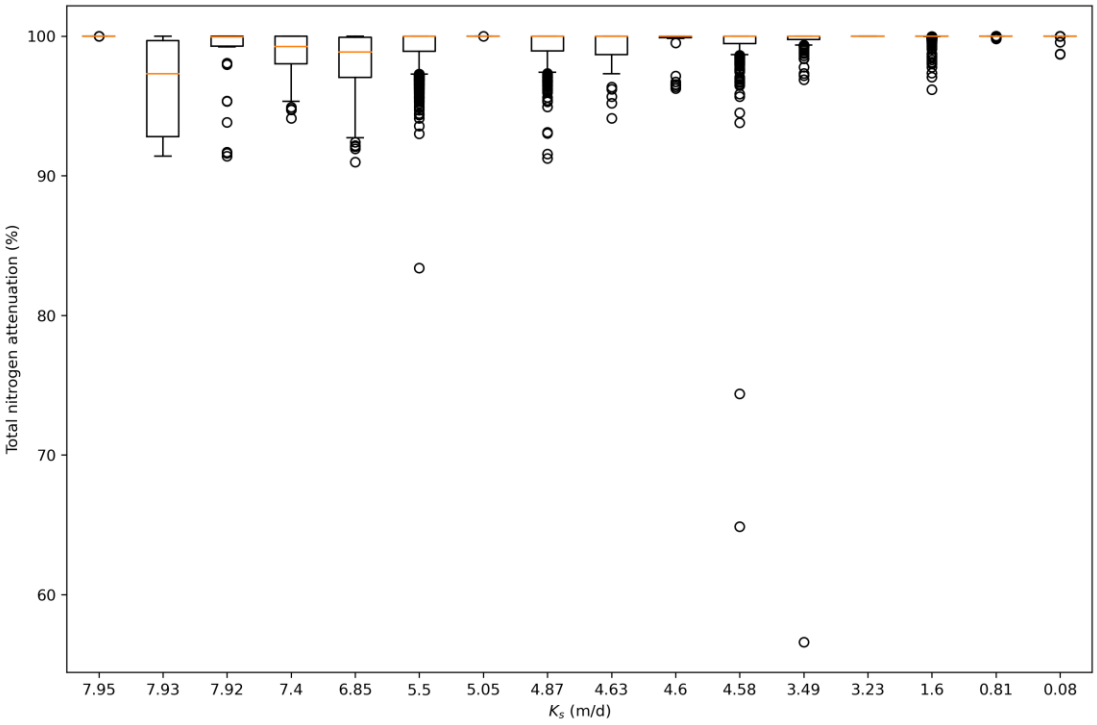

Fig. 2.60. The boxplot of $(1-C_{WB}/C_{DF})\times 100\%$ categorized by saturated hydraulic conductivity.

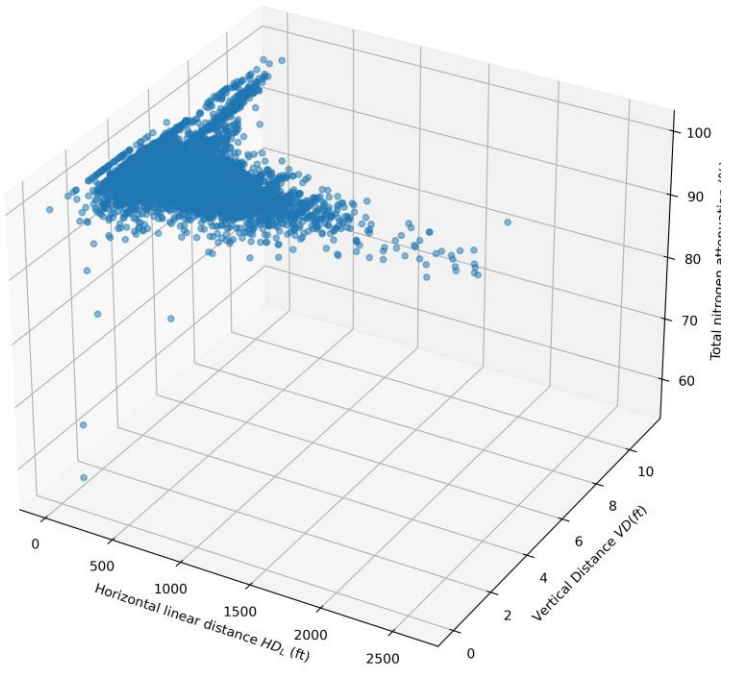

Fig. 2.61. Relations between horizontal linear distance HD_L, vertical distance VD, and total nitrogen attenuation rate ($1-C_{WB}/C_{DF}$).

A sensitivity analysis was conducted to understand the relation between the total nitrogen attenuation rate and the two setback distances with consideration of multiple factors discussed above. Below is a description of the values of multiple factors considered in the sensitivity analysis:

(1) To determine the values of horizontal setback distance, we selected eight OSTDS located in an aera between the Groseclose and Jones homes. As shown in Fig. 2.62, the flow paths from the eight OSTDS are parallel and toward a canal. The longest linear distance is 857.8 ft (Fig. 2.62). We added three virtual OSTDS (Fig. 2.62), and the shortest distance is 75 ft, which is the current setback distance for OSTDS environmental regulation. The sensitivity analysis thus has 11 values of horizontal setback distance.

(2) Each of the 11 OSTDS has its own value of hydraulic gradient estimated by ArcNLET, and these values were used for the sensitivity analysis. These values represent well the hydraulic gradient of the study area, and this is illustrated in Fig. 2.63 that plots the histogram of hydraulic gradient for the entire study area. The sensitivity analysis thus has 11 values of hydraulic gradient associated with he 11 values of horizontal setback distance.

(3) To determine the values vertical setback distance, we assumed that the distance varies between 0.3 ft and 9.8 ft, which is the range estimated by VAMOD for the study site. This range is uniformly divided into 29 intervals. The sensitivity analysis thus has 30

values of vertical setback distance.

(4) To determine the values of hydraulic conductivity, we used the SSURGO values for sand, sandy clay loam, sandy loam, and loamy sand, which are the soil types of the study area. The sensitivity analysis thus considers four values of hydraulic conductivity.

Therefore, we have a total of 1,320 = 11 × 30 × 4 combinations of 11 horizontal linear distances/hydraulic gradient, 30 different vertical distances, and 4 hydraulic conductivity. VZMOD and ArcNLET simulations were conducted for one OSTDS for the 1,320 combinations to determine the relation between the total nitrogen reduction rate and the two setback distances.

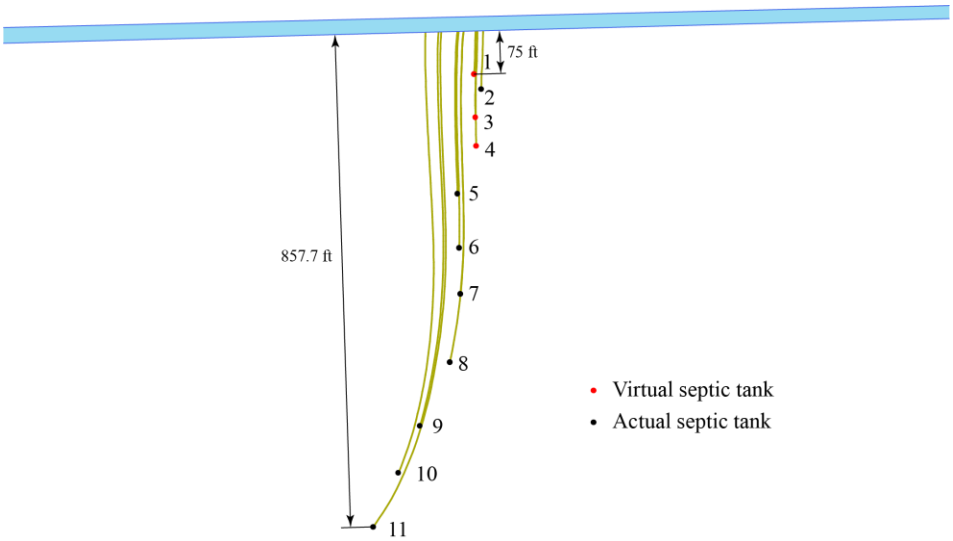

Fig. 2.62. Actual and virtual OSTDS used for sensitivity analysis to determine the relation between total nitrogen attenuation rate and two setback distances.

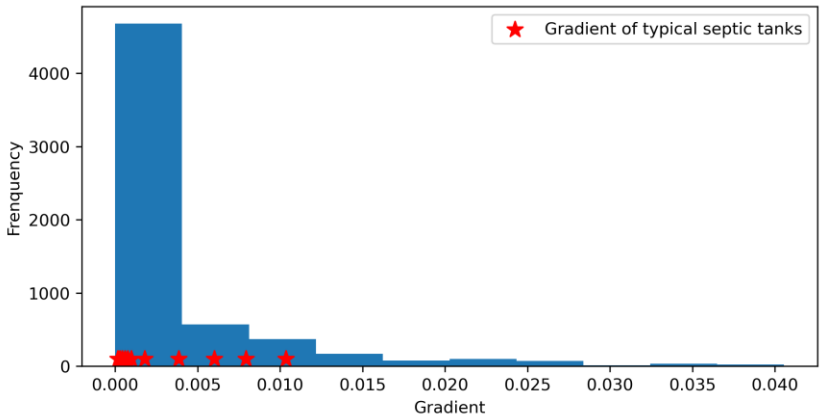

Fig. 2.63. Histogram of hydraulic gradient for the entire study. The eleven hydraulic gradient values used for the sensitivity analysis are marked by the star.

Based on the results of the 1,320 model simulation results, for each soil type, we plotted the contours of the total nitrogen attenuation rate with the horizontal and vertical setback distances. We also did this for the concentrations of NH_4-N and NO_3-N entering the canal (i.e., at the end of the groundwater flow paths). These contours are shown in Fig. 2.64. The

figure shows that increasing either the linear horizontal distance or the vertical distance can increase the rate. The vertical distance is more influential than the horizontal distance, because the attenuation rate changes more quickly with the vertical distance than with the horizontal distance.

The attenuation rate is affected by soil types. For sandy loam and sandy clay loam, when the horizontal linear distance is greater than 75 ft and the vertical distance is greater than 2 ft, an attenuation rate of 90% can be achieved when. The reason is that, when the vertical distance is greater than 2 ft, for sandy loam and sandy clay loam, NH_4-N can be completely converted to NO_3-N, and NO_3-N can be denitrified in both vadose zone and surficial aquifer. This however is not the case for loamy sand and sand (especially sand), for which achieving a 90% attenuation requires a large vertical and/or horizontal setback distance. Increasing the vertical distance alone for loamy sand, especially sand is not as effective as for the other two soil types.

The concentration contours in Fig. 2.64 show that, when both the horizontal linear distance and vertical distance are small, the concentrations of NH_4-N and NO_3-N are large, especially for the concentrations of NH_4-N. For a small vertical distance, the NH_4-N concentrations at water table are large due to inadequate nitrification, and corresponding NO_3-N concentrations are small. The relationship between the concentrations of NH_4-N and NO_3-N at water table and the vertical distance for the four soil types are shown in Fig. 2.65. The figure shows a threshold of 2 ft for the vertical distance, because NH_4-N concentrations decrease rapidly when the distance is smaller than 2 ft. Accordingly, the NO_3-N concentrations increase rapidly when the distance is smaller than 2 ft. When the distance is larger than 2 ft, the NH_4-N concentrations do not vary or vary slightly, but the NO_3-N concentrations decrease due to denitrification.

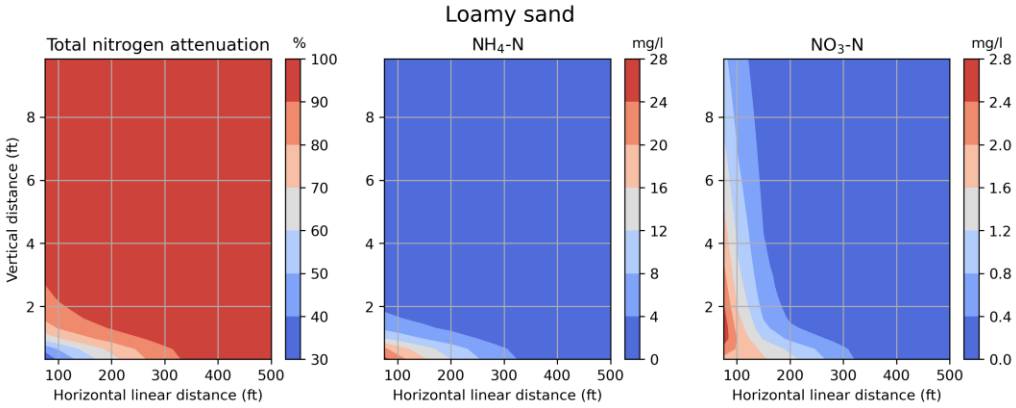

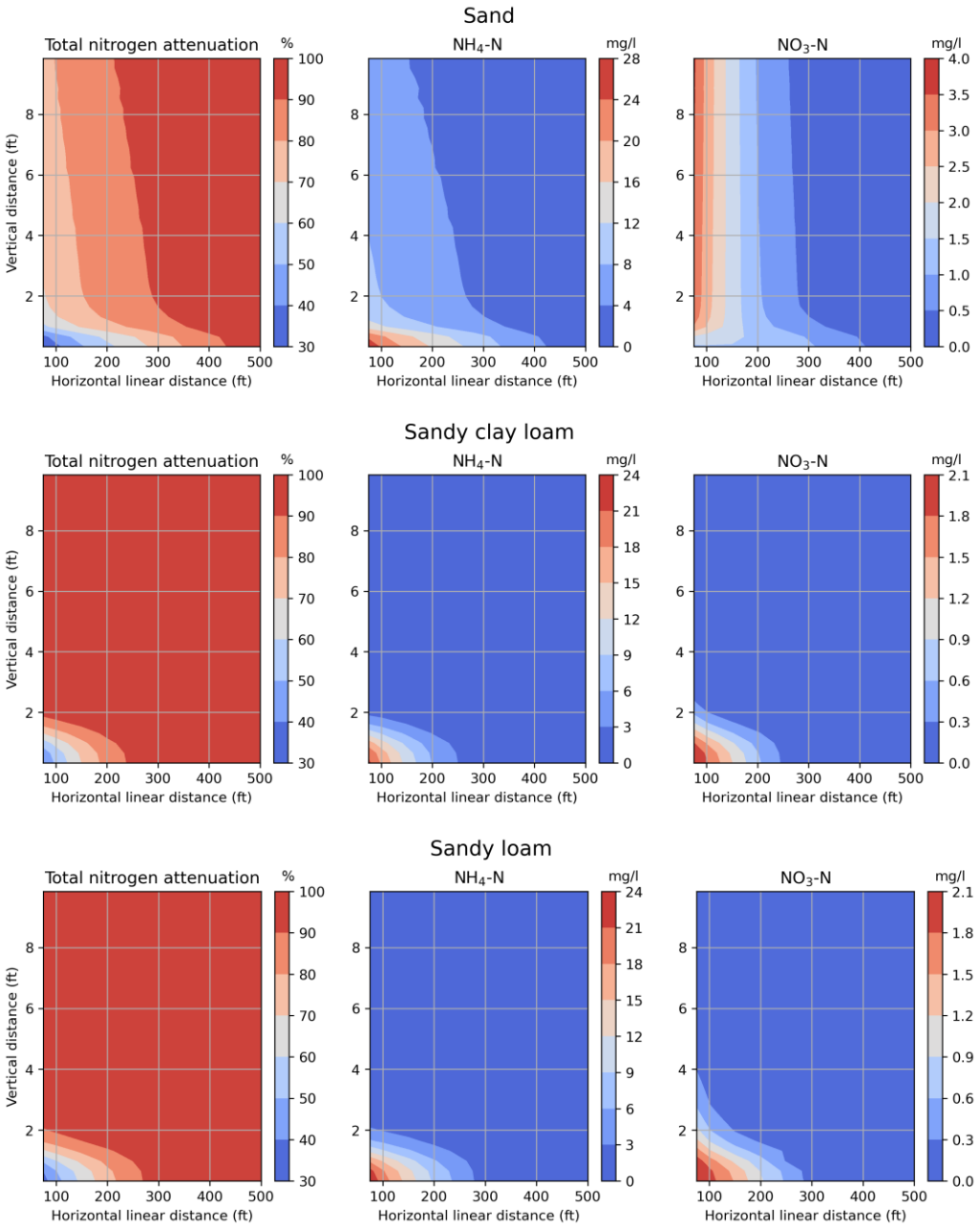

Fig. 2.64. Relations between nitrogen attenuation as well as concentrations of NH_4-N and NO_3-N entering the canal and the horizontal linear distance and vertical distance for four soil types. The smallest horizontal distance is 75 ft.

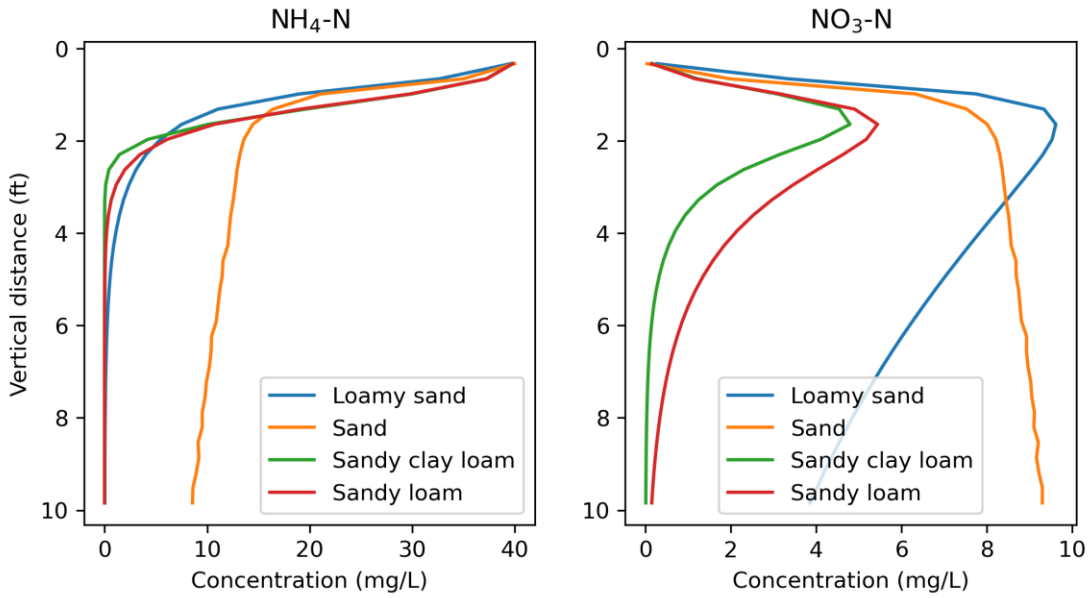

Fig. 2.65. The relationship between concentration of NH_4-N and NO_3-N entering the groundwater table and vertical distance categorized by different soil types.

2.10 Summary and conclusions

This chapter presented our work of setting up VZMOD and ArcNLET models, calibrating the models against observed hydraulic heads and NH_4-N and NO_3-N concentrations at the Groseclose and Jones sites, and used to calibrated models to simulate flow and nitrogen reactive transport at a study site with 6,096 OSTDS. The simulation results, together with a sensitivity analysis of 1,320 simulations, were used to explore the relation between nitrogen attenuation rates with the vertical and horizontal setback distances.

Our modeling results indicate that the nitrogen attenuation in vadose zone is significantly affected by the vertical distance from drainfields to water table and soil types. Loamy soils with sufficient water retention are suitable for nitrification and denitrification reactions, and thus have a large nitrogen attenuation rate. Sandy soils with insufficient water retention have less extent of nitrification and denitrification, and thus have a smaller nitrogen attenuation rate. Although there is no clay soil in the study site, it is expected that clay soils can be easily saturated, and do not support nitrification, which may lead to a small attenuation rate. The VZMOD simulations and the sensitivity analysis suggest that a vertical setback distance of 2 ft from drainfields to water able is a threshold for achieving a satisfactory (about 80%) of nitrogen attenuation in the vadose zone. This however does not apply to sandy soils that always have smaller attenuation rate due to a less extent of nitrification and denitrification.

Our modeling results indicate that the nitrogen attenuation rate in groundwater depends on hydraulic conductivity and groundwater gradient, which jointly determine groundwater velocity. We developed an empirical expression to describe the relation between the nitrogen attenuation rate and hydraulic conductivity and linear horizontal distance. The expression does not include hydraulic gradient, because it is largely unknown

in practice. Hydraulic conductivity can be found in SSURGO, and linear horizontal distance can be estimated by using ArcGIS or other tools. Our results show that, for the 75ft horizontal setback distance, the nitrogen attenuate rate is 93.5%, 83.9%, 79.0%, and 84.5% for sandy loam, loamy sand, sand, and sandy clay loam, respectively. Increasing the linear horizontal distance from OSTDS to waterbodies leads to a larger nitrogen attenuation rate. If the horizontal distance is large enough, nitrate can be completely removed by denitrification. However, a large horizontal distance is not realistic in practice.

The contours of total nitrogen attenuation rate produced by the sensitivity analysis can be used for simultaneously considering the vertical and horizontal setback distances. The contours suggest that it is necessary to consider the two distances for effective nitrogen attenuation. Taking the contours of sandy clay loam and sandy loam as an example, the vertical setback distance of 2 ft and the horizontal setback distance of 75 ft yield a 100% attenuation rate. If the vertical setback distance is reduced to 1 foot, the horizontal setback distance needs to about 250 ft for achieving 100% attenuation. For sand soil, 100% attenuation is practically impossible, unless the vertical and/or horizontal setback distance are set unrealistically large values such as 10 ft for the vertical distance or 400 ft for the horizontal distance.

References

Ayres Associates, 1993. An investigation of the surface water contamination potential from on-site sewage disposal systems (OSDS) in the Turkey Creek Sub-Basin of the Indian River Lagoon Basin.

Bakker, M., Post, V., Langevin, C.D., Hughes, J.D., White, J.T., Starn, J.J., 2016. Scripting MODFLOW Model Development Using Python and FloPy. Groundwater, 54(5), 733-739. doi: 10.1111/gwat.12413.

Lush, M.G., Toor, G.S., Yang, Y.Y., Mechtensimer, S., De, M., Obreza, T.A., 2017. A review of the fate and transport of nitrogen, phosphorus, pathogens, and trace organic chemicals in septic systems. Critical Reviews in Environmental Science and Technology. doi:10.1080/10643389.2017.1327787.

Chapter 3. Numerical Investigation of OSTDS Setback Distances for St. Lucie River of Indian River Lagoon

This chapter presents our modeling investigation of OSTDS setback distances based on the data collected by Belanger and Price (2007) at four sites along the St. Lucie River of the Indian River Lagoon. Since the procedure of modeling investigation is similar to that discussed in Chapter 2 for the Turkey Creek sub-basin, this chapter only presents necessary details related to the St. Lucie River, and does not include a discussion on the methods behind the numerical investigation.

3.1. Study Area and Study Sites

Belanger and Price (2007) selected four sites, B2, C2, D2, and E2, and their locations are shown in Fig. 3.1. Necessary information of the four study sites are summarized in Table 3.1. In this chapter, the four sites are referred to as study sites, and the area that includes the four sites is referred to as study area.

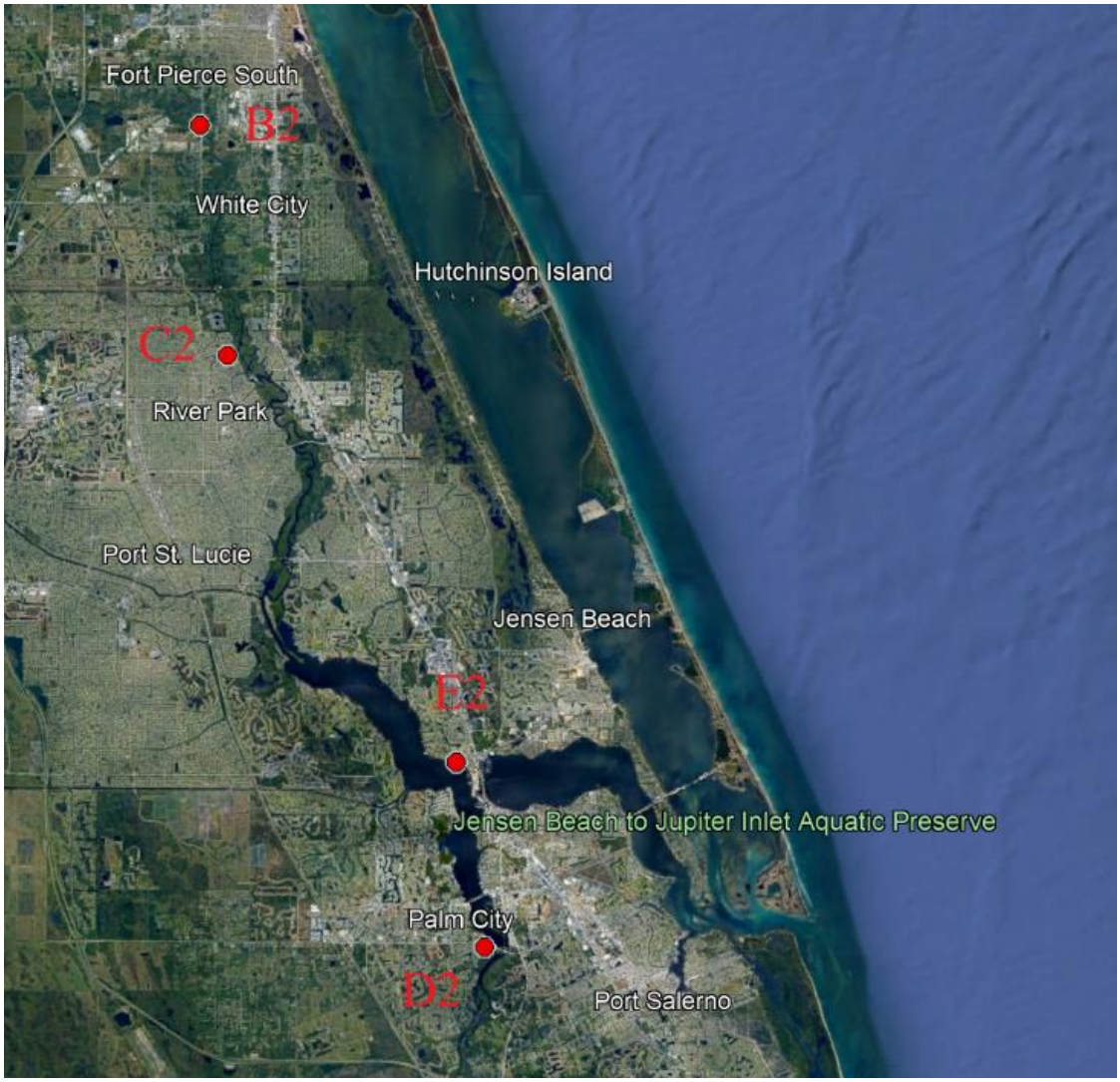

Fig. 3.1. Locations of the four study sites selected by Belanger and Price (2007).

Table 3.1. Summary information of the four study sites.

	B2	C2	D2	E2
Location	2502 Isola Bella in Ft. Pierce	354 Surfside in Port St. Lucie	701 N.W. Sunset Drive in Stuart	3679 S.W. St. Lucie Shores in Palm City
Build year	1985	1986	1975	1970
Number of people	4	4	4	3-5
Septic tank	-	-	750 gal	1050 gal
Drainfield	-	-	200 ft^2	300 ft^2
Distance to river	117 ft	22 ft	68 ft	200 ft
Property	Natural low gradient site	Bulkhead backyard	Bulkhead backyard	Natural low gradient site

3.2 Data for ArcNLET Modeling

The septic data were obtained from the Florida Water Management Inventory (FLWMI) project at https://ww10.doh.state.fl.us/pub/bos/Inventory/FloridaWaterManagementInventory/. The study area includes portions of the St. Lucie County and Martin County. The procedure of generating the ArcGIS file of septic tank for ArcNLET modeling is the same as that described in Section 2.2.1. The septic tank locations are shown in Fig. 3.2. To reduce computational cost only about 1,000 septic tanks were selected at each of the four sites (B2 – E2).

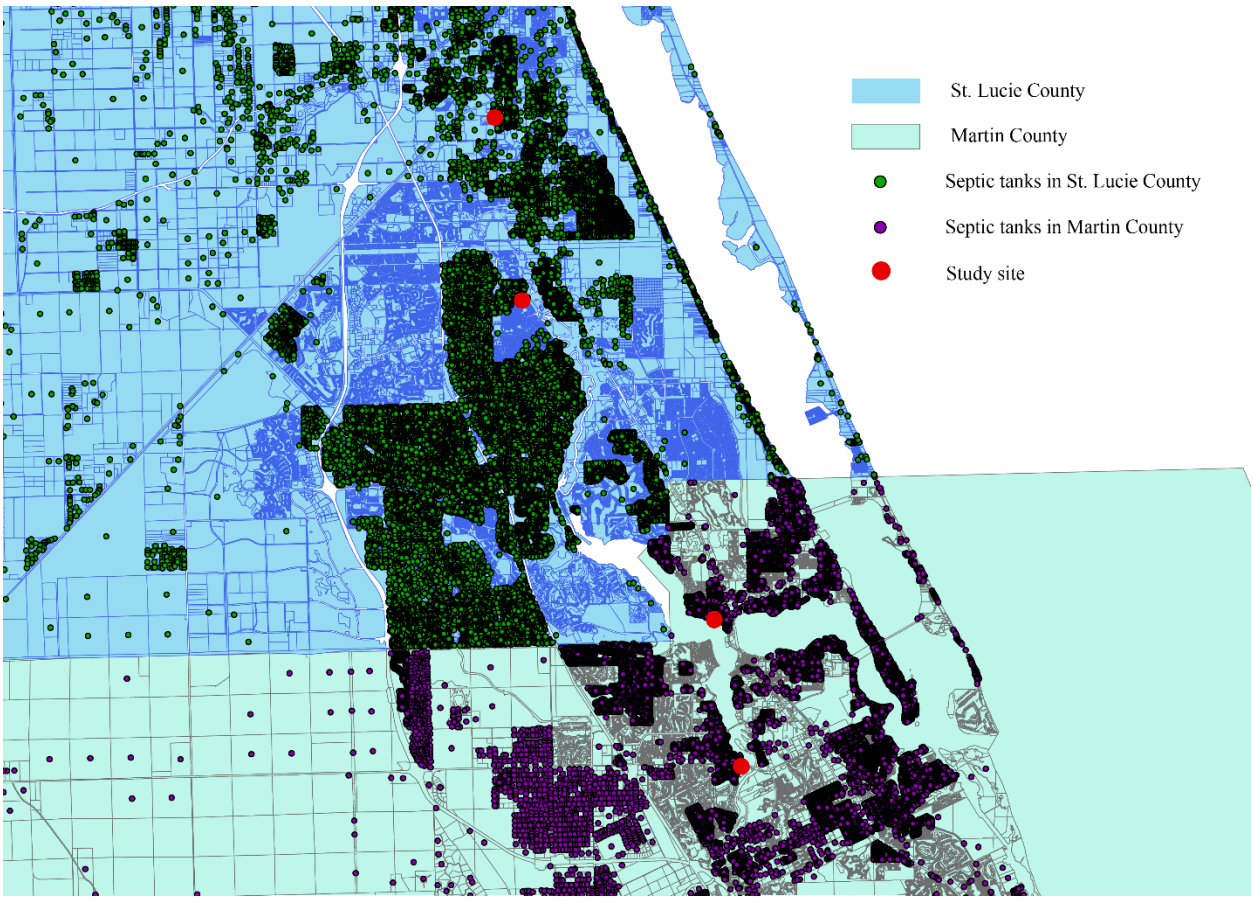

Fig. 3.2. Locations of septic tanks in the study area. Note that only about 1,000 septic tanks were used at each study site (red dots) to reduce computational cost.

The DEM data were downloaded from the USGS website at https://apps.nationalmap.gov/downloader/. The spatial discretization of the data is 3.28 ft × 3.28 ft. The NAD_1983_UTM_Zone_17N projected coordinate system was selected as the projected coordinate system for this study. The DEM data are shown in Fig. 3.3. The DEM used for ArcNLET modeling has the resolution of 32.8 ft × 32.8 ft, and the reasons are given in Section 2.3.

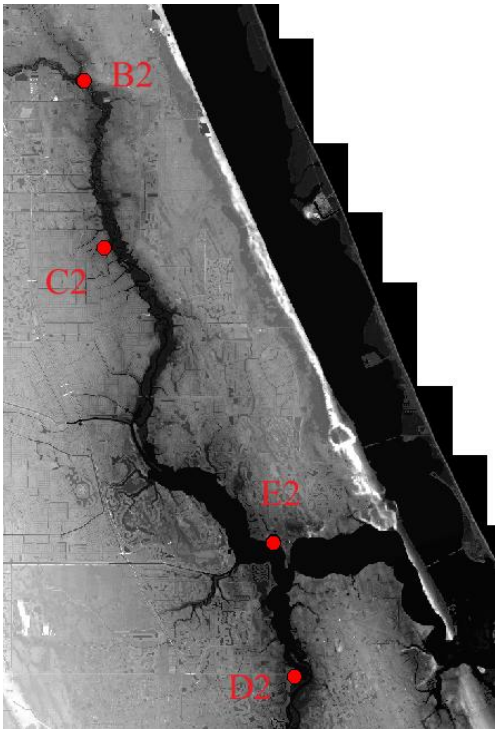

Fig. 3.3. DEM data of the study area. B2 – E2 are the four study sites selected by Belanger and Price (2007).

The water body data were download from the Florida Geographic Data Library at https://fgdl.org/fgdlmap/, and the data were processed in the same way as that described in Section 2.2.3. The drainage network in the area was modified, and canal width was corrected by using Google Earth, which was time consuming. For the St. Lucie River, wetlands of the river were also counted as the river, assuming that nitrogen loading to the wetland flows into the river. This is illustrated in Fig. 3.4.

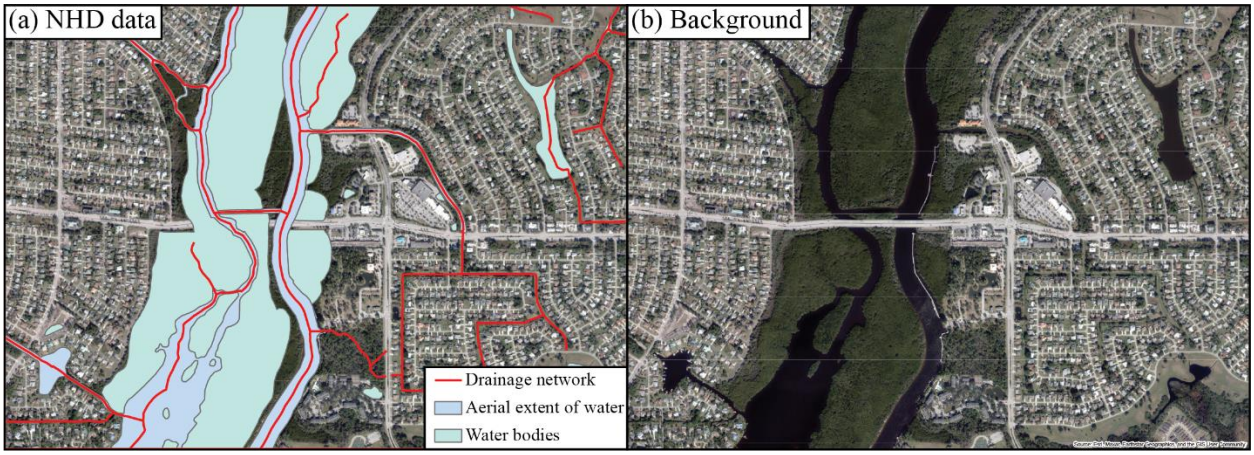

Fig. 3.4. (a) Illustration of processed NHD data and (b) Google Earth view of the same aera. Note that wetlands connected with the St. Lucie River are counted as the river.

The conductivity and porosity data of the study area were obtained from the SSURGO dataset with the assistance of the soilDB package. The soil zone indices of the study area are fl085 and

fl111. The process of processing the SSURGO data is the same as that described in Section 2.2.4. The soil type is sand at the four sites B2 – E2.

3.3 Calibration of ArcNLET Groundwater Flow Module

Although the DEM of fine resolution of 3.28 ft × 3.28 ft was available, the DEM used for ArcNLET modeling has the resolution of 32.8 ft × 32.8 ft for a computational reason. A very large smoothing factor and smoothing cell parameters were needed for the finer resolution, and the smoothing process was time consuming. A smoothing process with smoothing factor of 200 and smoothing cell of 30 took about one hour. This is computationally unaffordable, because smoothing needs to be conducted for tens of times for model calibration in a trial-and-error manner.

In this study, the DEM with the resolution of 32.8 ft × 32.8 ft was first smoothed with a smoothing factor of 40 and a smoothing cell of 7. Afterward, the DEM of water bodies was first extracted and then merged into the smoothed DEM for further smoothing, During the second round of smoothing, the smoothing factor was 5 and the smoothing cell was 7. For the third round of smoothing with the DEM of water bodies merged into the smoothed DEM, the smoothing factor was 2, and the smoothing cell was 7. Based on the smoothed DEM, the simulated flow paths are shown in Fig. 3.5 for the four study sites.

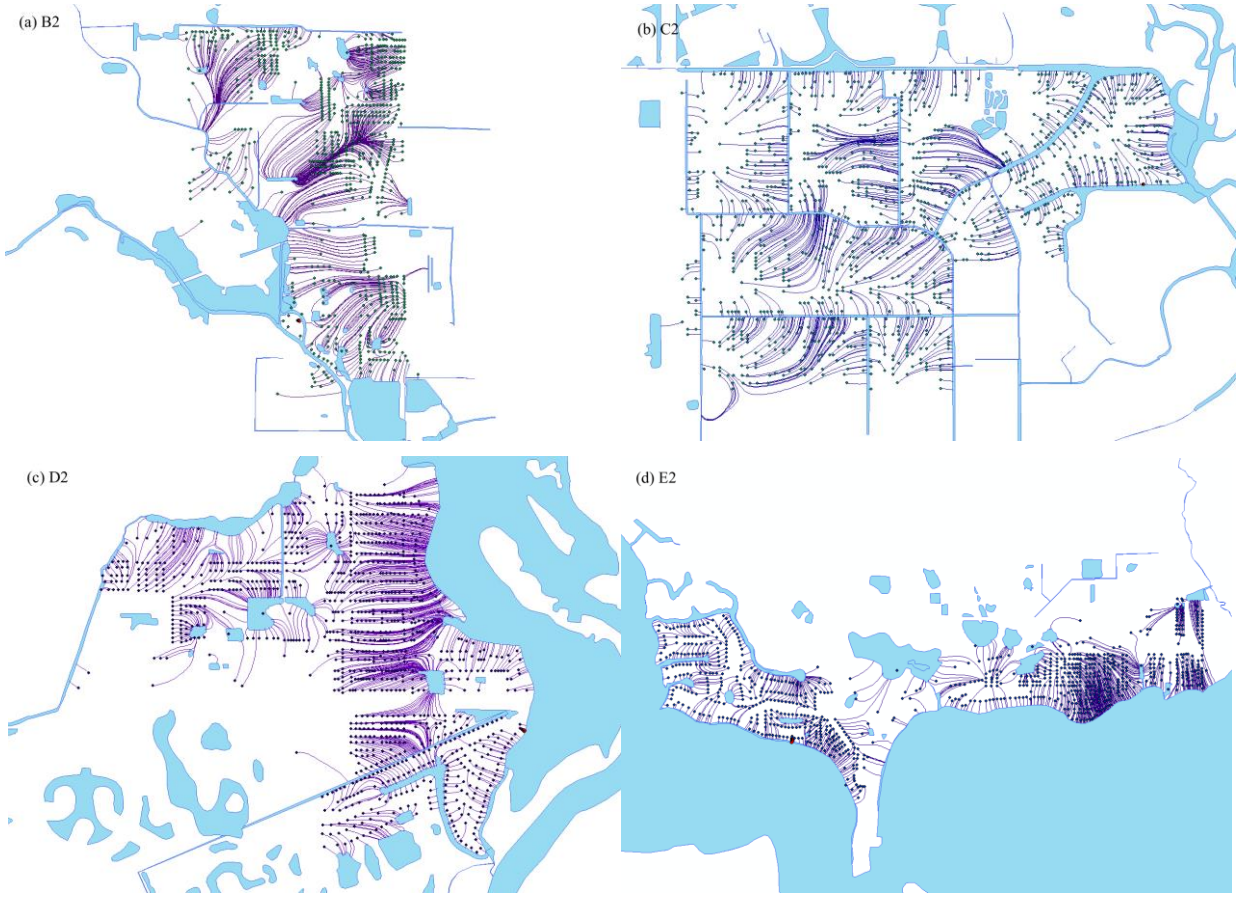

Fig. 3.5. ArcNLET-simulated flow paths from septic tanks to surface water bodies for the four study sites.

The report of Belanger and Price (2007) did not include any measurements of hydraulic head, and we contacted Dr. Belanger, but did not hear from him. The hydraulic heads used for

calibrating the ArcNLET flow module were downloaded from USGS (https://nwis.waterdata.usgs.gov/fl/nwis/gwlevels) and South Florida Water Management District (http://my.sfwmd.gov/dbhydroplsql/show_dbkey_info.main_menu). There are unfortunately no hydraulic head data in the B2 and C2 sites, and there are only four data in the D2 and E2 sites, as shown in Fig. 3.6. Three data locations are in D2 site, and one location in E2 site. The average head values were used to calibrate the groundwater module.

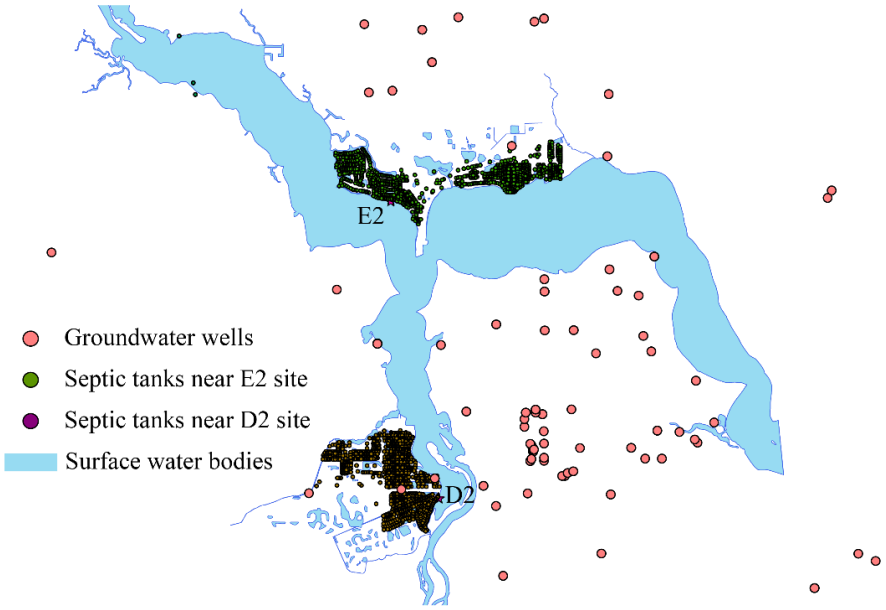

Fig. 3.6. Locations of head data near the D2 and E2 sites.

Fig. 3.7 plots comparison between the four average observed heads and smoothed DEM. While the slope of the fitted line between the two sets of data is 0.95 (close 1), the R^2 value is only 0.443. Fig. 3.7 also indicates that the fit between smoothed DEM and hydraulic head is not as good as that of the Turkey Creek Site discussed in Chapter 2. Nonetheless, the regression curve shown in Fig. 3.7 is comparable with that of Ye and Sun (2013) based on flow module calibration against hydraulic head data in the City of Port St. Lucie. The slope and intercept of the regression line shown in Fig. 3.7 are 0.95 and 3.92, respectively. Their corresponding values given in Ye and Sun (2013) are 1.05 and 5.47. We thus accepted the flow module calibration.

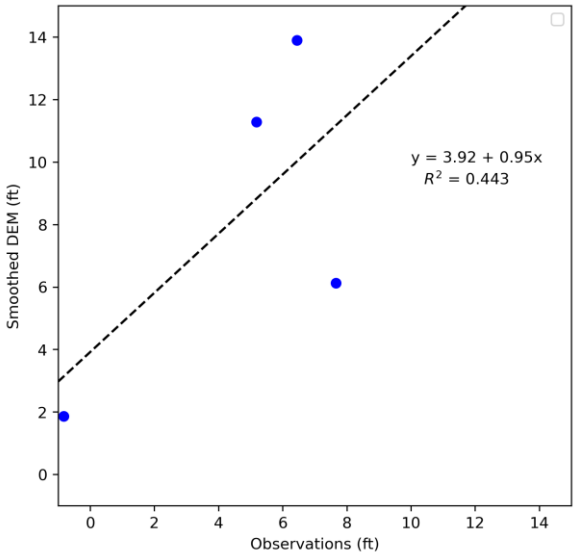

Fig. 3.7. Comparison between average groundwater levels of observation wells in D2 and E2 sites and smoothed DEM.

3.4. Calibration of VZMOD Solute Transport Module

Different from the report of Ayres Associates (1993) that provided a large amount of information to support VZMOD modeling, the report of Belanger and Price (2007) provided a limited amount of information. To determine ammonium and nitrate concentrations at drainfield, we relied on literature data. The average concentration of total dissolved nitrogen concentration in raw wastewater entering septic tanks, effluent leaving septic tanks, and effluent leaving leaching fields are 72, 68, and 44 mg/L, respectively (Valiela et al., 1997). From Toor et al. (2020) and Lowe et al. (2007), the total nitrogen concentration in septic effluent is in the range of 30-170 mg/L with the average of 60 mg/L. This is similar to the mean value of 61 mg/L (median value of 65 mg/L) of four sites reported by Lowe et al. (2009).

The nitrogen concentration of septic effluent can also be estimated. A number of studies used 4.8 kg/y (13.15 g/d) for annual nitrogen release per people (Watson et al., 1967; Branders 1978; Seigrist et al., 1976; North Carolina Department of Natural Resources and Community Development, 1986; Valiela et al., 1997). Assuming household population of 2.5 people (Ye and Sun, 2013), nitrogen release per household is 32.88 g/d. Each person in Florida produces about 100 gallons of domestic wastewater each day (https://floridadep.gov/water/domestic-wastewater#:~:text=Each%20person%20in%20Florida%20generates,aesthetic%20appeal%20of%20our%20waterways). According to the Florida Department of Health, 69.3 gallons of wastewater flows to OSTDS per person per day (https://floridadep.gov/water/domestic-wastewater/content/general-facts-and-statistics-about-wastewater-florida). As a result, the nitrogen concentration of wastewater entering septic tanks is between 34.74 mg/L and 50.13 mg/L. The estimates are smaller than the literature values discussed above.

In septic tanks, nitrogen is present in the form of NH_4-N, NO_3-N, and organic nitrogen. NH_4-N accounts for approximately 70% to 90% of the total nitrogen, and organic nitrogen makes up around 10% to 30%, and NO_3-N can be ignored. In the drainfield, the concentration of NH_4-N reaches the maximum value. We assumed in this study that, at the drainfield, NH_4-N and NO_3-N concentrations are 40 mg/L and 0.01 mg/L, respectively.

For other VZMOD parameters, we only calibrated the first-order nitrification rate K_{nit} and the first-order denitrification rate K_{dnt}, and used the VZMOD default values for other parameters. The default and calibrated K_{nit} and K_{dnt} values are listed in Table 3.2. The calibrated values are within the ranges given by McCray et al. (2005). To estimate the distance from the drainfield infiltrative surface to water table, we again used a formula A−B, as discussed in Section 2.5. The value of A is 3.92 ft, as shown in Fig. 3.7, and the B value is 18 inches for B as suggested in the VZMOD user manual. Therefore, the distance (DTW) from the drainfield to water table is 2.42 feet (73.76 cm). Fig. 3.8 is the user interface of the VZMOD simulation with all parameter values shown.

Table 3.2 Comparison of parameters used by VZMOD and the parameter ranges given in McCray et al. (2005).

	Default	Calibrated	McCray et al., 2005
K_{nit} (1/d)	2.9	0.25	0.0768~211.2
K_{dnt} (1/d)	0.025	0.4	0.004~2.27

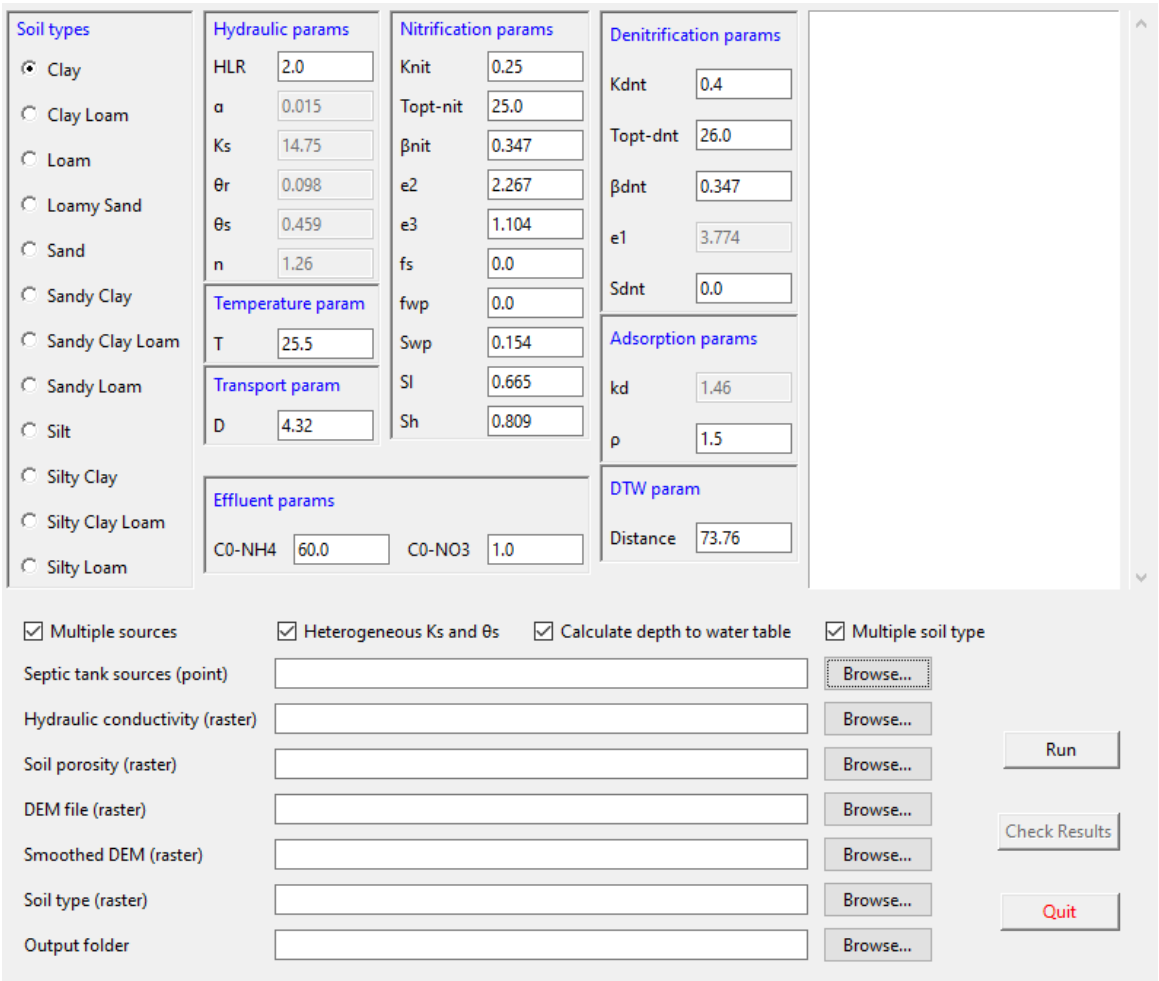

Fig. 3.8. VZMOD parameters used for the St. Lucie River modeling.

Fig. 3.9 plots the histograms of VZMOD-simulated NH_4-N and NO_3-N concentrations at water table at the four sites B2 – E2. NH_4-N concentrations are significant, because the soil types of the four sites are all sand and the nitrification process did not convert all NH_4-N into NO3-N. If the distance between drainfield and water table is small, the NH_4-N concentration can be high, close

40 mg/L. The NO_3-N concentrations are also relatively high, indicating inadequate denitrification in the vadose zone. This is confirmed by Fig. 3.10 that plots the vertical profiles of NH_4-N and NO_3-N concentrations, water saturation, nitrification factor, and denitrification factors at sites B2 – E2. Because the soil types at the four sites are all sand, the nitrification and denitrification factors are small. As a result, ammonium and/or nitrate concentrations are high even at the depth of 3 – 5 ft.

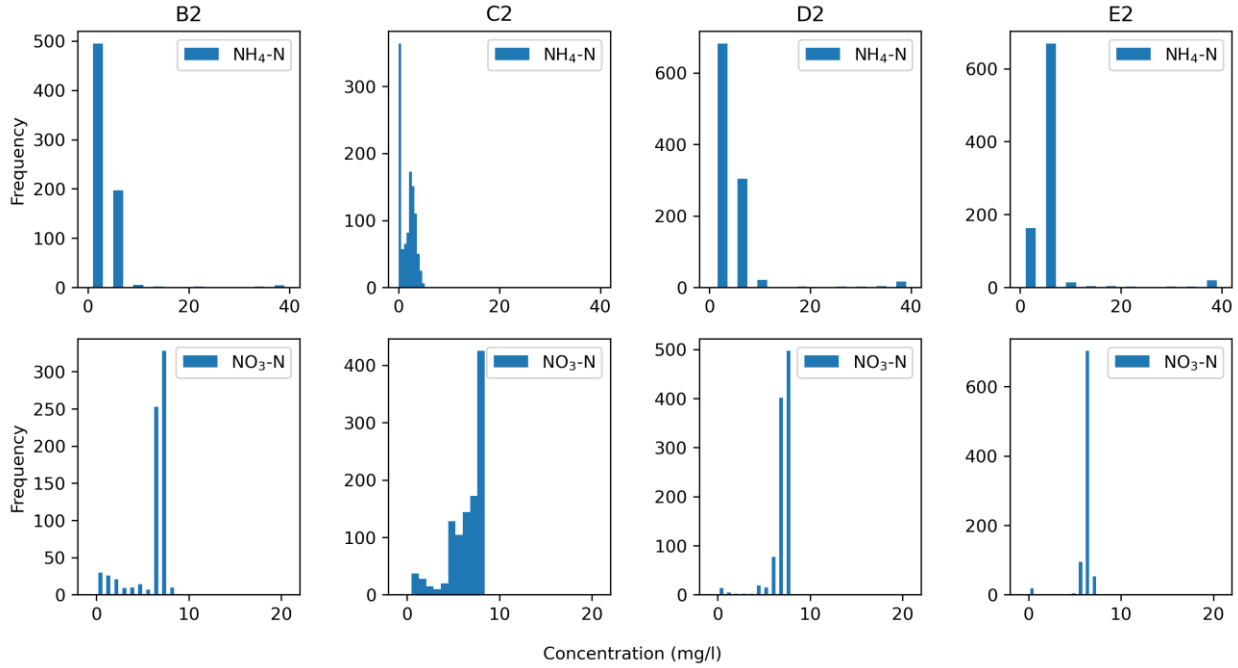

Fig. 3.9. Histogram of VZMOD-simulated concentrations of NH_4-N and NO_3-N at water table.

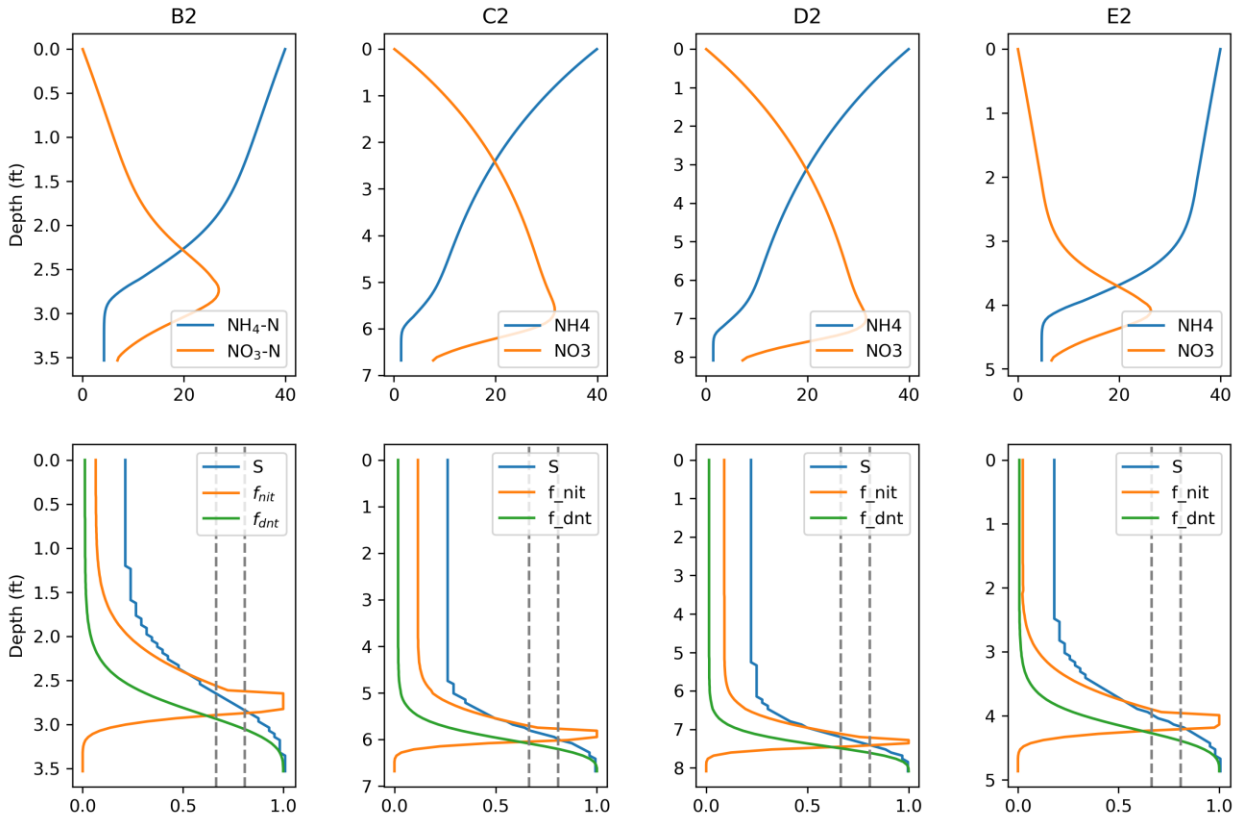

Fig. 3.10. Vertical profiles of NH_4-N and NO_3-N concentrations, water content, and water content related factors of nitrification and denitrification at sites B2 – E2.

3.5. Calibration of ArcNLET Solute Transport Module

ArcNLET simulated NH_4-N and NO_3-N concentrations in groundwater for about 1,000 OSTSD at each of the four sites. The ArcNLET default parameter values were used for the simulation, and they are shown in Fig. 3.10. We attempted to adjust the values of longitudinal dispersivity and horizontal transverse dispersivity, but it did not improve model simulation results in comparison with those given by the default parameter values. It should be noted that drainfield locations were not given by Belanger and Price (2007) for the four sites. This can substantially affect ArcNLET simulation results.

Fig. 3.11 plots together the ArcNLET-simulated NO_3-N and NH_4-N plumes and the observed values for sites B2, C2, D2, and E2. For site B2, while the observation points are located in the simulated plumes, the observed NH_4-N and NO_3-N concentrations are negligible and substantially smaller than the simulated concentrations. Belanger and Price (2007) suspected that the flow direction is not in the northeast direction, which is the ArcNLET simulated flow direction, and thus abandoned site B2. For site C2, ArcNLET did not simulate the observed concentrations well. This is not surprising, because the spatial distribution of the observed concentrations is not symmetric, while the ArcNLET simulated plume is symmetric. For site D2, the observed NH_4-N concentrations are large at locations far away from a hypothetical drainfield, but small at locations close to the drainfield. This may be caused by other nitrogen sources (e.g., fertilizer uses), but ArcNLET only considers nitrogen reactive transport due to OSTDS. For site E2, the spatial

distribution of observed NH_4-N and NO_3-N concentrations is also unexpected, in that larger values occurs in the middle observation locations. Due to the unknown locations of drainfields and unknown potential nitrogen sources, ArcNLET did not simulate well spatial patterns of observed nitrogen concentrations.

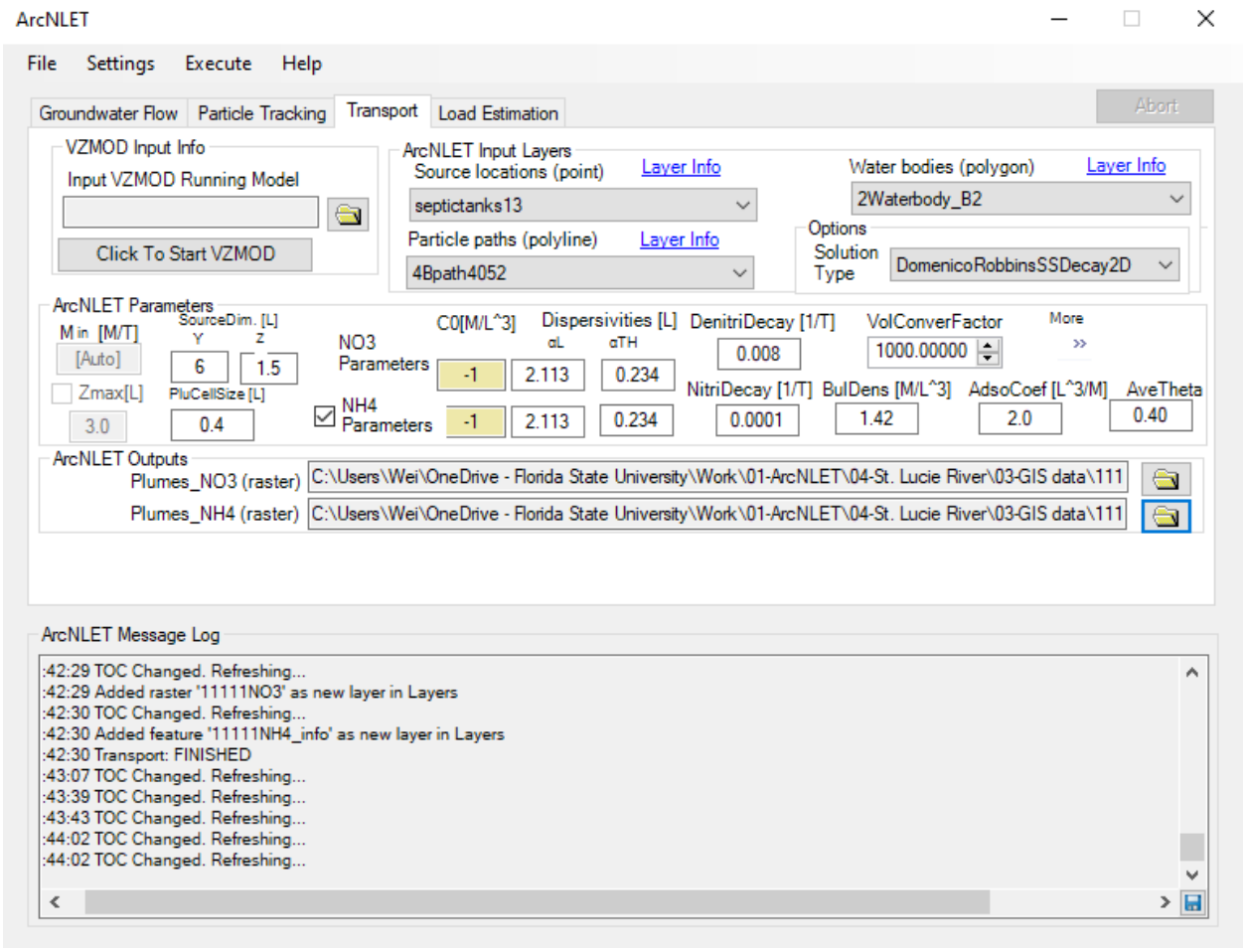

Fig. 3.10. ArcNLET interface for simulating ammonium and nitrate concentrations in groundwater.

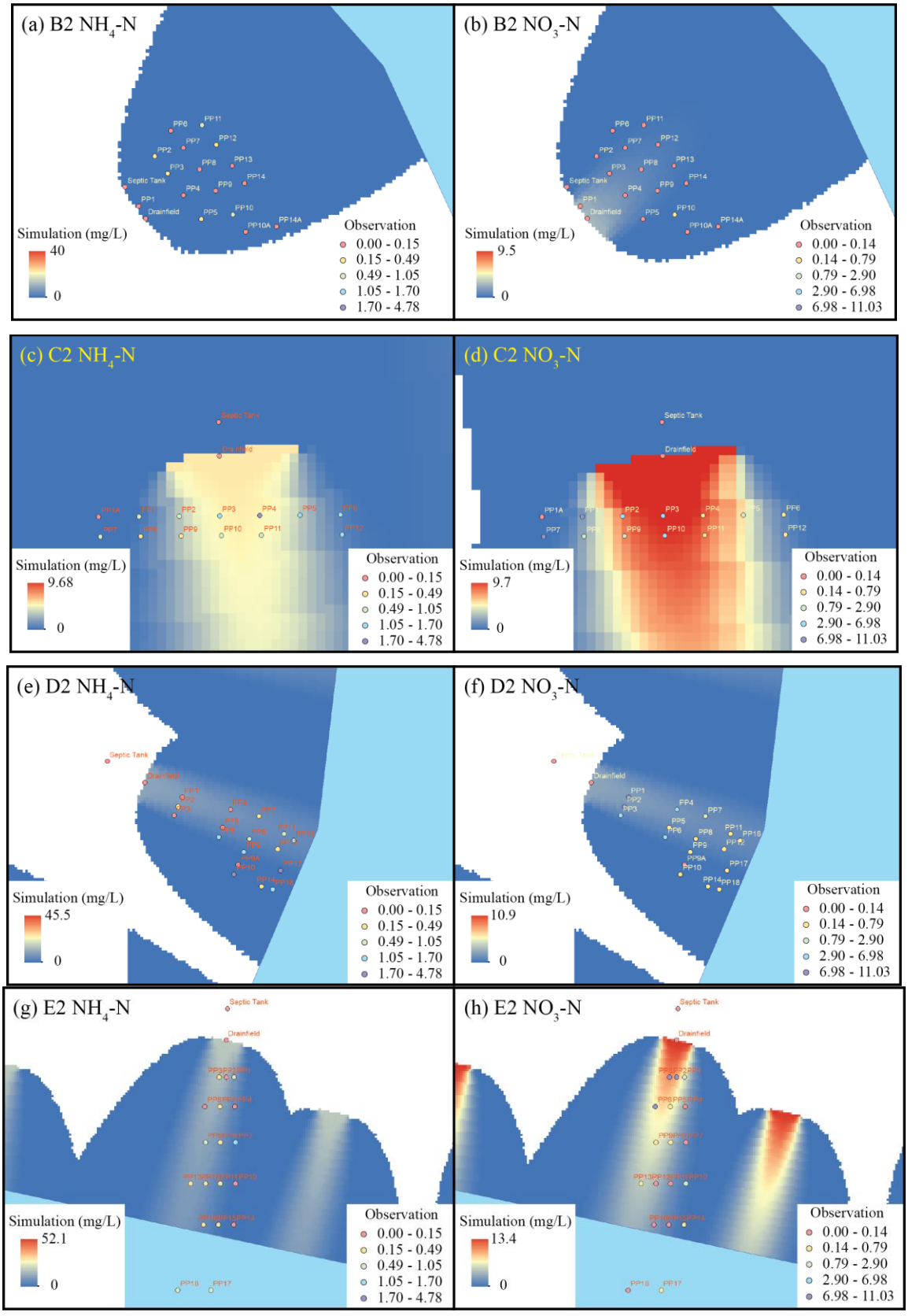

Fig. 3.11 Simulated NO_3-N and NH_4-N plumes and observed concentrations at sites B2 – E2.

Fig. 3.12 plots the observed NH_4-N and NO_3-N concentrations and their corresponding model simulations at the four sites. These data do not fall on the 1:1 lines, indicating that the model did not simulate well the observations. However, the observed and simulated concentrations are within the same range at sites C2 – E2. Fig. 3.13 thus compares the averages of the simulated and observed NH_4-N and NO_3-N concentrations. The average simulations match the average observations reasonably well, except at site B2. We thus accepted the calibrated ArcNLET transport module.

The calibrated VZMOD and ArcNLET models were used to simulate nitrogen reactive transport due to about 1,000 OSTDS at each of the four sites for investigating the vertical and horizontal setback distances.

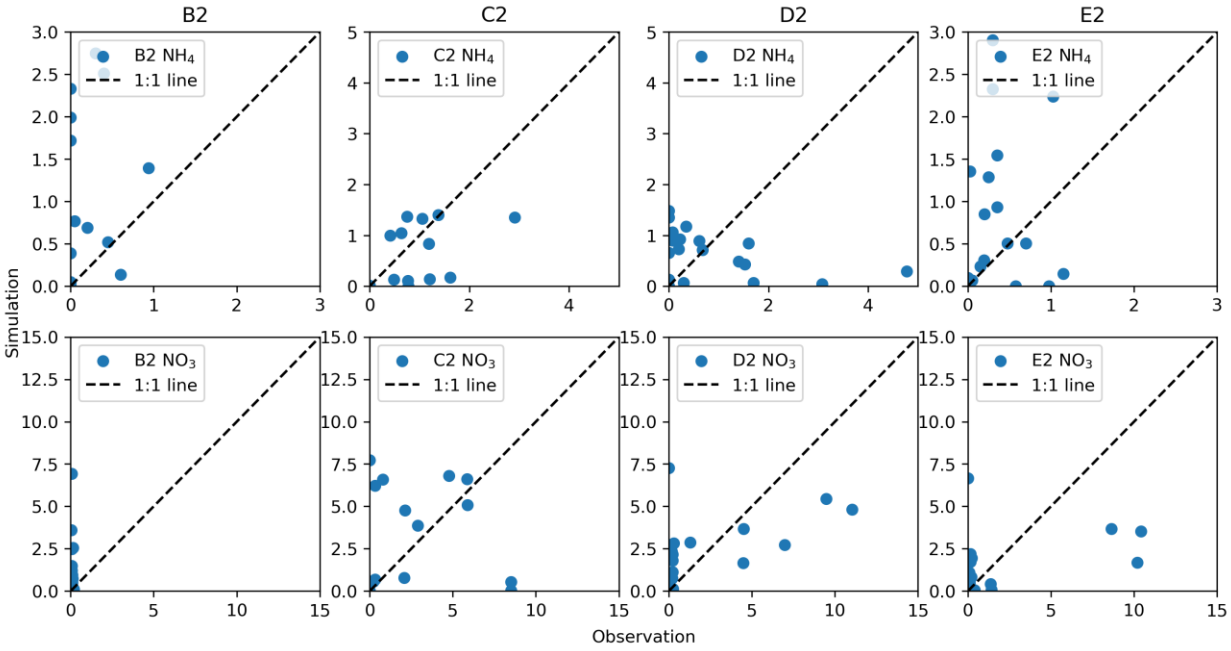

Fig. 3.12. Comparison of simulated and observed NH_4-N and NO_3-N concentration at the four sites of B2 – E2.

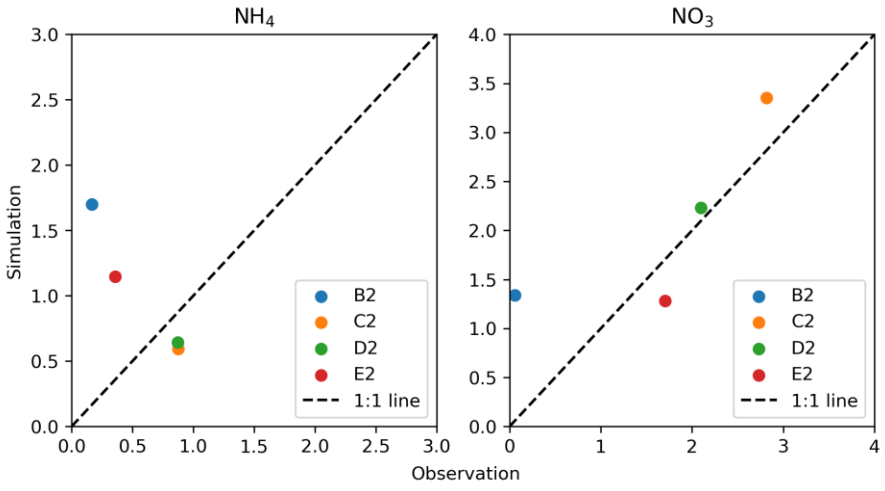

Fig. 3.13. Comparison between the averages of simulated and observed NH_4-N and NO_3-N concentrations at sites B2 – E2.

3.6 Vertical Setback Distance from Drainfield to Water Table

Fig. 3.15 plots the vertical nitrogen attenuation rate ($1 - C_{WT}/C_{DF}$) with the vertical distance (VD) from drainfield to water table groundwater for four soil types in the study area. Although the soil type is sand at the four study sites B2 – E2, the study area, which is substantially larger than the study sites, has four soil types. The numbers of OSTDS in the sand, sandy clay loam, sandy loam, and loamy sand soils are 3207, 7, 173, and 319, respectively. The soil types of the Turkey Creek sub-basin are also sand, sandy clay loam, sandy loam, and loamy sand (Chapter 2). Similar to Fig. 2.42 of Chapter 2 for the Turkey Creek sub-basin, Fig. 15 also shows that the vertical nitrogen attenuation rate increases with the vertical distance for all soil types. Different from the Turkey Creek sub-basin where the threshold value of vertical distance is 2ft, Fig. 3.15 shows that the threshold is about 2.5 ft. For the sand and loamy sand, the maximum attenuation rate is about 80% and 90%, respectively, even with large vertical distance. This is also shown in Fig. 3.16 that plots the histogram of the vertical nitrogen attenuation rate for each soil type. For sandy loam and sandy clay loam, the attenuation rates can be 100%. The rates are less than 90% for sand and loamy sand, due to relatively small nitrification and denitrification for the two soil types, as discussed in Section 3.4.

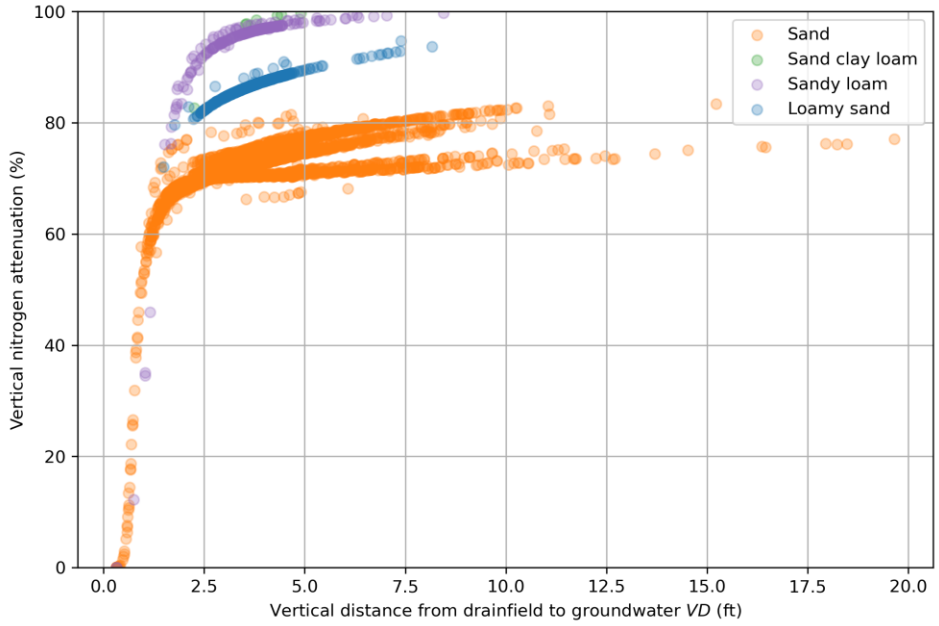

Fig. 3.15. Relation between vertical nitrogen attenuation rate ($1 - C_{WT}/C_{DF}$) and the vertical distance, VD, from drainfield to groundwater VD for four soil types.

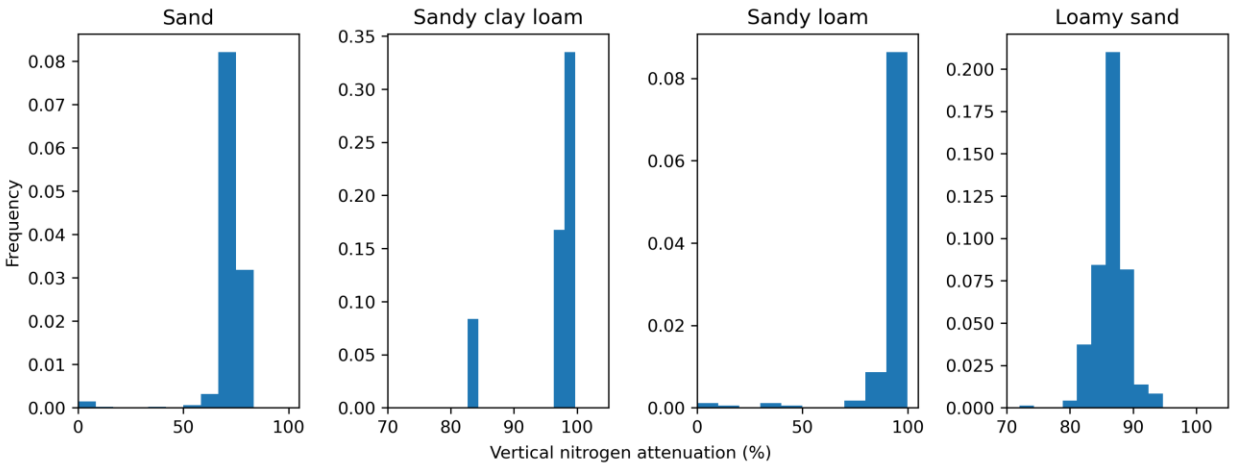

Fig. 3.16. Histograms of vertical nitrogen attenuation rate for four soil types.

3.7 Horizontal Setback Distance from Water Table to Water Body

Figs. 3.17 and 3.18 plot the histograms of NH_4-N and NO_3-N concentrations at water table (C_{WT}) and water body (C_{WB}) for the four soil types. The two figures show that, for each soil type, nitrogen concentrations at water body are smaller than the nitrogen concentrations at water table. Taking NO_3-N concentrations of sand as an example, the concentrations at water table are between 5.0 and 7.5 mg/L (Fig. 3.17), but they are reduced to 0 and 2 mg/L at water body (Fig. 3.18). The attenuation of NH_4-N is attributed to adsorption and a small amount of nitrification in groundwater, and the attenuation of NO_3-N is attributed to the denitrification.

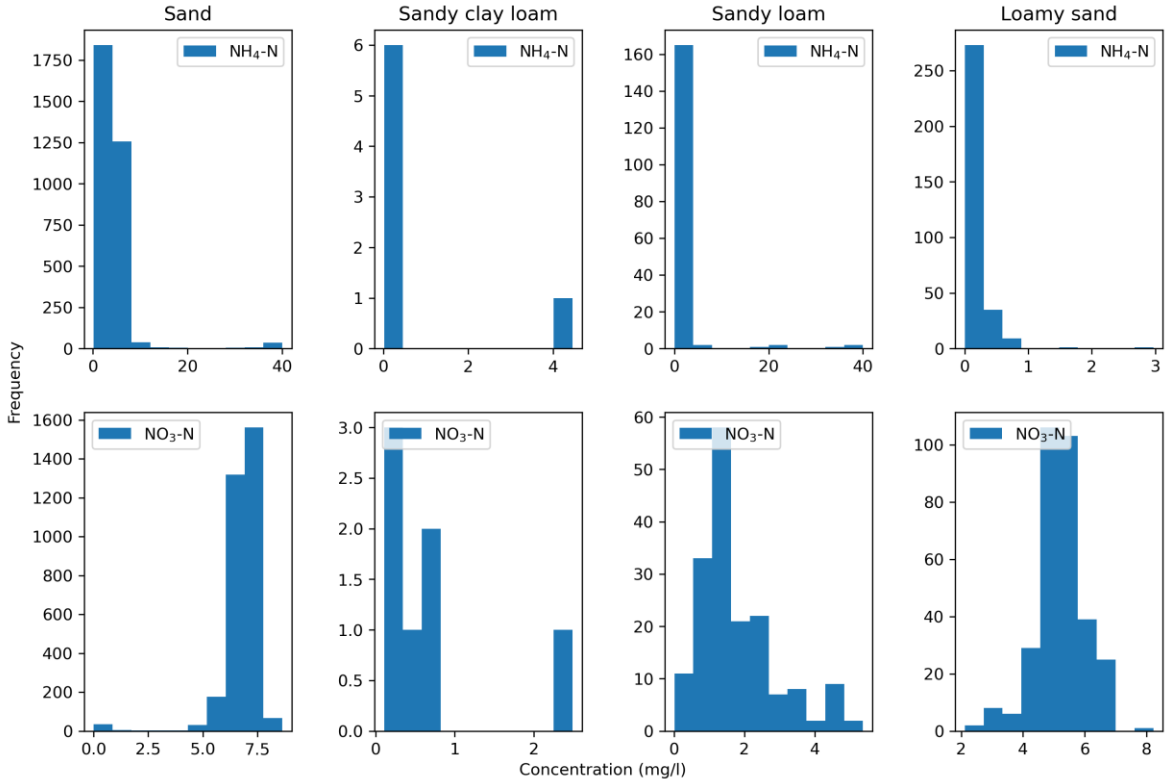

Fig. 3.17. Histograms of C_{WT} (NH_4-N and NO_3-N) for four soil types.

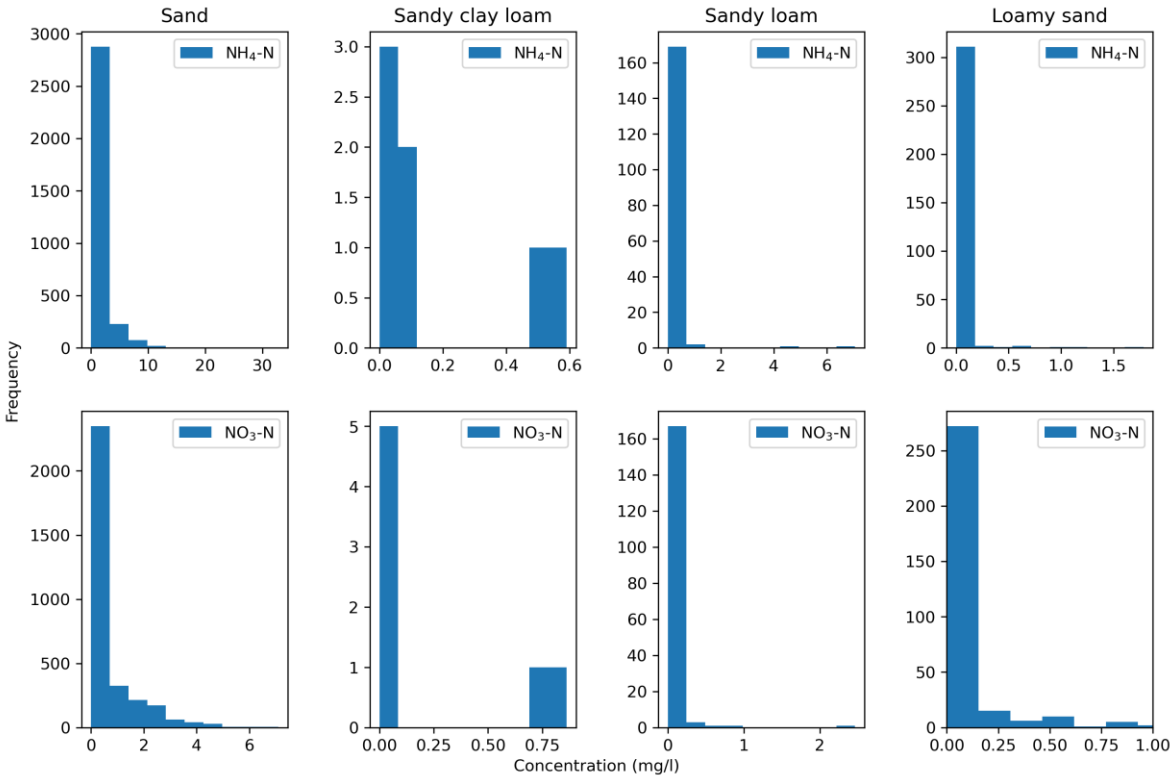

Fig. 3.18. Histograms of C_{WB} (NH_4-N and NO_3-N) for four soil types.

Fig. 3.19 plots the relations between horizontal nitrogen attenuation rate ($1 - C_{WB}/C_{WT}$) and the horizontal linear distance from drainfields to water bodies. The figure shows that, for all soil types, the horizontal nitrogen attenuation rate ($1 - C_{WB}/C_{WT}$) gradually increases with the linear horizontal distance HD_L. Fig. 3.20 is similar to Fig. 3.19, but plots the averaged horizontal nitrogen attenuation rate for every 10 ft of horizontal distance. Fig. 3.20 also plots the empirical expression

$$1 - C_{WB}/C_{WT} = 100 \times AF \times (1 - e^{((-HD_L)/(4\times K_s+20))}) \quad (3.1)$$

obtained in Chapter 2 for the Turkey Creek sub-basin, where AF is the adjust factor for the maximum nitrogen attenuation when the horizontal linear distance is large enough. The AF value was set as 95% for sand and 100% for the other three soil types.

Plume overlaps also affect the calculation of nitrogen attenuation rate, because nitrogen concentrations (C_{WB}) at the end of a flow path may be affected by concentrations of other plumes. This is illustrated in Fig. 3.21 for an area near site E2. For the condition of plume overlap, C_{WB} may be overestimated, and the horizontal nitrogen attenuation rate may be underestimated.

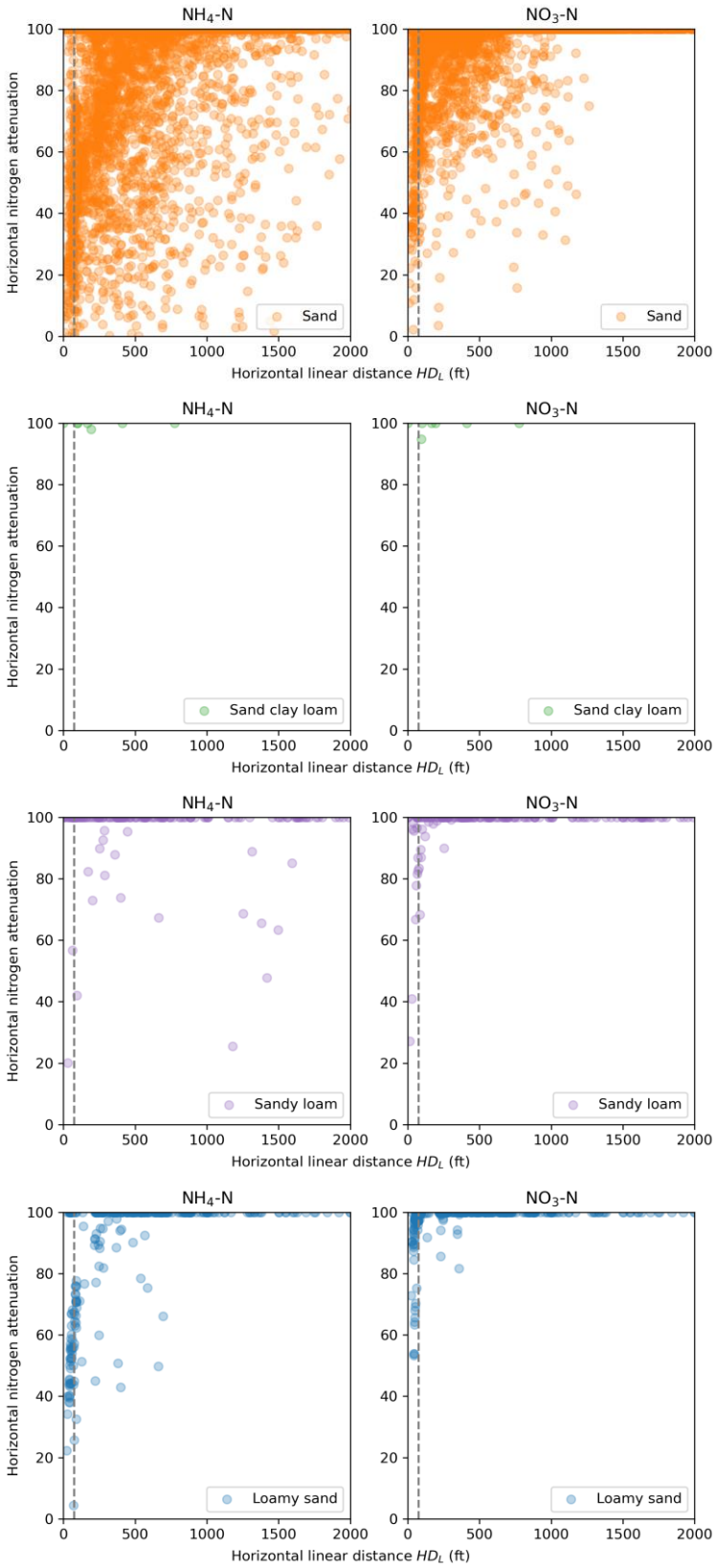

Fig. 3.19. Relations between horizontal nitrogen attenuation rate ($1 - C_{WB}/C_{WT}$) and linear horizontal distance (HD_L) from drainfield to waterbody for four soil types.

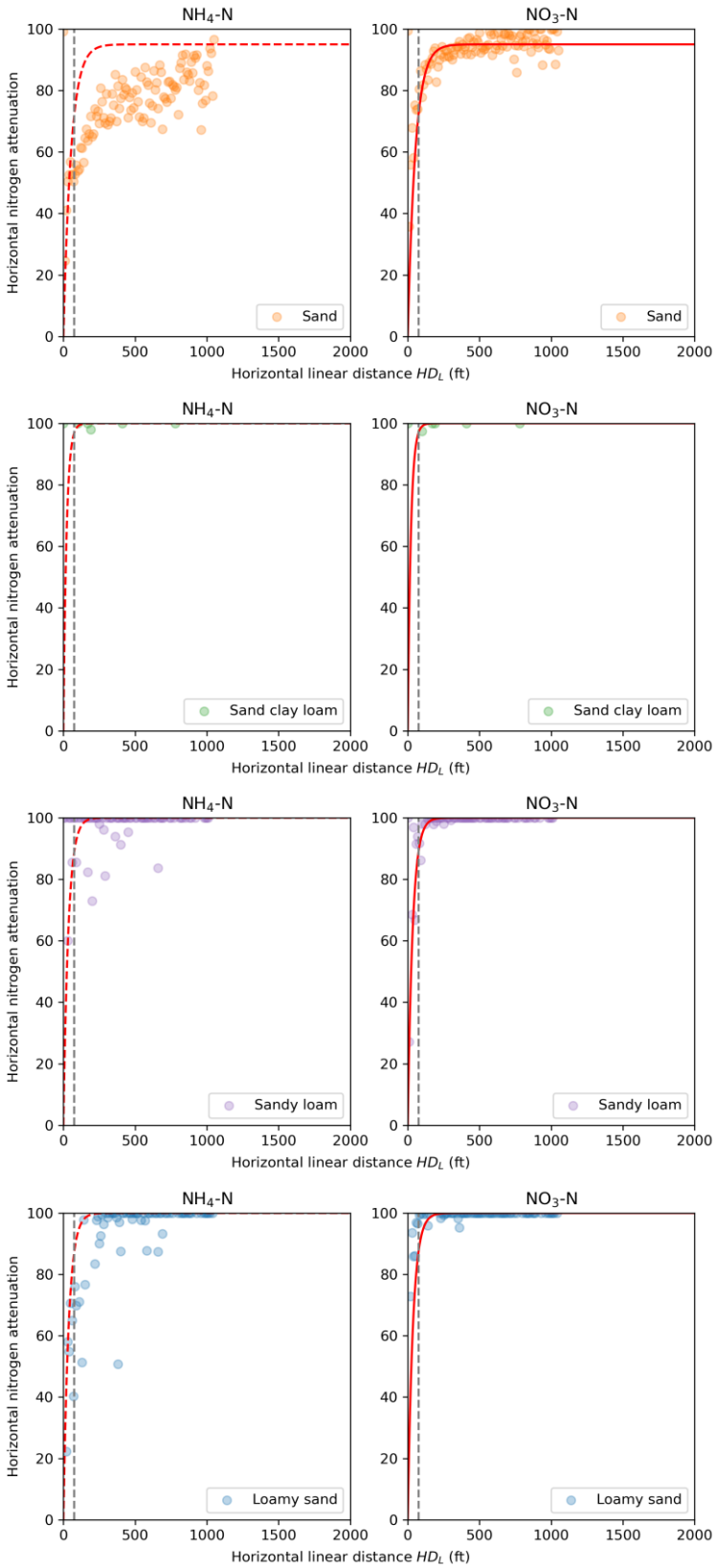

Fig. 3.20. Relations between horizontal nitrogen attenuation and the linear horizontal distance after averaging hydraulic gradient for every 10 feet of the distance.

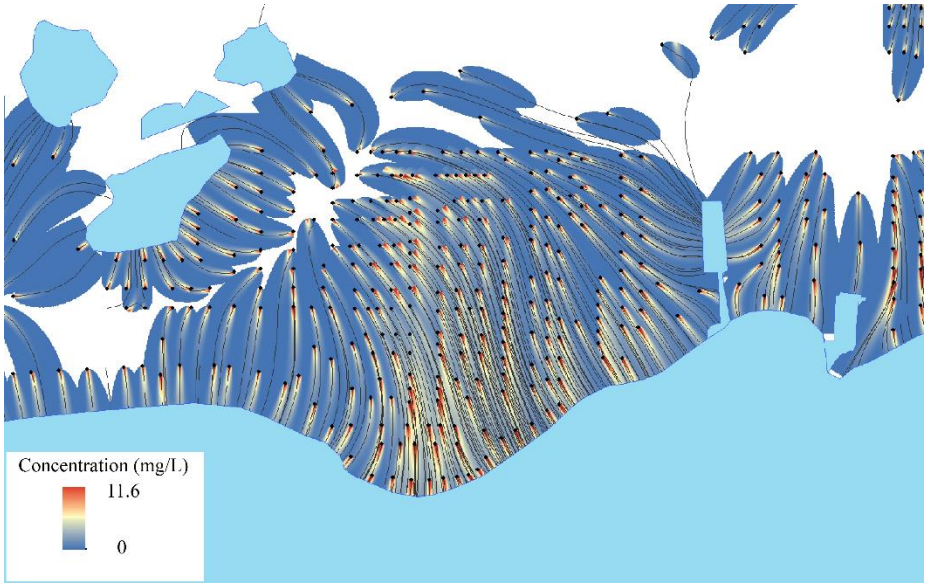

Fig. 3.21. Illustration of overlapped of NO_3-N plumes near site E2.

3.8 Sensitivity analysis to simultaneously determine vertical and horizontal setback distances

Seven actual OSTDS were chosen and three virtual OSTDS were added in an area near site D2 for the sensitivity analysis to simultaneously determine the vertical and horizontal setback distances. The locations of the ten OSTDS are shown in Fig. 3.22, and the linear horizontal distance between the OSTDS and the St. Lucie River are listed in Table 3.3. The vertical distance of each septic tank varies between 0.3 ft and 9.8 ft, and the range was divided into 29 intervals with 30 vertical distances. Four values of hydraulic conductivity were used, and they are those for sandy clay loam, sandy loam, and loamy sand. We thus run VZMOD and ArcNLET for a total of 1,200 = 10 × 30 × 4 combinations of horizontal distance/hydraulic gradient, vertical distance, and hydraulic conductivity.

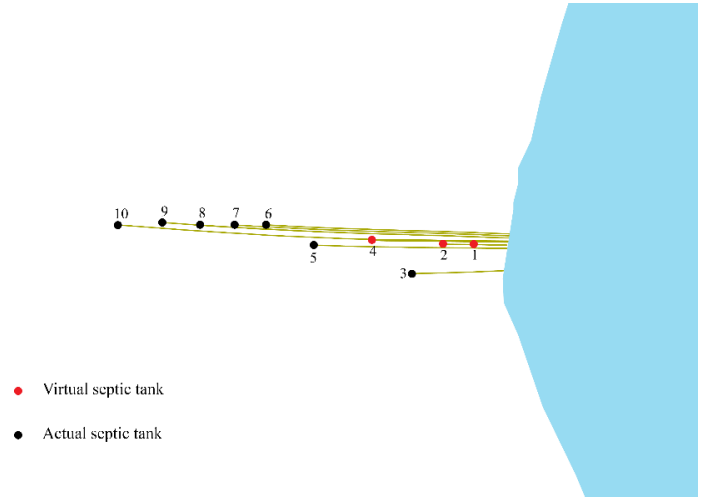

Fig. 3.22. Actual and virtual OSTDS used for sensitivity analysis to determine the relation between total nitrogen attenuation rate and two setback distances.

Table 3.3. Linear distance from OSTDS to water body for ten OSTDS.

OSTDS Index	1	2	3	4	5	6	7	8	9	10
Linear distance (ft)	75	135	187	274	387	486	547	615	689	776

Based on the results of the 1,320 model simulation results, for each soil type, we plotted the contours of the total nitrogen attenuation rate with the horizontal and vertical setback distances. We also did this for the concentrations of NH_4-N and NO_3-N entering the canal (i.e., at the end of the groundwater flow paths). These contours are shown in Fig. 3.23. This figure is similar to Figure 2.64 of Chapter 2 for the Turkey Creek sub-basin, and leads to the same conclusions discussion in Section 2.9.3. One of the conclusion is that, for the current regulation criterion of 75 ft horizontal setback distance, it should be adequate for nitrogen attenuation, as long as the vertical distance between drainfields and water table is 2 ft. Otherwise, a larger horizontal setback distance is needed. For sand soil, a larger horizontal setback distance may be still needed even when the vertical distance is 2 ft, due to relatively small amount of nitrification and denitrification in the vadose zone.

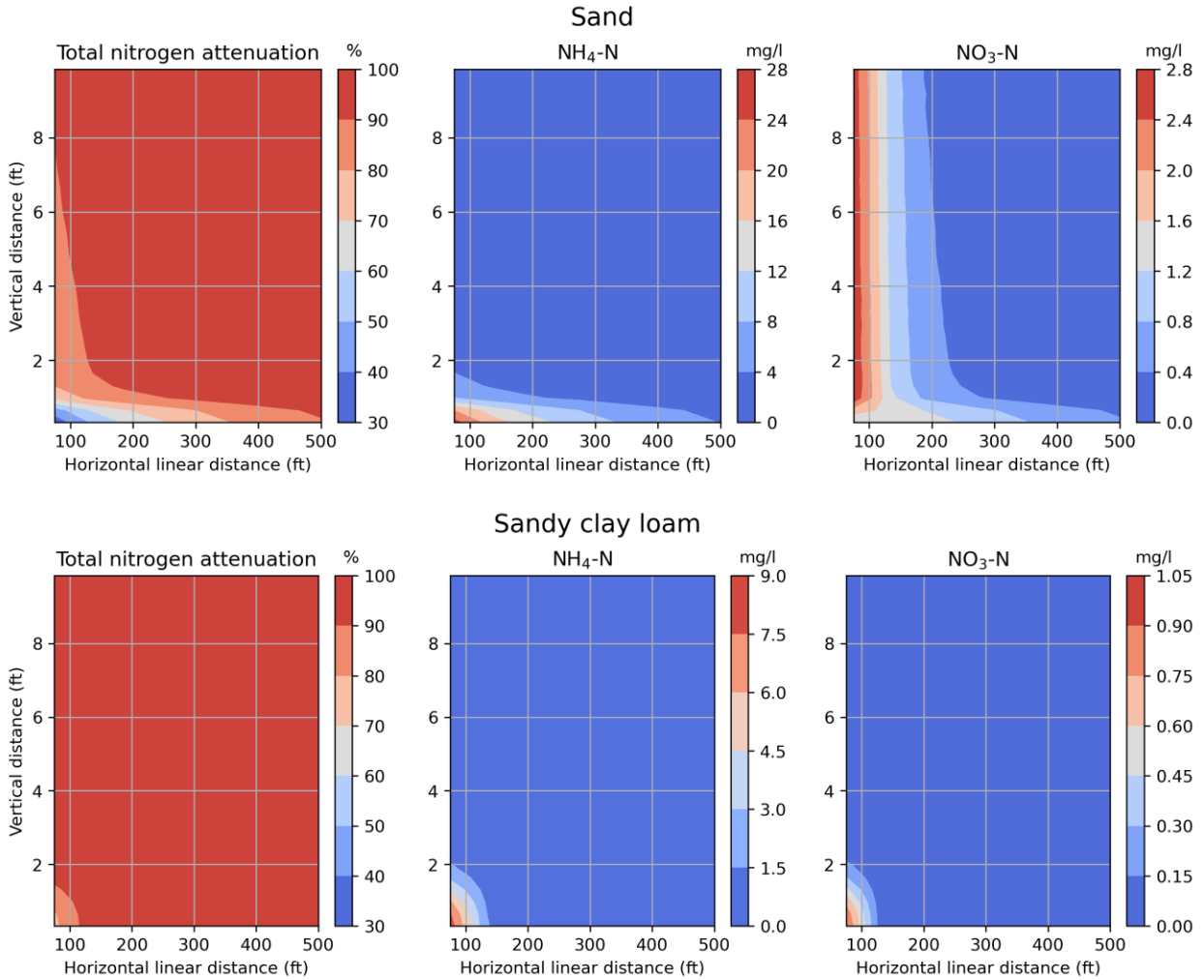

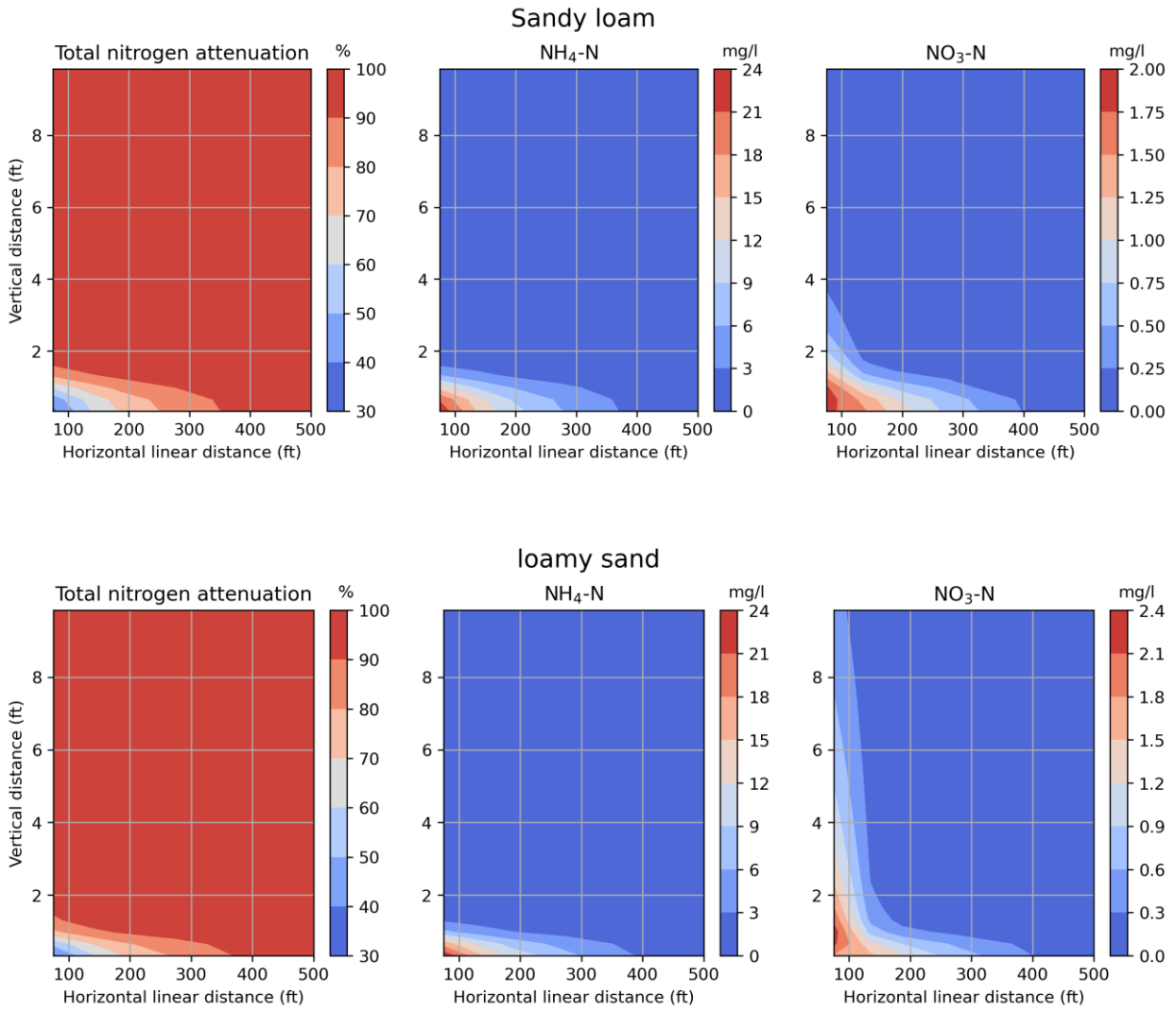

Fig. 3.23. Relations between nitrogen attenuation as well as concentrations of NH_4-N and NO_3-N entering the canal and the horizontal linear distance and vertical distance for four soil types. The smallest horizontal distance is 75 ft.

3.9. Summary and Conclusions

This chapter presented our work of setting up VZMOD and ArcNLET models, calibrating the models against observed hydraulic heads and NH_4-N and NO_3-N concentrations at four sites (B2 – E2) near the St. Lucie River, and used to calibrated models to simulate flow and nitrogen reactive transport at a study area with about 4,000 OSTDS. The simulation results, together with a sensitivity analysis of 1,200 simulations, were used to explore the relation between nitrogen attenuation rates with the vertical and horizontal setback distances.

The results and conclusions presented in this chapter are similar to those presented in Chapter 2. This is not surprising, because the results are based on the same models (VZMOD and ArcNLET). The difference between the simulations of Chapter 2 and this chapter is that different values of certain parameters were used. Nonetheless, the similarity in the results and conclusions between the two study sites is still meaningful for investigating vertical and horizontal setback

distance. It appears that consistent conclusions can be reached across multiple sites, given that the VZMOD and ArcNLET models were calibrated against site-specific data. In addition, all the data for the sensitivity analysis are real-world data, and the results of the sensitivity analysis are similar. More interestingly, the empirical equations for the horizontal attenuation rate works for the two sites. This however is empirical, and needs to be further evaluated by conducting VZMOD and ArcNLET modeling for other sites, which is ongoing.

References

Belanger, T.V., Price, T.L. 2007. OSDS impacts on the St. Lucie River and Indian River Lagoon. St. Lucie River Issues Team.

Lowe, K.S., Tucholke, M.B., Tomaras, J.M.B., Conn, K., Hoppe, C., Drewes, J.E., McCray, J.E., Munakata-Marr, J., 2009. Influent Constituent Characteristics of the Modern Waste Stream from Single Sources. Water Environment Research Foundation. Technical Report 04-DEC-01.

Lowe, K.S., Rothe, N.K., Tomaras, J.M.B., DeJong, K., Tucholke, M.B., Drewes, J.E., McCray, J.E., Munakata-Marr, J., 2007. Influent Constituent Characteristics of the Modern Waste Stream from Single Sources: Literature Review. Water Environment Research Foundation. Technical Report 04-DEC-1a.

Toor, G.S., Lusk, M., Obreza, T., 2020. Onsite sewage treatment and disposal systems: nitrogen. UF/IFAS Extension, Gainesville, FL 32611.

Valiela, I., G. Collins, J. Kremer, K. Lajtha, M. Geist, B. Seely, J. Brawley, C.H. Sham. 1997. Nitrogen loading from coastal watersheds to receiving estuaries: new method and application. Ecological Applications, 7(2), 358–380.

Ye, M., Sun, H. 2013. Estimation of nitrogen load from removed septic systems to surface water bodies in the city of Port St. Lucie, the city of Stuart, and Martin County. Department of Scientific Computing, Florida State University, Tallahassee, FL 32306.

Chapter 4. Numerical Investigation of OSTDS Setback Distances for Three Sites with Loading to Lower St. Johns River Basin and its Tributaries

This chapter presents our modeling investigation of OSTDS setback distances based on the data collected by Belanger et al. (2011) at three study sites with loading to the lower St. Johns River Basin and its tributaries. Since the procedure of the modeling investigation is similar to that discussed in Chapter 2 for the Turkey Creek sub-basin, this chapter only presents necessary details related to the Lower St. Johns River Basin.

4.1. Study Sites and Study Areas

Belanger et al. (2011) considered five sites as follows: Eggleston Heights, Julington Creek (this site includes Julington Creek, Hood Landing, and Julington Hill; for the convenience of discussion, the three sites are referred to as Julington Creek here), Lakeshore, Murray Hill B, and Oak Lawn. The former three sites (Fig. 4.1) were considered in this study, because OSTDS were converted into public sewers in Murray Hill B and there was only one monitoring location in Oak Lawn. In this chapter, the homes where monitoring data were obtained by Belanger et al. (2011) are referred to as study sites, and our ArcNLET modeling domains are referred to as study areas. Each area has more than 3,000 OSTDS including those studied by Belanger et al. (2011).

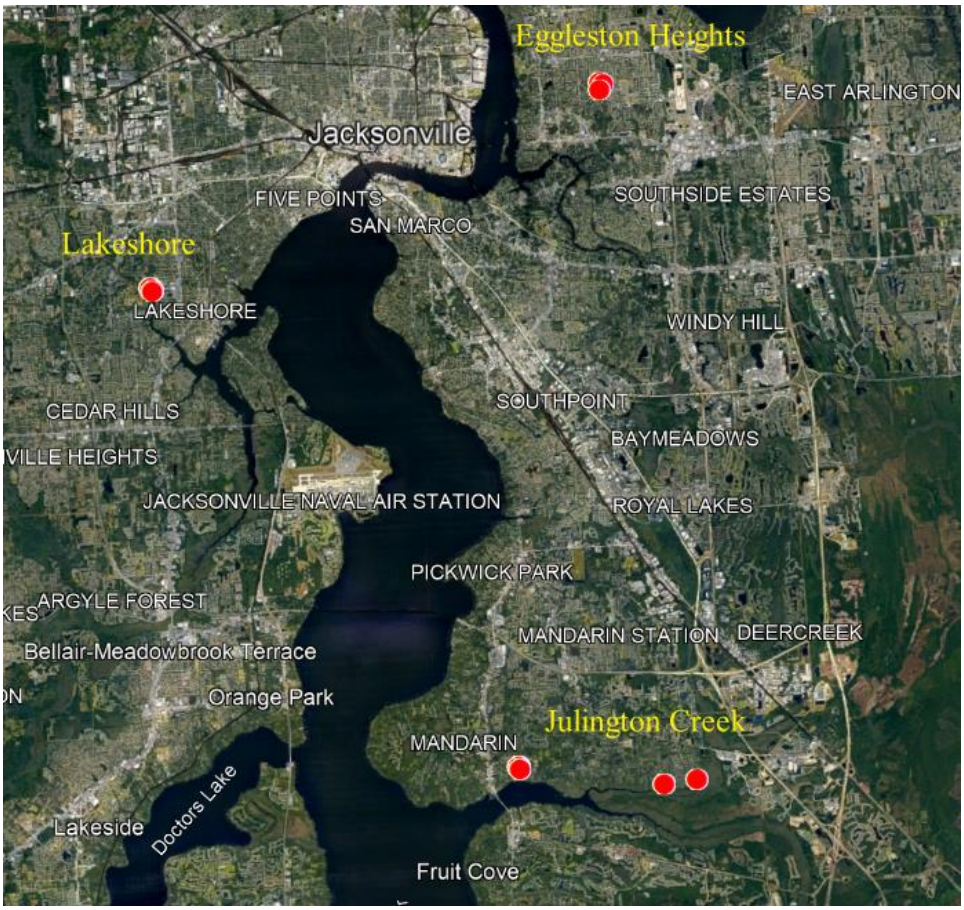

Fig. 4.1. Location of three study areas of Eggleston Heights, Julington Creek, and Lakeshore and locations of ten study sites of Belanger et al. (2011).

Summary information of OSTDS at the three sites is listed in Table 4.1. The Eggleston Heights area is an older subdivision with a high density of OSTDS, and OSTDS of three homes were monitored in the study of Belanger et al. (2011). The Lakeshore area also has a high density of OSTDS, and has three OSTDS monitored. The Julington Creek area has newer homes than the other two areas, and has four OSTDS monitored. Since all these three study areas are located in Duval County, their data were downloaded together, as discussed in section 4.2. However, OSTDS modeling was conducted for three areas separately.

Table 4.1. Summary information of the monitoring septic tanks.

Monitoring points	Location	Build year	Number of people	Sample time	Belonging
WH	1629 Aletha	1968	Two since 1980	December 2009	Eggleston Heights
MR	7186 King Arthur Rd.	1970	Seven since 1995	-	
CS	2020 Woodleigh	1980	Three since 1980	-	
RT	5428 Waterside	1951	Five until 1975 and then two	-	Lakeshore
DE	5476 Waterside	1959	Two since 1959	-	
NJ	5436 Waterside	1980	Two since 1980	June 2010	
LP	12827 Julington Road	1984	Two since 1984	-	Julington Hills/Julington Creek/Hood landing
CST	5180 Siesta Del Rio	2010	Five since 1985	-	
MM	12511 Cormorant	1967	Two since 1967	-	
DH	12537 Cormorant	1997	Four since 1997	-	

4.2. Data for ArcNLET Modeling

The septic tank data were obtained from the Florida Water Management Inventory (FLWMI) project at https://ww10.doh.state.fl.us/pub/bos/Inventory/FloridaWaterManagementInventory/. The procedure of generating the ArcGIS file of septic tank for ArcNLET modeling is the same as that described in Section 2.2.1. The septic tank locations are shown in Fig. 4.2. The numbers of septic tanks are 3,613, 3,585, and 3,080 for Eggleston Heights, Lakeshore, and Julington Creek, respectively.

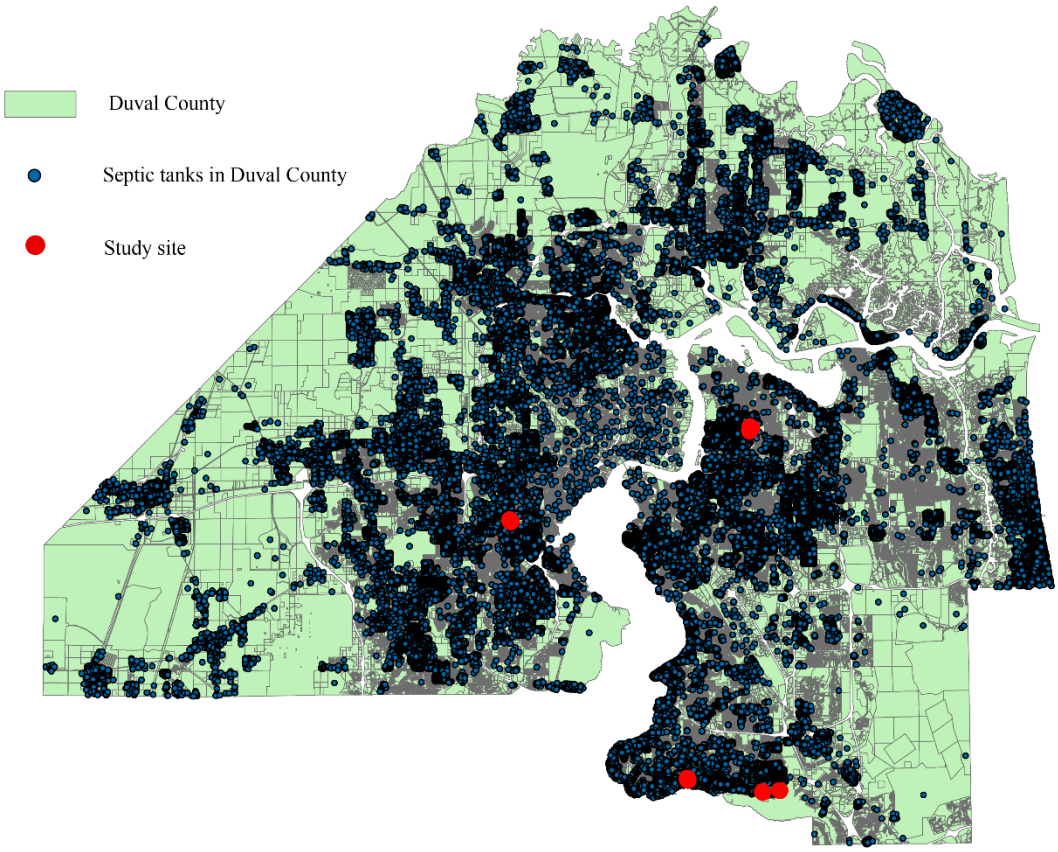

Fig. 4.2. Locations of septic tanks in the study areas.

The DEM data were downloaded from the USGS website at https://apps.nationalmap.gov/downloader/. The Lidar DEM data with the resolution of 16.4 ft × 16.4 ft were used for Eggleston Heights. The DEM data with the resolution of 32.8 ft × 32.8 ft was used for Julington Creek and Lakeshore. The water body data were download from the Florida Geographic Data Library at https://fgdl.org/fgdlmap/, and the data were processed in the same way as that described in Section 2.2.3 and Section 3.2.

The saturated conductivity and porosity were obtained from the SSURGO dataset with the assistance of the soilDB package. The soil zone index of the study area is fl031. The SSURGO data were processed in the way described in Sections 2.2.4 and 3.2.

4.3. ArcNLET Simulation for Eggleston Heights

The DEM with the resolution of 16.4 ft × 16.4 ft was used for Eggleston Heights. This resolution can better simulate particle paths and plumes results than the coarse resolution of 32.8 ft × 32.8 ft, and makes the ArcNLET modeling computationally affordable for more than 3,000 OSTDS. The DEM was first smoothed with a smoothing factor of 100 and a smoothing cell of 7. The elevation of the surface water bodies was then merged with the smoothed DEM, and another round of smoothing was performed with a smoothing factor of 2 and a smoothing cell of 7. More details of the smoothing process were given in Section 2.3.1.

The comparison of smoothed DEM and measured water table is shown in Fig. 4.3. The four red points represent four monitoring wells at Eggleston Heights, numbered AM-MW1, AM-MW2,

AM-MW3, and AM-MW4. Since the report of Belanger et al. (2011) did not include measurements of hydraulic head, the head data were obtained from a dataset provided by Richard Hicks to Ming Ye in a separate project. The solid black line is the fitted line of this study, and the dashed blue line is the fitted line by Zhu et al. (2017). The two lines are similar but not the same, because the resolution of the DEM used in Zhu et al. (2017) was 32.8 ft × 32.8 ft and the smoothing factor used in Zhu et al. (2017) is 60. The results of this study are better than those of Zhu et al. (2017) in that the slope of this study are close than one than that of Zhu et al. (2017). The simulated flow paths from septic tanks to surface water bodies are shown in Fig. 4.4.

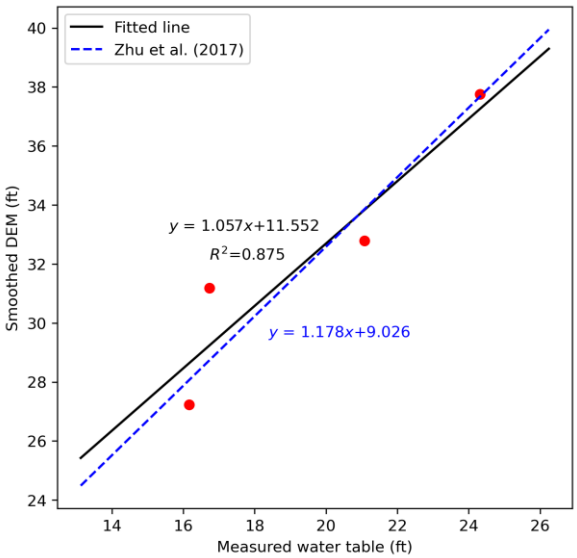

Fig. 4.3. Comparison of smoothed DEM and measured water tables.

Fig. 4.4. Simulated flow paths from septic tanks to surface water bodies of Eggleston Heights.

For the VZMOD simulation, the concentrations of 1.0 mg/L for NO_3-N and 40 mg/L for NH_4-N were used for all the individual septic tanks. These values were used for the study sites discussed in Chapters 2 and 3. The default parameter values of VZMOD were used, except maximum first-order nitrification rate K_{nit} and the maximum first-order denitrification rate K_{dnt}. The values of K_{nit} and K_{dnt} were adjusted to match the simulated and observed NH_4-N and NO_3-N values in groundwater. The final values of K_{nit} and K_{dnt} were 0.36 and 0.7, respectively. As indicated by Table 4.2, the adjusted value of K_{dnt} is substantially larger than the default value, but still in the parameter range reported in McCray et al. (2005).

Table 4.2. Comparison of parameters used by VZMOD and the parameter ranges given in McCray et al. (2005).

	Default value	Calibrated value	McCray et al., 2005
K_{nit} (1/d)	2.9	0.36	0.0768~211.2
K_{dnt} (1/d)	0.025	0.7	0.004~2.27

To estimate the distance from infiltrative surface to the water table, we used the formula A−B, where A is the distance between the smoothed DEM and the water table, and B is the distance between the infiltration surface and the land surface. A is the intercept of the fitted line shown in Fig. 4.3, which is 11.552 ft. Additionally, 18 inches for B is suggested in the VZMOD user manual. Therefore, the distance from the infiltrative surface to water table (DTW) is 10.052 feet (306.385 cm). The VZMOD modeling interface is shown in Fig. 4.5. The histograms of simulated NH_4-N and NO_3-N concentrations at the water table are shown in Fig. 4.6.

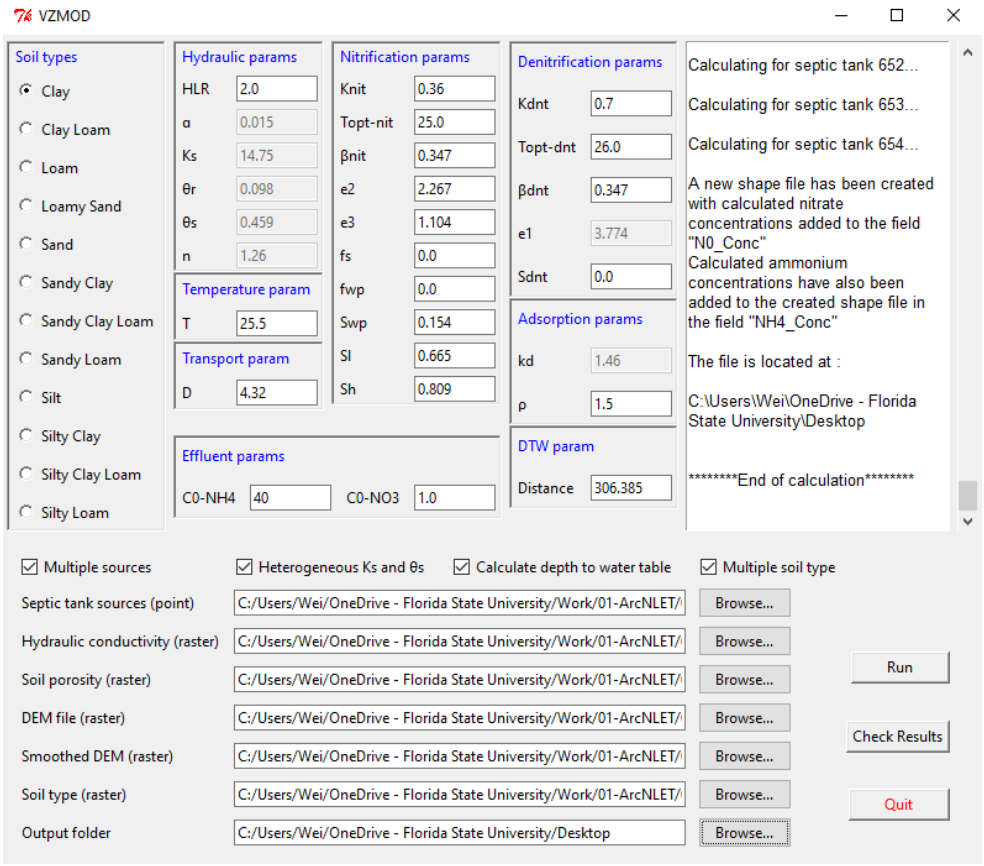

Fig. 4.5. VZMOD parameters used for Eggleston Heights modeling.

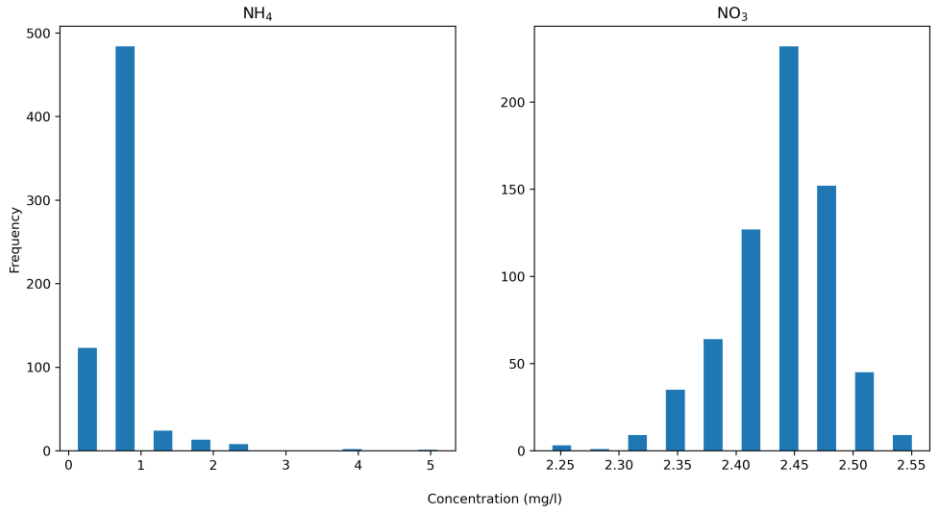

Fig. 4.6. Histograms of the concentrations of NH_4-N and NO_3-N at water table.

The simulated concentrations of NH_4-N and NO_3-N entering the groundwater were used as the input values of solute transport simulation in ArcNLET. The default parameter values were used for the ArcNLET simulation. The comparison between the simulated NO_3-N and NH_4-N plumes and the observation plumes is shown in Fig. 4.7. ArcNLET simulation was not conducted at the CS site, where the septic tank was already converted to central sewer. Fig. 4.7 shows that,

while the simulated plumes qualitatively reflect the spatial patterns of the observed concentrations, the simulated concentrations do not match the observed concentrations. The simulated and measured concentrations of NH_4-N and NO_3-N are further compared in Fig. 4.8. It shows that the simulation concentrations do not match the observed concentrations. Although spatial variability of the concentrations cannot be simulated, the average values simulated by our model are close to the observed average values. The averages of observed values of NH_4-N and NO_3-N are 1.08 and 0.78 mg/L, respectively. The averages of simulated values of NH_4-N and NO_3-N are 0.92 and 0.75 mg/L. In other words, the average simulations are comparable with the average observations. With the calibrated model, the simulated NH_4-N and NO_3-N concentrations are plotted in Figs. 4.9 and 4.10, respectively.

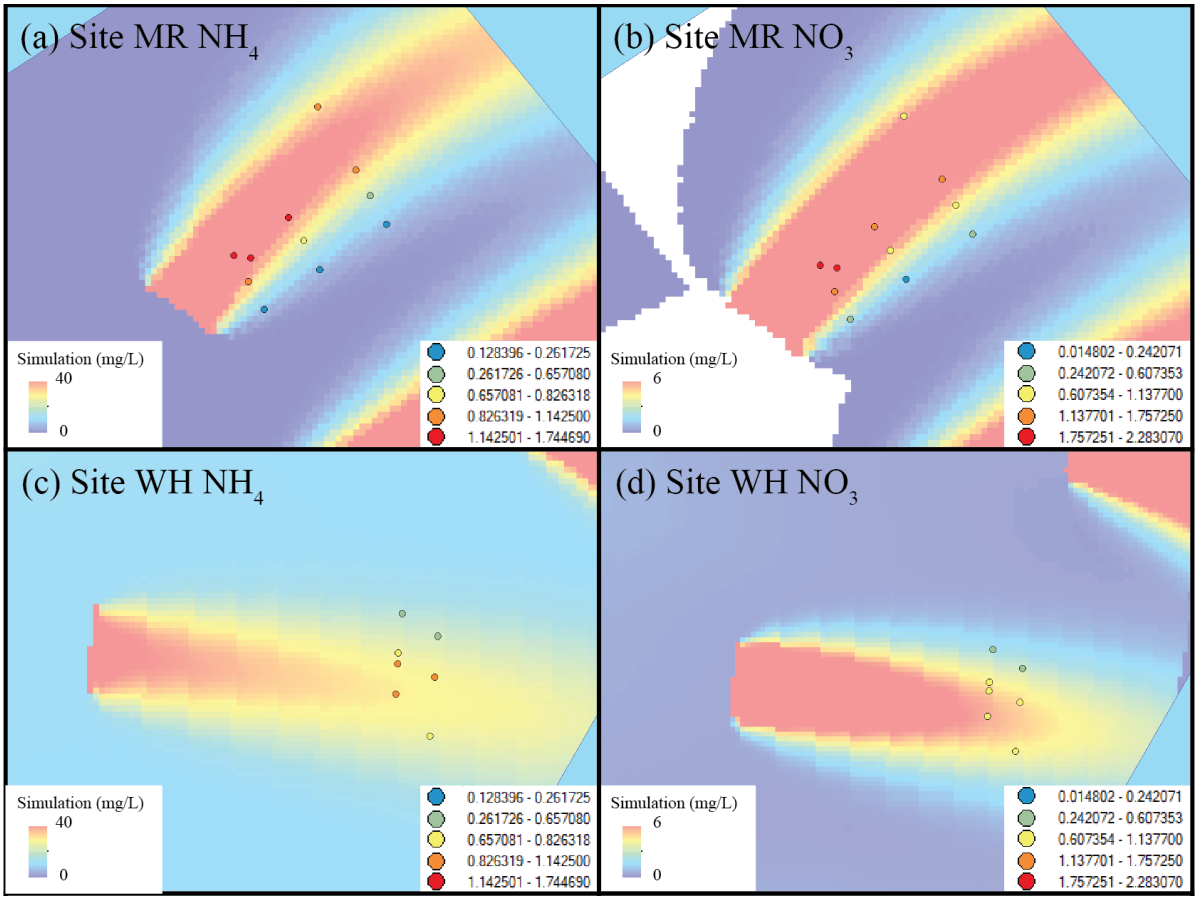

Fig. 4.7 Simulated NO_3-N and NH_4-N plumes and observed concentration at Eggleston Heights.

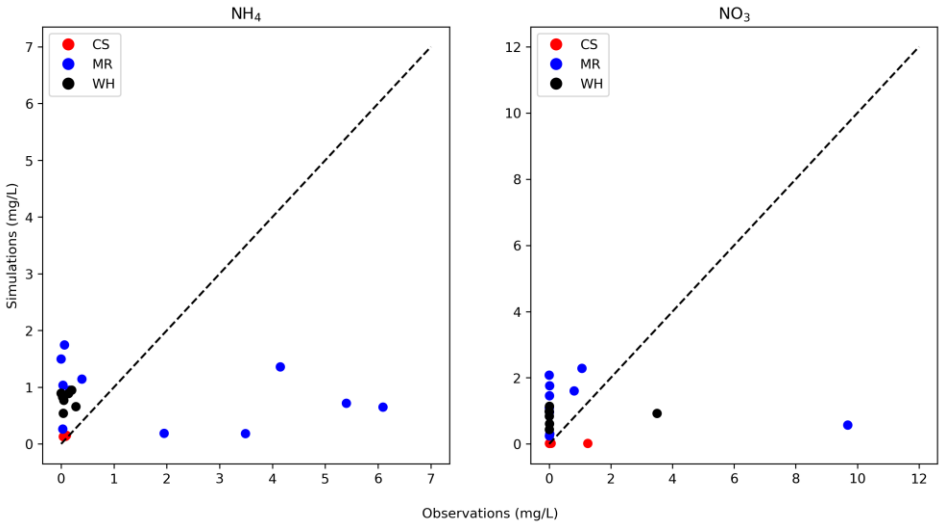

Fig. 4.8. Comparison of simulated and observed NH_4-N and NO_3-N concentrations for Eggleston Heights.

Fig. 4.9. Spatial distribution of simulated NH_4-N concentrations for Eggleston Heights.

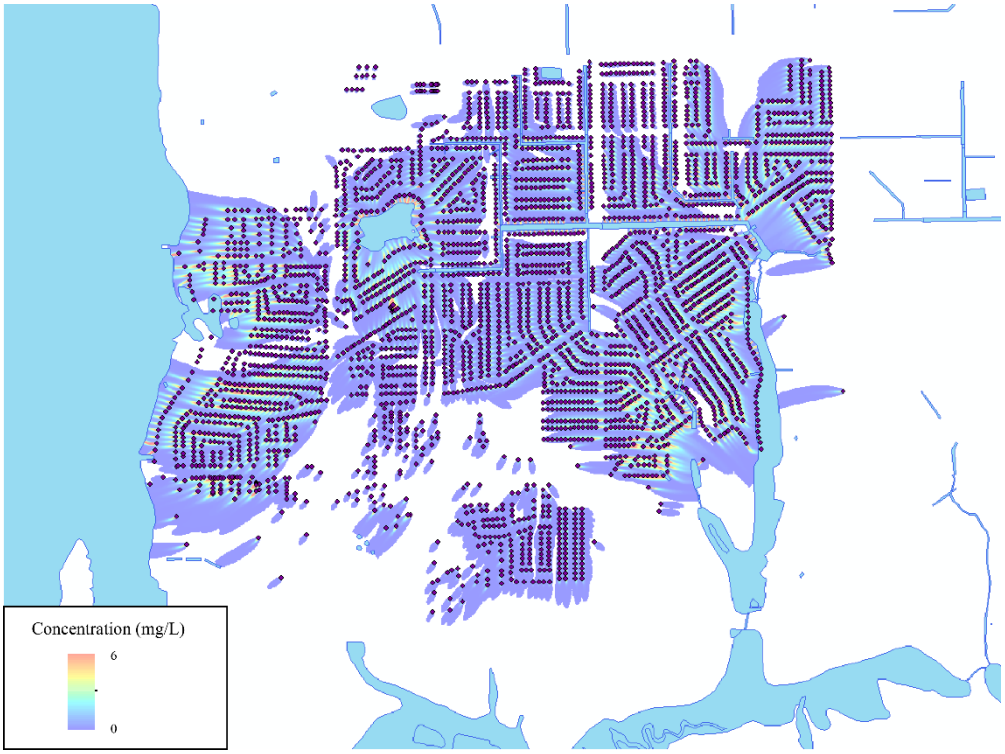

Fig. 4.10. Spatial distribution of simulated NO_3-N concentrations for Eggleston Heights.

4.4. OSTDS Setback Distances for Eggleston Heights

Fig. 4.11 plots the vertical nitrogen attenuation rate ($1 - C_{WT}/C_{DF}$) with the vertical distance (VD) from drainfield to water table groundwater for different soil types in the study area. Among the 3,613 OSTDS at the study area, only 2 OSTDS are located in clay soil, and the rest OSTDS in sandy soil. The discussion about OSTDS setback discussion is thus focused on sandy soil. Similar to Fig. 2.42 of Chapter 2 for the Turkey Creek sub-basin and Fig. 4.15 of Chapter 3 for the St. Lucie River of Indian River Lagoon, Fig. 4.11 also shows that the vertical nitrogen attenuation rate increases with the vertical distance. The vertical nitrogen attenuation in this study area is larger than the study areas of Turkey Creek and St. Lucie River. The histogram of the vertical nitrogen attenuation rate plotted in Fig. 4.12 indicates that the majority of the vertical nitrogen attenuation rate is close to 100%. The reason is that the maximum first-order nitrification rate (K_{nit}) and the maximum first-order denitrification rate (K_{dnt}) of VZMOD are large, as discussed above. The large values lead to a large amount of nitrification and denitrification in the vadose zone, and thus a large nitrogen attenuation. As a result, bigger vertical nitrogen attenuation values were obtained in this study area.

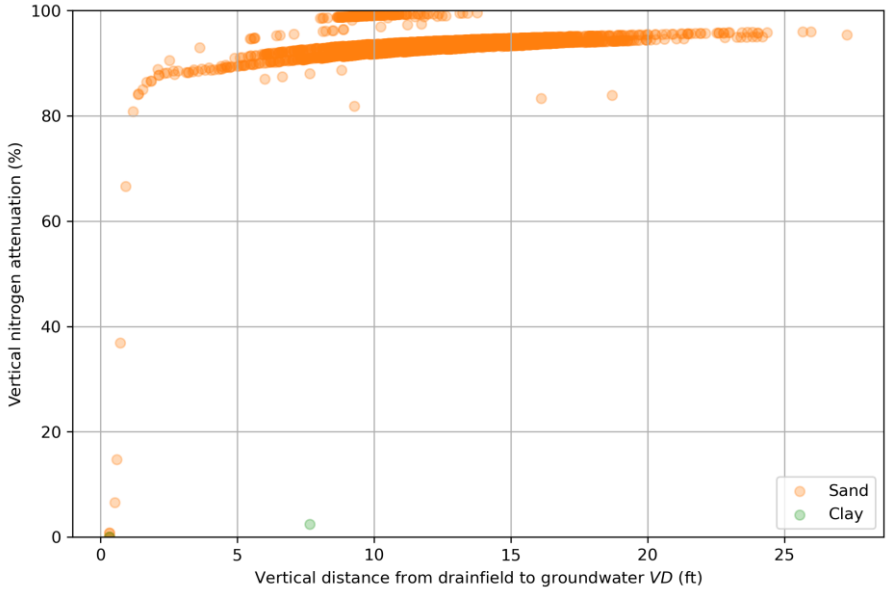

Fig. 4.11. Relation between vertical nitrogen attenuation rate ($1 - C_{WT}/C_{DF}$) and the vertical distance, *VD*, from drainfield to groundwater *VD* for Eggleston Heights.

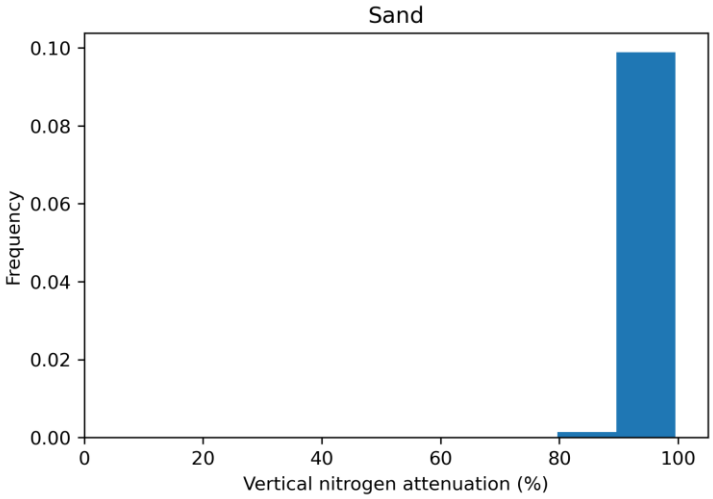

Fig. 4.12. Histogram of vertical nitrogen attenuation rate for Eggleston Heights.

Figs. 4.13 and 4.14 plot the histograms of NH_4-N and NO_3-N concentrations at water table (C_{WT}) and water body (C_{WB}), respectively, for Eggleston Heights. The two figures show that the concentrations of NO_3-N at water body are smaller than those at water table, which is attributed to the denitrification in groundwater. The concentrations of NH_4-N are close to zero at both water table and water body, indicting that NH_4-N is converted to NO_3-N in the vadose zone.

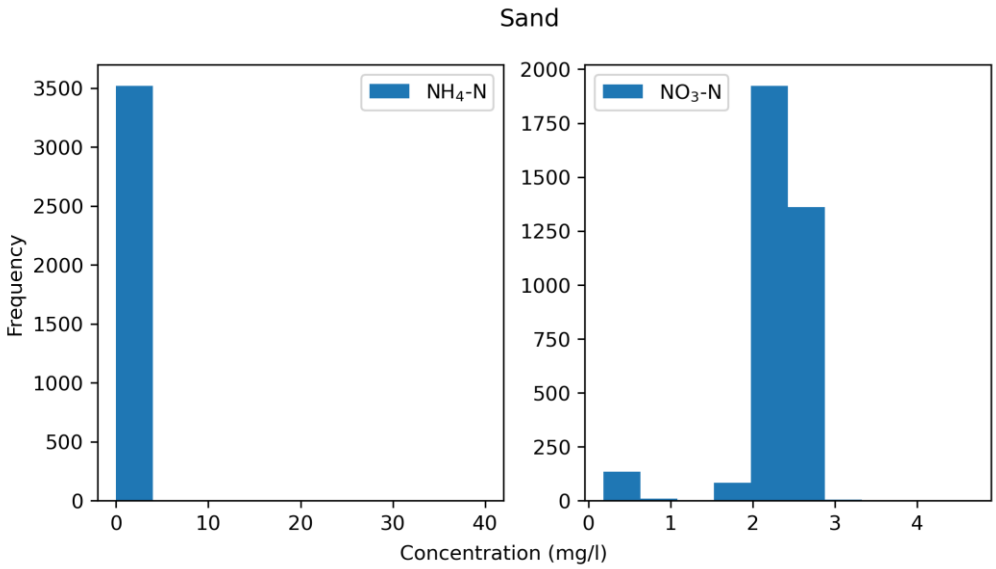

Fig. 4.13. Histograms of concentrations of NH_4-N and NO_3-N at water table (C_{WT}) at Eggleston Heights.

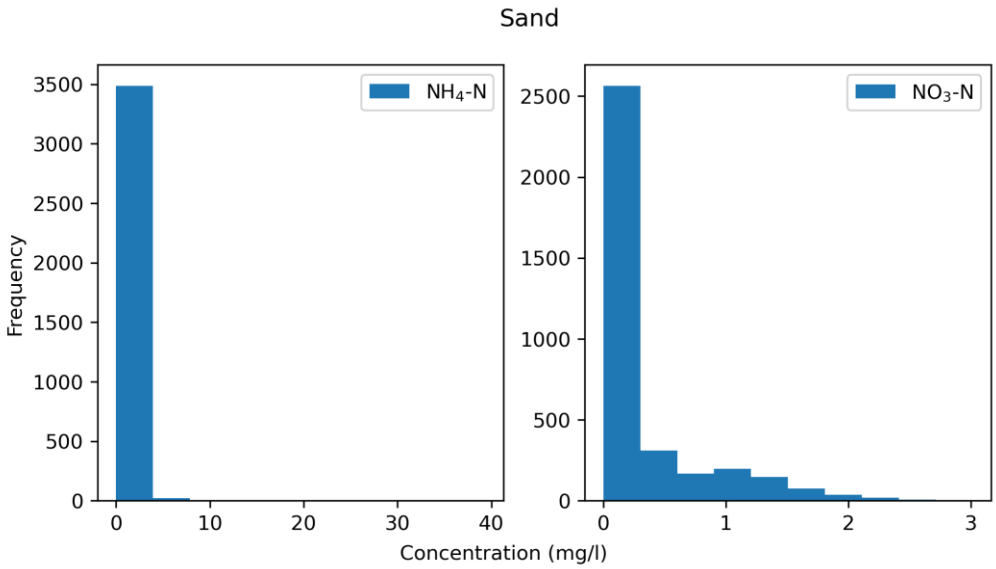

Fig. 4.14. Histograms of concentrations of NH_4-N and NO_3-N at water able (C_{WB}) at Eggleston Heights.

Fig. 4.15 plots the relations between the horizontal nitrogen attenuation rate ($1 - C_{WB}/C_{WT}$) and the horizontal linear distance from drainfields to water bodies. Fig. 4.16 is similar to Fig. 4.15, but plots the averaged horizontal nitrogen attenuation rate for every 10 ft of horizontal distance. Fig. 4.16 also plots the empirical expression

$$1 - C_{WB}/C_{WT} = 100 \times AF \times (1 - e^{((-HD_L)/(4\times K_s+20))}) \quad (4.1)$$

obtained in Chapter 2 for the Turkey Creek sub-basin, where *AF* is the adjust factor for the maximum nitrogen attenuation when the horizontal linear distance is large enough. The *AF* value was set as 95% for sand. Fig. 4.16 indicates that the empirical expression obtained in Chapter 2 for the Turkey Creek sub-basin is applicable for Eggleston Heights.

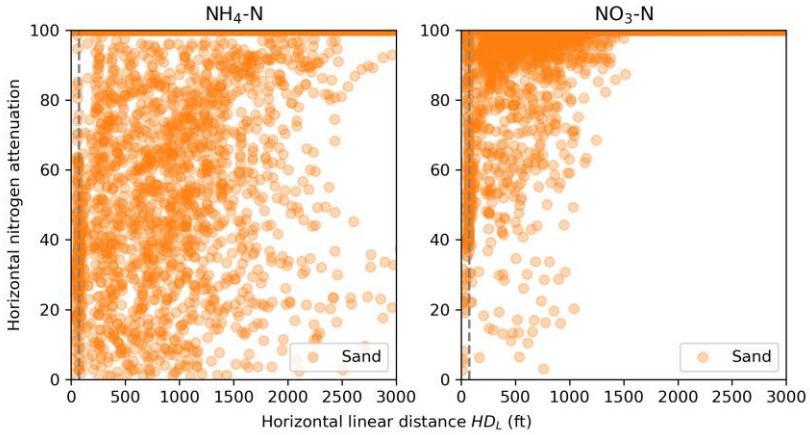

Fig. 4.15. Relations between horizontal nitrogen attenuation rate ($1 - C_{WB}/C_{WT}$) and linear horizontal distance (HD_L) from drainfield to waterbody for Eggleston Heights.

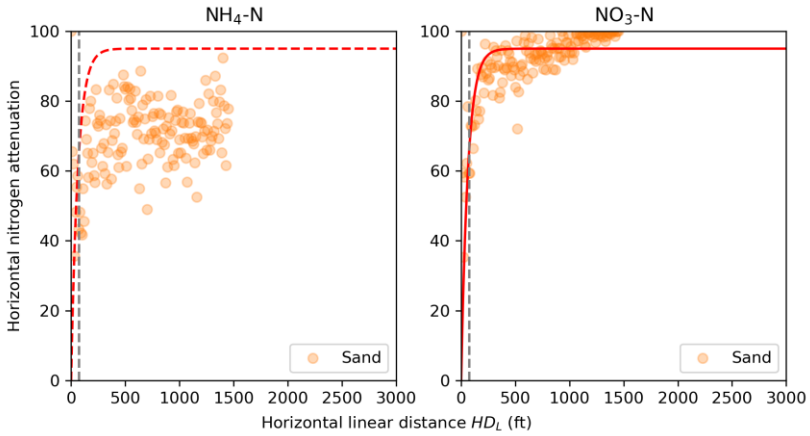

Fig. 4.16. Relations between horizontal nitrogen attenuation and the linear horizontal distance after averaging hydraulic gradient for every 10 feet of the distance.

For the sensitivity analysis of vertical and horizontal setback distances, nine OSTDS near the study sites (WH, MR and CS) in Eggleston Heights were chosen, and their locations are shown in Fig. 4.17. The vertical distance of the OSTDS varies between 0.3 ft and 9.8 ft, and the range was divided into 29 intervals with 30 vertical distances. Only sand was studied in this study area, and the contours of horizontal and vertical setback distances and total nitrogen attenuation rate for sand are shown in Fig. 4.18. This figure is similar to Figure 2.64 of Chapter 2 for the Turkey Creek sub-basin. However, for the same setback distance, the total nitrogen attenuation rate for Eggleston Heights is significantly larger due to the larger K_{nit} and K_{dnt} values, as discussed above.

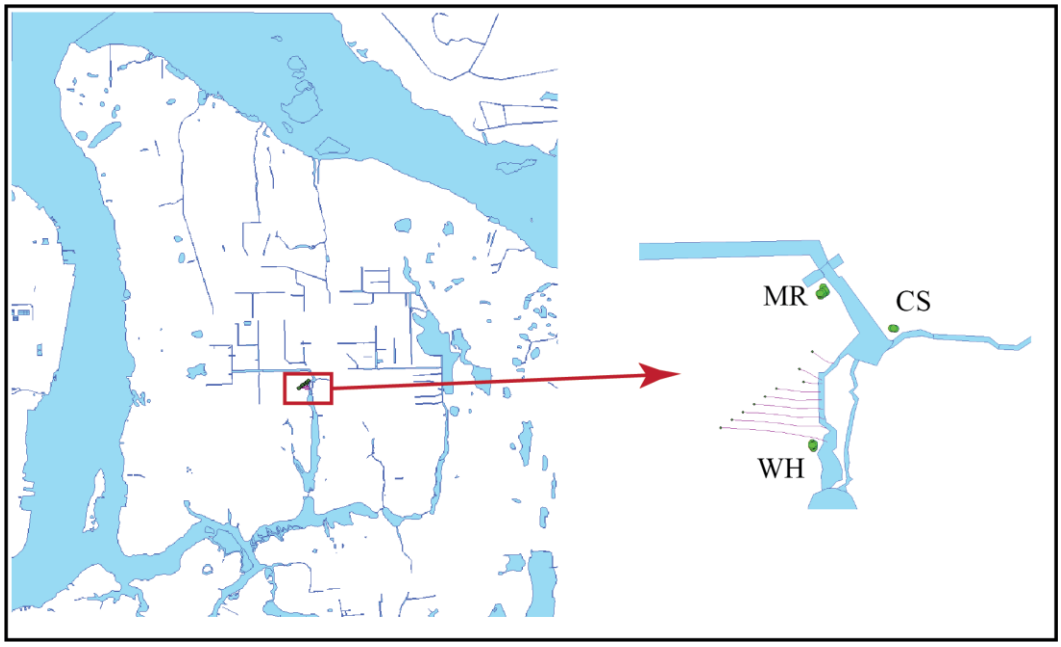

Fig. 4.17. OSTDS used for sensitivity analysis to determine the relation between total nitrogen attenuation rate and setback distances.

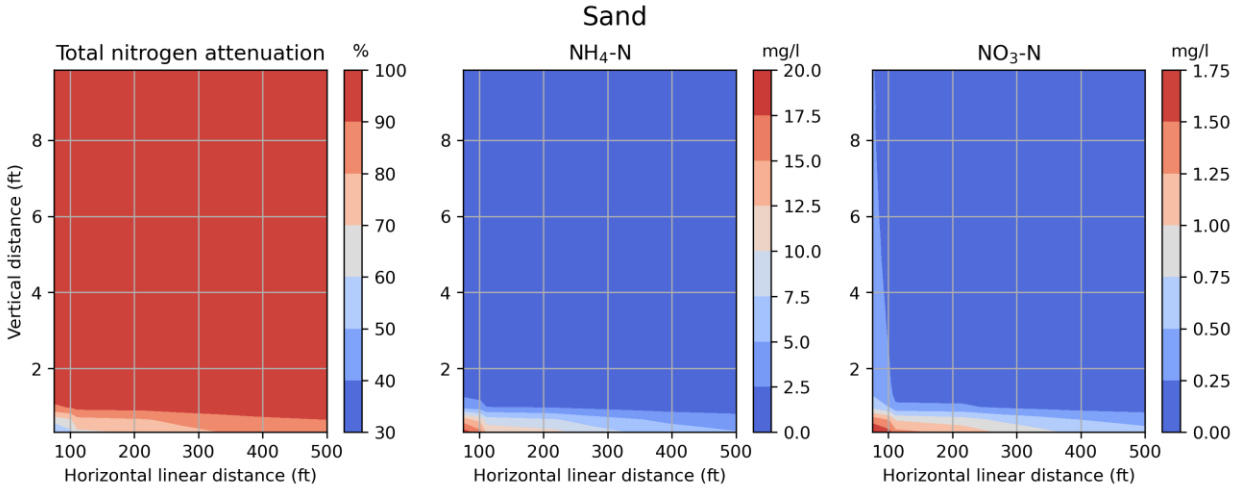

Fig. 4.18. Relations between nitrogen attenuation as well as concentrations of NH_4-N and NO_3-N entering the canal and the horizontal linear distance and vertical distance for Eggleston Heights. The smallest horizontal distance is 75 ft.

4.5. ArcNLET Simulation for Julington Creek

The DEM with the resolution of 32.8 ft × 32.8 ft was used for Julington Creek. Following Wang et al. (2011) and Ye and Wang (2012), the original DEM was first smoothed with a smoothing factor of 100 and a smoothing cell of 7. The elevation of the surface water bodies was then merged with the smoothed DEM, and another round of smoothing was performed with a smoothing factor of 2 and a smoothing cell of 7. The comparison of smoothed DEM and measured water table for Julington Creek is shown in Fig. 4.19, and the simulated flow paths from septic

tanks to surface water bodies are shown in Fig. 4.20. The 17 measured groundwater level is from Wang et al. (2011) and Ye and Wang (2012). The slope of the fitted line between measured water table and smoothed DEM is near 1, which indicates that the smoothed DEM is a reasonable approximation of the groundwater levels. In Wang et al. (2011) and Ye and Wang (2012), the intercepts were 7.11 ft and 9.37 ft, respectively. The intercept of this study was 7.4 ft, which is consistent with those of the previous studies.

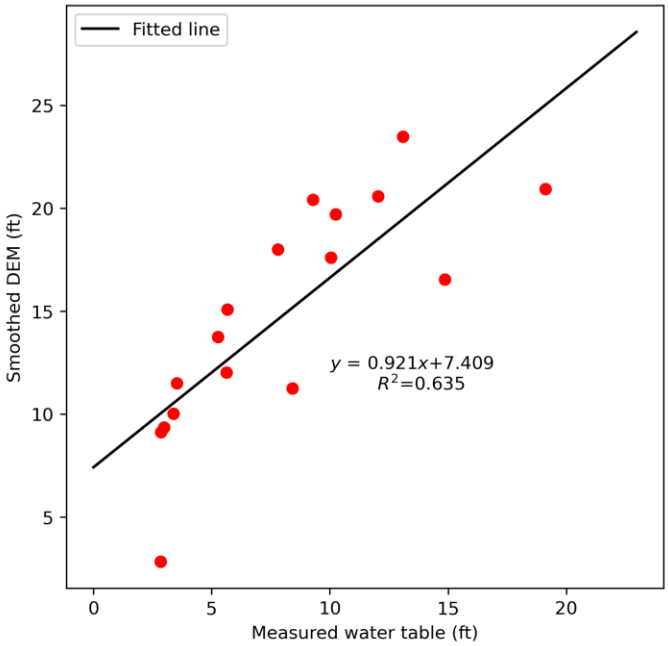

Fig. 4.19. Comparison of smoothed DEM and measured water tables for Julington Creek.

Fig. 4.20. Simulated flow paths from septic tanks to surface water bodies of Julington Creek.

The constant concentrations of 1.0 mg/L for NO_3-N and 60 mg/L for NH_4-N were used for all the individual septic tanks. The default parameter values of VZMOD were used in this study, except those of the maximum first-order nitrification rate K_{nit} and the maximum first-order denitrification rate K_{dnt}. The values of K_{nit} and K_{dnt} were adjusted based on the comparison of simulated and observed NH_4-N and NO_3-N values in groundwater. The final values of K_{nit} and K_{dnt} were 0.25 and 0.3, respectively. These values are within the range given by McCray et al. (2005), as indicated by Table 4.3. To calculate the distance from infiltrative surface to the water table, we used the formula A−B, which has been explained previously. A is the intercept of the fitted line, which is 7.409 ft. Additionally, 18 inches for B is suggested in the VZMOD user manual. Therefore, the distance from the infiltrative surface to water table (DTW) is 5.91 feet (180.14 cm). The interface of VZMOD modeling is shown in Fig. 4.21. The histograms of simulated NH_4-N and NO_3-N concentrations at water table are shown in Fig. 4.22 for the four sites at Julington Creek. The concentrations of both NH_4-N and NO_3-N are higher than those at Eggleston Heights, because the nitrification and denitrification reactions in the unsaturated zone are less substantial than at Eggleston Heights.

Table 4.3 Comparison of parameters used by VZMOD and the parameter ranges given in McCray et al. (2005).

	Default value	Calibrated value	McCray et al., 2005
K_{nit} (1/d)	2.9	0.25	0.0768~211.2
K_{dnt} (1/d)	0.025	0.3	0.004~2.27

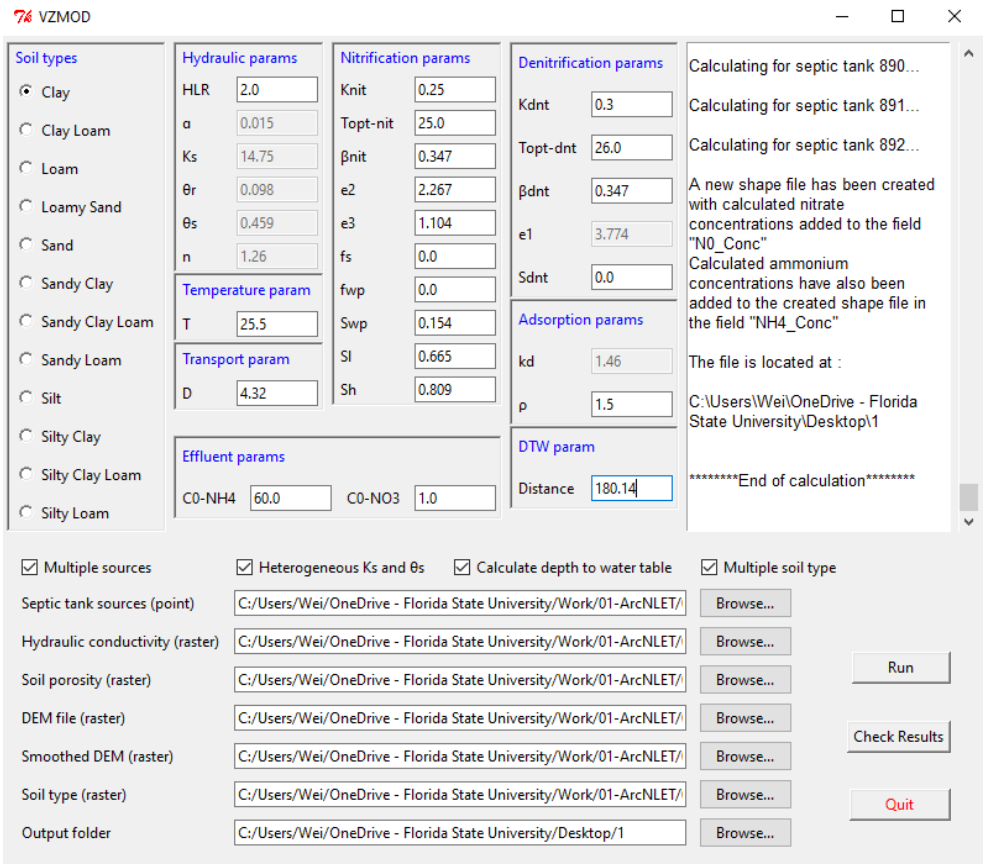

Fig. 4.21. VZMOD parameters used for Julington Creek modeling.

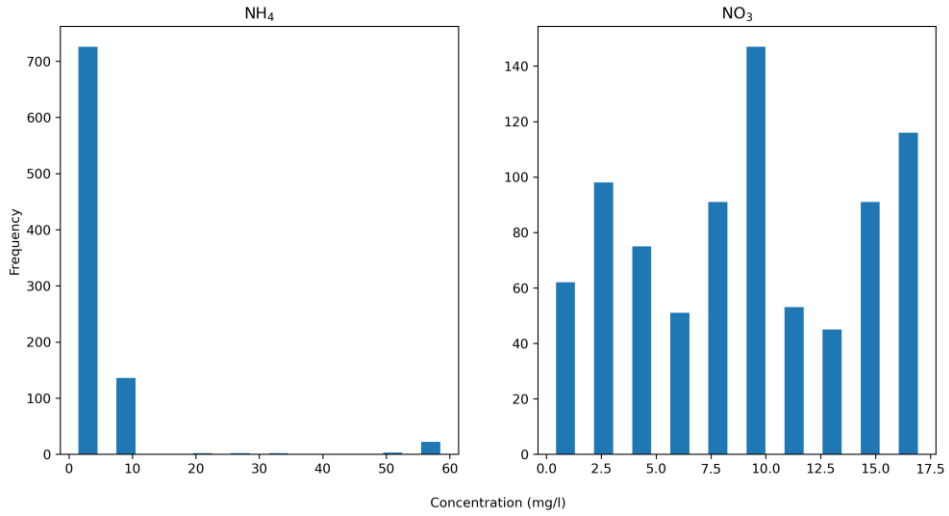

Fig. 4.22. Histogram of concentration of NH_4-N and NO_3-N at water table.

The comparison between the simulated and measured values of NH_4-N and NO_3-N is shown in Fig. 4.23. The simulated NH_4-N and NO_3-N plumes are plotted in Figs. 4.24 and 4.25, respectively. The fit between simulated and observed concentrations is similar to that of Eggleston Heights. The majority of observed concentrations for NO_3-N are less than 5 mg/L, and the majority of observed concentrations for NH_4-N are close to 0 mg/L. However, a few observed values are

very large, with the maximum NO_3-N concentration about 40 mg/L and the maximum NH_4-N concentration over 60 mg/L. Our simulation results cannot reproduce the large variability. Therefore, the mean value is used to evaluate the simulation results. The average values of observed NH_4-N and NO_3-N concentrations are 4.39 and 5.45 mg/L, respectively. The average values of simulated NH_4-N and NO_3-N concentrations are 3.46 and 4.47 mg/L, respectively. The two sets of values are close, indicating that the simulation results are reasonable.

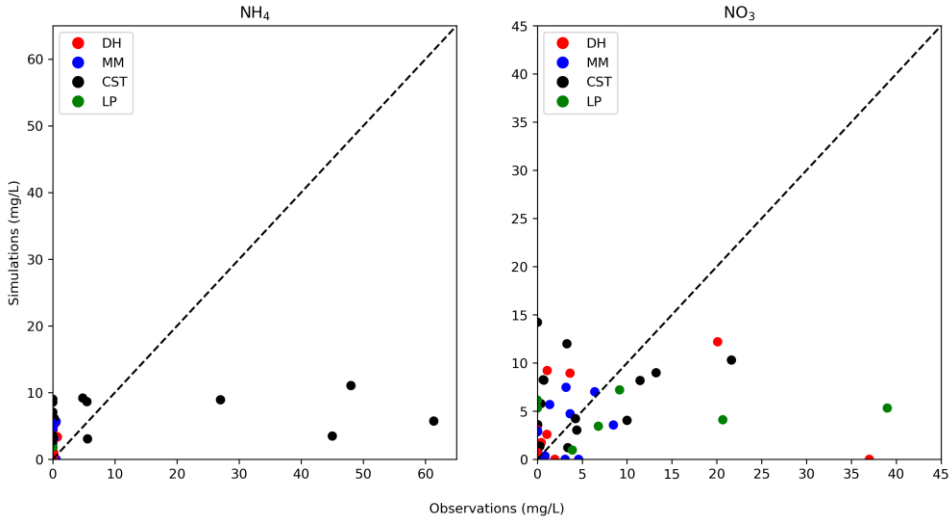

Fig. 4.23. Comparison of simulated and observed NH_4-N and NO_3-N concentrations for Julington Creek.

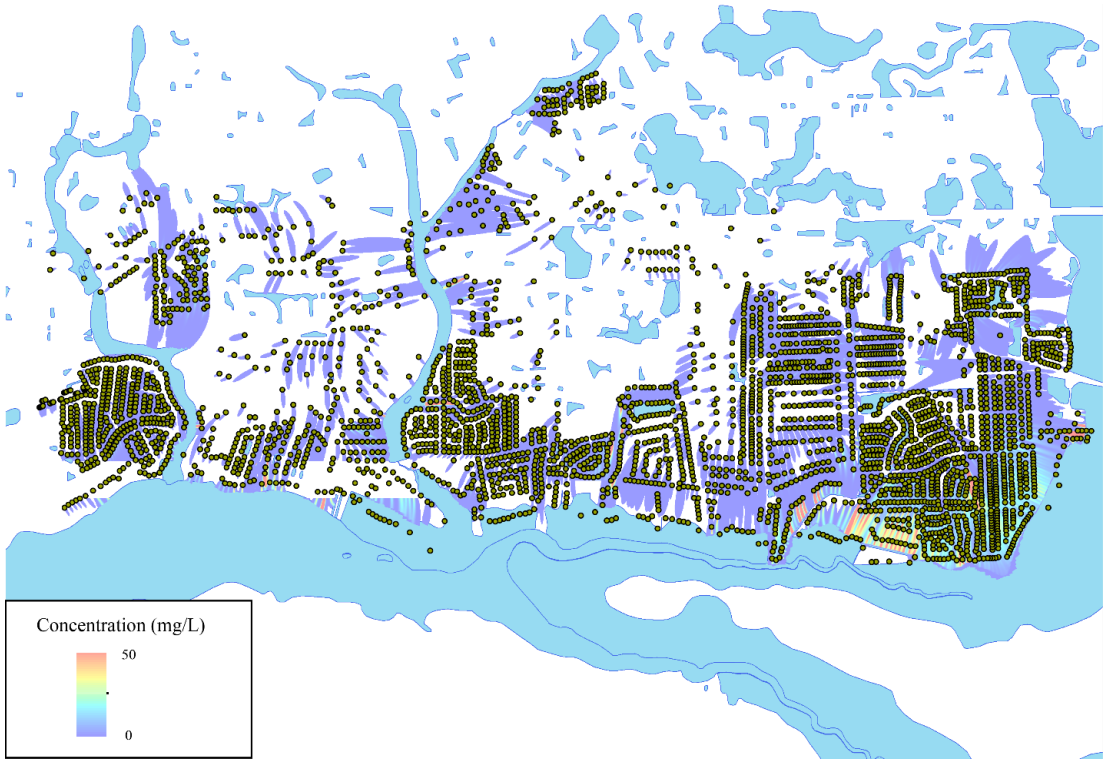

Fig. 4.24. Spatial distribution of NH_4-N concentrations at Julington Creek.

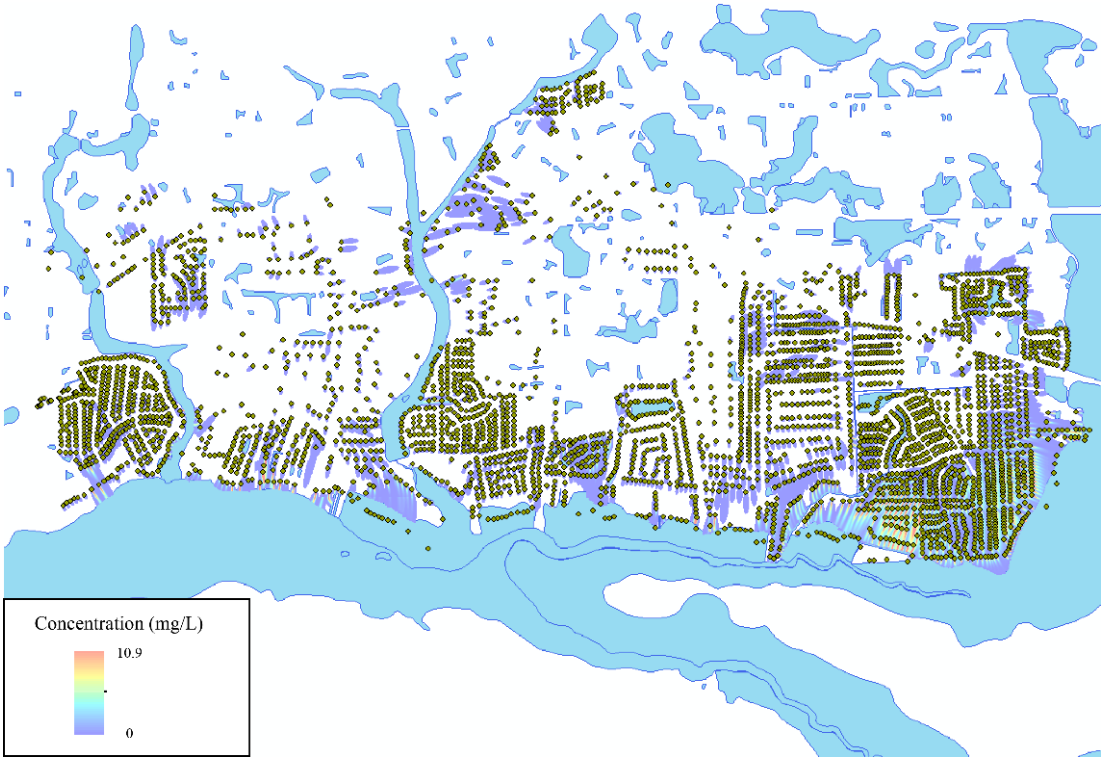

Fig. 4.25. Spatial distribution of NO_3-N concentrations for Julington Creek.

4.6. OSTDS Setback Distances for Julington Creek

Fig. 4.26 plots the vertical nitrogen attenuation rate ($1 - C_{WT}/C_{DF}$) with the vertical distance (VD) from drainfield to water table for the three soil types in Julington Creek. This figure is similar to those for Turkey Creek sub-basin and St. Lucie River of India River Lagoon, and this is attributed to the similar values of the maximum first-order nitrification rate (K_{nit}) and the maximum first-order denitrification rate (K_{dnt}) used for the three sites. The histogram of the vertical nitrogen attenuation rate is shown in Fig. 4.27, and the figure shows that the vertical nitrogen attenuation is smaller for sandy soil than for the other two soil types.

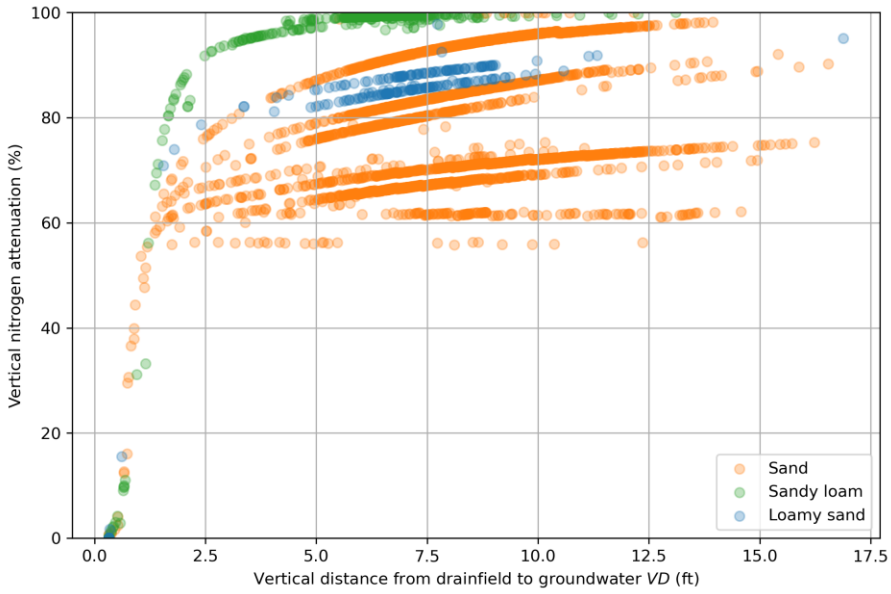

Fig. 4.26. Relation between vertical nitrogen attenuation rate ($1 - C_{WT}/C_{DF}$) and the vertical distance, *VD*, from drainfield to groundwater *VD* for Julington Creek.

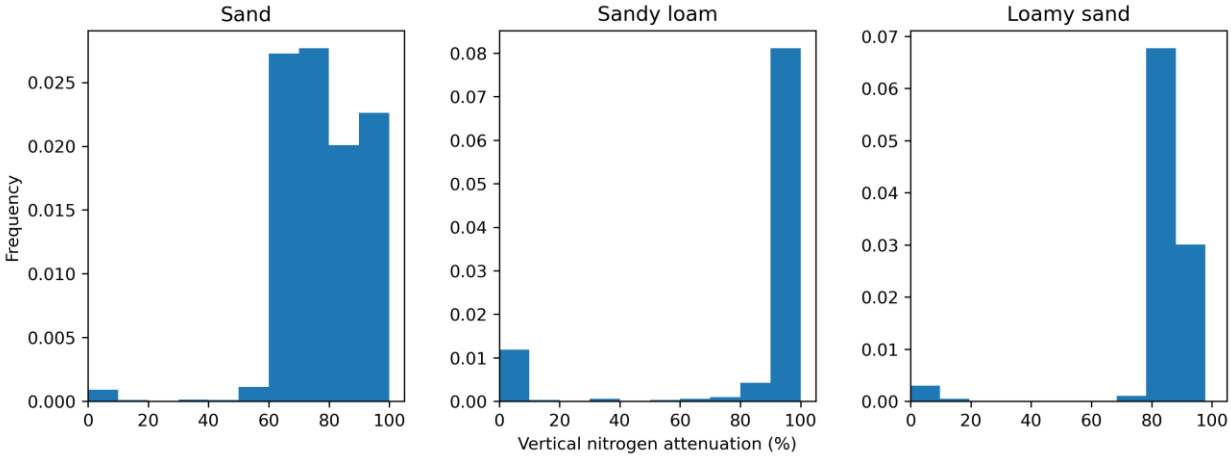

Fig. 4.27. Histograms of vertical nitrogen attenuation rate for Julington Creek.

Figs. 4.28 and 4.29 plot the histograms of simulated NH_4-N and NO_3-N concentrations at water table (C_{WT}) and water body (C_{WB}) for Julington Creek. The two figures show that the nitrogen concentrations at water body are smaller than those at water table, especially for NO_3-N, which indicates significant denitrification in groundwater.

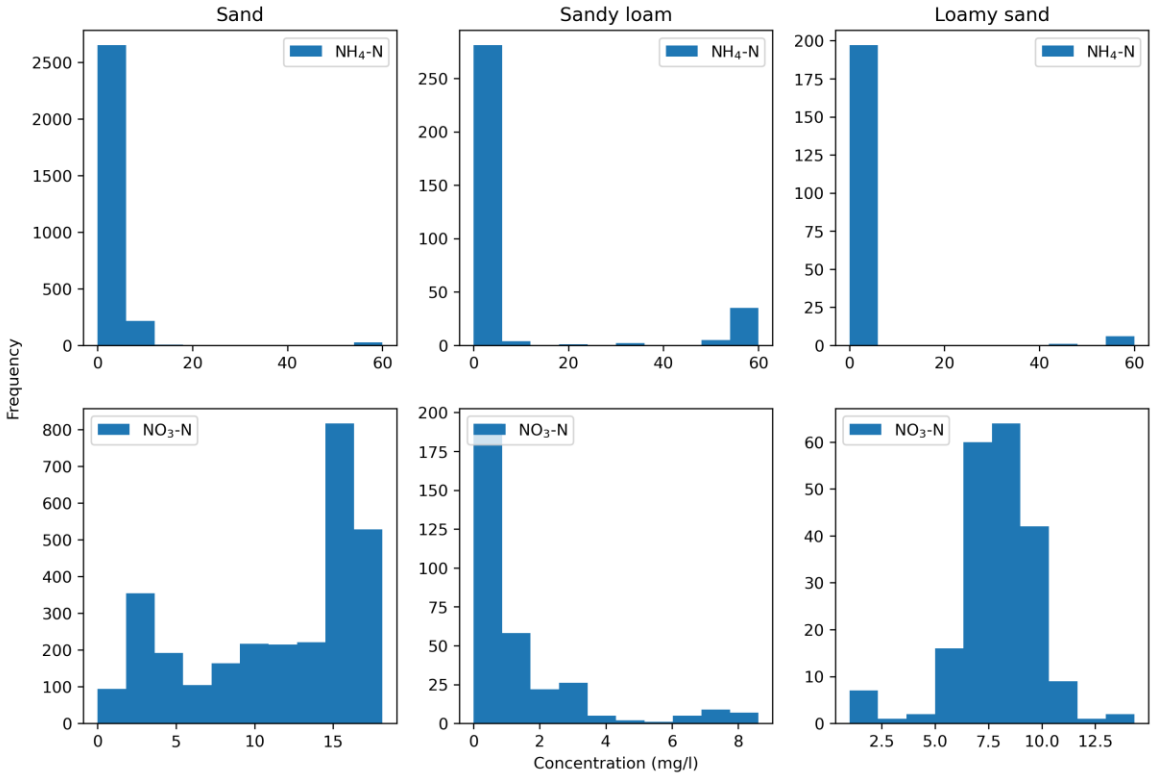

Fig. 4.28. Histograms of C_{WT} (NH_4-N and NO_3-N) for Julington Creek.

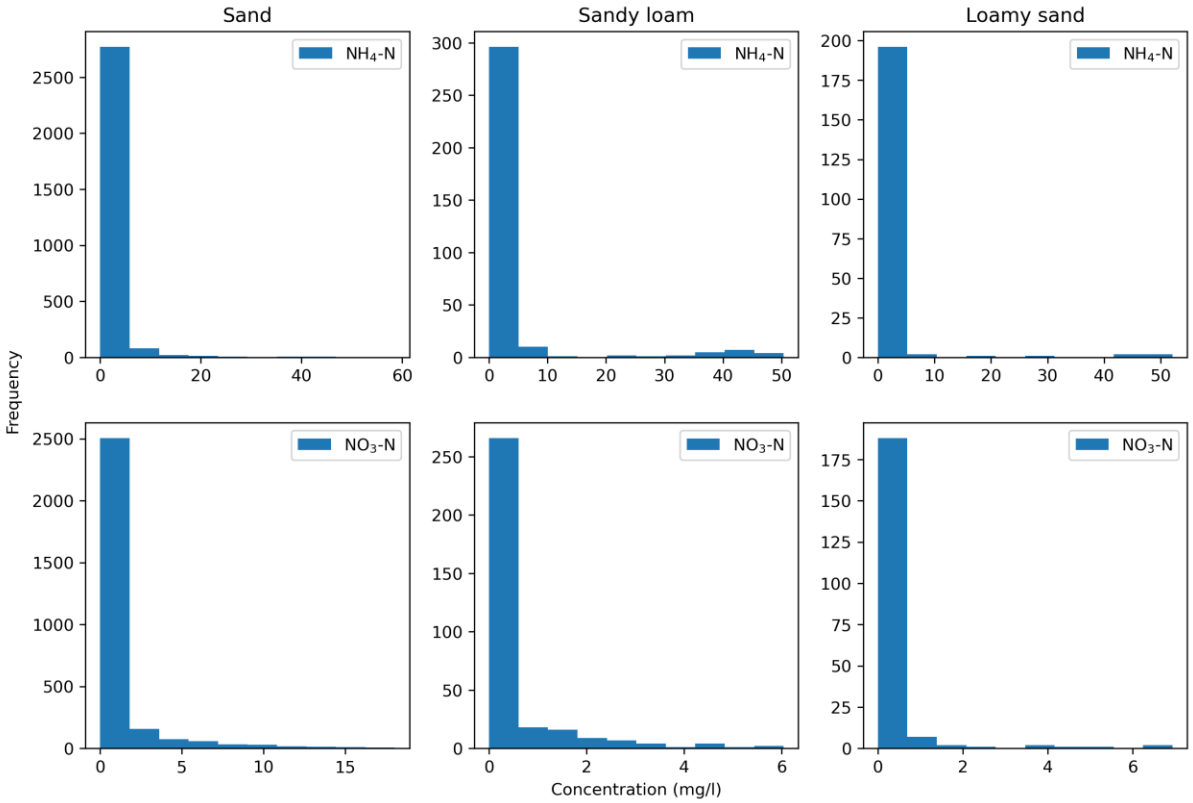

Fig. 4.29. Histograms of C_{WB} (NH_4-N and NO_3-N) for Julington Creek.

Fig. 4.30 plots the relations between the horizontal nitrogen attenuation rate ($1 - C_{WB}/C_{WT}$) and the horizontal linear distance from drainfields to water bodies for Julington Creek, and Fig. 4.31 plots the averaged horizontal nitrogen attenuation rate for every 10 ft of horizontal distance. Fig. 4.31 also pots equation (1) with the *AF* value set as 98% for sand and 100% for the other two soil types. Fig. 4.31 shows that the empirical equation still works for Julington Creek,.

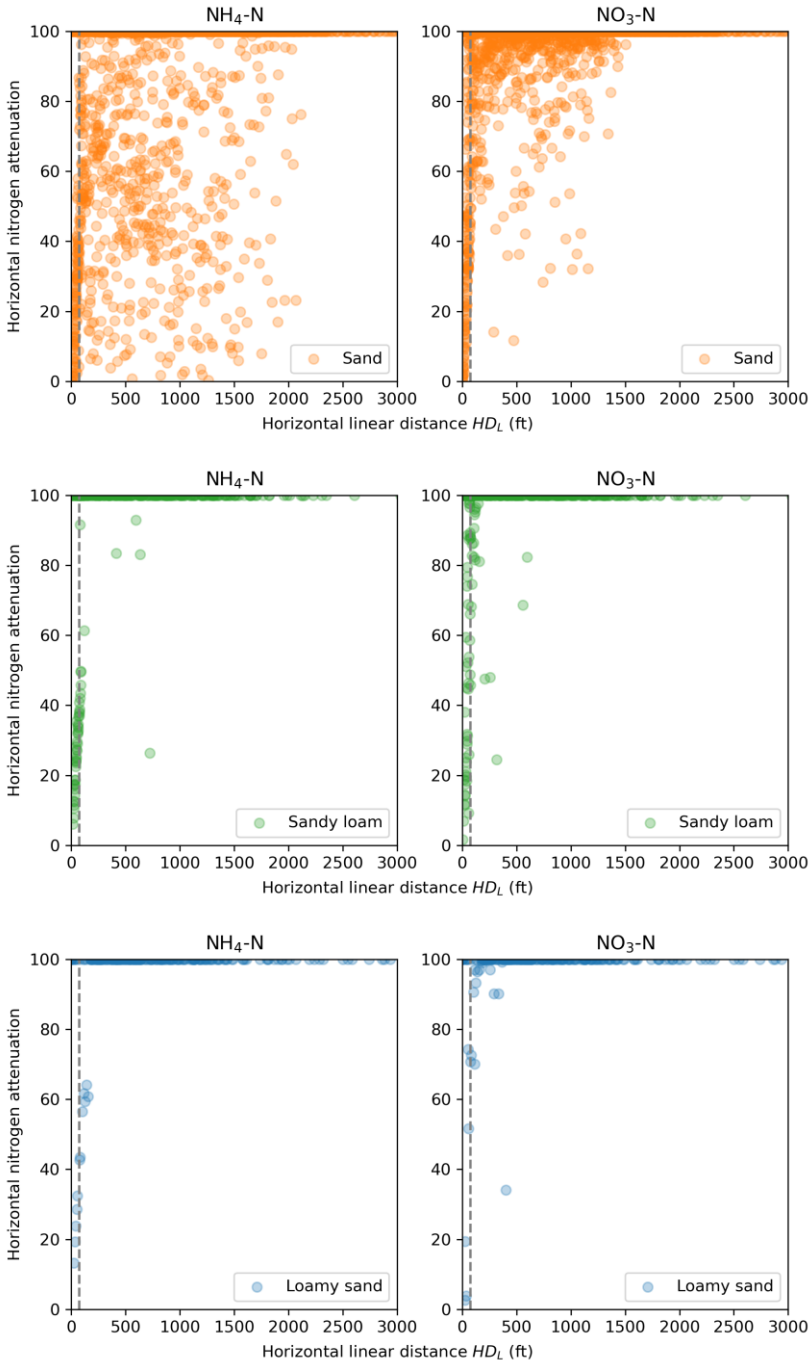

Fig. 4.30. Relations between horizontal nitrogen attenuation rate ($1 - C_{WB}/C_{WT}$) and linear horizontal distance (HD_L) from drainfield to waterbody for Julington Creek.

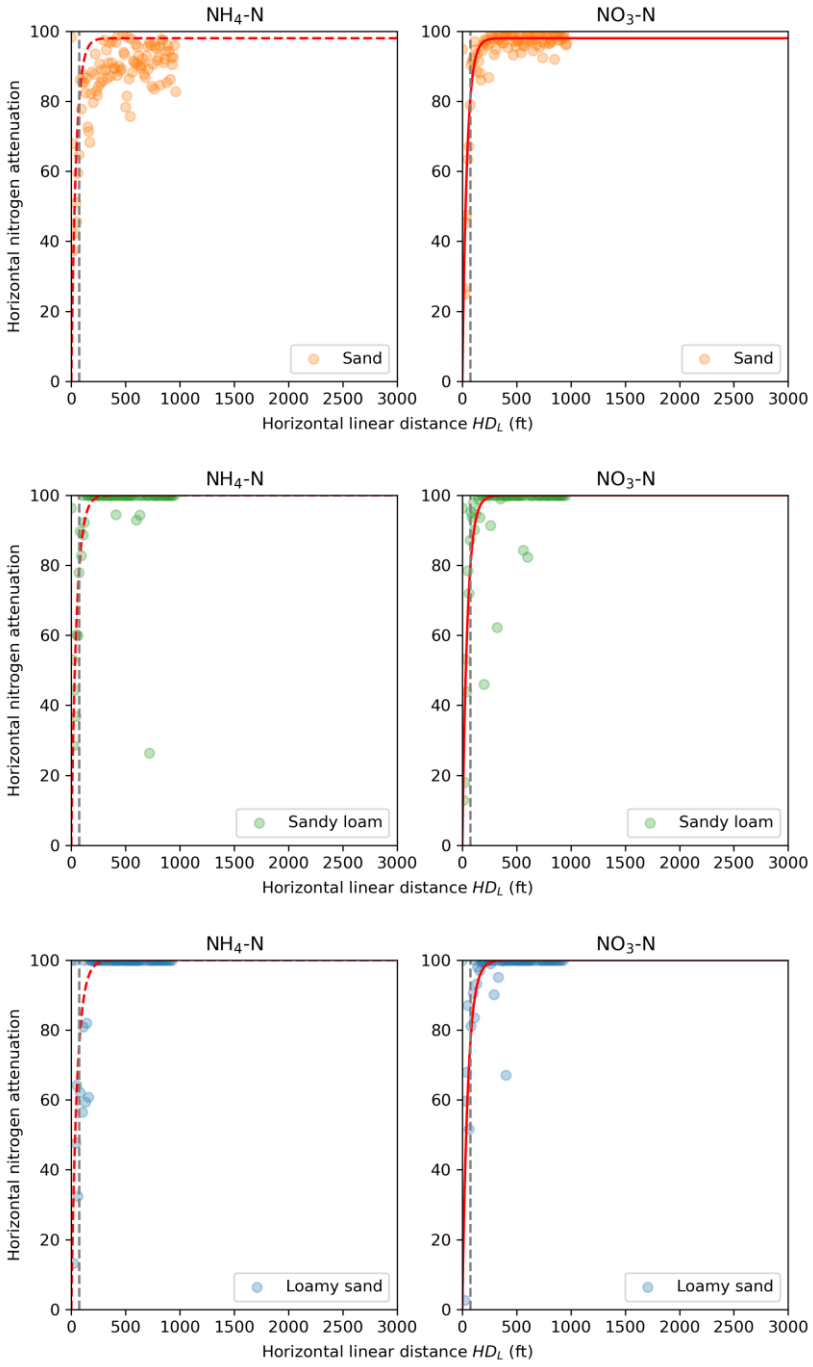

Fig. 4.31. Relations between horizontal nitrogen attenuation and the linear horizontal distance after averaging hydraulic gradient for every 10 feet of the distance.

For the sensitivity analysis of vertical and horizontal setback distances, ten OSTDS near the monitoring sites LP in Julington Creek were chosen. The locations of the ten OSTDS are shown in Fig. 4.32. Fig. 4.33 plots the contours of the total nitrogen attenuation rate against the horizontal and vertical setback distances for sand, sandy loam and loamy sand. This figure is similar to Figure 2.64 of Chapter 2 for the Turkey Creek sub-basin.

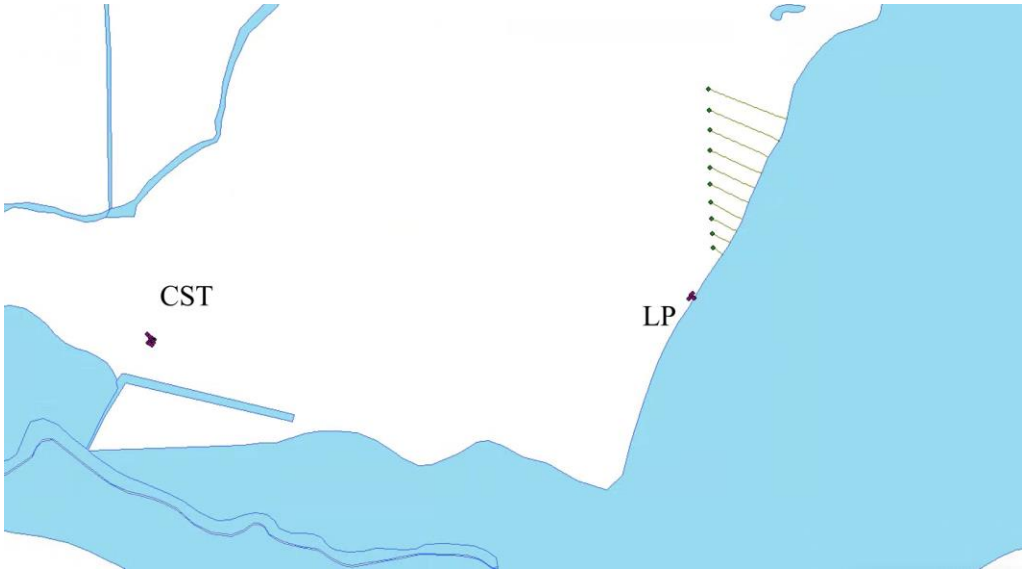

Fig. 4.32. OSTDS used for sensitivity analysis to determine the relation between total nitrogen attenuation rate and setback distances.

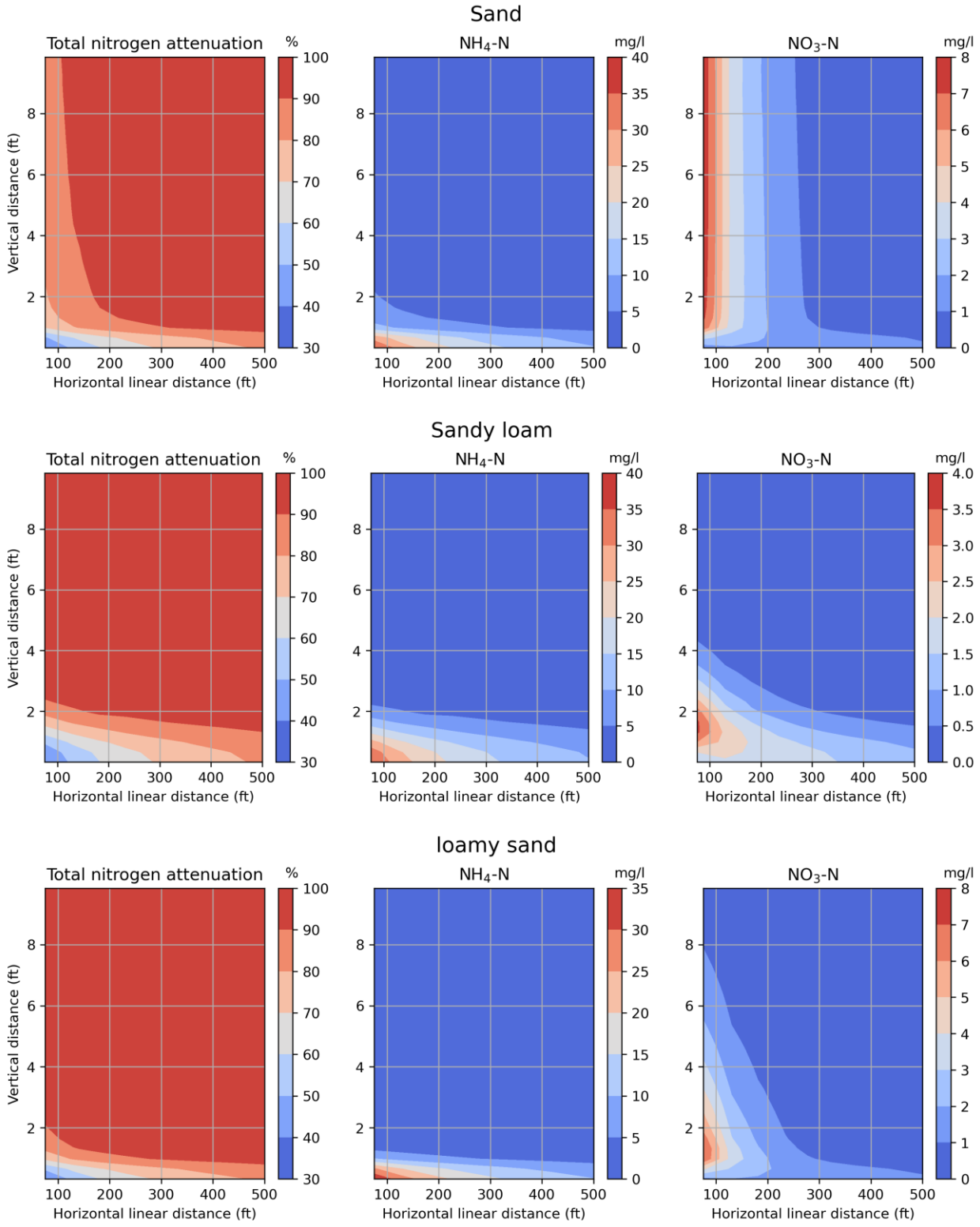

Fig. 4.33. Relations between nitrogen attenuation as well as concentrations of NH_4-N and NO_3-N entering the canal and the horizontal linear distance and vertical distance for Julington Creek. The smallest horizontal distance is 75 ft.

4.7. ArcNLET Simulation for Lakeshore

The DEM with a resolution of 32.8 ft × 32.8 ft was used for Lakeshore. The DEM was first smoothed with a smoothing factor of 100 and a smoothing cell of 7. The elevation of the surface water bodies was then merged with the smoothed DEM, and another round of smoothing was performed with a smoothing factor of 10 and a smoothing cell of 7. Since observations of hydraulic heads were unavailable at Lakeshore, calibration of the ArcNLET flow model was not conducted. The simulated flow paths from septic tanks to surface water bodies of Lakeshore are shown in Fig. 4.34.

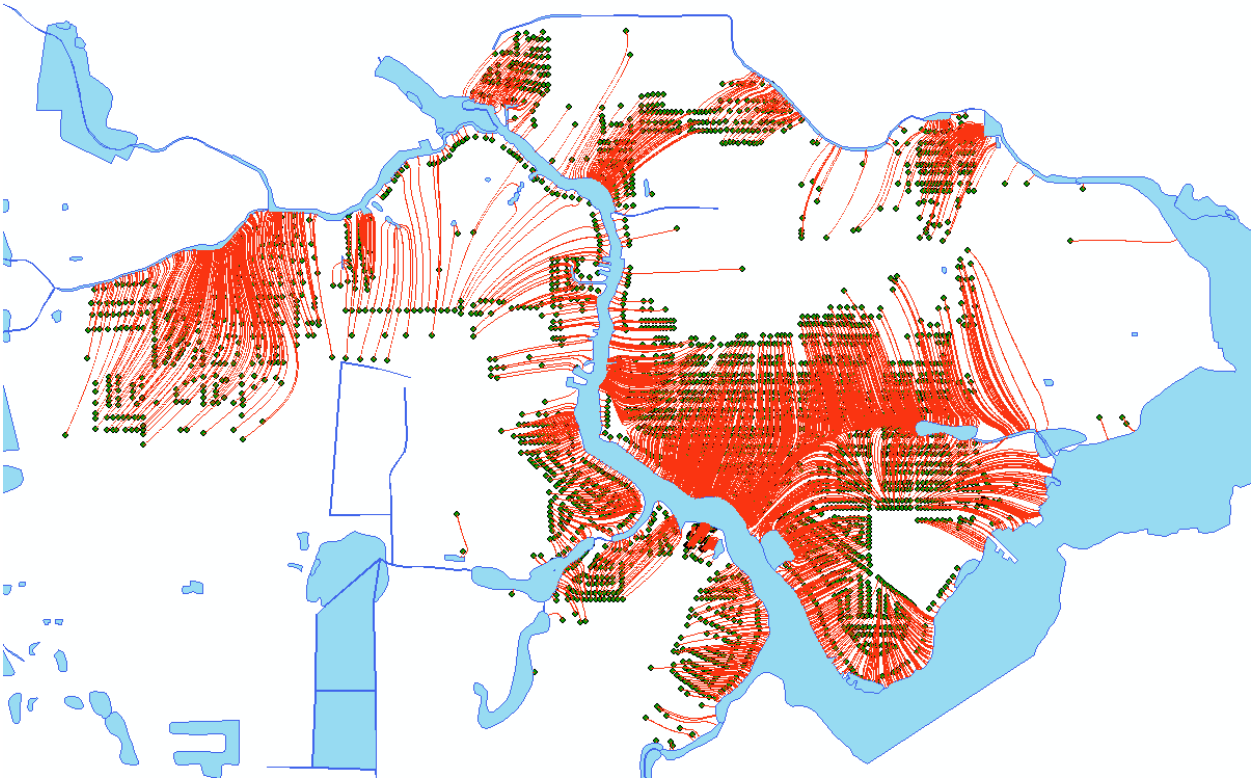

Fig. 4.34. Simulated flow paths from septic tanks to surface water bodies of Lakeshore.

The constant concentrations of 1.0 mg/L for NO_3-N and 40 mg/L for NH_4-N were used for all the individual septic tanks. The default parameter values of VZMOD were used in this study, except the maximum first-order nitrification rate (K_{nit}) and the maximum first-order denitrification rate (K_{dnt}). The calibrated values of K_{nit} and K_{dnt} were was 0.5 and 0.8, respectively, to match simulated and observed NO_3-N and NH_4-N concentrations in groundwater. Table 4.4 indicates that the calibrated parameter values are within the parameter range given by McCray et al. (2005). It should be noted that these parameter values are the largest all the five study areas of this project.

Table 4.4 Comparison of parameters used by VZMOD and the parameter ranges given in McCray et al. (2005).

	Default value	Calibrated value	McCray et al., 2005
K_{nit} (1/d)	2.9	0.5	0.0768~211.2
K_{dnt} (1/d)	0.025	0.8	0.004~2.27

In order to estimate the distance from infiltration surface to water table that is needed for VZMOD simulation, we still used the formular A-B. Since the ArcNLET flow model was not calibrated and the value of A was unknown, we used the estimated depth to water table available online at https://geodata.dep.state.fl.us/datasets/FDEP::estimated-depth-to-water-table-surficial-aquifer-system/about. According to the website, the mean depth from ground surface to water table for all the 3,080 OSTDS at Lakeshore area is 7.11 ft. For the B value, we used 18 inches for B given in the VZMOD user manual. Therefore, the distance from the infiltrative surface to water table (DTW) is 5.61 feet (170.95 cm).

Fig. 4.35 plots the simulated and observed NH_4-N and NO_3-N concentrations. The figure shows again that the model cannot simulate variability of the observed concentrations. The average values of the observed NH_4-N and NO_3-N concentrations are 1.49 and 0.05 mg/L, respectively. The average values of the simulated NH_4-N and NO_3-N concentrations are 1.99 and 1.06 mg/L. The average of simulated NO_3-N concentrations is larger than that of observed concentrations, despite of the large K_{nit} and K_{dnt} values used in this study. The average NO_3-N concentration was substantially smaller than the average NH_4-N concentrations, indicating that the nitrification reaction in the study area was not sufficient to completely convert NH_4-N to NO_3-N. However, the lack of additional monitoring data, such as water levels, makes simulation more difficult. In general, the simulation results are reasonable. The simulated NH_4-N and NO_3-N plumes are plotted in Figs. 4.36 and 4.37, respectively. The histograms of simulated NH_4-N and NO_3-N concentrations at water table are shown in Fig. 4.38. The figure shows low NH_4-N and NO_3-N concentrations t water table.

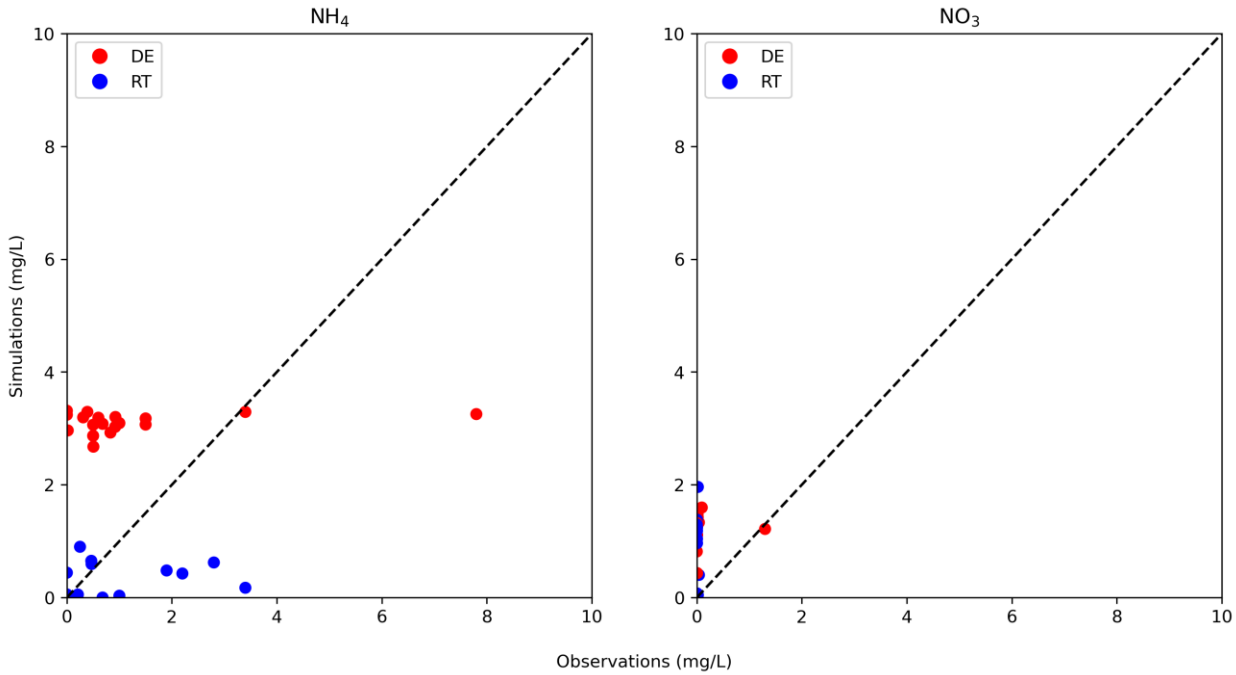

Fig. 4.35. Comparison of simulated and observed NH_4-N and NO_3-N concentrations for Lakeshore.

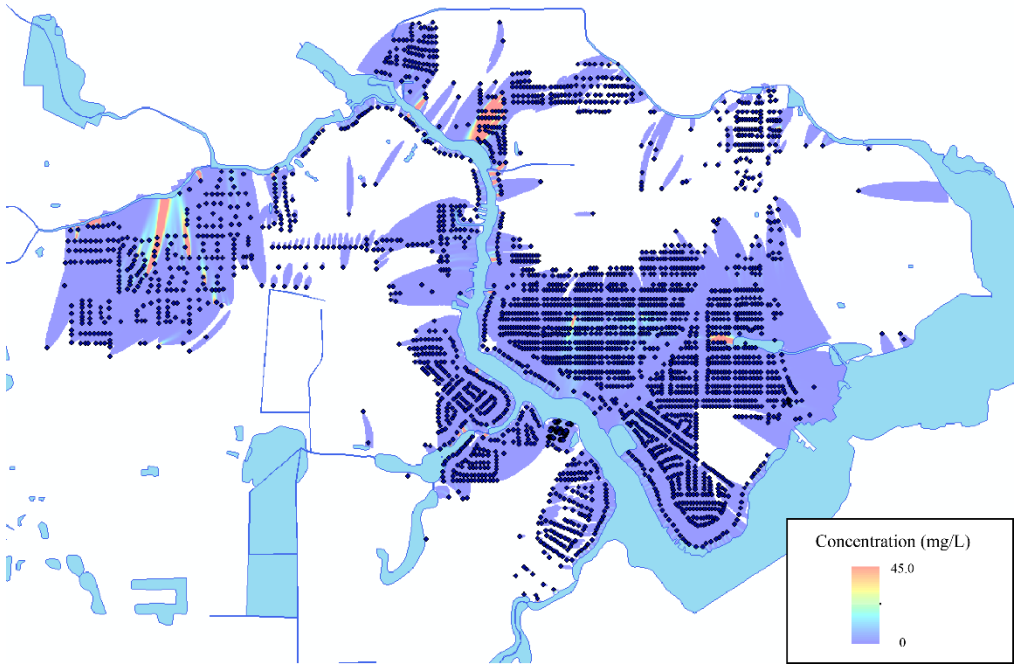

Fig. 4.36. Spatial distribution of NH_4-N concentrations at Lakeshore.

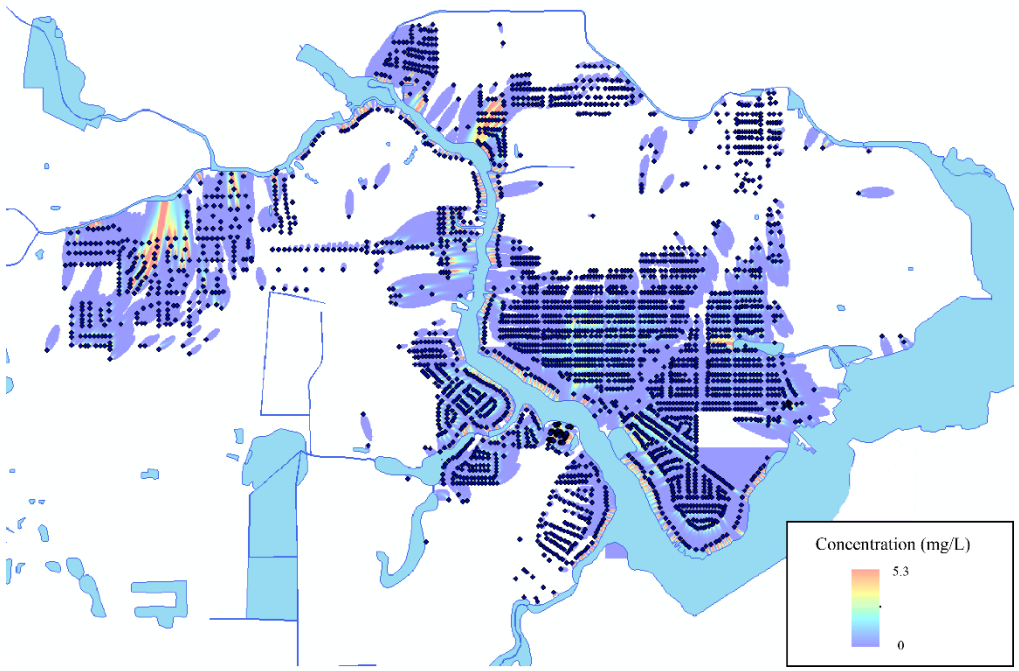

Fig. 4.37. Spatial distribution of NO_3-N concentrations for Lakeshore.

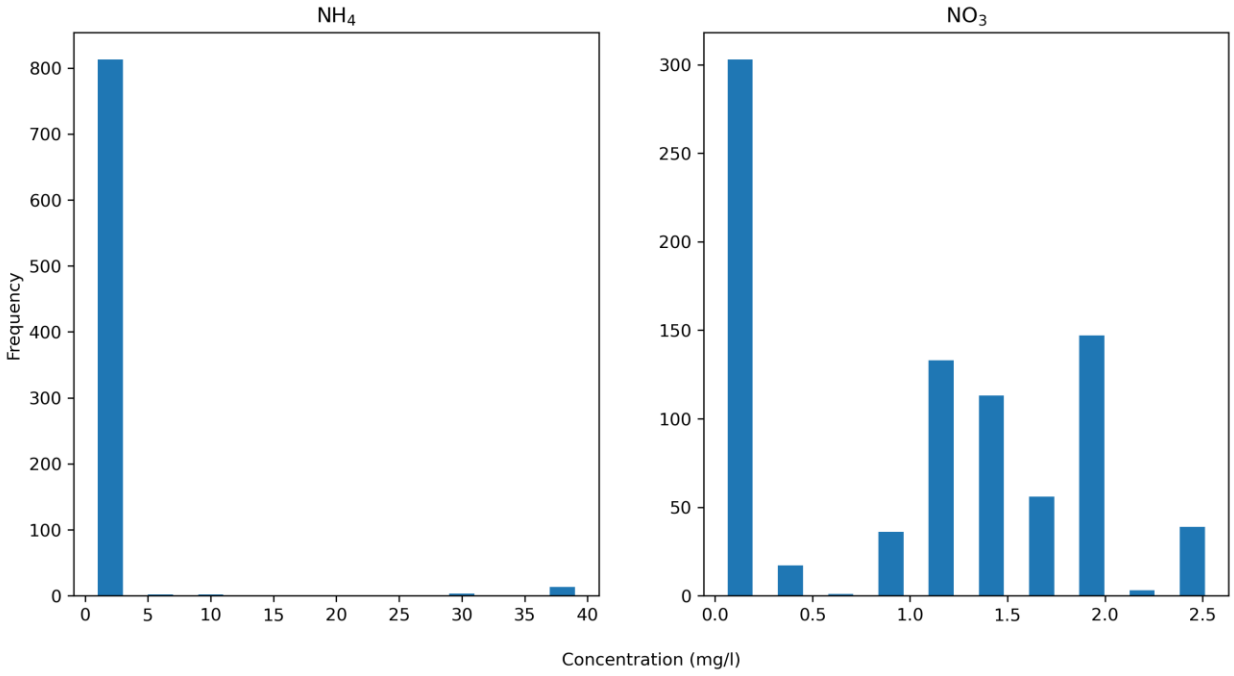

Fig. 4.38. Histogram of concentration of NH_4-N and NO_3-N at water table.

4.8. OSTDS Setback Distances for Lakeshore

Fig. 4.39 plots the vertical nitrogen attenuation rate ($1 - C_{WT}/C_{DF}$) with the vertical distance (VD) from drainfield to water table groundwater for the three soil types in Lakeshore. Because the values of K_{nit} and K_{dnt} used in this study area are the largest among all the study areas, the vertical nitrogen attenuation rate is large. Fig. 4.39 is similar to Fig. 4.11 for Eggleston Heights. The histogram of the vertical nitrogen attenuation rate (Fig. 4.40) is almost 100% for all the soil types because of the large values of K_{nit} and K_{dnt}. Figs. 4.41 and 4.42 plot the histograms of NH_4-N and NO_3-N concentrations at water table (C_{WT}) and water body (C_{WB}) for Lakeshore. The two figures show that the concentrations of NO_3-N and NO_4-N at water body are smaller than those at water table.

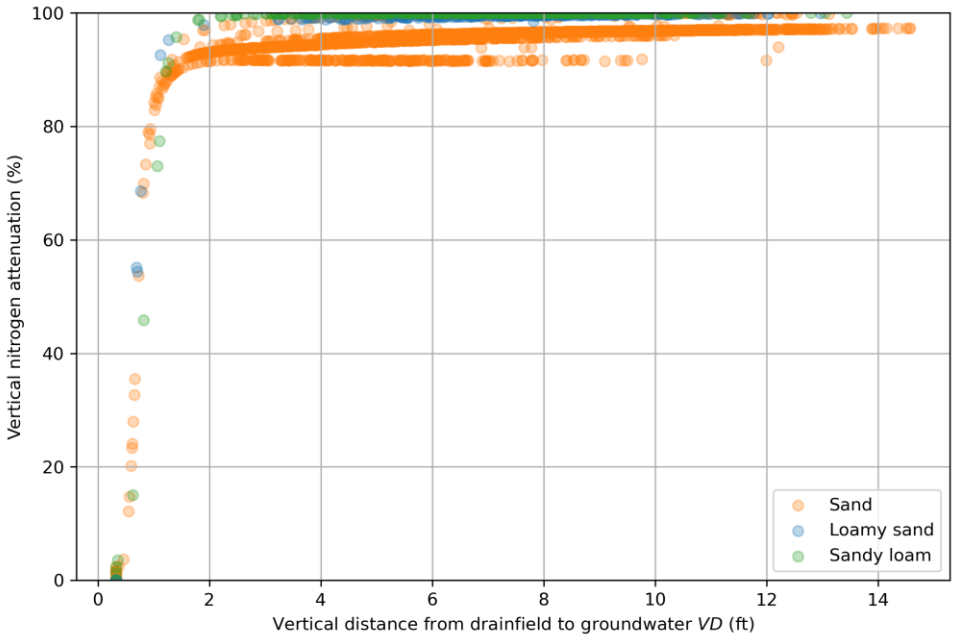

Fig. 4.39. Relation between vertical nitrogen attenuation rate ($1 - C_{WT}/C_{DF}$) and the vertical distance, VD, from drainfield to groundwater VD for Lakeshore.

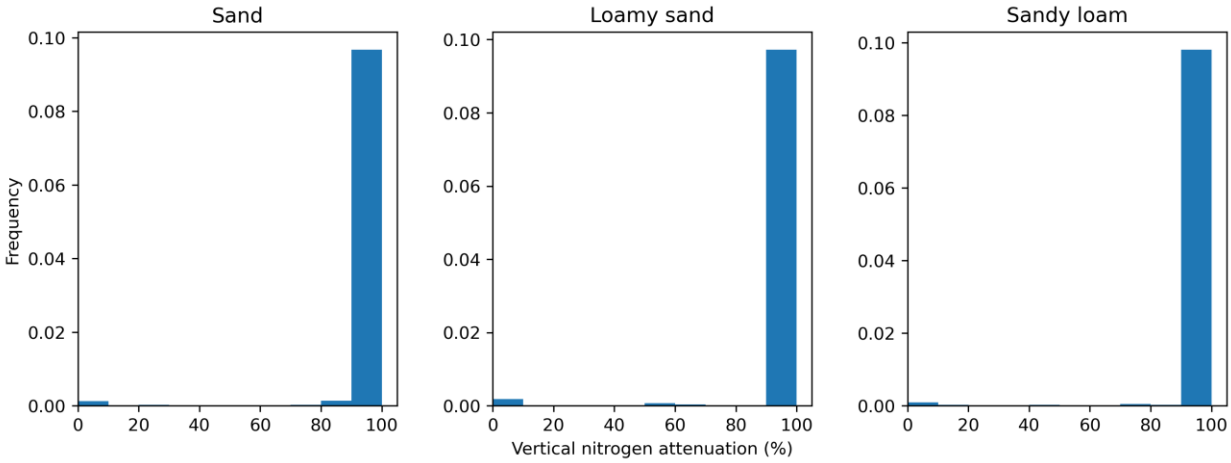

Fig. 4.40. Histograms of vertical nitrogen attenuation rate for Eggleston Lakeshore.

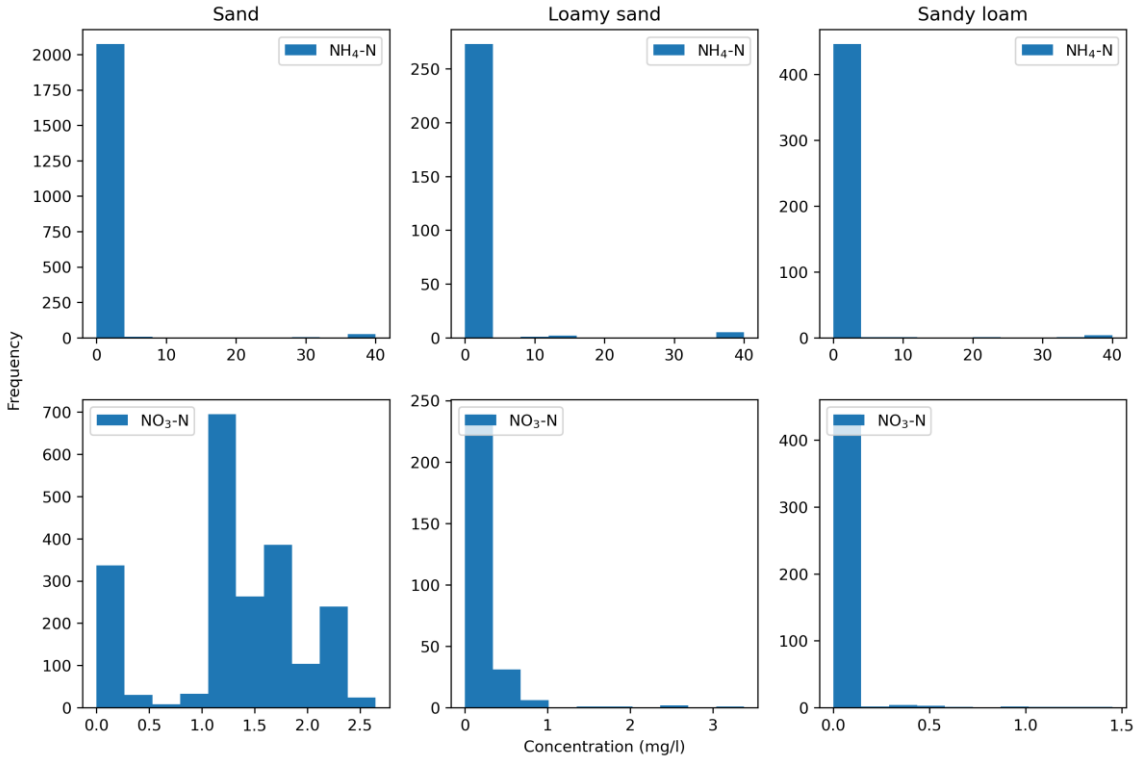

Fig. 4.41. Histograms of C_{WT} (NH_4-N and NO_3-N) for Lakeshore.

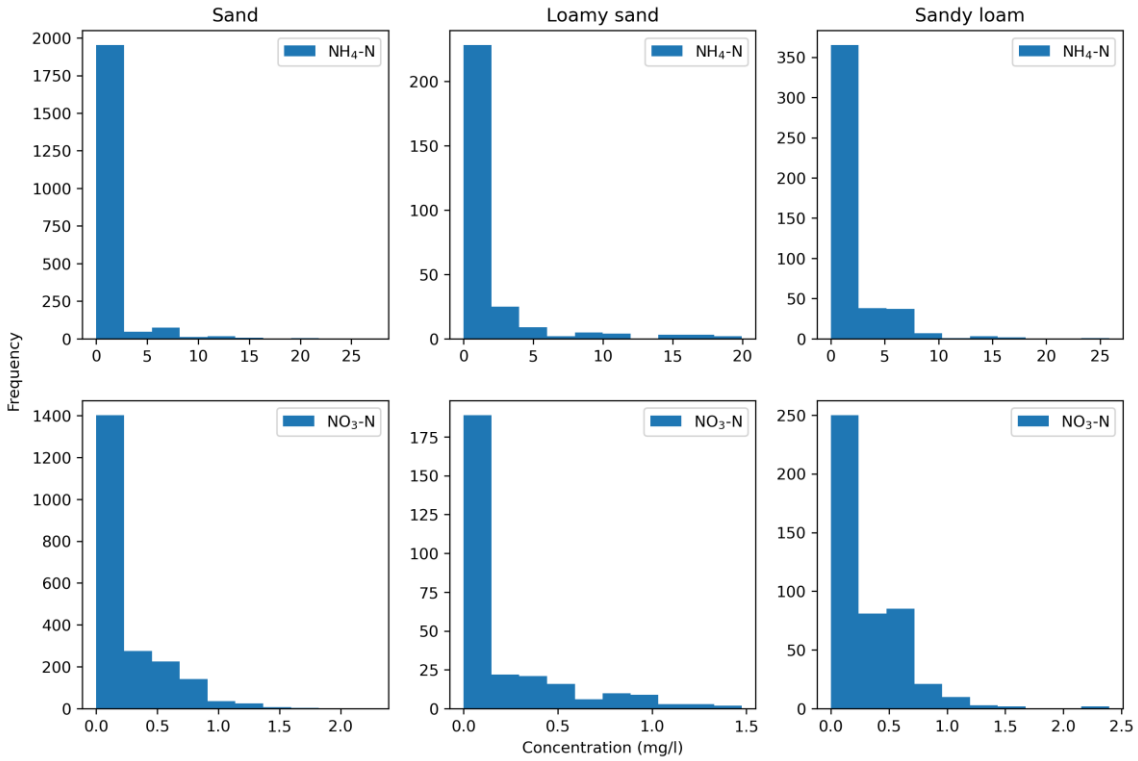

Fig. 4.42. Histograms of C_{WB} (NH_4-N and NO_3-N) for Lakeshore.

Fig. 4.43 plots the relations between the horizontal nitrogen attenuation rate ($1 - C_{WB}/C_{WT}$) and the horizontal linear distance from drainfields to water bodies for Lakeshore, and Fig. 4.44 plots the averaged horizontal nitrogen attenuation rate for every 10 ft of horizontal distance. The *AF* value was set as 98% for sand, while 100% for other soil types. Fig. 4.44 indicates that the empirical formula still works for Lakeshore.

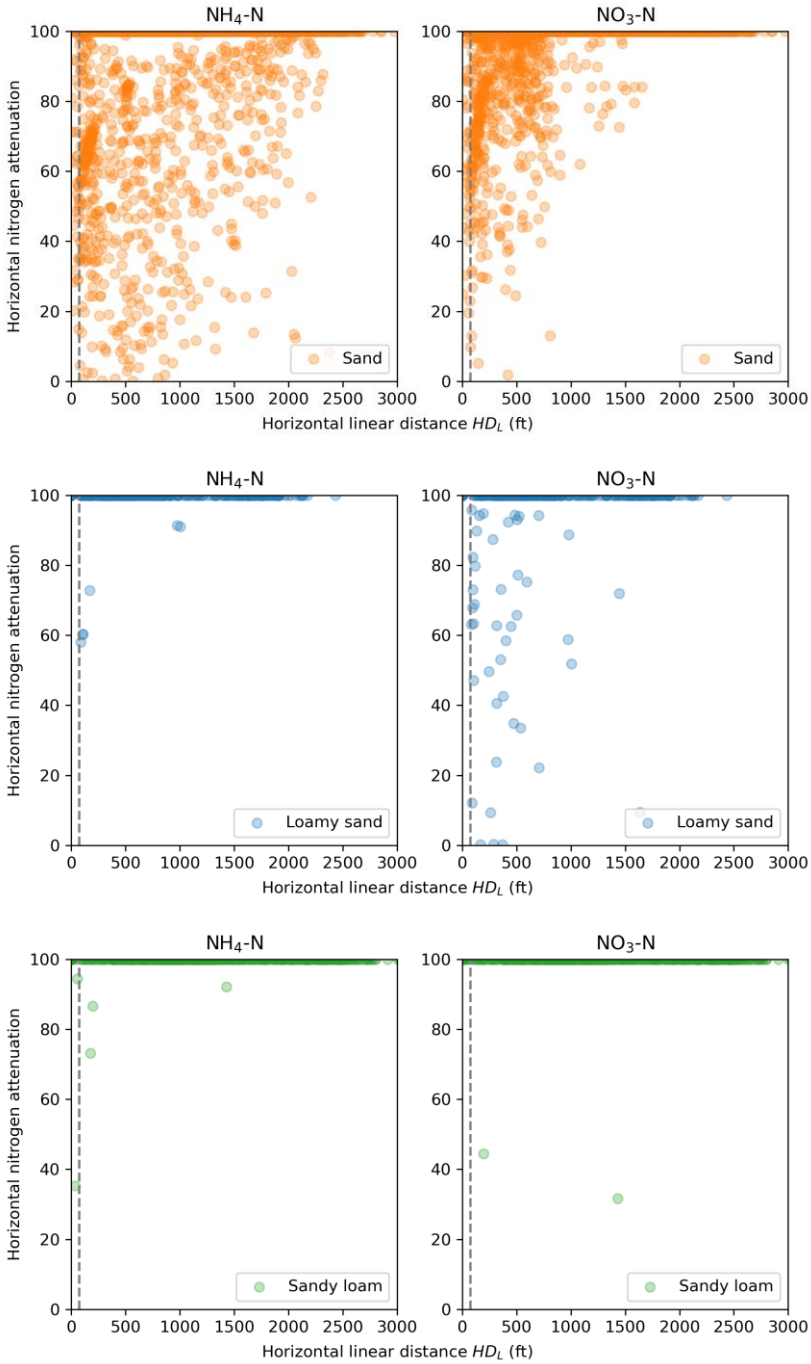

Fig. 4.43. Relations between horizontal nitrogen attenuation rate ($1 - C_{WB}/C_{WT}$) and linear horizontal distance (HD_L) from drainfield to waterbody for Lakeshore.

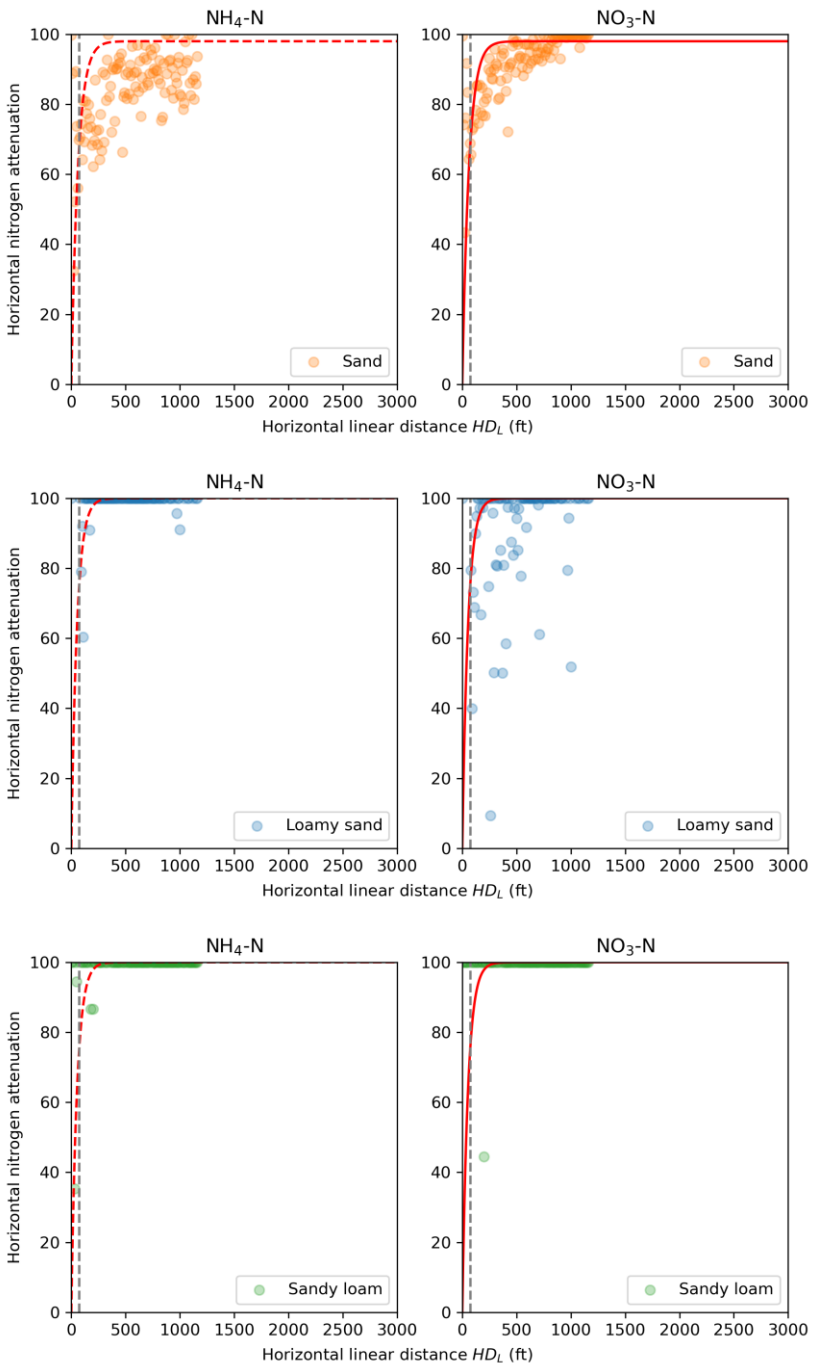

Fig. 4.44. Relations between horizontal nitrogen attenuation and the linear horizontal distance after averaging hydraulic gradient for every 10 feet of the distance.

For the sensitivity analysis of vertical and horizontal setback distances, ten OSTDS in Lakeshore were chosen, and their locations are shown in Fig. 4.45. The contours of the total nitrogen attenuation against the horizontal and vertical setback distances are plotted in Fig. 4.46

for sand, loamy sand, and sandy loam.

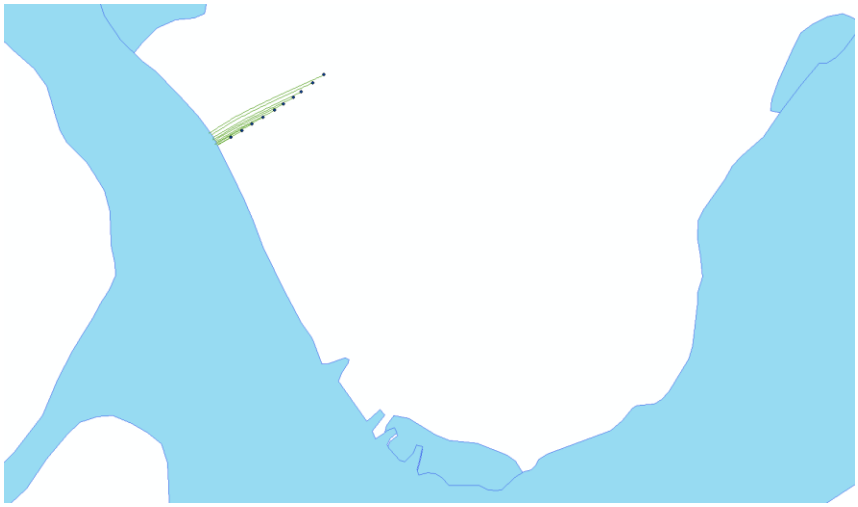

Fig. 4.45. OSTDS used for sensitivity analysis to determine the relation between total nitrogen attenuation rate and setback distances.

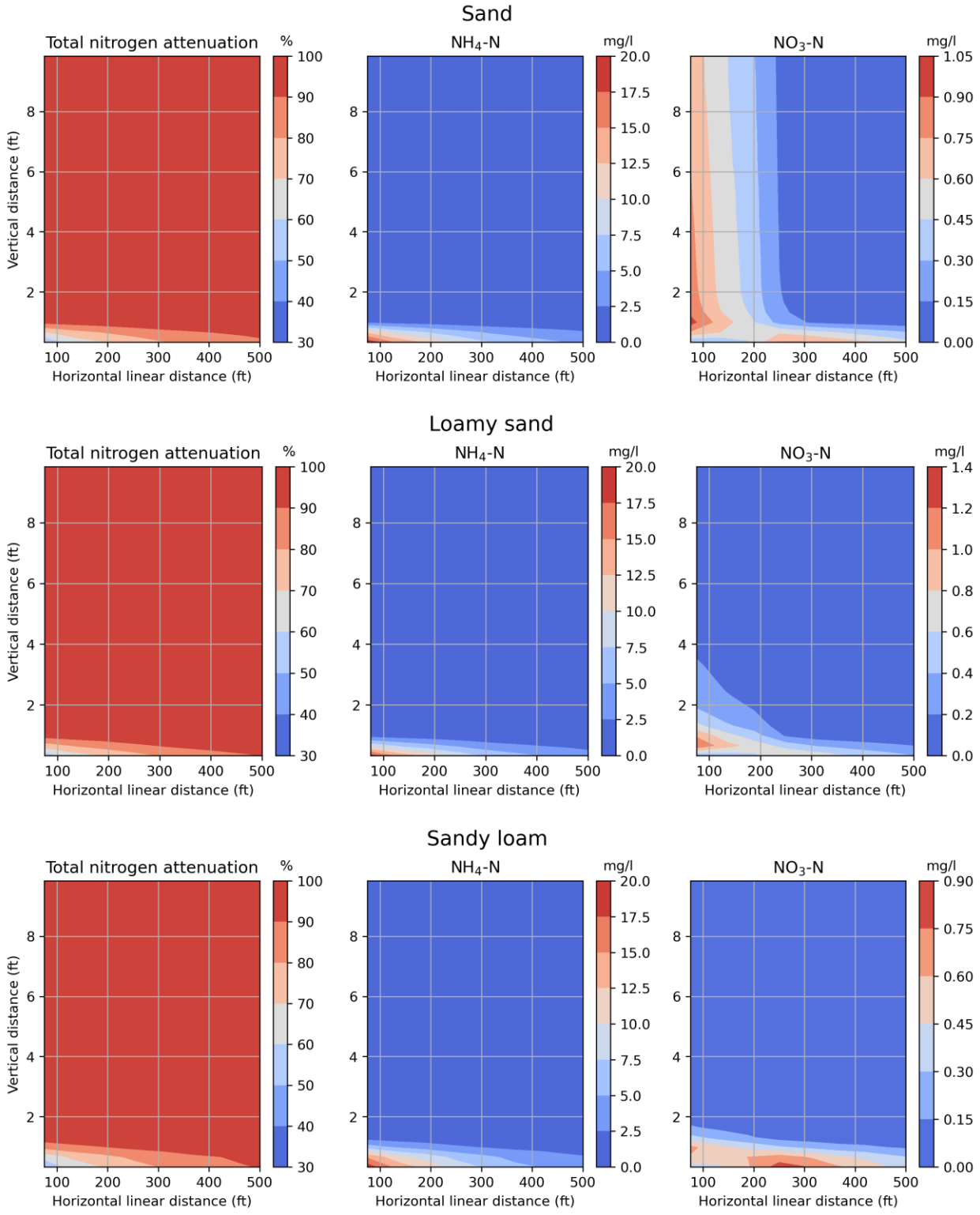

Fig. 4.46. Relations between nitrogen attenuation as well as concentrations of NH_4-N and NO_3-N entering the canal and the horizontal linear distance and vertical distance for Lakeshore. The smallest horizontal distance is 75 ft.

References

Belanger, T.V., Heck, H.H., Price Jr, T.L. 2011. Preliminary evaluation of septic tank influences on nutrient loading to the lower St. Johns River Basin and its tributaries.

Wang, L.Y., Ye. M., Rios, J.F., Lee, P. 2011. ArcNLET: an ArcGIS-based nitrate load estimation toolkit, application manual.

Ye, M., Wang, L.Y. 2012. Updated responses to SPRIM TAC evaluation of ArcNLET. FSU, Tallahassee.

Zhu, Y., Ye, M., Roeder, E., Hicks, R.W., Shi, L.S., Yang, J.Z. 2016. Estimating ammonium and nitrate load from septic systems to surface water bodies within ArcGIS environments. Journal of Hydrology. 532, 177-192.

Chapter 5. BN Analysis for Nitrogen and Phosphorus Attenuation from On-Site Treatment and Disposal Systems to Surface Water Bodies

5.1. Introduction

Surface water pollution caused by OSTDS is an increasing concern due to the potential impacts on water quality and public health (Clark 1996; US EPA 2015). The usage of OSTDS is widespread, and understanding their environmental impact is crucial for sustainable water resource management. Previous research has indicated that OSTDS can contribute significant nitrogenous compounds like nitrate (NO3), ammonia (NH3), and phosphorus to surface water bodies (Ayres Associates 1993; Troldborg et al. 2022). The objectives include identifying key risk factors associated with OSTDS pollution, incorporating site-specific data and expert knowledge to optimize model performance, and using the model to inform management strategies for groundwater protection. The goal of this study is to develop a Bayesian network (BN) model that estimates the probability of nitrate (NO3), total Kjeldahl nitrogen (TKN), and total phosphorous (TP) attenuation from OSTDS to surface water bodies.

Onsite sewage and waste disposal systems (OSTDS) are widely used for wastewater management, especially in areas without centralized sewer systems. However, their potential to contribute to surface water pollution by releasing NO3, TKN, and TP has raised concerns regarding water quality and public health (Troldborg et al. 2022). In addition, nitrogen and phosphorus pollution can lead to eutrophication, harmful algal blooms, and the deterioration of aquatic ecosystems (Clark 1996; US EPA 2015). Therefore, understanding and addressing the factors contributing to OSTDS pollution is crucial for preserving water resources and mitigating environmental impacts. Unfortunately, these compounds' transport and attenuation mechanisms in the environment are not thoroughly understood. Moreover, how different factors, such as setback distances from water bodies, influence these processes remains to be clarified (Glendell et al. 2021). These gaps in understanding limit our ability to manage the environmental impacts of OSTDS effectively.

The long-term project goal is to comprehensively understand the factors affecting NO3, TKN, and TP attenuation from OSTDS to surface water bodies and use this knowledge to inform effective groundwater protection strategies. The specific modeling objectives are identifying factors associated with OSTDS pollution in the Turkey Creek Basin of the Indian River Lagoon, St. George Island, and St. Johns River in Florida (Fig. 5.1). This study uses BN models to investigate the OSTDS-induced nitrogen load and its relationship with distances of attenuation. The models allow researchers to identify influential parameters that cause substantial changes in nitrogen attenuation (Glendell et al. 2021; Troldborg et al. 2022).

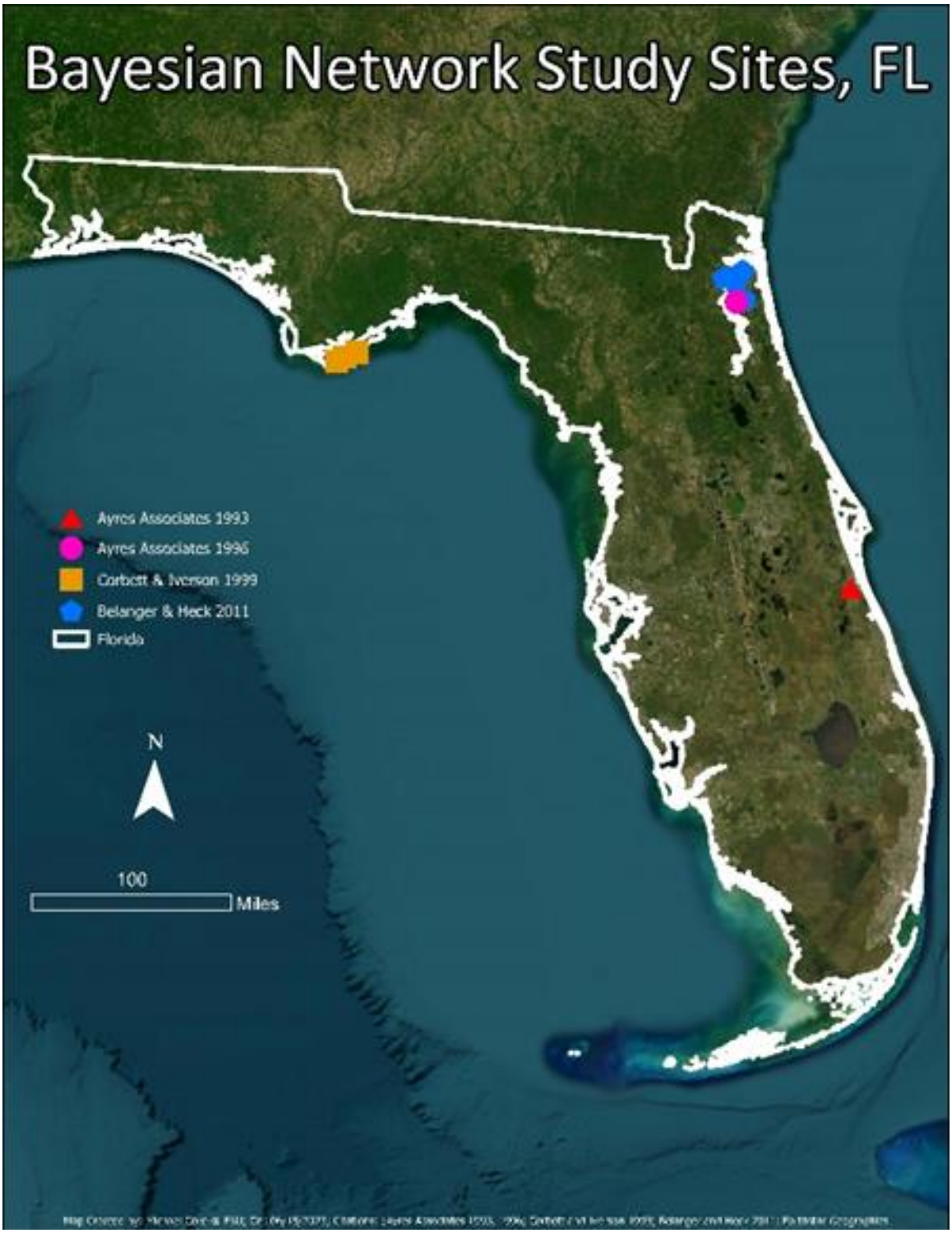

Fig. 5.1. Map of the Florida study sites from the literature used to build the BN. The map is of the study areas marked with colored shapes, and Florida is outlined in white.

Onsite Sewage Treatment and Disposal Systems (OSTDS) are vital in areas where centralized sewage treatment facilities are unavailable or impractical. These systems treat and dispose of household wastewater on the property where it is generated (Troldborg et al. 2022). OSTDS

consists of a septic tank, which collects and partially treats the waste, and a drain field, where the partially treated wastewater is discharged and further treated by soil-based processes (Clark 1996).

However, OSTDS are potential sources of nitrogenous compounds such as nitrate (NO3), ammonia (NH3), and phosphorus (TP), which can percolate into groundwater and eventually reach surface water bodies, thereby negatively impacting water quality (Clark 1996; US EPA 2015). High concentrations of these compounds can result in excessive algae growth, leading to eutrophication, reduced dissolved oxygen levels, and damage to aquatic life.

Given the widespread usage of OSTDS and the potential environmental implications, a detailed understanding of the nitrogen transport processes from OSTDS to surface water bodies is necessary for informed environmental decision-making. The study of attenuation distances between OSTDS, monitoring well locations, and water bodies and their effect on nitrogen is a crucial area of this research, as setback distances can significantly influence the amount of nitrogen reaching the surface waters (Glendell et al. 2021; Troldborg et al. 2022). This project employs BN models to probe this complex relationship. BNs are probabilistic graphical models representing the variables and conditional dependencies via a directed acyclic graph (Fenton and Neil 2018). Glendell et al. (2021) and Troldborg et al. (2022) offer a systematic approach to incorporate both quantitative data and expert judgments to quantify and analyze the impacts of OSTDS on nitrogen load.

The relevance of this study lies in its ability to advance our understanding of the environmental implications of OSTDS and its potential impacts on water quality. Troldborg et al. (2022) indicated that nitrogen loading from OSTDS to surface water bodies has been a primary environmental concern due to its potential to degrade water quality. Nevertheless, the complexity of nitrogen transport processes and the variability in system design, soil conditions, and operation practices pose challenges to assessing this impact accurately. The model's strength lies in its capacity to accommodate the complexity and uncertainty inherent in environmental systems (Fenton and Neil 2018). By systematically incorporating empirical data and expert judgments, the model allows a nuanced understanding of the variables and their conditional dependencies.

Moreover, by identifying the most and least influential parameters on nitrogen load, the findings of this study can guide policy decisions related to OSTDS installation and management. These decisions can reduce nitrogen pollution in surface waters, preserving water quality and aquatic ecosystems (Glendell et al. 2021). Ultimately, this study serves as a valuable tool for environmental decision-makers, helping to optimize strategies for OSTDS management to reduce their environmental impact and protect our valuable water resources.

During the comprehensive BN analysis, the data from Turkey Creek, Lakeshore, Julington Heights, St. George Island, and St. Johns sites were sourced from the FDEP and used to classify, categorize, and create data distributions to populate conditional probability tables (CPT) within various iterations of BN models representing both individual sites, entire studies (i.e., Turkey Creek (Ayres Associates 1993)), and all five studies combined into one BN model. The CPTs were trained with data from the FDEP-supplemented literature via the Expectation Maximization (EM) algorithm provided in the Norsys Software Corp (2007). First, individual models were designed, trained, and assessed for each previously mentioned location. Afterward, one network was designed and trained to accommodate all the data from all five locations mentioned above. Several findings emerged from this study, such as estimates of the distances needed to attenuate various analytes in the groundwater from an OSTDS. The network was used to estimate the attenuation

rates for NO3-N, NH3-N, and TP for the combined data set for Turkey Creek, Lakeshore, Julington Heights, St. George Island, and St. Johns. These analytes and the combined BN were chosen as they demonstrated the lowest error rates and consistently pointed towards the attenuation distance as a significant factor during sensitivity analysis.

The study leveraged the strengths of the BN to predict the necessary attenuation distances from the groundwater source of pollution originating from an OSTDS towards the downgradient adjacent surface waterbody via entering the evidence of an attenuation rate into one of the output nodes of the network and having the results propagate the parent nodes. For example, the evidence of a 0% to 25% attenuation rate was entered into the NO3-N attenuation node, and the evidence's results of 10ft to 25ft of the distance needed to achieve the evidential attenuation rate were observed in the distance of the attenuation node. Likewise, the distances required for various attenuation rates (0% to 25%, 25% to 50%, 50% to 75%, 75% to 95%, and 95% to 100%) changed but generally fell between 10ft and 50 ft for NO3-N, NH3-N, and TP. The juvenile network with limited training believes that for 100% attenuation, distances of 50 ft were needed across all analytes (NO3-N, NH3-N, and TP) for the combined dataset (Turkey Creek, Lakeshore, Julington Heights, St. George Island, and St. Johns). These findings agree with the results of earlier studies by Ayres Associates (1993), which reported that nitrogen levels should approach or revert to background levels within approximately 40 feet of the OSTDS but are not recommended for a setback due to the fledgling nature of the BN. The attenuation rate, analyte concentrations, and distances of attenuation data can be seen in the scatterplots in Figs. A26 – A30 in the appendix. These data plots generally show that analyte concentrations are attenuated 80% to 100% within 75 ft of the OSTDS.

The specialized BN utilized in this study demonstrated varying success in predicting nutrient attenuation rates from OSTDS to adjacent surface water bodies. While the model showed excellent performance in certain areas, with 0% error rates for predicting NO3-N and ammonium (NH4-N) groundwater attenuation, other nutrients, such as TN and nitrate (NOx), showed higher error rates of 50% and 66.67%, respectively. These results emphasize the complexity of nutrient behavior in the subsurface environment and the need for ongoing model refinement and validation. Furthermore, this study unearthed several findings about the relationship between OSTDS, nitrogenous compounds, and the attenuation rates as they travel toward surface water bodies. The calculated OSTDS-based pollutant attenuation rates and distances the analyte traveled are in the appendix. These findings reveal pivotal factors influencing nutrient transport and transformation in soil and groundwater systems within the network. The distance of attenuation, organic carbon, dissolved oxygen concentration, and groundwater source concentration was most responsive to change, emphasizing their critical role in the system. Alternatively, groundwater flow characteristics such as hydraulic gradient and ground elevation were less impactful to the network. These findings can guide mitigation strategies for managing nitrogen load in surface water bodies originating from OSTDS. In summary, our sensitivity analysis has revealed that although some factors within the network exert less influence on OSTDS analyte attenuations, their exact impact may be context-dependent. This underscores the necessity for a comprehensive and tailored approach when managing OSTDS performance and its potential impact on water quality (Glendell et al. 2021).

5.2. Combined BN Model

The analytical methodology applied to this study leveraged a combination of commercial and specialized software, each tailored to specific steps of the data collection, analysis, and

interpretation process. Data originating from the literature was systematically organized, and calculations were executed using Microsoft Excel for Microsoft 365 MSO (Version 2305 Build 16.0.16501.20074) 64-bit. Excel's robust data manipulation, analysis, and visualization features were crucial in managing the data's complexity and ensuring its readiness for analysis. Spatial analysis and visualization were performed using ArcGIS Pro (Version 3.1.2). ArcGIS Pro was instrumental in providing the necessary geographic context for our study locations, offering the ability to manipulate, analyze, and display geospatial data effectively. Its extensive suite of tools provided the versatility required to handle the geospatial elements of our study. The centerpiece of the analytical toolkit was Netica (Version 6.09 64 bit for MS Windows 7 to 10), a leading software package for working with Bayesian networks (BN). This software facilitated the construction of the complex BNs that underpinned the study. Netica enabled the derivation of detailed error rate analyses and sensitivity analyses of the nodes within our networks, which was crucial for evaluating the robustness and reliability of the models. Together, these software packages provided the computational capabilities and versatility to handle the multi-dimensional data and complex analyses required for the study. This diverse software suite reflects the interdisciplinary nature of the research, encompassing fields ranging from statistical analysis and hydrogeology to geographic information systems.

The BN model applied in this study is a graphical model used to represent the probabilistic relationships among several variables. In the context of our research, it allows users to estimate the attenuation rates of nitrogen, ammonia, and phosphorus transport from an onsite sewage and waste disposal system (OSTDS) to a surface water body while accounting for the inherent uncertainty in these systems (Glendell et al. 2021; Troldborg et al. 2022). This decision network was specifically developed to incorporate the influences of various environmental and anthropogenic factors. Variables such as soil porosity, depth to groundwater, wastewater quality, and setback distances are all integrated within the network. Each variable (or 'node') in the network is connected to others through direct links, representing the dependencies between these factors (Fig. 5.2)(Fenton and Neil 2018).

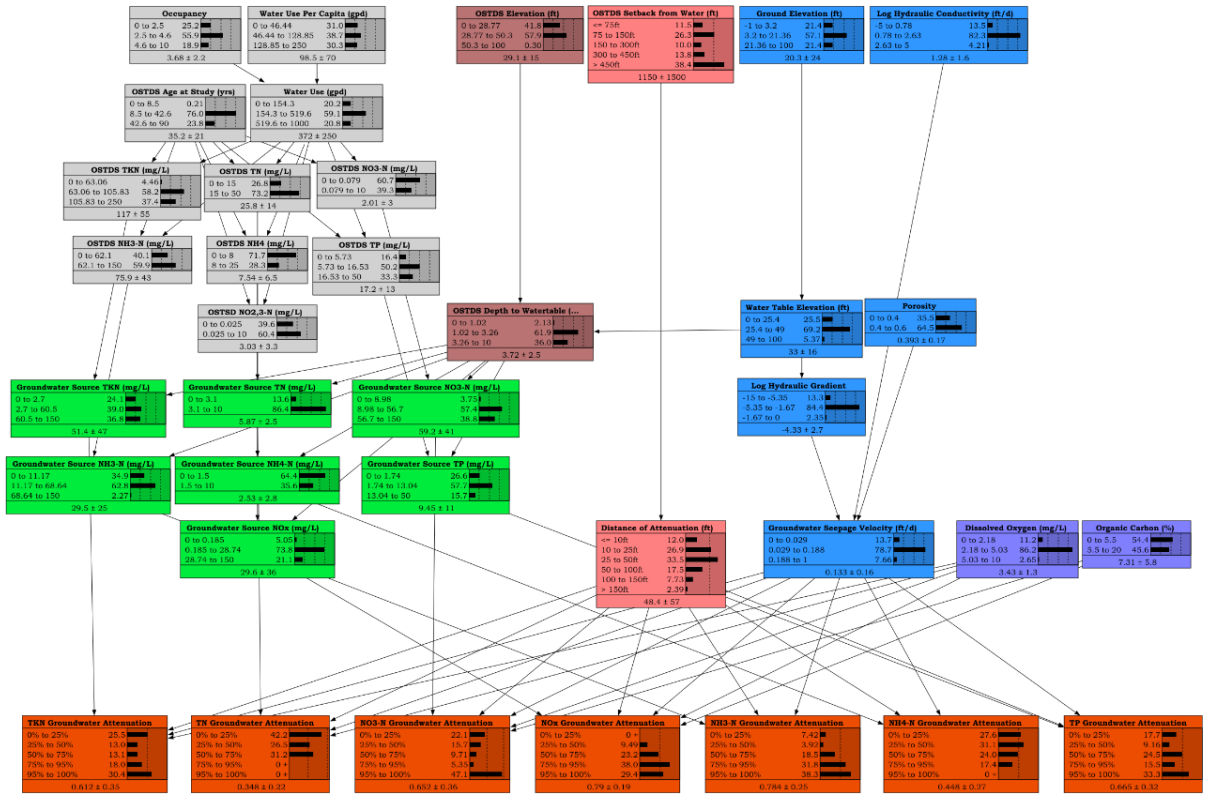

Fig. 5.2. The combined Turkey Creek, Lakeshore, Julington Heights, St. George Island, and St. Johns Bayesian network. The BN output attenuation nodes are in orange. The node links are black lines, which connect parent and children nodes.

As a part of the BN, conditional probability tables were established for each node to quantify the relationships between nodes based on prior knowledge and observational data (Fenton and Neil 2018). In this way, the BN provides a robust decision-making framework, integrating quantitative data and expert judgment. The strength of a network model lies in its capacity to handle non-linear, complex relationships and to incorporate uncertainty, making it an ideal tool for investigating the relationship between setback distances, analyte attenuation, and OSTDS-induced nitrogen load to surface waters (Troldborg et al. 2022).

The BN model, at its core, utilizes the principles of Bayesian probability theory, in which prior knowledge is updated with new data to estimate the likelihood of an outcome (Fenton and Neil 2018). For this study, the result of interest is the attenuation rate of nitrogen, ammonia, and phosphorus transport from an OSTDS to a surface water body. First, a researcher identifies key variables or parameters influencing the system under study (Troldborg et al. 2022). These variables (called 'nodes') comprise the network and are connected through directed links representing causal relationships. In this study, these variables included but were not limited to setback distances, the distance of analyte attenuation, soil porosity, hydraulic gradient, Darcian seepage velocity, depth to groundwater, and OSTDS wastewater quality. Each node has an associated probability distribution, conditioned on the state of its parent nodes (if any) (Glendell et al. 2021). This interdependence between variables is captured through conditional probability tables, quantifying node relationships (Fenton and Neil 2018). Furthermore, the states of each node, such as the

setback distance, were defined based on the relevant literature and expert opinion. This variability in the input parameters captured the heterogeneity seen in real-world scenarios (Fenton and Neil 2018).

Once the network is established, it is operationalized through data input. As new information becomes available, Bayes' theorem updates the conditional probabilities. The updated probabilities then propagate through the network, influencing the probabilities of downstream nodes (Fenton and Neil 2018). In our study, the BN model was utilized to predict the attenuation rates of nitrogen, ammonia, and phosphorus in different scenarios, providing insights into the interplay of the variables affecting these rates. The model's predictive power allowed for an evaluation of the impacts of various environmental and anthropogenic factors on the OSTDS-induced nitrogen attenuation rates (Glendell et al. 2021; Troldborg et al. 2022).

The output parameters of the Bayesian network (BN) model were primarily the estimated attenuation rates for nitrogen, ammonia, and phosphorus, represented as attenuation rate nodes (i.e., Attn_NOxN_mg_L, Attn_NH3N_mg_L, Attn_NH4N_mg_L, and Attn_TP_mg_L). These parameters represented the percentage of these compounds that were attenuated as they traveled from the OSTDS to the nearest surface water body. By using these input and output parameters, the network model could estimate the nitrogen attenuation rates from OSTDS to surface water bodies under different scenarios, providing a comprehensive tool for understanding and predicting the behavior of these systems (Glendell et al. 2021; Troldborg et al. 2022).

The steps below were followed to create each individual network and then the combined one. First, a site was selected using report data to choose areas monitoring locations where nitrogen and phosphorus concentrations were highest at the wells adjacent to the OSTDS and decreased downgradient. The data leveraged for this project came from FDEP reports, where observations of Florida residents were recorded from 1993 to 2011. Secondly, data and figures were georeferenced, and attenuation rates were calculated for each study site by using report data and figures to calculate the percent reduction of nitrogen and phosphorus and the distance from the groundwater contamination source locations near the OSTDS to the downgradient monitoring well. During this phase, report data was used to identify an analyte plume from the OSTDS traveling downgradient for eight residents and one state park study site. The calculated attenuation rates were used in the cross-validation process for the BN. Likewise, the distance and attenuation rates were plotted and compared (see the appendix). Thirdly, the data was characterized and classified into bin ranges using histograms, and then probabilities were calculated for each bin range for a total of 89 monitoring locations with a possible 36 records for each location. The data characterization and discretization were used to create the conditional probability tables (CPT) in the untrained BN. The EM algorithm was used during the BN training to fill in missing data points (Norsys Software Corp 2007). For example, NOx was not measured at every location used to build the combined BN, but using the EM algorithm, a likely value for NOx groundwater concentrations and attenuation rates could be generated for each monitoring location. Fourthly, a separate BN was trained with the monitoring location records for each study site, generally 10 to 20 records per network. During training, 1 to 3 records were removed and used as evidence in the cross-validation of the BN-predicted attenuation rates for real-world monitoring locations. Afterward, one BN was created that was trained with data from all the monitoring wells except 1 for each site that was used as evidence for the cross-validation of predicted attenuation rates. Lastly, the BN attenuation rate nodes were tested for sensitivity to all other nodes in the network to help determine the BN’s critical data points.

5.2.1 Model Results

The BN model provided an understanding of OSTDS-induced nitrogen loadings to surface water bodies in various hydrogeologic settings. The results focused on the estimated attenuation rates for nitrogen, ammonia, and phosphorus. Regarding nitrate-nitrogen (NO3-N) groundwater attenuation, the model predicted relatively lower error rates, particularly for the 75% to 95% and 95% to 100% categories, resulting in an overall error rate of 0.0% for the combined BN. This was an increase in performance from an error rate of 53% when only the Turkey Creek data (Ayres Associates 1993) was used. The decrease in error rates suggests better network performance as more data is added to the learning process. The higher error rates represent a complex interplay of factors affecting nitrate-nitrogen attenuation, warranting further investigation.

Regarding ammonia-nitrogen (NH3-N) (i.e., Attn_NH3N_mg_L) groundwater attenuation, the model's prediction yielded a lower percent error rate of 25%, especially in the higher attenuation categories. Likewise, the BN was able to predict the NH3-N attenuation rate with a 50% error rate for the Lakeshore and Julington Heights sites (Belanger et al. 2011) with fewer data points. These findings indicate a somewhat accurate representation of ammonia-nitrogen behavior in the system.

Monitoring Location	Analyte	Error Rate
G13; G14; G15	TKN	100%
G13; G14; G15	NO3-N	0%
G13; G14; G15	TP	0%
G15; J8; CST1120100601; DH920100927; MM720100602; RTPZ420091229; JA9; SP8; TW151993; TW151995	TKN	40%
G15; J8; CST1120100601; DH920100927; MM720100602; RTPZ420091229; JA9; SP8; TW151993; TW151995	TN	50%
G15; J8; CST1120100601; DH920100927; MM720100602; RTPZ420091229; JA9; SP8; TW151993; TW151995	NO3-N	0%
G15; J8; CST1120100601; DH920100927; MM720100602; RTPZ420091229; JA9; SP8; TW151993; TW151995	NOx	67%
G15; J8; CST1120100601; DH920100927; MM720100602; RTPZ420091229; JA9; SP8; TW151993; TW151995	NH3-N	25%
G15; J8; CST1120100601; DH920100927; MM720100602; RTPZ420091229; JA9; SP8; TW151993; TW151995	NH4-N	100%
G15; J8; CST1120100601; DH920100927; MM720100602; RTPZ420091229; JA9; SP8; TW151993; TW151995	TP	25%

Table 5.1. Results of the combined Turkey Creek, Julington Heights, Lakeshore, St. George Island, and St. Johns Bayesian network. The network shows improved performance with more data in the training process.

The ammonium-nitrogen (NH4-N) groundwater attenuation category revealed a significant challenge with an error rate of 100%. This result pointed to significant missing parameters in the model or a more complex behavior of ammonium in groundwater, which might still need to be fully understood (Glendell et al. 2021). Furthermore, in the total phosphorus (TP) Groundwater attenuation category, the model demonstrated a reasonable level of accuracy with an error rate of 25%, robust in the 95% to 100% category. This suggested that the model was relatively reliable in predicting the behavior of total phosphorus in the environment.

These results provide insights into the setback distances and their influence on nutrient attenuation from OSTDS to nearby surface water bodies. Further model refinement and research are necessary to increase prediction accuracy, especially for NOx and NH4-N. However, the findings here are an essential step forward in estimating and potentially mitigating nutrient loading from OSTDS. The model's overall prediction error rates for each nutrient provided valuable insights. In the case of NOx, the error rate of 66.67% (Table 5.1) signified that the prediction model needs refinement, potentially indicating a more complex attenuation process influenced by numerous parameters, some of which might not be adequately accounted for in the current model

(Troldborg et al. 2022). This analysis highlighted the model's strengths and areas needing improvement, emphasizing the necessity for continuous research and model refinement. The data interpretation provides critical guidelines for OSTDS management practices, highlighting the impact of setback distances on nutrient attenuation. Still, it also points to the need for a more holistic approach considering the complexity of the environmental and geochemical processes.

5.2.2 Model sensitivity

A sensitivity analysis was performed on the Bayesian network (BN) model to evaluate how changes in various parameters would impact the model's outputs (Tables 5.2 and 5.3). A model's sensitivity to specific input parameters indicates the degree to which these variables influence predictions. It aids in identifying the most (or least) influential parameters that can cause the most significant (or slightest) change in the network’s nodes (Norsys Software Corp 2007).

Node	Influential Nodes
TKN Attenuation	Distance of attenuation; GW Source TKN; OSTDS TKN; NH3-N Attenuation
TN Attenuation	Distance of attenuation; Seepage Velocity; GW Source TN; Dissolved oxygen
NO3-N Attenuation	Distance of attenuation; NH3-N Attenuation; Organic carbon; TP Attenuation
NOx Attenuation	Distance of attenuation; NH3-N Attenuation; TP Attenuation; GW Source NOx
NH4-N Attenuation	Distance of attenuation; Seepage Velocity; TKN Attenuation; TN Attenuation
NH3-N Attenuation	Distance of attenuation; TP Attenuation; TKN Attenuation; GW Source NH3-N
TP Attenuation	Distance of attenuation; GW Source TP; NH3-N Attenuation; OSTDS TP

Table 5.2. Most influential factors impacting attenuation rates for the combined network. As seen in the table, the attenuation distance continually shows influence over the network's beliefs.

Node	Non-Influential Nodes
TKN Attenuation	Log Hydraulic Conductivity; OSTDS NH3-N; Ground Elevation; Log Hydraulic Gradient
TN Attenuation	Occupancy; OSTDS TKN; Water Use Per Capita; Groundwater Source NH4-N
NO3-N Attenuation	Log Hydraulic Conductivity; OSTDS TN; OSTDS NH4; OSTDS Age
NOx Attenuation	Ground Elevation; Log Hydraulic Gradient; OSTDS TKN; OSTDS NO3-N
NH4-N Attenuation	Occupancy; OSTDS TKN; GW Source NOx; GW Source NO3-N
NH3-N Attenuation	Ground Elevation; Water Table Elevation; Log Hydraulic Gradient; GW Source NH4-N
TP Attenuation	Log Hydraulic Conductivity; OSTDS NH3-N; GW Source NH3-N; OSTDS NO3-N

Table 5.3. Least influential factors impacting attenuation rates for the combined network. The table shows that hydraulic conductivity has the least influence on the network.

For each of the analytes, total Kjeldahl nitrogen (TKN), total nitrogen (TN), nitrate nitrogen (NOx & NO3-N), ammonia nitrogen (NH3-N), ammonium nitrogen (NH4-N), and total phosphorus (TP), the Turkey Creek, Lakeshore, Julington Heights, St. George Island, and St. John model's sensitivity was assessed. The model appeared to be most responsive to the changes in the distance of attenuation, adjacent attenuation rates of the previously mentioned analytes, and the groundwater source concentrations of a given analyte. This aligns with the literature stating that these factors are critical in controlling nutrient transport and transformation in the soil and groundwater system (Ayres Associates 1993, 1996). For instance, increasing the distances of attenuation from the OSTDS showed a considerable reduction in nitrogen load, highlighting the role of distance as a critical buffer in nutrient transport (Clark 1996).

In the context of our combined Bayesian network for Turkey Creek, Lakeshore, Julington Heights, St. George Island, and St. Johns, a closer examination of attenuation nodes reveals their sensitivity to specific factors in the network. Each attenuation node's influence was reported for the four most and least influential nodes for attenuation rates (Table 5.2). This critical interaction indicates that these interrelationships significantly influence the model's predictive capability.

The TKN attenuation node, for example, is sensitive to changes in the distance of attenuation, groundwater (GW) source concentration of TKN, OSTDS concentration of TKN, and NH3-N attenuation rate nodes. Similarly, the TN attenuation node was most sensitive to the attenuation distance, groundwater seepage velocity, GW source concentration of TN, and dissolved oxygen concentration nodes. The sensitivity of the NO3-N and NOx attenuation nodes underscore the interconnectedness of nutrient cycles. These nodes were sensitive to changes in the distance of attenuation, NH3-N attenuation, and TP attenuation nodes. Furthermore, the NO3-N attenuation node was sensitive to the organic carbon concentration node, and the NOx attenuation node was sensitive to the GW source NOx concentration node. A similar pattern was observed when focusing on the NH4-N and NH3-N attenuation nodes. Both nodes were sensitive to the distance of the attenuation node. In addition, the NH4-N attenuation node was sensitive to the groundwater seepage velocity, TKN attenuation, and TN attenuation nodes. Conversely, the NH3-N attenuation node was sensitive to the TP attenuation, TKN attenuation, and GW Source NH3-N concentration nodes. Finally, the TP attenuation node displayed sensitivity to the attenuation distance, GW source TP concentration, NH3-N attenuation, and OSTDS TP concentration nodes.

Understanding these sensitivities is crucial as it provides deeper insights into how variations in these specific nodes might influence the performance and output of the attenuation nodes. These findings form an integral part of our ongoing model refinement process. Future improvements to the model's performance may be realized by focusing on these influential nodes and their interplay within the network. On the other hand, the model was less sensitive to changes in other factors, such as occupancy, water use (gpd), and ground elevation (ft), suggesting that these parameters might have a lesser direct impact on the nitrogen attenuation rates. These findings emphasize the need for a comprehensive understanding of different site-specific parameters and their impacts on nutrient loading. It underlines the importance of tailor-made OSTDS management strategies considering these influential factors, as Glendell et al. (2021) highlighted.

The factors that have the least to negligible impact across various types of analyte attenuation provide insight into the complex interplay within these systems (Table 5.3). In the context of TKN attenuation, changes in parameters such as log hydraulic conductivity, OSTDS NH3-N concentration, ground elevation, and log hydraulic gradient show minimal impact on the rate of TKN attenuation. In the network, these factors do not significantly sway TKN attenuation rates. Furthermore, a different pattern emerges when considering TN attenuation. The factors such as occupancy, OSTDS TKN concentration, water use per capita, and groundwater source NH4-N concentration show a diminished influence. This highlights the nuanced complexity of TN attenuation, in which these factors have a reduced yet present role. For NO3-N attenuation rates, the sensitivity analysis indicates a limited influence of factors like log hydraulic conductivity, OSTDS TN concentration, OSTDS NH4 concentration, and the OSTDS age at the time of the study. While these factors are also part of the more extensive system, their impact on NO3-N attenuation remains relatively minor in the BN.

The least impactful factors in NOx attenuation include ground elevation, log hydraulic gradient, OSTDS TKN concentration, and OSTDS NO3-N concentration. Once again, despite their presence

in the network, the influence of these factors on NOx attenuation is less significant. NH4-N attenuation offers another perspective where occupancy, OSTDS TKN concentration, groundwater source NOx concentration, and groundwater source NO3-N concentration demonstrate the most negligible impact. Their limited influence accentuates the intricate balance within the NH4-N attenuation process. Regarding NH3-N attenuation, ground elevation, water table elevation, log hydraulic gradient, and groundwater source NH4-N concentration show the most negligible impact. While integral to the network, these factors exert minimal influence on the NH3-N attenuation rates. Finally, considering TP attenuation, factors like log hydraulic conductivity, OSTDS NH3-N concentration, groundwater source NH3-N concentration, and OSTDS NO3-N concentration are the least impactful.

To summarize, the sensitivity analysis illuminates how certain factors, although part of the larger network, influence different OSTDS analyte attenuations less. However, it is essential to note that these factors' exact interplay and significance could depend on site-specific characteristics and conditions. These least impactful factors may still be relevant, underscoring the need for a comprehensive approach when analyzing and managing OSTDS performance and its potential impact on water quality.

5.3. BN for Turkey Creek Site (Ayres Associated, 1993)

The study area is in the Turkey Creek Basin of the Indian River Lagoon, Florida (Fig. 5.3). This region consists of two main sites, Jones, and Groseclose, with unique geological and hydrogeological characteristics that influence the transport and attenuation of pollutants from OSTDS to surface water bodies (Ayres Associates 1993).

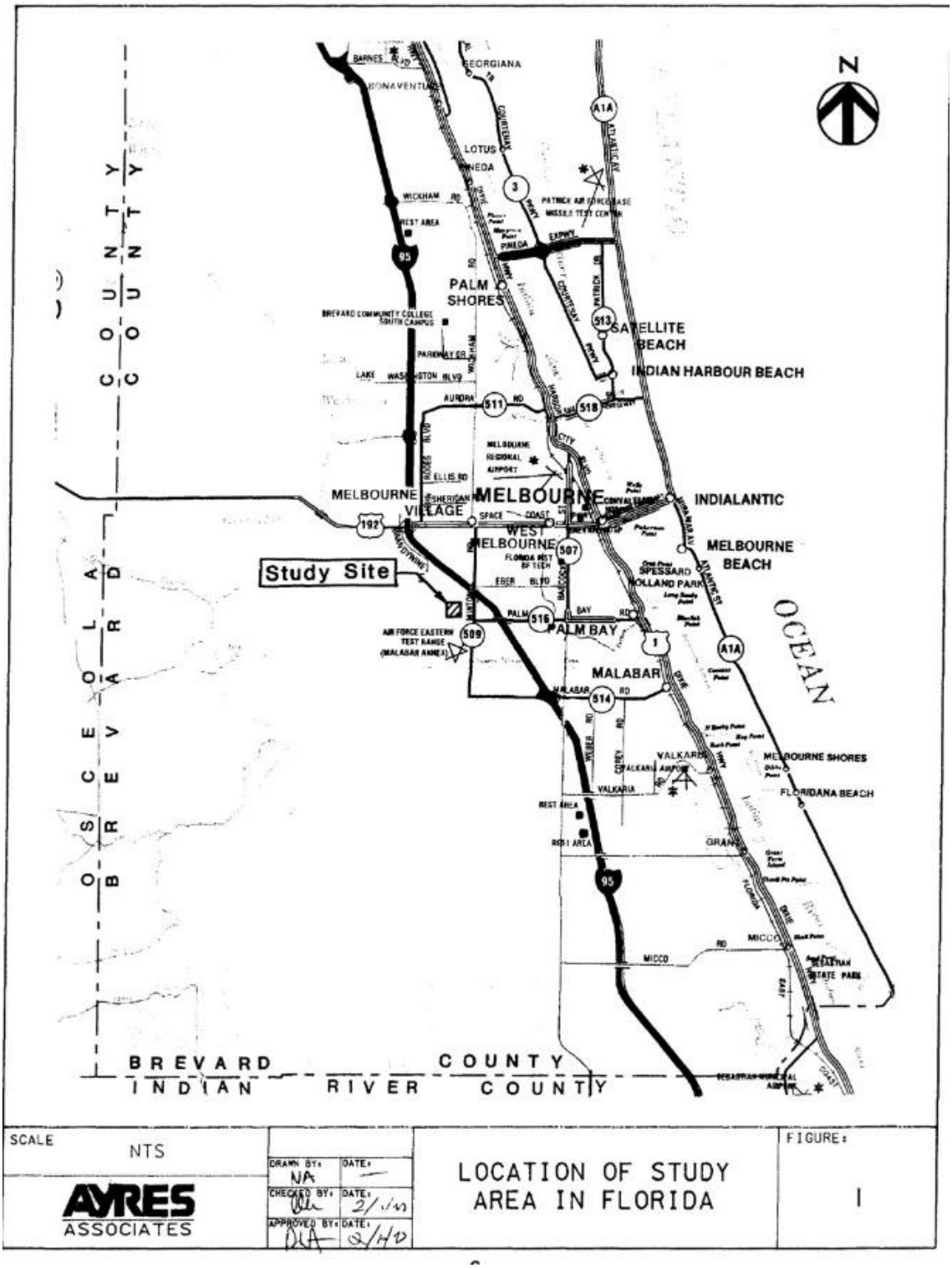

Fig. 5.3. Map of the Melbourne area from Ayres Associates (1993). Survey of Melbourne, Florida, with roads and boundaries in black.

The study area experiences significant recharge from precipitation and surface water infiltration. The Jones site has a predominantly northeasterly groundwater flow direction (Fig. 5.4), while the Groseclose site exhibits a predominantly northwesterly flow direction (Fig. 5.5).

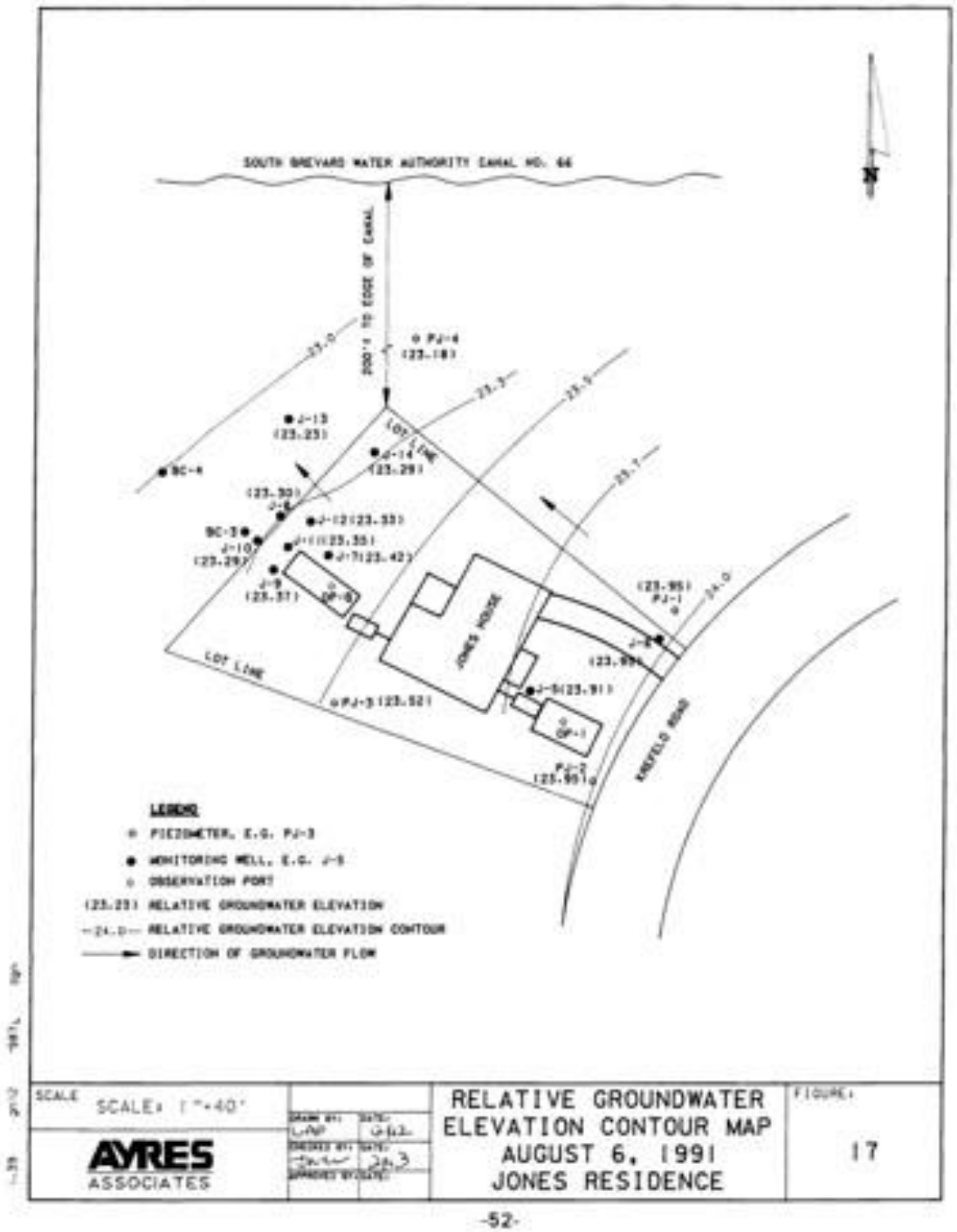

-52-

Fig. 5.4. Groundwater flow direction at the Jones Site, Turkey Creek, Ayres Associates (1993). The boundary survey shows the Jones residents in a black outline and the groundwater elevation in black contour lines.

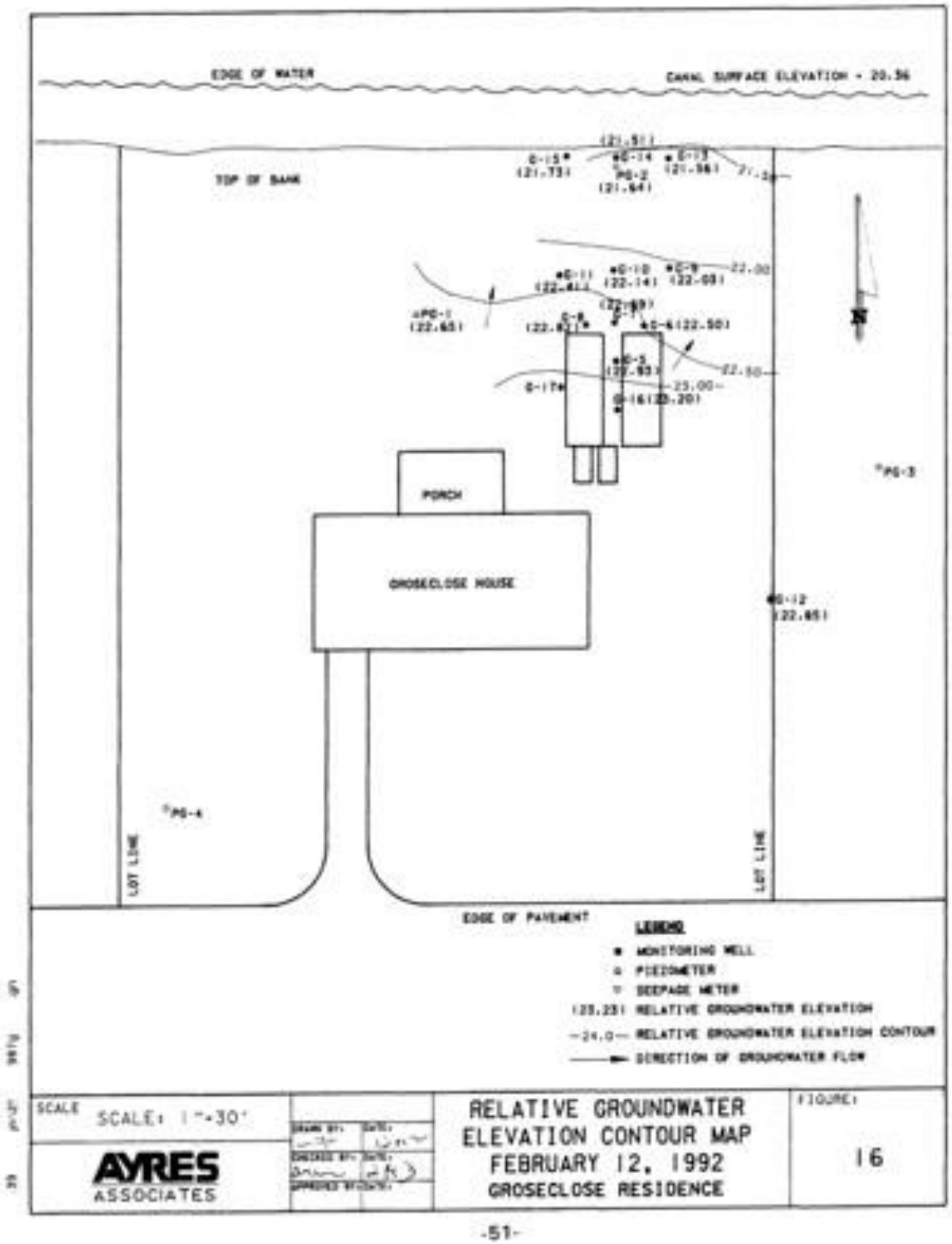

-51-

Fig. 5.5. Groundwater flow direction at the Groseclose Site, Turkey Creek, Ayres Associates (1993). The boundary survey shows the Groseclose residents in a black outline and the groundwater elevation in black contour lines.

The hydrostratigraphic units are defined based on the site-specific geological composition, including soil type and hydraulic conductivity. For example, the Jones site has moderate to high

hydraulic conductivities, ranging from 1.22 ft/day to 4.18 ft/day, with an average of 2.52 ft/day (Fig. 5.6). In contrast, the Groseclose site has lower hydraulic conductivities due to silts and clays, ranging from 0.47 to 4.74 ft/day, with an average of 1.81 ft/day (Fig. 5.6). The hydraulic gradients at the Jones site vary from 8.14x10-4 to 6.46x10-3 ft/ft, with an average of 3.22x10-3 ft/ft (Fig. 5.7). At the Groseclose site, the gradients range from 3.15x10-4 to 0.04 ft/ft, with an average of 0.02 ft/ft (Fig. 5.7). These gradients and the hydraulic conductivities influence the seepage velocities at both sites (Fig. 5.8). However, hydraulic conductivity and hydraulic gradient are not directly related because increased hydraulic conductivity automatically decreases the hydraulic gradient or vice versa (Fig. 5.9). Instead, independent factors influence fluid flow rate through a porous medium (Fetter 2018).

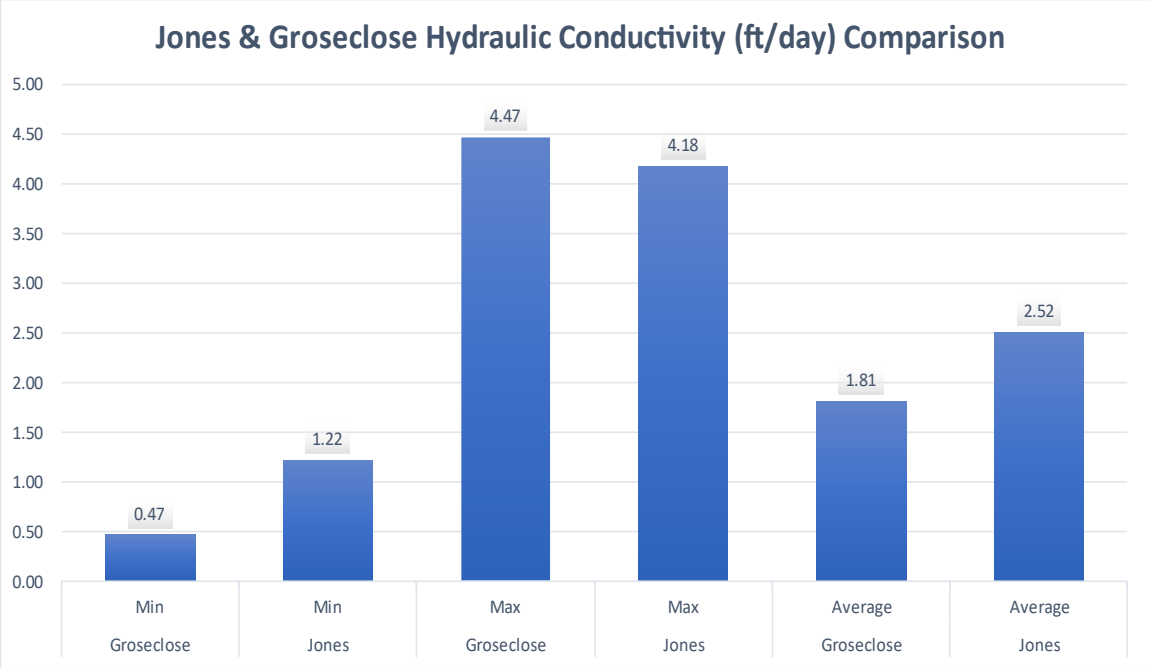

Fig. 5.6. Chart of Jones and Groseclose, Turkey Creek, hydraulic conductivity (ft/day) comparison reported in Ayres Associates (1993). The chart shows the min and max hydraulic conductivity values, the Groseclose average hydraulic conductivity values, and the Jones average hydraulic conductivity values in blue.

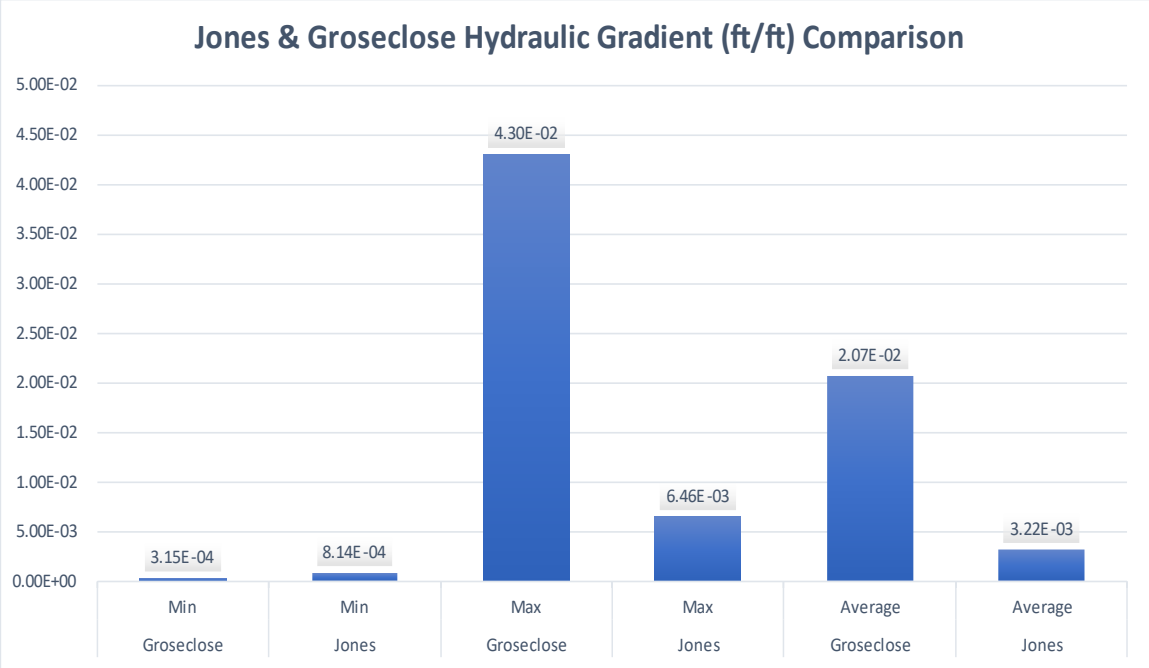

Fig. 5.7. Chart of Jones and Groseclose, Turkey Creek, hydraulic gradient (ft/ft) comparison as reported in Ayres Associates (1993). The chart shows the min and max hydraulic gradient values. The chart shows the Groseclose average hydraulic conductivity values and the Jones average hydraulic conductivity values in blue.

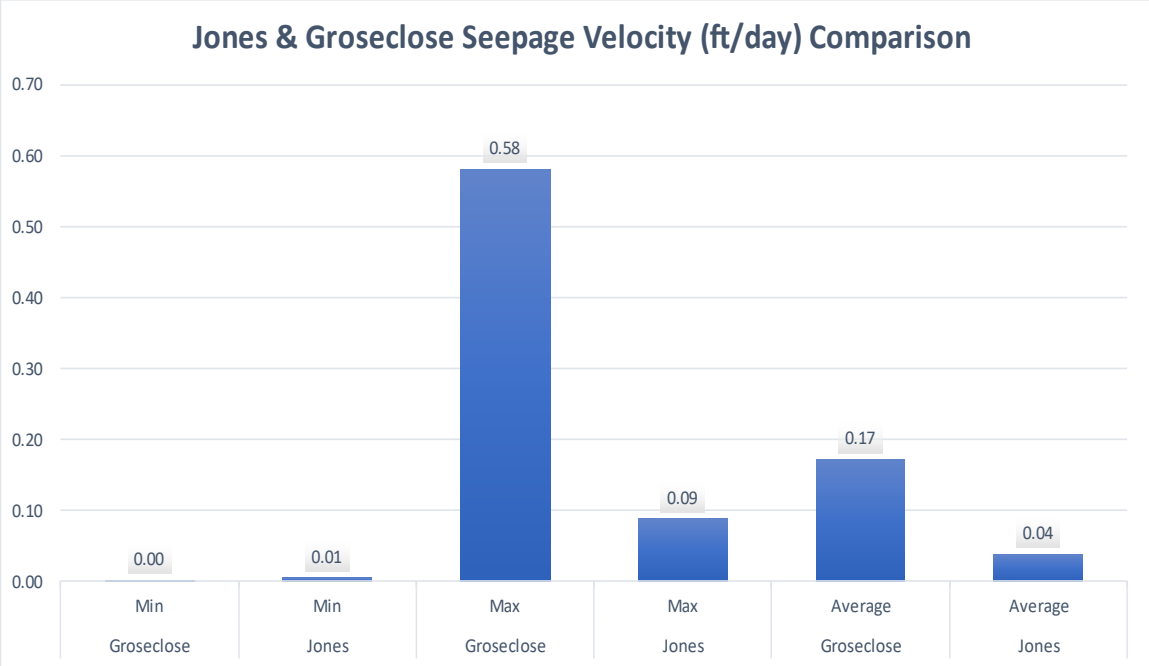

Fig. 5.8. Chart of Jones and Groseclose, Turkey Creek, seepage velocity (ft/day) comparison as reported in Ayres Associates (1993). The chart shows the min and max seepage velocity values. The bar chart shows the Groseclose average seepage velocity values and the Jones average seepage velocities values in blue.

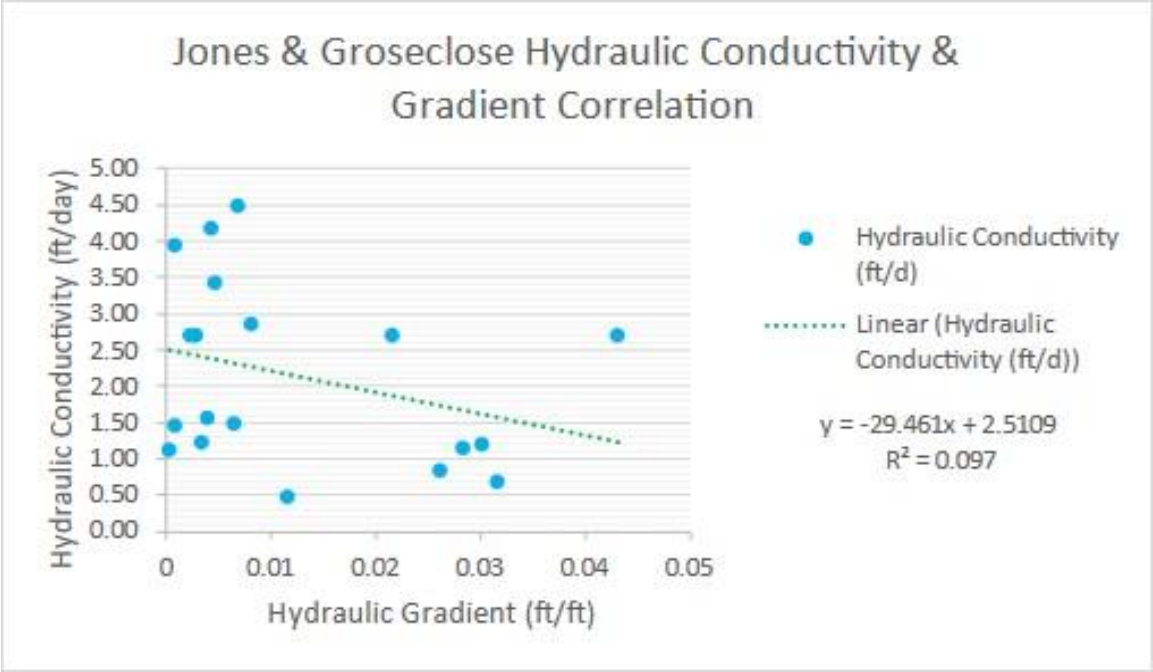

Fig. 5.9. Scatterplot of Jones and Groseclose, Turkey Creek, hydraulic conductivity and gradient correlation. The hydraulic conductivity values are blue dots, and the correlation line is green.

Nonetheless, if considering a specific flow rate (Q) to be maintained in a system, an increased hydraulic conductivity could decrease the required hydraulic gradient to achieve that flow rate. Per Darcy's Law, this is because the flow rate is proportional to the hydraulic conductivity and gradient product. Therefore, if the hydraulic conductivity increases and the flow rate remains constant, the hydraulic gradient may decrease to maintain a steady state (Fetter 2018). Observations of hydraulic heads, hydraulic gradients, and seepage velocities provide essential information for developing the hydraulic part of the conceptual model. In addition, the flow system in the study area can be considered a steady state. Therefore, yearly averaged recharge values are appropriate for analyzing the transport and attenuation of pollutants in this setting.

The first BN to be developed was for the Groseclose site, as Ayres Associates (1993) reported. The model incorporated site-specific data (Fig. 5.10) and expert knowledge (Glendell et al. 2021; Troldborg et al. 2022) to estimate the probability of NO3, TKN, and TP attenuation from OSTDS to surface water bodies. The specific modeling objectives are first to validate the model using monitoring location data from the Jones and Groseclose sites (Figs. 5.10 and 5.11) and then second, to generate probability beliefs for nitrogen and phosphorus attenuation rates for pollutants originating from OSTDS at multiple locations in Florida to assess pollution risks and inform management strategies (Fig. 5.12).

Fig. 5.10. The Groseclose site, Turkey Creek, with seepage velocity and flow paths from Ayres Associates (1993). The map of the Groseclose property shows the house in an orange outline, the monitoring locations in gray and blue dots, and the flow paths in blue and white lines.

Fig 5.11. Map of the Jones Site, Turkey Creek, with nitrate levels from Ayres Associates (1993). The map of the Jones property shows the residents in an orange outline and the monitoring well locations in green, orange, and red dots based on nitrate concentrations.

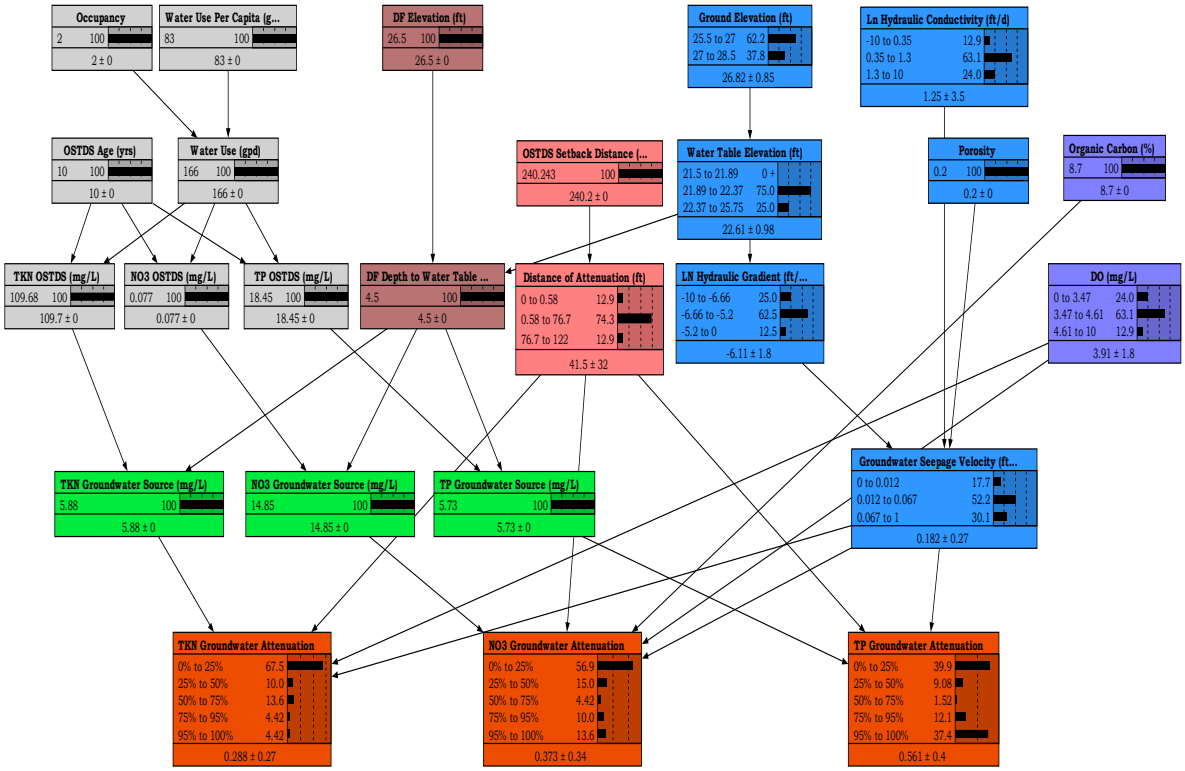

Fig. 5.12. BN for Jones, Turkey Creek, monitoring location J-13. The BN shows the output nodes in orange, the parent nodes of the network are in various colored rectangles, and the node links are black lines.

This research builds upon previous work by Troldborg et al. (2022), who employed a BN approach to analyze OSTDS pollution risks. The present study expands upon Troldborg's work by incorporating site-specific data from the Turkey Creek Basin (Ayres Associates 1993) and integrating insights from Glendell et al. (2021) and Fenton & Neil (2018). This integration allows for a more comprehensive understanding of the factors affecting OSTDS pollution and the development of an accurate model on a parcel scale. The general approach to accomplishing the goals and objectives involves developing a BN model representing the relationships among key risk factors, such as hydraulic conductivity, hydraulic gradients, and seepage velocities (Fig. 5.12). Combining site-specific data with expert knowledge. The model can estimate the probability of nitrogen and phosphorus attenuation from OSTDS to surface water bodies, thus informing more effective management strategies for groundwater protection.

5.3.1 Conceptual model

The conceptual model is based on the study area's geology, hydrology, and hydrogeology. It incorporates the geological composition, and hydrogeological parameters, such as hydraulic conductivity, hydraulic gradient, and seepage velocity, to predict the attenuation of NO3, TKN, and TP from OSTDS to surface water bodies. This model is developed with a BN approach, which integrates site-specific data and expert knowledge (Ayres Associates 1993; Glendell et al. 2021) to estimate the probability of pollutant attenuation and inform groundwater protection strategies.

The BN model (Fig. 5.12) was developed using site-specific data and expert knowledge to organize, characterize, and discretize the data for hydraulic conductivity, hydraulic gradient, and groundwater seepage velocity (Figs. 5.13-5.15). The conceptual model was transferred into a numerical model by discretizing the study area into nodes representing the key hydrogeological parameters: hydraulic conductivity, hydraulic gradient, and seepage velocity. The model parameters were assigned based on site-specific data and expert knowledge (Ayres Associates 1993; Fenton and Neil 2018; Glendell et al. 2021). Boundary and initial conditions were defined according to the hydrogeologic settings of the Jones and Groseclose sites, including groundwater flow direction, seepage velocities, and hydraulic head distributions. The network output represents NO3, TKN, and TP attenuation values moving away from an OSTDS and towards the nearest surface water body. The nodes in the BN represent all variables (Fig. 5.12 and 5.16).

NO3, TKN, and TP are this network's focus for groundwater attenuation, ln hydraulic conductivity, ln hydraulic gradient, and groundwater seepage velocity are among these nodes for probability beliefs. The OSTDS setback distance represents the horizontal distance between the OSTDS and the nearest surface water body. The drainfield depth to the water table node represents the vertical setback distance between the OSTDS and groundwater. Finally, the network outputs are the TKN Groundwater attenuation, NO3 Groundwater attenuation, and TP Groundwater attenuation nodes.

The model was then trained using monitoring location data from both sites and validated through cross-validation. The results from the combined Jones and Groseclose BN tests indicate varying performance across different groundwater attenuation measures. For example, in the first test involving wells G13, G14, and G15, the model accurately predicted NO3 attenuation with a 0% error rate (Table 5.4).

Monitoring Location	BN	Analyte	Error Rate
G13	Groseclose Network	TP	100%
G13	Groseclose Network	NO3	0%
G13	Groseclose Network	TKN	100%
J13	Jones Network	TP	0%
J13	Jones Network	NO3	100%
J13	Jones Network	TKN	100%

Table 5.4. Results of Turkey Creek, Ayres Associates 1993 BN. The table shows the monitoring locations used to cross-validate each BN and the associated analyte attenuation error rate. Analytes with a 0% error rate are in green.

However, it struggled with TKN and TP attenuation, yielding 100% error rates. The TKN, NO3, and TP attenuation calculated from the values reported in Ayres Associates (1993) for location G13 were 59%, 99.2%, and 98.7%, respectively. The values for location G13 were withheld from the network during the training process. Afterward, the data for the location (i.e., ground elevation, occupancy, seepage velocity, the distance of attenuation) was entered into the

network as evidence to predict the TKN, NO3, and TP groundwater attenuation rates for these locations. These attenuation rates were withheld from the network while entering the evidence. Lastly, the network determined the most probable attenuation rates for location G13. The network predicted that TKN groundwater attenuation is 0% to 25%, the NO3 groundwater attenuation is 95% to 100%, and the TP groundwater attenuation is 50% to 75%. The groundwater seepage velocity influences these findings, the distance of attenuation, and the groundwater source concentrations of analytes from the OSTDS.

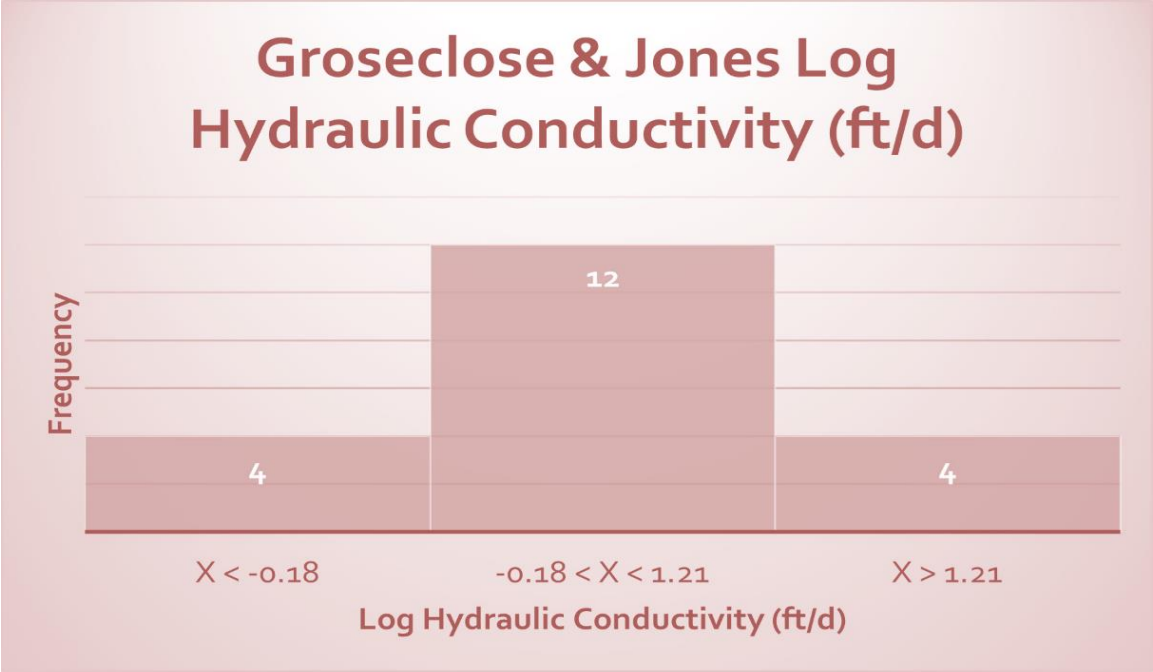

Fig. 5.13. Groseclose and Jones, Turkey Creek, log hydraulic conductivity (ft/day). These data bin ranges and frequencies were used to calculate the probabilities in the BN's conditional probability tables (CPT). The probabilities were calculated based on the dataset's normal distribution, mean, and standard deviation.

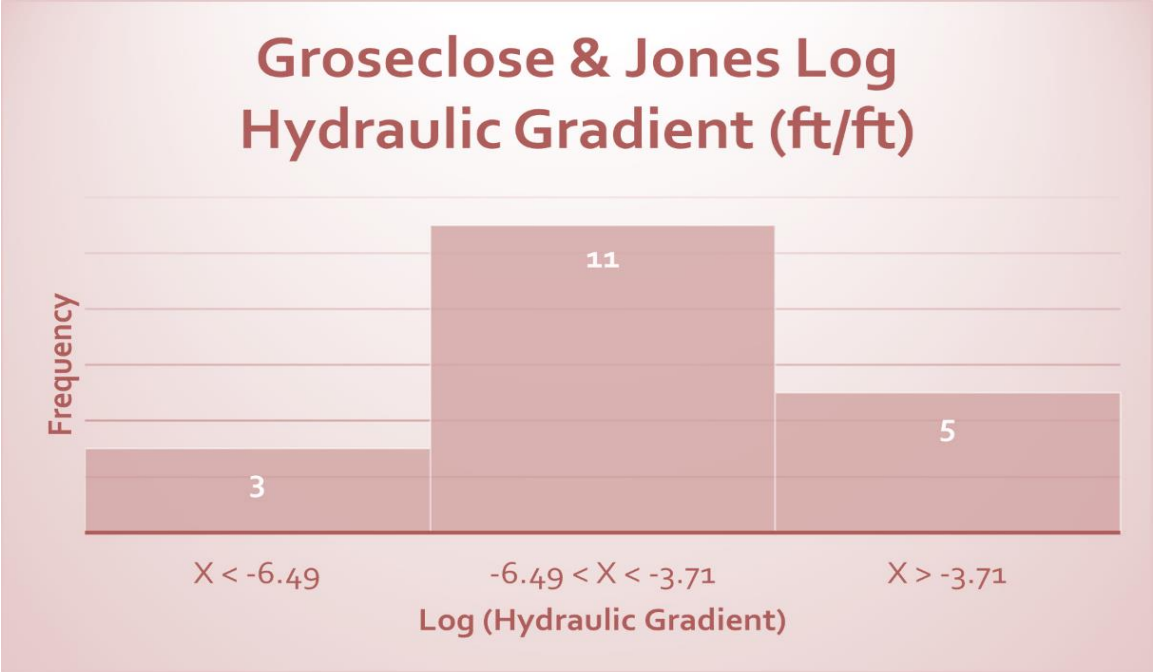

Fig. 5.14. Groseclose and Jones, Turkey Creek, log hydraulic gradient (ft/ft). These data bin ranges and frequencies were used to calculate the probabilities in the BN's conditional probability tables (CPT). The probabilities were calculated based on the dataset's normal distribution, mean, and standard deviation.

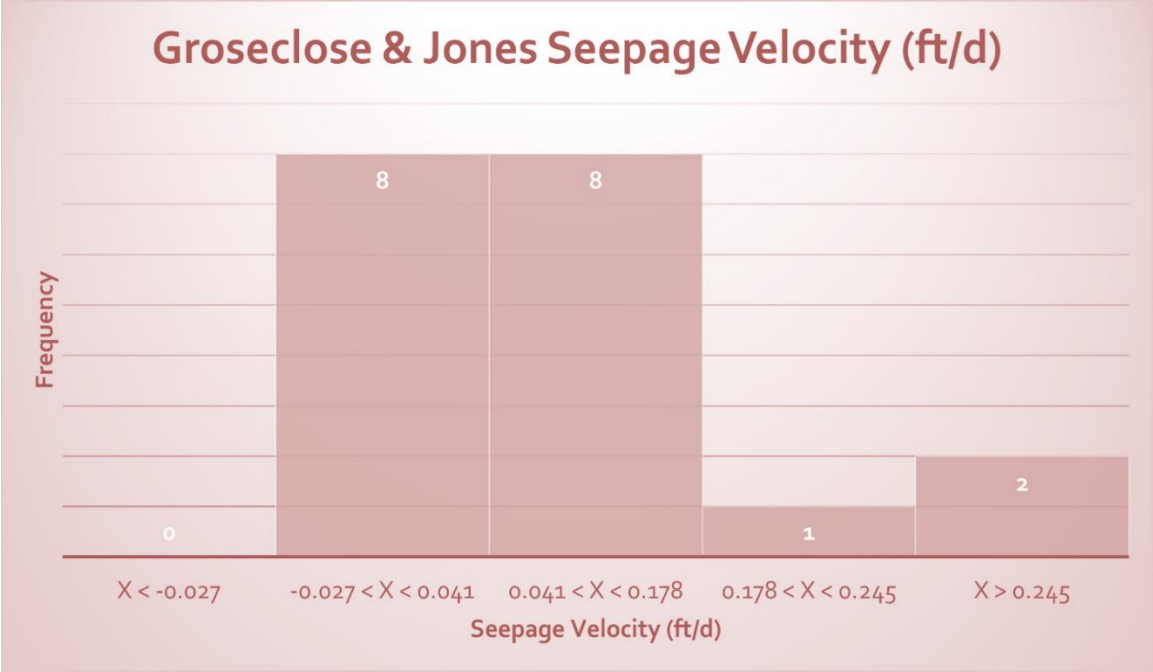

Fig. 5.15. Turkey Creek groundwater seepage velocity (ft/day) node. These data bin ranges and frequencies were used to calculate the probabilities in the BN's conditional probability tables (CPT). The probabilities were calculated based on the dataset's normal distribution, mean, and standard deviation.

Likewise, the Jones decision network was tested with the updated monitoring location J13 (Fig. 5.16). The TKN, NO3, and TP attenuation calculated from the values reported in Ayres Associates (1993) for location J13 were 71.26%, 98.56%, and 98.78%, respectively. The values for location J13 were withheld from the network during the training process. Afterward, the data for the location was entered into the network as evidence to predict the TKN, NO3, and TP groundwater attenuation rates for this location. These attenuation rates were withheld from the network while entering the evidence. Lastly, the network was used to determine the most probable attenuation rates for location J13. The network predicted that TKN groundwater attenuation was 0% to 25%, the NO3 groundwater attenuation was 0% to 25%, and the TP groundwater attenuation was 95% to 100%. The groundwater seepage velocity and the attenuation distance influence these findings (Table 5.3).

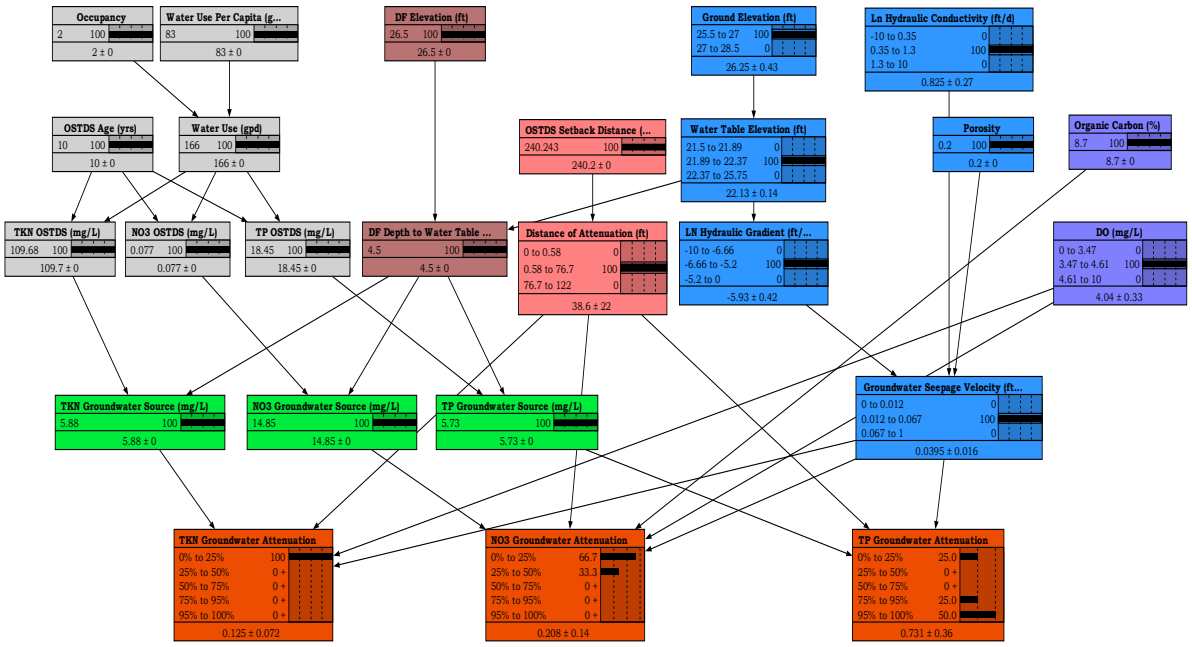

Fig. 5.16. Jones, Turkey Creek, network with J-13 withheld. The BN output attenuation nodes are in orange. The node links are black lines, which connect parent and children nodes. The evidence can be seen in the black bars in the parent nodes and the beliefs in the black bars in the orange output nodes.

The data for the Groseclose and the Jones sites were combined to create one decision network. Afterward, four locations were chosen to test the BN. The locations G7, G11, J8, and J14 were randomly selected in Excel to test the combined BN. Data from these locations were withheld from the BN during the training process. Afterward, data from these locations (less the analyte concentration attenuation percentages) were used as evidence to test the combined decision network. The results are shown in Table 5.5 below.

Site	**Well ID**	**BN-Estimated Attenuation**			**Data-based Attenuation**		
		TNK	**NO3**	**TP**	**TKN**	**NO3**	**TP**
Groseclose	G7	0% to 25%	95% to 100%	75% to 95%	0%	72.6%	66.4%
Groseclose	G11	0% to 25%	95% to 100%	95% to 100%	41%	98.8%	58.8%
Jones	J8	0% to 25%	0% to 25%	95% to 100%	0%	6.9%	95.3%
Jones	J14	0% to 25%	0% to 25%	95% to 100%	48.8%	92%	97%

Table 5.5. Results of the combined Groseclose and Jones, Turkey Creek, network. The correctly predicted attenuation values are highlighted in green.

Calibration targets included hydraulic head and flow measurements from the study area. The calibration method employed a Bayesian approach, incorporating prior knowledge and updating model parameters based on site-specific data. The final models generated probability belief maps

for NO3, TKN, and TP attenuation at the Jones and Groseclose sites. The model's match to the predicted attenuation values with the observed data was used to verify the predictive ability of the network. The error rates for TKN and TP attenuation were high, indicating that the model's calibration may need further improvement. Cross-validation, where possible, was performed to evaluate the model's performance and ensure its robustness.

Sensitivity analyses were conducted after cross-validation to identify the most influential model parameters and evaluate their impact on the attenuation predictions. This analysis helped to improve the model's performance. The study demonstrated that the model's calibration for NO3 attenuation was satisfactory, with an error rate of 0%. However, the high error rates for TKN and TP attenuation indicate a need for further improvement in the model. Additional data, such as more accurate estimates of hydrogeological parameters, site-specific attenuation processes, and spatial distribution of pollutants, may be needed to improve the BN. This could help reduce uncertainties in the model predictions and provide a more accurate representation of the groundwater attenuation processes at the Jones and Groseclose sites.

The analysis demonstrated that the individual site models' performance was satisfactory, capturing the fundamental processes governing the transport and attenuation of NO3 pollutants in the study area. However, the model needs more data to improve the predictions of TKN and TP. Areas for potential improvement include refining the hydrogeological parameter estimates and incorporating additional field data to reduce uncertainties in the model predictions. Likewise, soil parameters related to phosphorous sorption and retardation are needed to improve the TP belief predictions (Glendell et al. 2021; Troldborg et al. 2022).

The BN model performed well in estimating the pollution risks associated with OSTDS for NO3 attenuation, moderately for TKN attenuation, and inaccurately for TP attenuation. The model's calibration and sensitivity analysis have identified areas where additional data and refinements are required to improve the model's predictive capabilities for TKN and TP attenuation. With further improvements and data collection efforts, the BN model can provide valuable insights into the complex interactions between hydrogeological parameters and their influence on groundwater pollution attenuation at the Jones and Groseclose sites.

Monitoring Location	BN	Node	Influential Nodes
G13	Groseclose Network	TKN Attenuation	Distance of attenuation; TP Attenuation; NO3 Attenuation; Seepage Velocity
G13	Groseclose Network	NO3 Attenuation	Distance of attenuation; TP Attenuation; TKN Attenuation; DO
G13	Groseclose Network	TP Attenuation	Distance of attenuation; TKN Attenuation; NO3 Attenuation; Seepage Velocity
J13	Jones Network	TKN Attenuation	NO3 Attenuation; Distance of attenuation; TP Attenuation; Seepage Velocity
J13	Jones Network	NO3 Attenuation	TKN Attenuation; Distance of attenuation; TP Attenuation; Seepage Velocity
J13	Jones Network	TP Attenuation	Seepage Velocity; Log Hydraulic Gradient; Log Hydraulic Conductivity; NO3 Attenuation
G7; G11; J8; J14	Combined Groseclose & Jones	TKN Attenuation	Seepage Velocity; TKN GW Source; Distance of attenuation; TP Attenuation
G7; G11; J8; J14	Combined Groseclose & Jones	NO3 Attenuation	Organic carbon; NO3 GW Source; DF Depth to WT; NO3 OSTDS
G7; G11; J8; J14	Combined Groseclose & Jones	TP Attenuation	Seepage Velocity; TP GW Source; Distance of attenuation; DF Depth to WT

Table 5.6. Turkey Creek 1993 BN node sensitivity. The table shows the most influential nodes for each Turkey Creek study area BN. The distance of attenuation and seepage velocity nodes were noted as influential to the BN.

5.4. Julington Creek and Lakeshore Sites (Belanger et al., 2011)

Belanger et al. (2011) reported on five sites along the St. Johns River near the City of Jacksonville in Lakeshore and Julington Heights. The areas represent locations impacted by OSTDS. ArcGIS Pro was used to georeference the site surveys recorded by Belanger et al. (2011). Furthermore, the monitoring well locations were digitized to calculate the change in distance between monitoring locations and attenuation for septic tank analyte concentrations. The distance and analyte concentration changes were calculated using adjacent monitoring location well pairs. Likewise, the calculations followed the flow path from the OSTDS to the surface water body. Unfortunately, the monitoring well locations Belanger et al. (2011) reported were inconsistent between monitoring dates. During the study at many residents monitoring sites, monitoring well locations and nomenclature changed from date to date. For example, for 5180 Siesta Del Rio, site CST, for July 2009, there are only two piezometers and one monitoring well, which does not have associated analyte concentration data recorded in Table 3 of Belanger et al. (2011). Because there is no analyte concentration data in Table 5.3 for this date, the December monitoring wells were removed for the analysis. Alternatively, for site CST for December 31st, 2009, there is data recorded in Table 3 of Belanger et al. (2011) for the piezometers and the monitoring well, and

there are nine monitoring wells and two piezometers listed for this date and location. Monitoring well number one at the site, CST changed locations between dates to compound the issue. Thus, monitoring well one for July is at a different location in December. As Belanger et al. (2011) reported in the Appendix, for the site DE, the septic tank and drainfield changed places on the site plan. For example, for the December 2009 site survey, the drainfield changed orientation. Furthermore, for site DE for the September 2010 site survey, the septic tank and drainfield are shifted southwest nearly 15 feet.

Several sites, CST (Fig. 5.17), DH (Fig. 5.18), and MM (Fig. 5.19), as reported in Belanger et al. (2011), were identified as having OSTDS impacting the surrounding groundwater. Likewise, site RT (Fig. 5.20) at Waterside Drive had isotope values consistent with septic tank effluent as the source of the nitrate. Belanger et al. (2011) organized piezometer groundwater monitoring locations by site and date. For this study, monitoring locations, sites, and dates were chosen where a discernable NH3-N and NOx plume of higher analyte concentrations near the OSTDS and a decreasing magnitude of NH3-N or NOx towards the adjacent surface waterbody were observed via analyte concentrations. Data from these sites, dates, and monitoring locations were used to calculate NH3-N and NOx attenuation from the OSTDS towards the adjacent surface water body. The analyte attenuation concentration is the output and most critical node of the BN for determining the necessary setback distance needed to attenuate OSTDS nitrogen pollutants to 95% or greater of the NH3-N and NOx groundwater source concentrations from an OSTDS to a proximal surface water body.

Fig. 5.17. Map of Julington Heights, CST locations for BN. The maps show the CST site with the septic tank marked as a black rectangle, the drainfield marked as a brown rectangle, and the monitoring wells in blue and yellow dots.

Fig. 5.18. Map of Julington Heights, DH locations for BN. The maps show the DH site with the septic tank marked as a black rectangle, the drainfield marked as a brown rectangle, and the monitoring wells in blue and yellow dots.

Fig. 5.19. Map of Julington Heights, MM locations for BN. The maps show the MM site with the septic tank marked as a black rectangle, the drainfield marked as a brown rectangle, and the monitoring wells in blue and yellow dots.

Fig. 5.20. Map of Lakeshore, RT locations for BN. The maps show the MM site with the septic tank marked as a black rectangle, the drainfield marked as a brown rectangle, and the monitoring wells in blue and yellow dots.

ArcGIS Pro version 3.1.2 (Esri, 2023) was used to estimate variables needed for the BN. Firstly, the ground elevations were assigned to each piezometer location from the USGS one-meter resolution digital elevation model (DEM) 3D Elevation Program (3DEP) (USGS 2022) to aid in determining the flow direction of the NH3-N and NOx plumes within the groundwater. The flow direction of the contaminant plume was generally considered to travel from the groundwater source location and piezometers with higher elevations to piezometers with lower elevations (Fetter 2018).

The attenuation was calculated as such, the piezometer monitoring well closest to the OSTDS, with the highest NH3-N or NOx concentration, and the highest elevation was denoted as the groundwater source location for the given site and date. The groundwater source location is the point from which attenuation was calculated. Afterward, the analyte concentration attenuation was calculated as a percent reduction of NH3-N and NOx groundwater concentration, as reported by Belanger et al. (2011). Furthermore, the attenuation distance between piezometers was estimated in ArcGIS Pro. The decision network uses the attenuation distance to estimate the distance that NH3-H or NOx will need to travel before the analyte concentration is reduced to at least 95% of the initial introduction from the OSTDS into the groundwater.

Unfortunately, site JB in Murry Hill B was removed from the analysis because it was a location where a septic tank was no longer in service. Locations where OSTDS were not used, were out of this project's scope and therefore removed from the analysis. Furthermore, dates of observations with no discernable analyte concentration attenuation from the OSTDS as the source of the NH3-N or NOx to the surface waterbody, as reported by Belanger et al. (2011), were also out of this project's scope and therefore were removed. These are locations where the piezometer monitoring well with the highest concentration of NH3-N or NOx was not amongst the closest to the OSTDS (i.e., where at least one row of monitoring wells separates the well with the highest analyte concentration and the OSTDS). For example, for the site CST in Julington Hills on December 31, 2009, piezometer nine had a NOx concentration of 30 mg/L. Piezometer nine's value contrasts the analyte concentrations for piezometers two, three, and four, where NOx was less than 2 mg/L. Unfortunately, piezometers two, three, and four were closest (within 5 ft) to the OSTDS, while piezometer nine was over 25 ft downgradient of the OSTDS and towards the surface water body. For many locations, fertilizer use, surface water interactions, and other human interactions were reported by Belanger et al. (2011), causing higher analyte concentration observations at piezometer monitoring locations unrelated to OSTDS analyte contamination. Table 5.7 below shows the monitoring well sites, dates, and locations used to calculate analyte attenuation for the OSTDS to the surface waterbodies.

Site	Date	Monitoring Locations	Analyte
CST	12/31/2009	4, 8, & 9	NH3-N
CST	12/31/2009	4 & 8	NOx-N
CST	6/1/2010	4, 8, 9, 10, & 11	NH3-N
CST	6/1/2010	2,8,9,10,11	NOx-N
CST	9/27/2010	4, 9A, & 11	NH3-N
DH	6/1/2010	2, 7, & 8	NOx-N
DH	9/27/2010	1A, 1, 2, 7, 8, & 9	NH3-N
DH	9/27/2010	1A, 1, 8, & 9	NOx-N
MM	6/2/2010	PZ1, 1, 2, 4, 5, 6, & 7	NOx-N
MM	9/27/2010	1A, 1, 2, 4, & 5	NH3-N
RT	12/29/2009	1, 2, & PZ4	NH3-N
RT	6/2/2010	3B, 3, & PZ2	NH3-N

Table 5.7. Lakeshore and Julington Heights sites used for analysis. The table shows the monitoring locations, sites, and dates for each analyte used for the BN.

The hydraulic conductivity (K80) values Belanger et al. (2011) reported were decreased by two orders of magnitude. The average hydraulic conductivity (K80) values for sites MM, DH, RT, and CST were 0.48 cm/s (1360.63 ft/d), 0.51 cm/s (1445.67 ft/d), 1.06 cm/s (3004.72 ft/d), and 1.34 cm/s (3798.43 ft/d), respectively. The aforementioned hydraulic conductivity values were compared with results from similar studies. For example, Ayres Associates (1993) estimated hydraulic conductivity with tracer tests. The results of tracer test number one were 2.70 ft/d and tracer test number two was 1.36 ft/d, as reported in Ayers Associates (1993) and McNeil (1994). Likewise, hydraulic conductivity values between 25.9 ft/d and 2.3 ft/d were estimated for Eggleston Heights (Zhu et al. 2016). The data used in the decision network is reported in Table 5.8.

Name	Type	Unit	Source	Notes
Occupancy	Integer	Persons per household	Belanger et al. (2011)	
OSTDS age	Integer	Years from built date to 2011.	Belanger et al. (2011)	
NOx-N & NH3-N groundwater source	Float	Mg/L	Belanger et al. (2011)	Piezometers near the OSTDS w/ the highest concentration
Log vertical hydraulic gradient	Float	Unitless	Belanger et al. (2011)	Values were log-transformed.
Log horizontal hydraulic gradient	Float	Unitless	Belanger et al. (2011)	Values were log-transformed.
Log hydraulic conductivity	Float	Ft/d	Belanger et al. (2011)	Values were decreased, converted, and transformed.
Groundwater seepage	Float	mL/m2/hr.	Belanger et al. (2011)	
Ground Elevation	Float	Feet	USGS DEM 3DEP	
Distance of attenuation	Float	Feet	GIS calculated	

Table 5.8. Data for the BN was used for Lakeshore and Julington Heights from Belanger et al. (2011).

The censored data above the detection limit reported by Belanger et al. (2011) were increased by 25%, and censored data lower than the detection limit was reduced to 75% of the value (Yang et al. 2020). Likewise, the vertical and horizontal hydraulic gradients and groundwater seepage velocities were reported in Table 2 by Belanger et al. (2011). Information was reported in the data Table 2 for piezometer destroyed (PD), lost piezometer (LP), low water level (LWL), bag leak (BL), high tide (HT), low tide (LT), and rising tide (RT). The report only contains information regarding the high and low tide relative to groundwater seepage at the DH site and LT, HT, and RT for the LP, MM, DH, RT, and DE sites. For the MM and RT sites, HT minimum and maximum values were separated with a "," (i.e., site MM on June 1, 2010, for groundwater seepage, the values of 442, 663 (HT) were recorded in Table 2); these values were averaged. In total, two cells for groundwater seepage values were averaged. Lastly, if there were no numerical data in a cell in Table 2, these data points were removed. In total, 5 LWL values, 31 NS values, 2 BL values, 2 PD values, and 2 LP values were converted to no data.

Water quality data reported by Belanger et al. (2011) were reported in Tables 3 – 6. Information for groundwater was reported for monitoring sites and as averages, while there were no average values for surface water data. Furthermore, for the CS site, for dissolved oxygen (DO) mg/L for sample CS-PZ1 on June 3rd, 2010, the values of 2.1/4.8 were recorded in Table 3 of Belanger et al. (2011). This record was averaged and updated to 3.45. Site-specific residential year-built data reported by Belanger et al. (2011) had the LP and CS sites listed as the 1970s and 1980s, respectively. These data points were adjusted to 1975 and 1985, respectively. Furthermore, the

information for residential dwellings was verified via the parcel record card/summary available via the county property appraiser's office.

An Excel formula was used to sort and list the unique site and location combinations. Likewise, an Excel formula was used to average the vertical hydraulic gradient, horizontal hydraulic gradient, groundwater seepage, coliform, Cl, SO4, NH3, TKN, NOx, TN, TP, δ15N, δ18O, B, Fe, K, TOC, specific conductance, temperature, DO, pH, triclosan, and caffeine. Lastly, ArcGIS Pro was used to estimate the attenuation distance.

5.4.1 Model design and results

Variables with continuous data were discretized for the Lakeshore and Julington Heights (Belanger et al. 2011) decision network. Data were assigned to bin ranges based on the mean and standard deviation of the sample set. Variables such as the log transformation of the hydraulic conductivity and groundwater seepage values were assigned to a normal distribution using three classifications $\mu - \sigma$, μ, and $\mu + \sigma$. The groundwater source concentrations were assigned the classifications of $\mu - 0.5\sigma$, μ, and $\mu + 0.5\sigma$. Alternatively, the occupancy, NOx attenuation, and NH3-N attenuation values were given an initial probability of occurrence based on frequency calculated from the piezometer analytes measurements from Belanger et al. (2011).

The K80 values, as reported in Table 1 of Belanger et al. (2011), represent the lower range for medium sand and are ideal representations for each site. As previously mentioned, the hydraulic conductivity values were logarithmically transformed to fit a standard distribution curve. Furthermore, the values were averaged if a site had more than one K80 value—the averaged K80 values for each.

The BN was created with NH3-N and NOx groundwater sources and attenuation nodes. Separating these nodes required organizing the data and categorization of the data. Unfortunately, separating the NH3-N and NOx data left missing data records in the data used to train the network. For example, for site RT and monitoring location PZ4 on December 29, 2009, NH3-N groundwater source and attenuation could be determined, while the NOx plume concentration and flow direction could not be determined using data from Belanger et al. (2011). Secondly, the BN was trained and tested with the five missing locations and later used to cross-validate the BN (Fig. 5.22). The locations for Julington Heights were site CST piezometer nine and ten on June 1, 2010, piezometer ten on September 27, 2010, and site DH piezometer eight on June 1, 2010. The location for Lakeshore was site RT piezometer PZ4 on December 12, 2009. Unfortunately, as mentioned above, some of the test locations chosen at random are missing the analyte concentration attenuation data required to check the predictions of the BN.

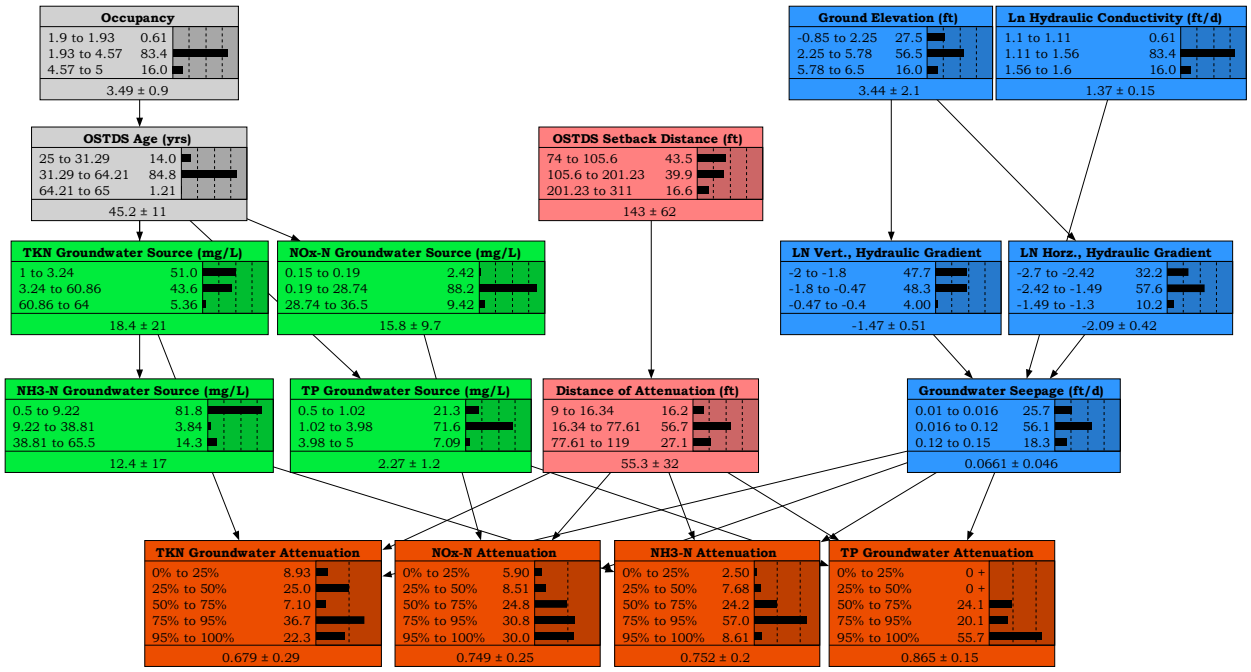

Fig. 5.21. Lakeshore and Julington Heights BN. The BN output attenuation nodes are in orange. The node links are black lines, which connect parent and children nodes.

Once the NH3-N and NOx groundwater source and attenuation rates were separated in the data for the decision network, it left locations where either the NH3-N groundwater source concentrations or concentration attenuation rates could not be determined from the data from Belanger et al. (2011). These missing records or data are unobserved cases for training the BN and therefore are estimated with the expectation maximization (EM) algorithm (Norsys Software Corp 2007) during the BN learning process. Therefore, new test locations with data for both NOx and NH3-N groundwater source concentrations and attenuation rates were chosen to test the performance of the combined analyte and separate analyte decision networks. Care was taken to choose two locations that do not represent the minimum or maximum of the data set. The NH3-N and NOx second test locations were for Julington Heights site DH piezometer nine on September 27, 2010, and site CST piezometer ten on June 1, 2010. (Figs. 5.22 and 5.23).

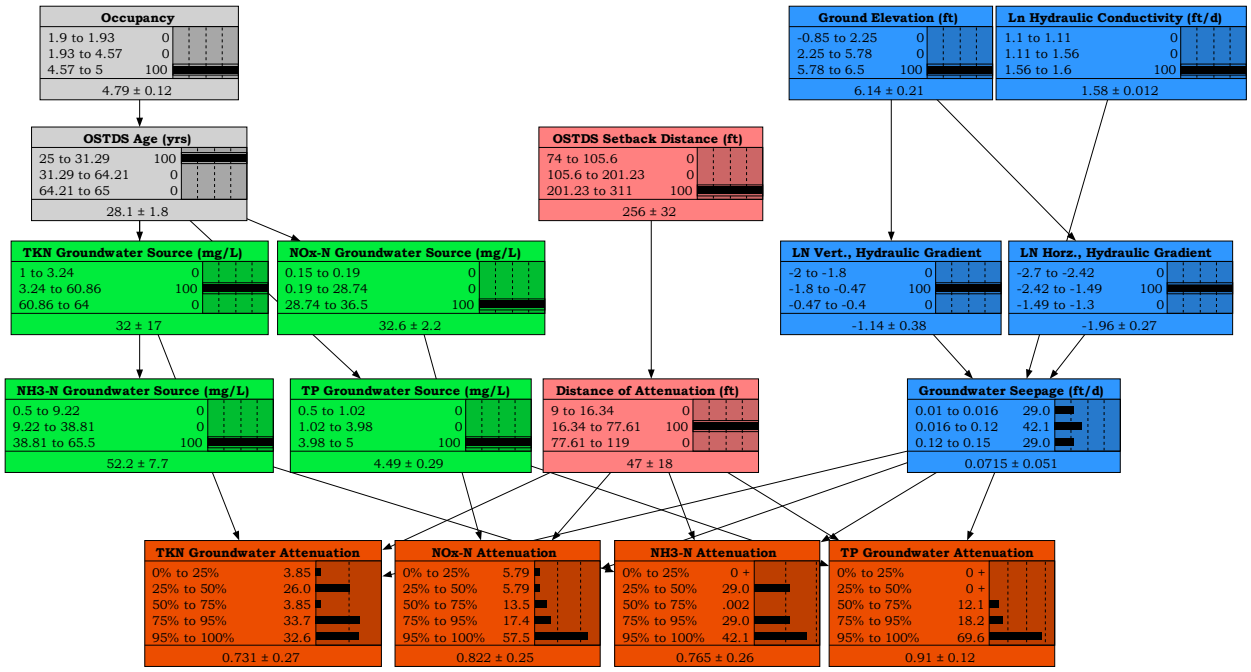

Fig. 5.22. Julington Heights, DH9, September 9, 2010, BN. The BN output attenuation nodes are in orange. The node links are black lines, which connect parent and children nodes. The evidence can be seen in the black bars in the parent nodes and the beliefs in the black bars with the highest percentage in the orange output nodes.

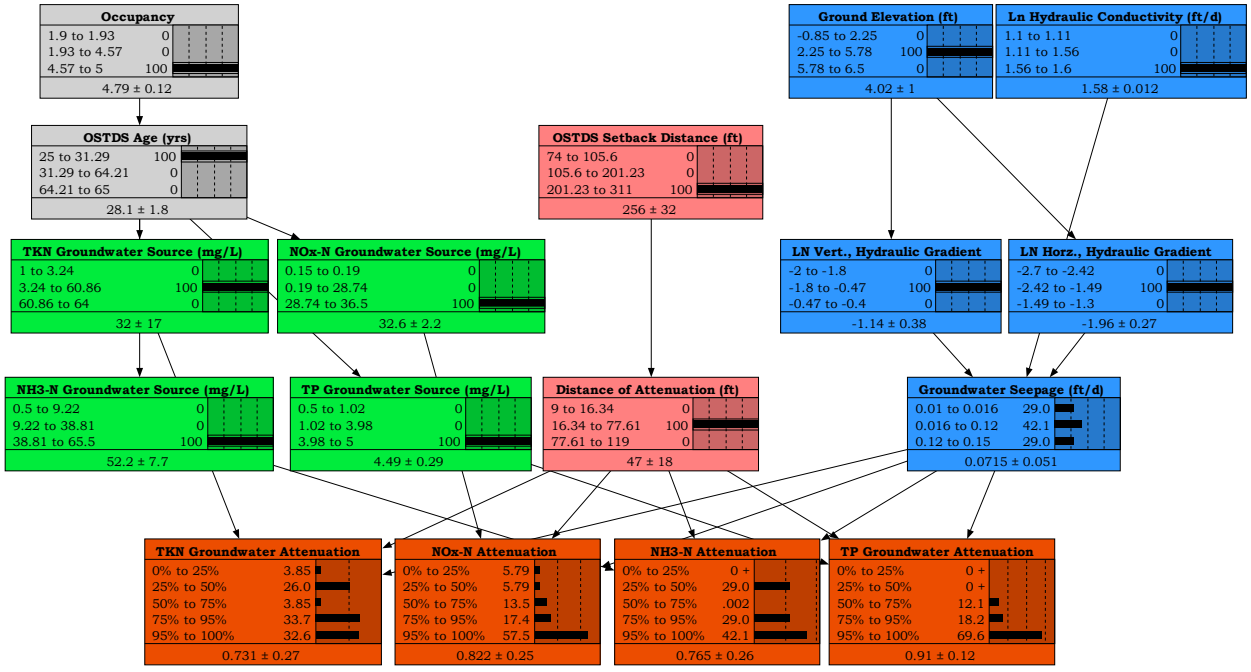

Fig. 5.23. Julington Heights, CST10, June 1, 2010, BN. The BN output attenuation nodes are in orange. The node links are black lines, which connect parent and children nodes. The evidence can be seen in the black bars in the parent nodes and the beliefs in the black bars with the highest percentage in the orange output nodes.

For testing, the BN 5 monitoring locations, dates, sites, and analytes were chosen randomly using the RANDBETWEEN function in Excel. The randomly chosen monitoring location, as described above, were given unique IDs, which were CST920100601NOx, DH820100601NOx, RTPZ420091229NH3, CST1020100601NH3, and CST1120100927NH3. These locations were removed from the training data that teaches the BN via the EM algorithm (Norsys Software Corp 2007). Afterward, these locations were used as evidence in the decision network to predict NH3-N and NOx attenuation, and the results and be seen in Table 5.9 below.

Furthermore, the network was tested with monitoring data reported by Belanger et al. (2011) for site Julington Heights, site CST on June 1, 2010, for piezometers nine, ten, and eleven (Table 5.10). These data were chosen due to an identifiable analyte concentration plume that started at the OSTDS and diminished downgradient and towards the adjacent surface water body for NOx, NH3-N, TKN, and TP.

Monitoring Location	BN	Analyte	Error Rate
CST920100601; DH820100601; RTPZ420091229; CST1020100601; CST1120100927	Unique to Belanger 2011	NH3-N	50%
CST920100601; DH820100601; RTPZ420091229; CST1020100601; CST1120100927	Unique to Belanger 2011	NOx	67%

Table 5.9. Results of initial Lakeshore and Julington Heights network. The table shows the monitoring locations used to cross-validate each analyte's BN.

Site (June 1st, 2010)	Well ID	Attenuation Predicted by BN				Attenuation Calculated from Observations			
		TNK	NOx-N	NH3-N	TP	TKN	NOx-N	NH3-N	TP
CST	9	75% to 95%	95% to 100%	95% to 100%	95% to 100%	87.1%	72.5%	89%	81.1%
CST	10	75% to 95%	95% to 100%	95% to 100%	95% to 100%	98.8	87.2%	99.9%	99.4%
CST	11	75% to 95%	95% to 100%	95% to 100%	95% to 100%	99.1%	94.7%	99.98%	99%

Table 5.10. Updated Lakeshore and Julington Heights BN attenuation predictions error rates. The correctly estimated attenuation values are in green.

A sensitivity analysis of the BN developed for the Belanger et al. (2011) study was conducted to investigate the dependence of crucial attenuation nodes on other elements within the network (Table 5.11). This process was facilitated using monitoring location data from three distinct locations from Julington Heights, site CST piezometers nine, ten, and eleven. The TKN attenuation

node displayed the highest sensitivity to the TKN groundwater (GW) source, ammonia nitrogen (NH3-N) attenuation, the distance of attenuation, and onsite sewage treatment and disposal systems (OSTDS) age. This suggests that these nodes play an integral role in the changes observed in the TKN attenuation node. The NOx attenuation node was most sensitive to the attenuation distance, NH3-N attenuation, GW seepage, and OSTDS setback distance.

Similarly, the NH3-N attenuation node demonstrated significant sensitivity to the same set of nodes with the addition of NOx attenuation. For the TP attenuation node, the distance of attenuation, GW seepage, OSTDS setback distance, and TP GW source concentration were observed to be the most influential nodes. The TKN attenuation notably influenced the NO3 attenuation node, the length of attenuation, TP attenuation rate, and seepage velocity nodes, indicating the interconnected dynamics among these elements. A similar pattern was observed for the TP attenuation node, but with the influence of seepage velocity, log hydraulic gradient, log hydraulic conductivity, and NO3 attenuation. This sensitivity analysis provides valuable insights into the dependencies among various nodes in the Belanger et al. (2011) BN model. The results highlight the interconnectedness of the environmental variables and their influence on attenuation rates.

Node	Influential Nodes
TKN Attenuation	TKN GW Source; NH3-N Attenuation; Distance of attenuation; OSRDS Age
NOx-N Attenuation	Distance of attenuation; NH3-N Attenuation; GW Seepage; OSTDS Setback Dist.
NH3-N Attenuation	Distance of attenuation; GW Seepage; OSTDS Setback Dist.; NOx-N Attenuation
TP Attenuation	Distance of attenuation; GW Seepage; OSTDS Setback Dist.; TP GW Source
NO3 Attenuation	TKN Attenuation; Distance of attenuation; TP Attenuation; Seepage Velocity
TP Attenuation	Seepage Velocity; Log Hydraulic Gradient; Log Hydraulic Conductivity; NO3 Attenuation
TKN Attenuation	Seepage Velocity; TKN GW Source; Distance of attenuation; TP Attenuation
NO3 Attenuation	Organic carbon; NO3 GW Source; DF Depth to WT; NO3 OSTDS
TP Attenuation	Seepage Velocity; TP GW Source; Distance of attenuation; DF Depth to WT

Table 5.11. Lakeshore and Julington Heights BN node sensitivity. The table shows the most influential nodes for the BN. The distance of attenuation and seepage velocity rank high amongst the most influential nodes in the network.

5.5. St. George Island Site (Corbett & Iverson, 1999)

Data for Corbett & Iverson (1999) for St. George Island for Jay Abott's (JA) site (Fig. 5.24) and the State Park (SP) (Fig. 5.25) were used to construct the BN. The decision was made to use the results from Table 2 (Corbet et al. 2002) for the groundwater source concentration and to calculate analyte attenuation percentages. The values reported in Table 2 of Corbett et al. (2002) are average nutrient concentrations from wells downfield from the OSTDS reported in Corbett & Iverson (1999). The St. George Island SP site was in the Dr. Julian G. Bruce State Park. The SP location was determined to be the restricted area north of the service road intersection intended for staff use and E. Gulf Beach Drive using historic aerials, site descriptions, and Figure 1.2 from Corbett & Iverson (1999). The JA site was at a single-family residence at 419 N Sawyer Street on St. George Island, Florida, as shown in Figure 2-C of Corbett et al. (2002). The analytes concentrations reported by Corbett et al. (2002) indicate the OSTDS as the groundwater source of the total nitrogen (NO2 and NO3 (mg N L^{-1})), ammonium (NH4 (mg N L^{-1})), and total phosphate (PO4 (mg P L^{-1})). The analyte concentrations were used to calculate a percent reduction from the OSTDS to the downgradient surface water body. Table 5.12 below shows the wells and sites used for analysis.

The BL site was removed from the analysis because it does not have a discernable total nitrogen (mg N L^{-1}) nor ammonium (mg N L^{-1}) concentration plumes in Table 2 (Corbett et al. 2002) for analyte concentration attenuation calculation. For example, the monitoring location closest to the OSTDS was well number three for total nitrogen. Location number three had an average total nitrogen (mg N L^{-1}) concentration of 1.0 +/- 0.1, while location numbers seven and eight which are approximately 82 ft downgradient of the OSTDS, have a total nitrogen (mg N L^{-1})

concentration of 1.1 +/- 0.1. In addition, the BL site was demolished, and a new house was built closer to the adjacent water body. Situations where analyte concentrations do not attenuate from the OSTDS towards the downgradient direction of the OSTDS are outside the scope of this analysis. These situations could be related to pet ownership, animal husbandry, lawn fertilization schedules, and not pollutants from OSTDS (Ayres Associates 1993; Clark 1996).

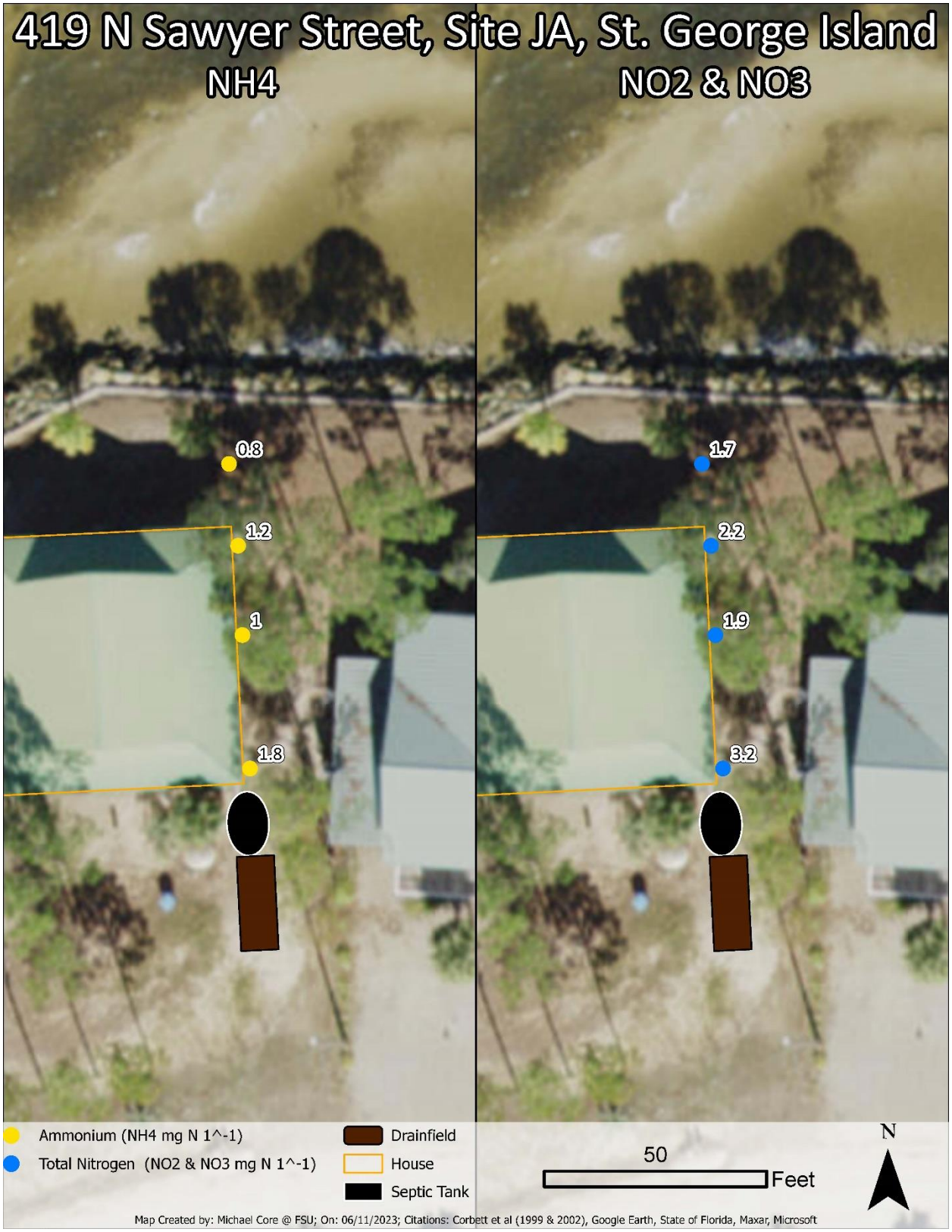

Fig. 5.24. JA site, St. George Island from Corbett & Iverson (1999) wells used for BN. The map shows the residents in an orange outline and the monitoring locations in blue and yellow dots.

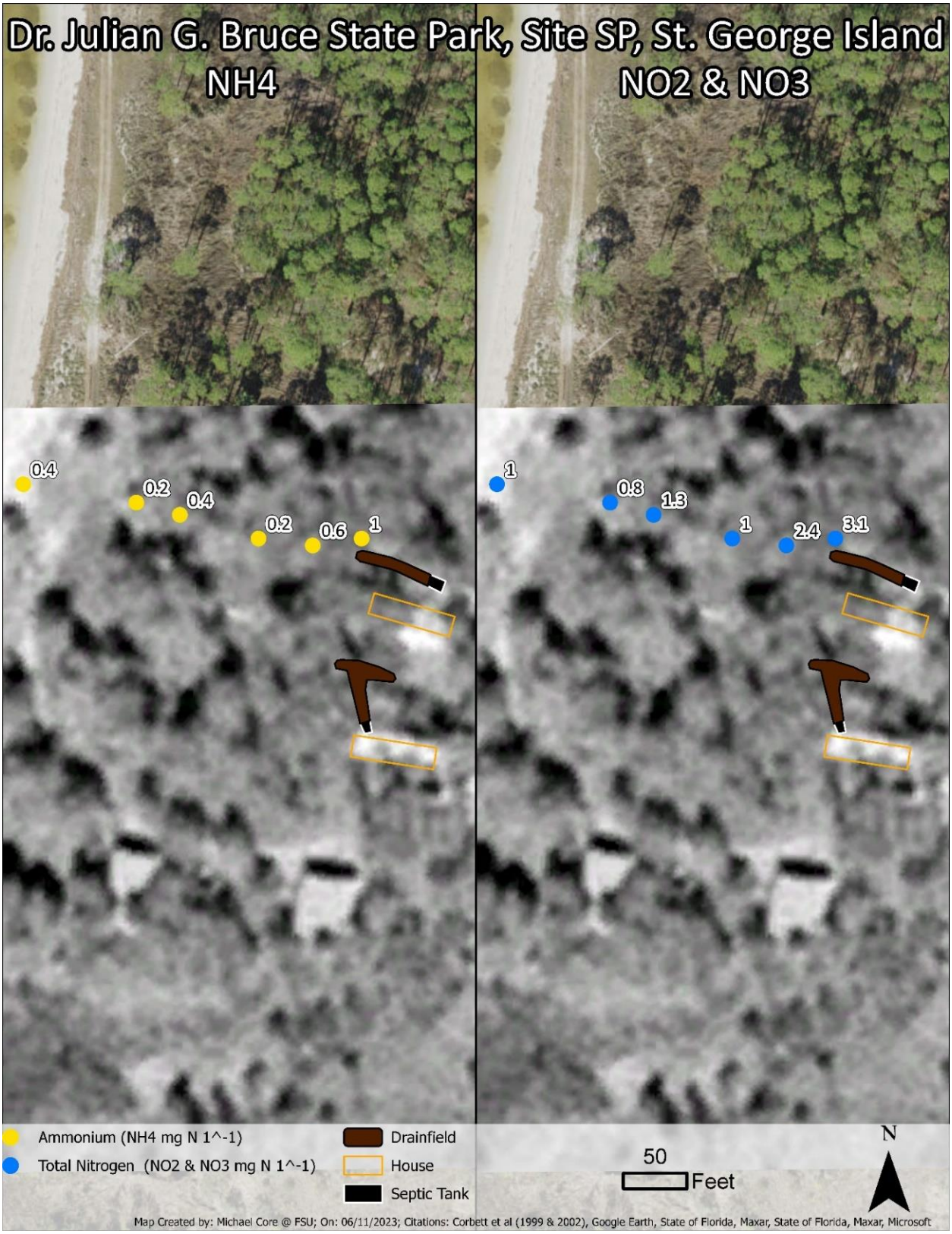

Fig. 5.25. SP site, St. George Island from Corbett & Iverson (1999) wells used for BN. The map shows the residents in an orange outline and the monitoring locations in blue and yellow dots.

Site	Monitoring Locations	Analyte
SP	7, 8, 9, 14, 15, & 17	NO2 & NO3; NH4
JA	4, 7, 8, & 9	NO2 & NO3; NH4

Table 5.12. St. George Island sites used for analysis. The table shows the monitoring locations and analytes used to train the BN for each site.

Corbett & Iverson (1999) reported that rain events influenced the groundwater calculations for monitoring location SP-17b and therefore were removed from the analysis. Furthermore, the values for locations 4a and 4b for the JA site were assumed to be at the exact location because they are not listed separately on the site survey, and therefore the hydraulic gradient and hydraulic conductivity values, as reported in Corbett & Iverson (1999) in Table 1.4 were averaged. Likewise, elevation data was sourced from the USGS 3DEM product (USGS 2022). The data recorded in Corbett & Iverson (1999) as ranges, for example, time and horizontal transport rates have data ranges for one date and monitoring well between 410 to 450 and 0.12 to 0.13, respectively. This range and all of the other reported ranges were averaged.

For data discretization for the Corbett & Iverson (1999) sites, the total nitrogen (TN) groundwater source sample had two values (Fig. 5.26); thus, the cumulative distribution function for the standard distribution was used to calculate the probability that the value will be less than or equal to 3.1 mg/L and the probability a given value will be larger than 3.1 mg/L, which were 22.06% and 77.94%, respectively. Furthermore, the following datasets: NH4 groundwater source, TP groundwater source, TN OSTDS concentration, NH4 OSTDS concentration, TP OSTDS concentration, and OSTDS setback distance (Fig. 5.27) from the adjacent waterbody, were classified into two groups based on the available data. Then the cumulative distribution was calculated for the range of values to create probabilities for the data ranges. The data for the JA site was used to create a network, and then the data from the SP site was used as evidence in the learned network to estimate the attenuation of analytes from the OSTDS for the monitoring locations for the SP site. The results can be seen in Table 5.13 below.

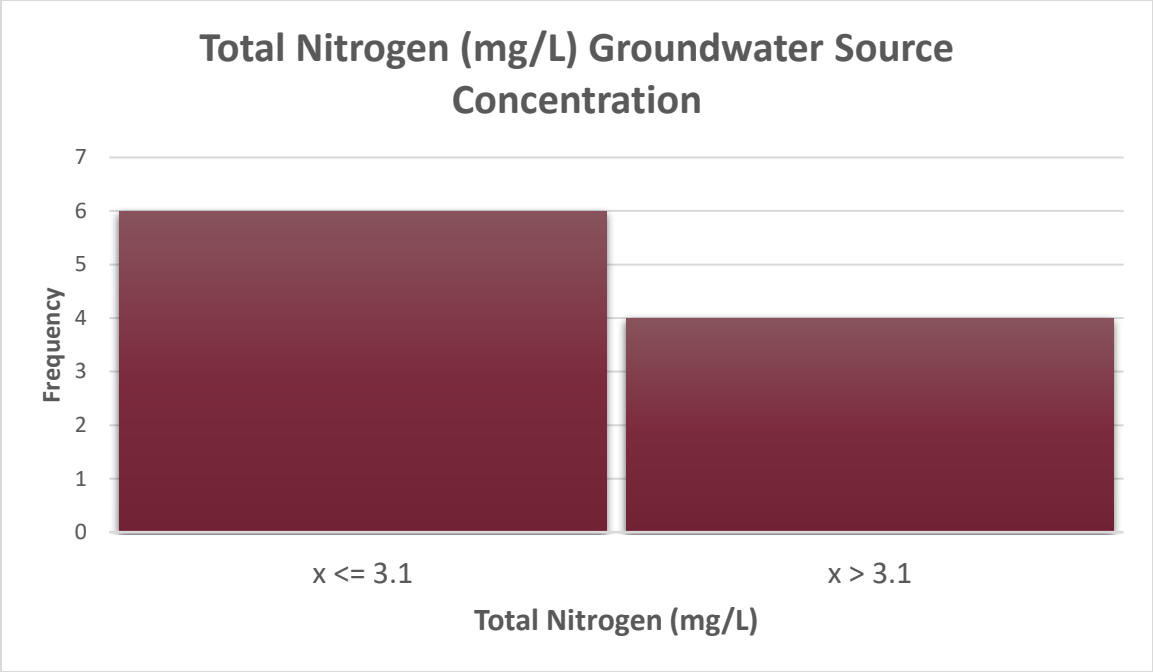

Fig. 5.26. Total nitrogen (mg/L) groundwater source Concentration histogram. The histogram was used for creating the bins in the BN.

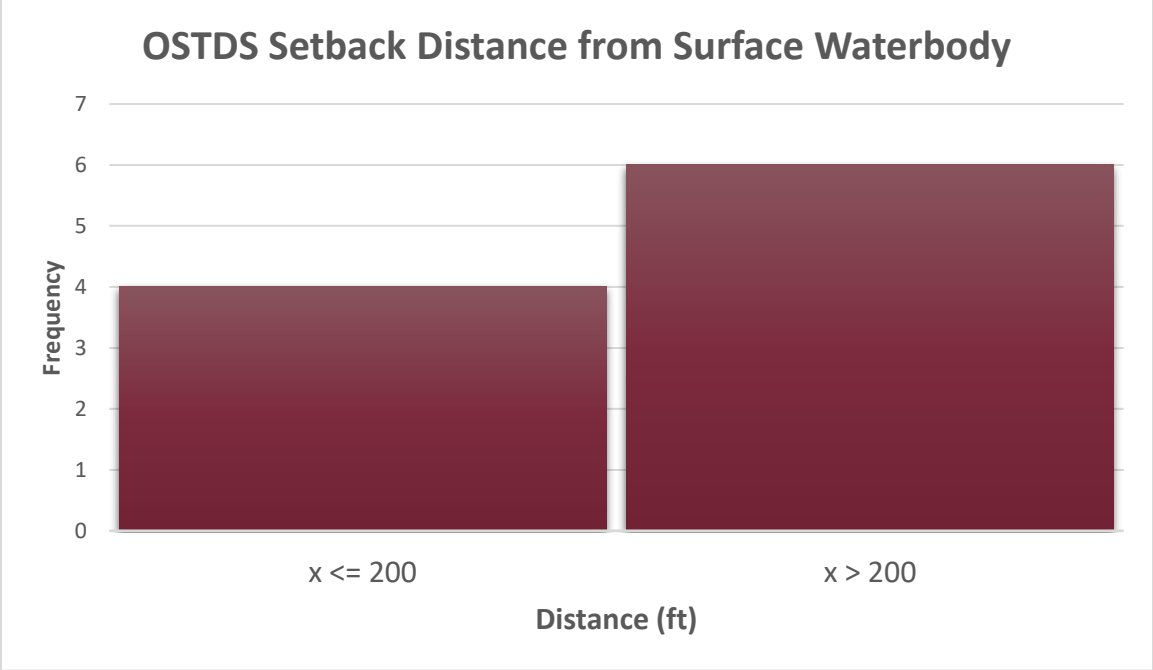

Fig. 5.27. OSTDS setback distance from a surface waterbody. The histogram was used to create the bin ranges in the CPT in the BN.

Secondly, the data for the SP site was used to create a network, and then the data from the JA site was used as evidence in the learned network to estimate the attenuation of analytes from the OSTDS for the monitoring locations for the JA site. Finally, Corbett & Iverson (1999) data were used to train the third network for St. George Island, leaving out the data for sites JA7 and SP14.

Afterward, the information from Corbett & Iverson (1999) sites JA7 and SP14 was used as evidence, and the network would then estimate the attenuation rate at sites JA7 and SP14. The network can be seen in Fig. 5.28. In contrast, the results of the error rate test for analyte attenuation can be seen in Table 5.13, and the sensitivity analysis for the attenuation nodes can be seen in Table 5.14.

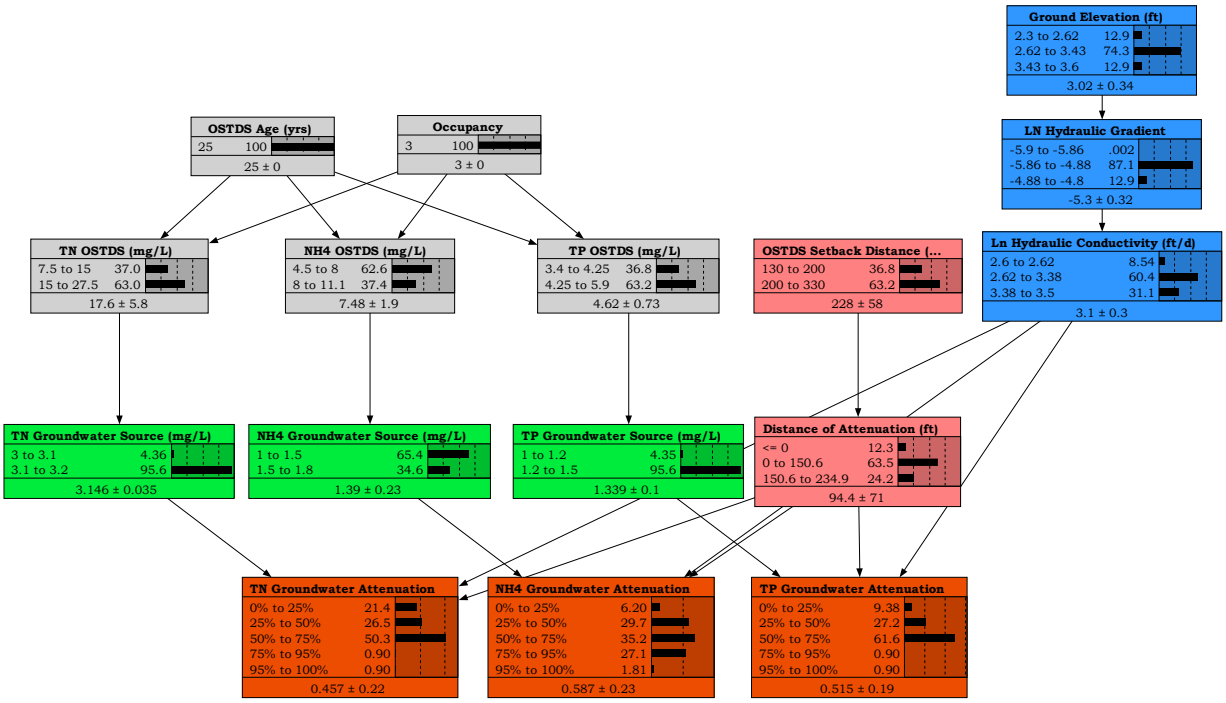

Fig. 5.28. St. George Island BN for sites JA and SP. The BN output attenuation nodes are in orange. The node links are black lines, which connect parent and children nodes.

Data from Corbett & Iverson (1999) was integrated into the BN, presenting a range of error rates across different wells and analytes. In the State Park (SP) wells with the Jay Abott (JA) BN, total nitrogen (TN) showed an error rate of 50%, ammonia (NH4) was at 83.3%, and total phosphorus (TP) was at 66.67%. When the JA wells were applied to the SP Network, TN showed a 75% error rate, while NH4 and TP had 50% error rates. Combining data from both JA7 and SP14 wells for the JA/SP network led to a 50% error rate for NH4 and TP but a 0% error rate for TN (Table 5.13). The reduction in the error rate for TP helps to illustrate the iterative nature of the BN design process.

Monitoring Location	BN	Analyte	Error Rate
SP wells	JA Network	TN	50%
SP wells	JA Network	NH4	83.3%
SP wells	JA Network	TP	66.67%
JA wells	SP Network	TN	75%
JA wells	SP Network	NH4	50%
JA wells	SP Network	TP	50%
JA7; SP14	JA/SP Network	TN	0%
JA7; SP14	JA/SP Network	NH4	50%
JA7; SP14	JA/SP Network	TP	50%

Table 5.13. St. George Island JA and SP BN error rates. The table shows the monitoring locations used for cross-validation and the associated attenuation error rates. The TN error rate of 0% is in green.

The node sensitivity of the combined JA/SP network exposes the role of specific parameters. In this network, TN attenuation was sensitive to the distance of attenuation, NH4 attenuation, TP attenuation, and TN Surface Water (SW) source. NH4 attenuation showed sensitivity to log hydraulic conductivity, TP attenuation, TN attenuation, and attenuation distance. Similarly, TP attenuation was sensitive to log hydraulic conductivity, NH4 attenuation, TN attenuation, and the attenuation distance (Table 5.14. St. George Island JA/SP BN node sensitivity). This information underscores the complexity and interconnectedness of the factors in the BN.

Well Location	Node	Influential Nodes
JA7; SP14	TN Attenuation	Distance of attenuation; NH4 Attenuation; TP Attenuation; TN SW Source
JA7; SP14	NH4 Attenuation	Log Hydraulic Conductivity; TP Attenuation; TN Attenuation; Distance of attenuation
JA7; SP14	TP Attenuation	Log Hydraulic Conductivity; NH4 Attenuation; TN Attenuation; Distance of attenuation

Table 5.14. St. George Island JA/SP BN node sensitivity. The table shows the most influential nodes for the combined JA/SP network. Notably, the distance of attenuation and hydraulic conductivity influence the network most.

5.6. St. Johns Site (Ayres Associates, 1996)

As Ayres Associates (1996) reported, the St. Johns site, The Soap and Detergent Association (SDA) site address was at 1291 Tangerine Dr., Fruit Cove, Florida (Fig. 5.29). This location has measurements for various depths below the ground surface (bgs) at each monitoring well site for one observation in 1993 and one in 1995. For example, monitoring well TW2 had analyte concentration observations at 6, 12, and 20 ft below the ground surface for 1993 and 1995.

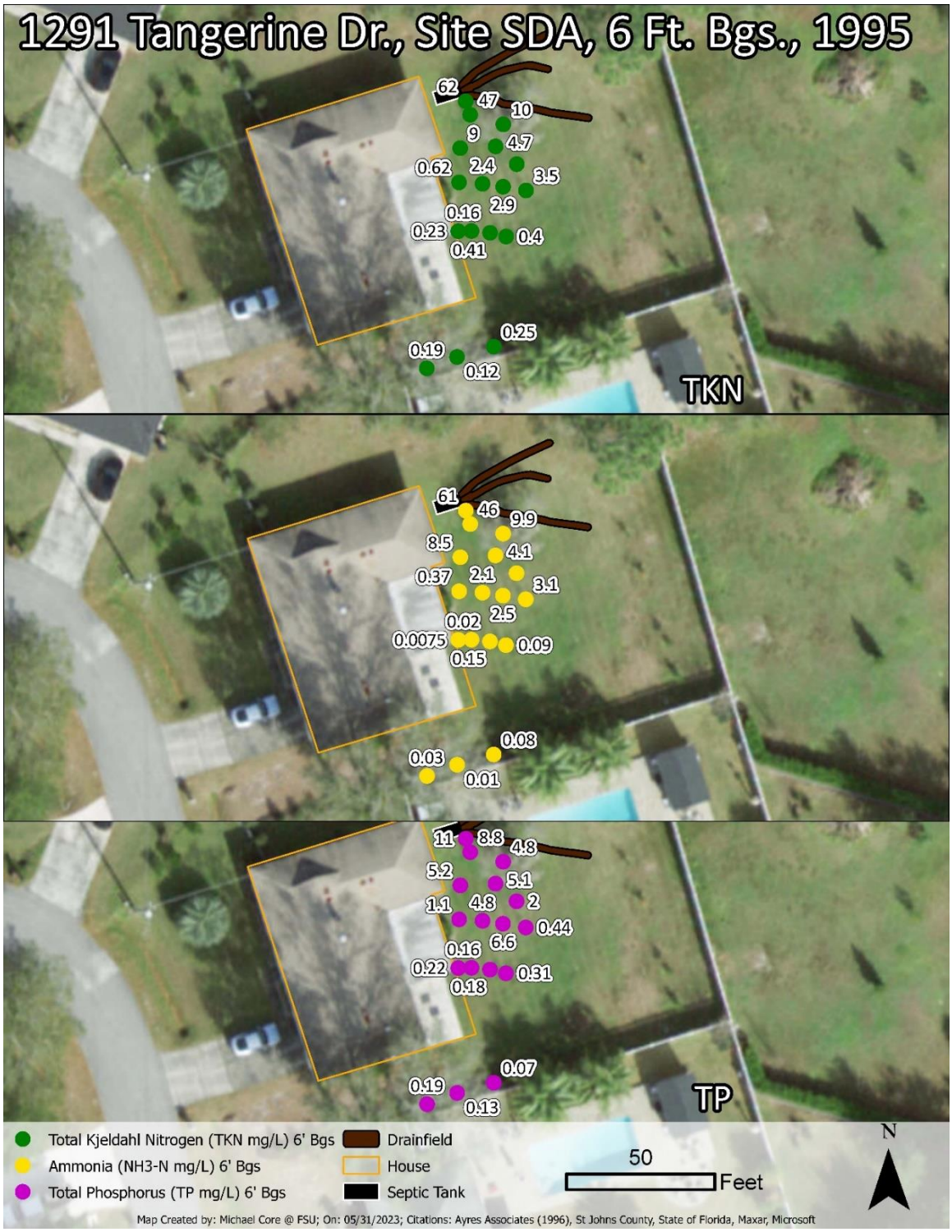

Fig. 5.29. St. Johns, Ayres Associates (1996) 6 ft bgs monitoring locations for BN. The residents are marked in orange, and the monitoring locations are colored dots.

Monitoring locations were chosen first by year and then by depth for TP, TKN, NH3-N, and NO3-N, where the concentration was highest at the OSTDS and decreased traveling southerly and downgradient from the OSTDS. This was done to calculate an analyte concentration attenuation

at various distances downgradient from the OSTDS. Sites with monitoring locations (wells and piezometers) closest to the OSTDS having the highest analyte concentration were considered sites where the OSTDS was the source of groundwater contamination. For example, as reported in Ayres Associates (1996) for NH3-N for 1995 for 6 ft bgs monitoring location TW19 was in the row nearest to the OSTDS and had an analyte concentration of 61 mg/L. Then, decreasing from this location southerly, monitoring locations TW1, TW5, TW6, TW7, TW8, TW9, TW10, TW11, and TW12 had NH3-N concentrations of 46 mg/L, 4.1 mg/L, 8.5 mg/L, 2.1 mg/L, 0.37 mg/L, 2.5 mg/L, 9.9 mg/L, 29 mg/L, and 3.1 mg/L respectively. The monitoring well locations, years, and depths used for analysis are in Table 5.15 below. For TP for 1995 for 6 ft bgs location TW19 with a concentration of 11 mg/L was chosen as the ground source location of the contamination due to the overall agreement between the highest analyte concentration of TKN, NH3-N, and the second highest concentration for TP.

Alternatively, location TW20 had the highest TP concentration measurement at 12 mg/L, was amongst the same row of monitoring wells as TW19, and is approximately 5 ft southeasterly from TW19 along the trench of the drainfield. Also, for 1995 for 6 ft bgs, NO3-N attenuation was not calculated because the peak concentration values of 15 mg/L and 14 mg/L were amongst the third and second rows, respectively, and were not adjacent to the OSTDS. These locations were out of this project's scope and therefore removed from the analysis. Data for 1995 for 12 ft bgs and 20 ft bgs were removed from this analysis due to the steep gradient of analyte concentrations. For example, as reported in Ayres Associates (1996), for monitoring location TW19, a concentration of 61 mg/L and 60 mg/L for TKN and NO3-N, respectively. The adjacent monitoring locations have concentrations of less than one mg/L and then spike to 3 mg/L at location TW28. These analyte attenuation interaction types are outside of this research's scope.

For 1993 for 6 ft bgs, as Ayres Associates (1996) reported, monitoring location TW16 had the highest measurements for NO3-N and TP, 59.15 mg/L and 16 mg/L, respectively. Likewise, TW16 represents the OSTDS as the source of groundwater contamination and, thus, the point from which the analyte concentration attenuation rate is calculated. The attenuation patterns for the analyte measurements for 1993 for 12 ft bgs and 20 ft bgs were removed from the analysis due to their attenuation patterns with steep attenuation gradients being outside this project's scope.

Year	Monitoring Location	Analyte
1995	TW1, TW5, TW6, TW7, TW8, TW9, TW10, TW11, TW12, TW13, TW14, TW15, TW19, TW25, TW26, TW27, & TW28	TKN, NH3-N, & TP
1993	TW1, TW2, TW3, TW5, TW6, TW7, TW8, TW9, TW10, TW11, TW12, TW13, TW14, TW15, & TW16	NO3-N & TP

Table 5.15. Sites used for analysis from St. Johns. The table shows the monitoring locations and analytes used to create the St. Johns BN.

The dissolved oxygen (DO) values, as reported in Ayres Associates (1996) in Table H.1, were averaged across monitoring locations. For example, in Table H.1 for location TW1, there are notations for monitoring locations TW1-6 and TW1-12 for August 31st, 1993. These values for these locations and times were averaged. The septic tank average estimated analyte concentration from Table 4.1 was used from August 1993 and November 1993 to May 1995 to represent TKN, NH3-N, NO3-N, and TP concentrations from 1993 and 1995, respectively. For total water use

(gpd), the value of 583.1 gpd from August 15th, 1993, to November 1st, 1993, was chosen for the 1993 data. Likewise, the value of 173.2 gpd for November 1st, 1993, to December 23rd, 1994, was selected for the 1995 data. Furthermore, for the water table elevation (ft) data in Figure 4-2, the data ranges were averaged for each location. As Ayres Associates (1996) reported, the seepage estimates consistently indicated an average velocity of approximately 0.13 ft/day downgradient of the OSTDS. The porosity observed at the drainfield ranged between 41.90% to 46.10%. The sample locations were noted as SC1, SC2, and SC3. Unfortunately, these locations were not depicted on the site surveys of the monitoring locations, and therefore the values were averaged to 43.43%. Likewise, the saturated hydraulic conductivity was only reported for sample locations SC1, SC2, and SC3 with 10.6 ft/d, 13.5 ft/d, and 16.9 ft/d, respectively. Therefore, the saturated hydraulic conductivity values were averaged to 13.6 ft/d. The relative groundwater elevation was derived from Ayres Associates (1996) Figure 4-2 during data processing. The drainfield depth to the water table was calculated using the averaged value from the contour lines straddling the OSTDS, as shown in Figure 4-2 in Ayres Associates (1996). Likewise, the drainfield elevation was reported as 47.74 ft via the observation port. The relative water table elevation averaged from the contour map was 46.23 ft. The relative water table elevation was then subtracted from the drainfield elevation, thus giving the drainfield depth to the water table estimate of approximately 1.5 ft. Lastly, the ground elevation data was sourced from the USGS National Map (USGS 2022).

A BN was developed and trained with the data for 1993 (Fig. 5.30) for St. Johns, as reported in Ayres Associates (1996). Afterward, the data for 1995 (Table 5.15), as reported in Ayres Associates (1996), was used to test the 1993 network and predict the analyte attenuation rates for 1995. Likewise, the 1993 data were used to test the 1995 trained network (Fig. 5.31).

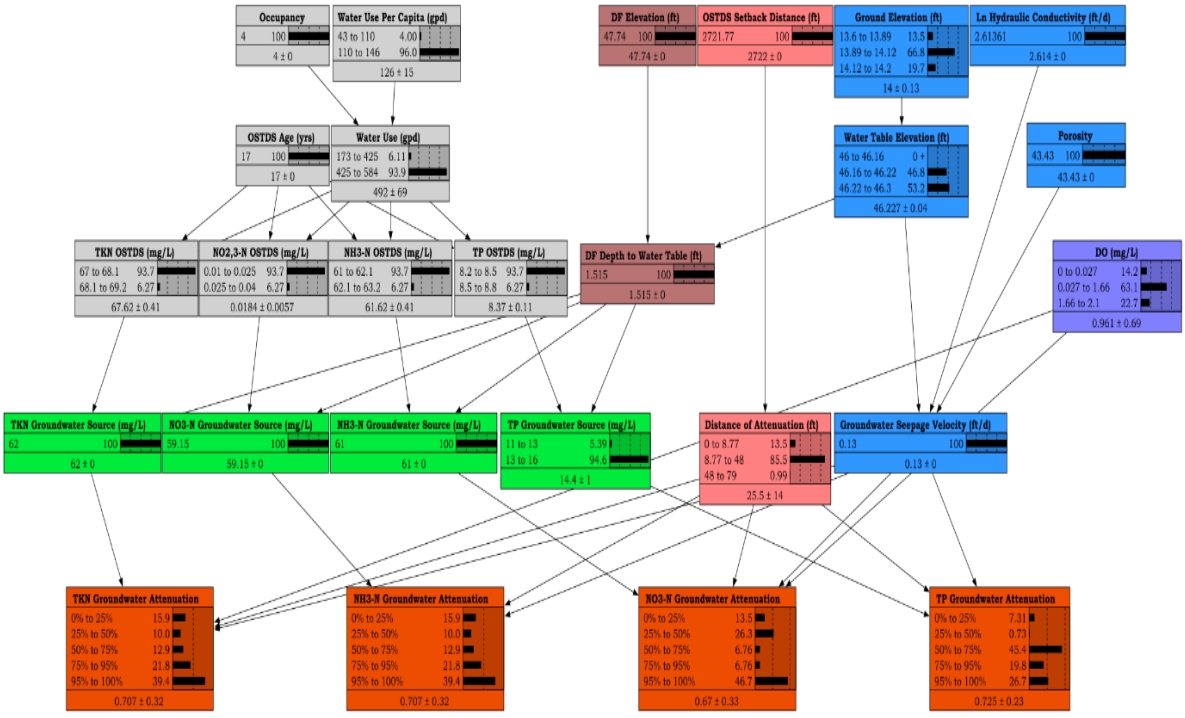

Fig. 5.30. St. Johns BN from 1993 data. The BN output attenuation nodes are in orange. The node links are black lines, which connect parent and children nodes.

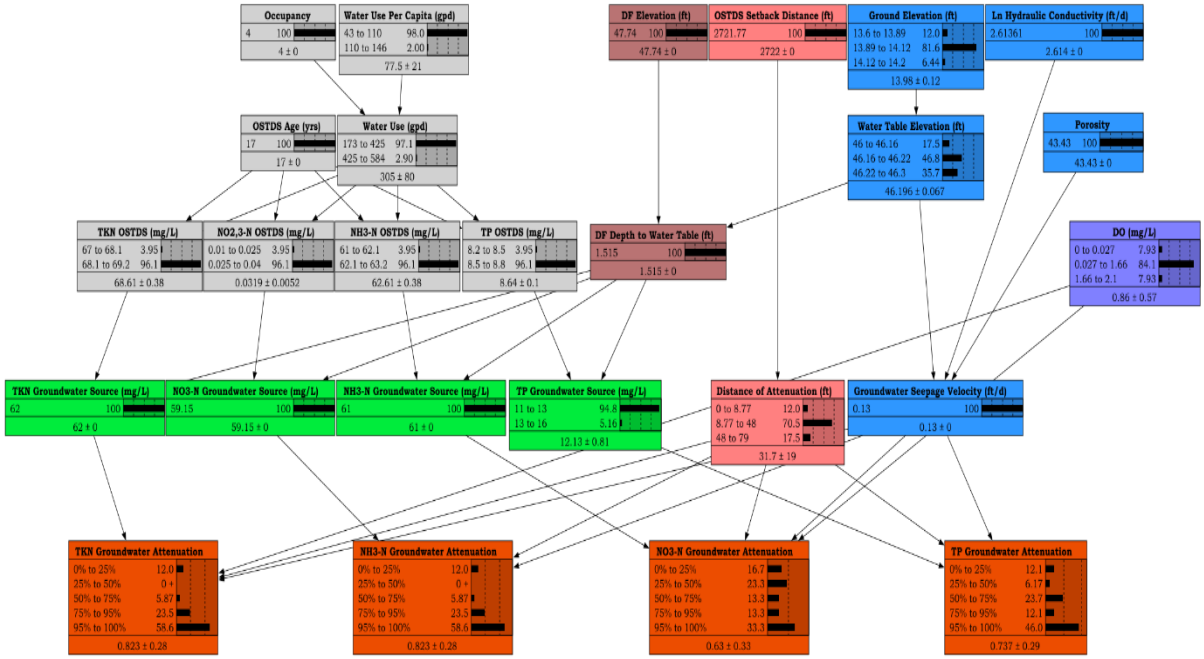

Fig. 5.31. St. Johns BN from 1995 data. The BN output attenuation nodes are in orange. The node links are black lines, which connect parent and children nodes.

A comparison of error rates from Ayres Associates (1996) literature and the Bayesian Network (BN) demonstrates varied results. The NH3 and TKN analytes in the 1995 wells with the SDA 1993 network showed an error rate of 41%, while TP had an error rate of 53%. On the other hand, the 1993 wells with the SDA 1995 network exhibited a 53% error rate for NO3-N and a 73% error rate for TP (Table 5.16).

Monitoring Locations	BN	Analyte	Error Rate
1995 wells	SDA 1993	NH3	41%
1995 wells	SDA 1993	TP	53%
1995 wells	SDA 1993	TKN	41%
1993 wells	SDA 1995	NO3-N	53%
1993 wells	SDA 1995	TP	73%

Table 5.16. St. Johns, Ayres Associates (1996) BN error rates. The table shows the monitoring locations used to cross-validate the BN for each analyte. The table also shows the error rate for estimating each analyte's attenuation rate.

Likewise, analyzing the sensitivity of nodes in the BN reveals intricate relationships. For example, in the 1995 wells' SDA 1993 network, the TKN attenuation node was sensitive to log hydraulic conductivity, porosity, seepage velocity, and NO3-N attenuation. The NH3-N attenuation node in the same network exhibited sensitivity to porosity, seepage velocity, log hydraulic gradient, and NO3-N attenuation. Meanwhile, the NO3-N attenuation node was sensitive

to dissolved oxygen, attenuation distance, TP attenuation, and TKN attenuation. Finally, the TP attenuation node was most responsive to the distance of attenuation, NO3-N attenuation, TP groundwater source, and TP OSTDS. These observations highlight the nuanced interplay of various factors within the network, significantly impacting the model's predictive capability (Table 5.17).

Well Locations	BN	Node	Influential Nodes
1995 wells	SDA 1993 Network	TKN Attenuation	Log Hydraulic Conductivity; Porosity; Seepage Velocity; NO3-N Attenuation
1995 wells	SDA 1993 Network	NH3-N Attenuation	Porosity; Seepage Velocity; Log Hydraulic Gradient; NO3-N Attenuation
1995 wells	SDA 1993 Network	NO3-N Attenuation	DO; Distance of attenuation; TP Attenuation; TKN Attenuation
1995 wells	SDA 1993 Network	TP Attenuation	Distance of attenuation; NO3-N Attenuation; TP GW Source; TP OSTDS

Table 5.17. St. Johns, Ayres Associates (1996) BN node sensitivity. The table shows the influential nodes for the SDA 1993 network. The distance of attenuation and seepage velocity are among the network's most influential nodes.

5.7 BN based on Data of All Sites

This study adopts an integrated approach, consolidating data from multiple sources to create a comprehensive and robust BN model. Data from four articles, Ayres Associates (1993, 1996), Corbett & Iverson (1999), Corbett et al. (2002), and Belanger et al. (2011), were combined to capture a broad spectrum of insights related to OSTDS-induced nitrogen attenuation from an OSTDS to surface waters. The cumulative distribution function for normal distribution was utilized to process and homogenize this multi-source data. This statistical method allowed for a standardized dataset despite their varying characteristics and scales. This ensured that each data source contributed evenly to the final model, avoiding potential skew from over-representing any single source (Fenton and Neil 2018). Following the data integration, a binning process was utilized to categorize the data into distinct ranges for the BN. The bins were formed based on the data distribution, dividing them into intervals representing a specific range of values. This process reduced potential noise and data complexity, simplifying the modeling and interpretation of results (Norsys Software Corp 2007; Fenton and Neil 2018).

The updated BN (Fig. 5.1), enriched with combined data from all four articles, provides a more holistic understanding of the OSTDS-induced nitrogen attenuation rate. It integrates a wide range of observations and experimental results, enhancing its validity and applicability in guiding environmental management and decision-making. The combined BN was trained using the Expectation Maximization (EM) algorithm on all data (and missing data), excluding monitoring locations G13, G14, and G15 from Ayres Associates (1993) (Figure 32). This selection provided a robust dataset for the model's training while retaining some locations for later validation.

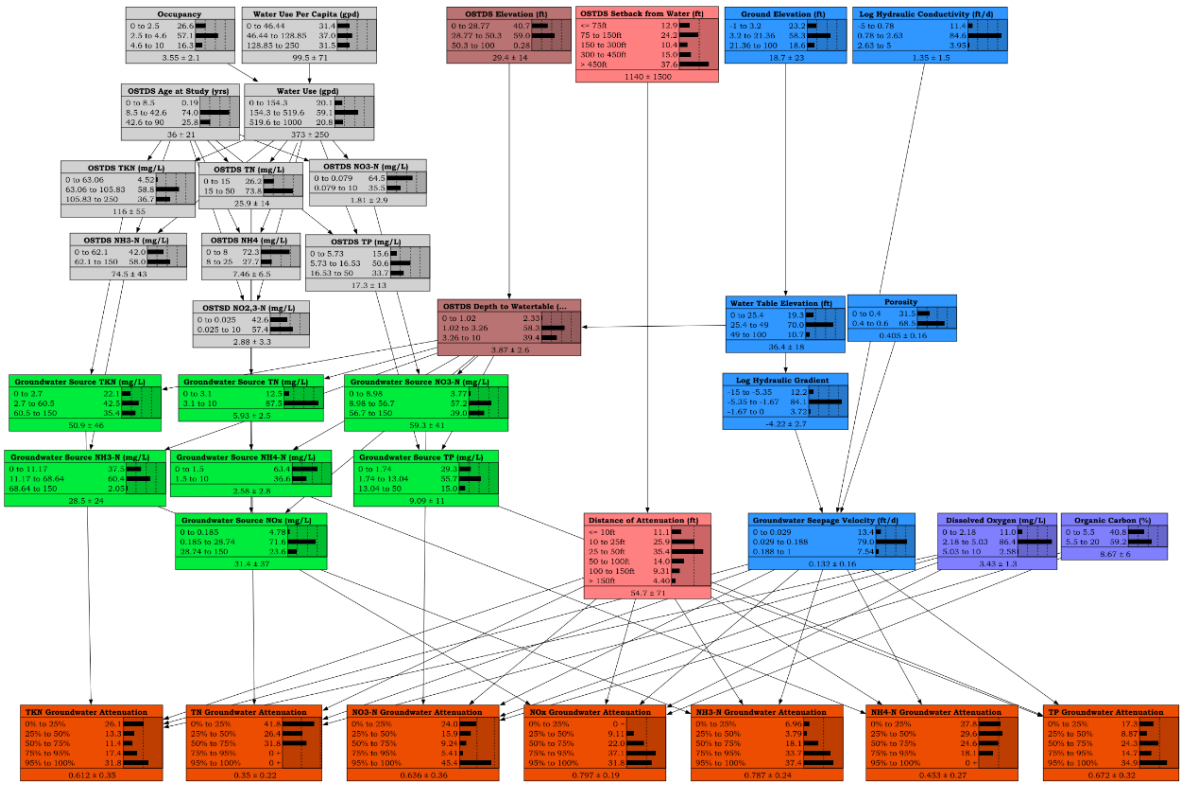

Fig. 5.32. Combined BN for testing Groseclose (13, 14, & 15). The BN output attenuation nodes are in orange. The node links are black lines, which connect parent and children nodes.

Following the training, the model was validated using the data from the monitoring locations initially excluded from the training phase. This approach helped ascertain the model's accuracy and generalization ability beyond the training data. The validation results were examined through confusion matrices for each response variable (Tables 5.1 and 5.2): TKN groundwater attenuation, TN groundwater attenuation, NO3-N groundwater attenuation, and TP groundwater attenuation. For TKN groundwater attenuation rates, the model exhibited an error rate of 100%, indicating that the model's predictions did not align with the validation data. Likewise, the model did not produce applicable cases for TN groundwater attenuation (50%).

In contrast, the model displayed an error rate of 0% for NO3-N and TP groundwater attenuation. The model's predictions for these parameters fell exclusively within the "95% to 100%" category, indicating that the model was entirely accurate within these ranges. These results provide a valuable benchmark for the model's performance and underscore the potential for further tuning and refinement to enhance its predictive accuracy, particularly for the TKN groundwater attenuation rates.

A specialized BN was created to predict analyte attenuation rates from the OSTDS to the adjacent surface water bodies. For this task, we implemented a training regimen using the EM algorithm, excluding data from several specific monitoring locations as follows: Turkey Creek (Ayres Associates 1993): Groseclose G15 and Jones J8; Julington Heights and Lakeshore (Belanger et al. 2011): CST 11 on June 1, 2010, DH 9 on September 27, 2010, MM 7 on June 2, 2010, and RT PZ4 on December 12, 2009; St. George Island (Corbett and Iverson 1999; Corbet et

al. 2002): JA9 and SP8; and St. Johns (Ayres Associates 1996): TW15 on 1993 and TW15 on1995. The selected locations for this model were primarily located near surface water bodies. Following the training, these excluded locations were used for validation to assess the model's predictive capacity specifically for OSTDS-to-surface-water scenarios. The validation results for this specialized network are detailed below.

For TKN groundwater attenuation, the model achieved an error rate of 40%. NO3-N groundwater attenuation had a 0% error rate which was a notable achievement for the model and suggested a strong understanding of the factors affecting NO3-N attenuation. NOx and TP groundwater attenuation showed error rates of 66.67% and 25%, respectively. These findings highlight the complex behavior of these nutrients in the subsurface environment and point to potential future research opportunities. Interestingly, for NH3-N groundwater attenuation and NH4-N groundwater attenuation, the error rates were 25% and 0%, respectively. These findings suggest a level of accuracy for these parameters. These validation results reveal the performance of the specialized BN when applied to situations where attenuation rates from OSTDS to adjacent surface water bodies are of interest. The diverse error rates across different analytes underscore the complexity of such predictions and highlight potential areas for further improvement and refinement of the model.

Alternatively, TN groundwater attenuation has an error rate of 50%, representing an opportunity for model enhancement. This could be achieved by focusing on variables impacting TN attenuation rates, such as the presence of specific microbial communities, vegetation, or the physical characteristics of the soil profile (Clark 1996; Glendell et al. 2021; Troldborg et al. 2022). Nonetheless, it is essential to maintain an iterative approach and continually test the model with new data sets to ensure its continued accuracy. Understanding the biogeochemical processes affecting these nutrients could reduce these error rates. While the specialized BN shows promise, there is still work. The varying error rates indicate that the model's ability to predict nutrient attenuation rates from OSTDS to surface water bodies depends mainly on the evaluated nutrient. This underlines the complexity of nutrient behavior in the subsurface environment and emphasizes the need for ongoing model refinement and validation.

In the context of the Combined BN (Fig. 5.1), a closer examination of attenuation nodes reveals their sensitivity to specific factors in the network (Table 5.2). Each attenuation node's influence was found to be largely dependent on particular nodes. This interaction indicates that these interrelationships significantly influence the model's predictive capability. The TKN Attenuation node, for example, is sensitive to changes in the distance of attenuation, Groundwater (GW) source TKN, OSTDS TKN concentrations, and the NH3-N attenuation nodes. Similarly, the TN attenuation node was most sensitive to the distance of attenuation, seepage velocity, GW Source TN concentration, and dissolved oxygen concentration nodes. The sensitivity of the NO3-N and NOx attenuation nodes underscore the interconnectedness of nutrient cycles. These nodes were sensitive to changes in the distance of attenuation, NH3-N attenuation, and TP attenuation nodes.

Furthermore, the NO3-N attenuation node was sensitive to the organic carbon node, and the NOx attenuation node was sensitive to the GW source NOx concentration node. A similar pattern was observed when focusing on the NH4-N and NH3-N attenuation nodes. Both nodes were sensitive to the distance of the attenuation node. In addition, the NH4-N attenuation node was sensitive to the seepage velocity, TKN attenuation, and TN attenuation nodes. Conversely, the NH3-N attenuation node was sensitive to the TP attenuation, TKN attenuation, and GW source

NH3-N nodes. Finally, the TP attenuation node displayed sensitivity to the distance of attenuation, GW source TP, NH3-N attenuation, and OSTDS TP concentration nodes.

Understanding these sensitivities is crucial as it provides deeper insights into how variations in these specific nodes might influence the performance and output of the attenuation nodes. These findings form an integral part of our ongoing model refinement process. Future improvements to the model's performance may be realized by focusing on these influential nodes and their interplay within the network.

5.8 Model Prediction

Considering multiple risk factors, the BN model predicts the likelihood of NO3, TKN, and TP attenuation from OSTDS to surface water bodies. In addition, the model's probabilistic nature allows for addressing uncertainties related to OSTDS use, condition, and maintenance (Glendell et al. 2021). This improved understanding of pollution risks can aid decision-makers in selecting appropriate mitigation measures and managing groundwater resources more effectively. During the comprehensive BN analysis, the combined data from Turkey Creek, Lakeshore, Julington Heights, St. George Island, and St. Johns sites into a unified Bayesian network. The inherent strength of the BN, as elucidated by Fenton & Neil (2018), lies in its ability to propagate beliefs or probabilities throughout interconnected nodes via the network's links. This interconnectedness facilitates evidence entry into a child node and subsequently impacts beliefs in the parent and grandparent nodes, thereby providing dynamic insights into the complex interplay within the system. Given the consistent sensitivity of NO3-N, NH3-N, and TP (Tables 5.1 and 5.2) to the attenuation distance, as reflected by their low error rates, these analytes were chosen for detailed examination. Predictions were made for the critical attenuation distance from the groundwater pollution source, originating from an OSTDS, towards a downgradient adjacent surface water body. The resulting distances required for various analyte attenuation rates ranged between 10 and 50 feet. Specifically, for complete 100% attenuation, a consistent distance of 50 feet was necessary across all analytes, NO3-N, NH3-N, and TP. These findings resonate with the results of earlier studies by Ayres Associates (1993), which reported that nitrogen levels should approach or revert to background levels within approximately 40 feet of the OSTDS. This consistency highlights the reliability of our findings and their implications for managing OSTDS on these sites.

The BN model is relatively nascent, with limited training, underscoring the potential for refining and enhancing its predictive capabilities. Additional data on OSTDS analyte concentrations and analyte measurements from monitoring wells and piezometers, particularly from reports in the FDEP OCULUS portal, would significantly enhance the network's accuracy and predictive prowess for analyte attenuation rates. With increased observations and data variability, initial bin ranges, distributions, and probabilities in the network's conditional probability tables (CPT) would be better representative before the training commences (Norsys Netica 2007). The untrained CPTs with fully described data characterizations based on observations of a greater number of real-world scenarios would inherently lead to more precise attenuation rate predictions. Further, training the network with a greater number of observations would provide the model with a more nuanced understanding of the ground reality, enabling it to make more accurate inferences. For instance, incorporating data from diverse environmental conditions in Florida, such as karst environments, would enrich the network's knowledge base, making it more reflective of unique geology.

This model enhancement approach underscores the iterative nature of BN models. As more data is incorporated and the model is re-trained, its ability to accurately simulate and predict environmental outcomes will continue to improve. The more we can align the model with the diverse and specific realities of Florida's environmental conditions, the better we can predict OSTDS impacts and make informed decisions to maintain water quality.

The findings of this study corroborate existing literature on the critical factors influencing nitrogen transport from OSTDS. These results align with research by Troldborg et al. (2022), who emphasized the significant role of soil type, depth to the water table, and setback distances in nitrogen attenuation. The variable error rates observed across different analytes in this study underscore the complexities of nitrogen transformation and attenuation in OSTDS. While NOx and NH4-N demonstrated relatively higher error rates, the model performed reasonably well for NH3-N and TP, which resonates with Glendell et al. (2021), who found diverse attenuation rates for different forms of nitrogen in OSTDS. Furthermore, the significant influence of setback distances on nitrogen loading, as demonstrated in this study, supports the findings of Ayres Associates (1993 & 1996). They proposed considerable setback distances to reduce OSTDS-induced nitrogen loading to surface waters, particularly in environmentally sensitive areas.

On the other hand, the lesser sensitivity of the model to occupancy and water use may reflect the specificity of the site conditions of our study compared to their broader geographic scope. This study underscores the need for ongoing research into OSTDS nitrogen loading. While this study aligns with much of the existing literature, differences are also observed, suggesting that site-specific factors may significantly influence nitrogen transport. These findings further testify to the complexity of nitrogen cycling and the necessity for further nuanced, context-specific research.

The model predictions provided valuable insights into the effectiveness of current and proposed setback distance for protecting groundwater resources in several counties in Florida. By identifying areas of high attenuation potential, the results can inform targeted measures to reduce the risk of groundwater pollution and safeguard the quality of surface water bodies. This information is essential for informed water resource management decision-making (Ayres Associates 1993). Based on the model predictions, several measures to enhance groundwater protection are recommended, such as implementing best management practices related to OSTDS setback distances from surface waterbodies to reduce the release of NO3, TKN, and TP into the water systems. Likewise, the vertical setback distance related to the distance between an OSTDS and the groundwater should be considered. Ample vertical distance allows space for nitrification and denitrification (Clark 1996) and, finally, regular updates to the BN model with new data and expert knowledge to continually refine the understanding of the hydrogeological system and improve the accuracy of predictions. By incorporating these recommendations into a water resources management strategy, we can help safeguard Florida’s groundwater and surface water resources and ensure long-term sustainability.

Despite its promising performance, the BN model has limitations. The model's accuracy depends on the quality of input data and expert knowledge used to develop it (Fenton and Neil 2018). Additionally, the model may only capture some of the complexities of the natural system, which could impact its predictive performance. One limitation of the current model is the reliance on existing data without collecting additional observations. While the available data provided a solid foundation for constructing the BN, incorporating new field measurements and monitoring data could further refine the model's accuracy and reliability. While the Bayesian network model utilized in this study offers valuable insights into the transport and attenuation of nitrogen in

OSTDS, its limitations may have influenced our results. The model operates based on conditional independence (Fenton and Neil 2018), assuming that each parameter independently impacts nitrogen loading. However, in the real world, the interaction between different factors may be more complex, with variables potentially having synergistic or antagonistic effects on nitrogen loading (Troldborg et al. 2022).

Furthermore, the model's sensitivity to specific parameters may have been underestimated due to the limited range of values used in the model setup. This study may not fully capture the effect of extreme conditions or outlier values. A point of note by Glendell et al. (2021) suggests that the attenuation of certain nitrogen forms may be under or overestimated depending on local environmental conditions not considered in the model. The model also assumes uniformity in the characteristics of OSTDS, soil properties, and hydrogeologic conditions across the study area, which may not hold in reality. The heterogeneity of these factors in the field may cause variability in nitrogen loading (Ayres Associates, 1993 & 1996). The lack of spatial variability may therefore represent a potential source of error in our predictions. For example, the conceptualization of the hydrogeological system, including the representation of hydrostratigraphic units and flow processes, may only partially capture the complexity of the real-world system (Glendell et al. 2021; Troldborg et al. 2022). Additionally, the assignment of model parameters, boundary conditions, and initial conditions was based on the available data and expert knowledge, which may only partially represent the study area's actual conditions (Fenton and Neil 2018). Lastly, the model assumes that the relationships between hydrogeological parameters and pollutant attenuation processes are stationary, which may not hold under changing environmental conditions or management practices.

Lastly, the model does not consider certain variables, such as the maintenance status of OSTDS, rainfall, or seasonal variations in the water table, which Glendell et al. (2021) suggest could significantly impact nitrogen loading from OSTDS. Despite these limitations, this study provides a basis for further research and can serve as a tool for preliminary decision-making regarding OSTDS management and policy development. Acknowledging these limitations allows for the continued improvement and refinement of the model.

Model calibration and prediction are inherently uncertain due to measurement errors, parameter uncertainty, and model structure uncertainty (Troldborg et al. 2022). The calibration process relies on matching the model outputs with observed data, which may contain measurement errors or be influenced by factors not explicitly considered in the model (Ayres Associates 1993, 1996; Corbett and Iverson 1999; Corbet et al. 2002; Belanger et al. 2011). Parameter uncertainty arises from the limited data for specific hydrogeological parameters, requiring expert judgment or interpolation methods that may introduce errors (Glendell et al. 2021). Finally, model structure uncertainty relates to the assumptions and simplifications made in the representation of the hydrogeological system, which may not fully capture the complex interactions between various components (Fenton and Neil 2018). Despite these limitations, the BN model still provides valuable insights into the attenuation processes of NO3, TKN, and TP in the study area. By acknowledging and understanding these limitations, the model results can be more effectively applied in groundwater resource management.

5.9. Summary and Conclusions

The implications of this study extend beyond the model's predictions, providing insights into the complex interplay between OSTDS, analyte attenuation, setback distances, and nitrogen

loading to surface water bodies. Understanding the significant influence of parameters such as OSTDS type, setback distance, and hydrogeologic conditions on nitrogen loading can guide more effective environmental policies and practices. These could include revising setback regulations, considering soil permeability in OSTDS site selection, and promoting using OSTDS types associated with lower nitrogen loading. Despite certain limitations, the Bayesian network model has proven helpful in environmental management, facilitating understanding of complex relationships and providing a probabilistic framework for decision-making (Glendell et al. 2021; Troldborg et al. 2022). Its predictive accuracy and application scope can be further enhanced with continued refinement and incorporation of diverse datasets.

This research underscores the need for an integrated and proactive approach to managing the impacts of OSTDS on water quality. The insights gleaned will inform the development of strategies that balance the needs of urbanization and infrastructure development with the preservation and restoration of Florida's precious water resources. This study's iterative research, modeling, and analysis process exemplifies the multidisciplinary collaboration necessary to address complex environmental issues. As we refine our models and deepen our understanding, we can better manage the health of our water systems for the benefit of all Floridians and the diverse ecosystems they support.

This study opens several avenues for future research. Expanding the geographical scope of the study to more areas of Florida could elucidate how different hydrogeological and climatic conditions influence OSTDS-induced nitrogen loading. Similarly, the study's Bayesian network model could be adapted to evaluate the impacts of other pollutants. In this study, we employed a BN approach to creating probability beliefs for nitrate (NO3), total Kjeldahl nitrogen (TKN), and total phosphorous (TP) attenuation from onsite sewage treatment and disposal systems (OSTDS) to surface waterbodies in Florida. Furthermore, the results can be extracted into a GIS to create probability belief maps for decision-makers and public planners (Morgan et al. 2012).

Looking forward, there are several areas for future work. One such area involves additional site characterization and data collection to refine the hydrogeological model and reduce uncertainties in model parameters, boundary conditions, and initial conditions. Another area of interest is expanding the model to incorporate temporal changes in environmental conditions, management practices, and soil conditions, enabling a more dynamic assessment of the nitrogen and phosphorus pollution attenuation processes. Lastly, developing and testing alternative conceptual models could help evaluate the sensitivity of model predictions to different hydrogeological system assumptions and representations. The BN model can be further enhanced by addressing these future works, contributing to better groundwater resource management.

References

Ayres Associates (1993) An Investigation of the Surface Water contamination Potential from On-Site Sewage Disposal Systems (OSDS) in the Turkey Creek Sub-Basin of the Indian River Lagoon Basin. Florida Department of Health and Rehabilitative Services (HRS)

Ayres Associates (1996) Contaminant Transport Investigation from an Onsite Wastewater Treatment System (OWTS) in Fine Sand.

Belanger TV, Heck HH (2011) Preliminary evaluation of septic tank influences on nutrient loading to the Lower St. Johns River Basin and its Tributaries. Florida Department of Environmental Protection

Clark (1996) Coastal Zone Management Handbook. Lewis Publishers

Corbet DR, Dillon K, Burnett W, Schaefer G (2002) The spatial variability of nitrogen and phosphorus concentration in a sand aquifer influenced by onsite sewage treatment and disposal systems: a case study on St. George Island, Florida. Environ Pollut Barking Essex 1987 117:337–345. https://doi.org/10.1016/s0269-7491(01)00168-3

Corbett DR, Iverson R (1999) Groundwater and Nutrient Dynamics on A Strip Barrier Island Served by On-Site Sewage Treatment and Disposal Systems in the Northeastern Gulf of Mexico. Florida Department of Health

Fenton N, Neil M (2018) Risk Assessment and Decision Analysis with Bayesian Networks, 2nd edition. Chapman and Hall/CRC, Boca Raton

Fetter CW (2018) Applied Hydrogeology, Fourth Edition, 4th edition. Waveland Press, Inc.

Glendell M, Gagkas Z, Richards S, Halliday S (2021) [Developing a probabilistic risk model to estimate phosphorus, nitrogen and microbial pollution to water from septic tanks] | CREW | Scotland's Centre of Expertise for Waters. In: Cent. Expert. Water. https://www.crew.ac.uk/publication/developing-probabilistic-risk-model-estimate-phosphorus-nitrogen-and-microbial-pollution. Accessed 22 Mar 2023

Morgan J, Rogers K, Hutchins M, Fox J (2012) A Methodological Framework focused on integrating GIS and BBN Data for Probabilistic Map Algebra Analysis

Norsys Software Corp (2007) Netica Help

Troldborg M, Gagkas Z, Vinten A, et al (2022) Probabilistic modelling of the inherent field-level pesticide pollution risk in a small drinking water catchment using spatial Bayesian belief networks. Hydrol Earth Syst Sci 26:1261–1293. https://doi.org/10.5194/hess-26-1261-2022

US EPA O (2015) History of the Hypoxia Task Force. https://www.epa.gov/ms-htf/history-hypoxia-task-force. Accessed 23 Feb 2023

USGS (2022) 1 meter Digital Elevation Models (DEMs) - USGS National Map 3DEP Downloadable Data Collection - ScienceBase-Catalog. In: 1 Meter Digit. Elev. Models DEMs

- USGS Natl. Map 3DEP. https://www.sciencebase.gov/catalog/item/543e6b86e4b0fd76af69cf4c. Accessed 16 Jun 2023

Yang J, Ye M, Tang Z, et al (2020) Using cluster analysis for understanding spatial and temporal patterns and controlling factors of groundwater geochemistry in a regional aquifer. J Hydrol 583:124594. https://doi.org/10.1016/j.jhydrol.2020.124594

Zhu Y, Ye M, Roeder E, et al (2016) Estimating ammonium and nitrate load from septic systems to surface water bodies within ArcGIS environments. J Hydrol 532:177–192. https://doi.org/10.1016/j.jhydrol.2015.11.017

Appendix

Location	Well Pair	Distance (ft)	Bin	Frequency
G5	G5 (GW Source)	0	x < 4.11	2
J9	J9 (GW Source)	0	4.11 < x < 64.5	15
G7	G7 & G5	11.03	x > 64.5	2
J11	J11 & J9	11.08		
G6	G6 & G5	12.94		
G8	G8 & G5	13.78		
J10	J10 & J9	15.72		
J7	J7 & J9	22.12		
J8	J8 & J9	24.49		
J12	J12 & J9	25.01		
G10	G10 & G5	26.47		
G11	G11 & G5	29.92		
G9	G9 & G5	30.36		
G14	G14 & G5	58.68		
G13	G13 & G5	60.03	**Distance**	
G15	G15 & G5	60.81	mean	34.30
J14	J14 & J9	61.51	STD	30.19
J13	J13 & J9	66.38	mean + STD	64.5
J5	J5 & J9	121.46	mean - STD	4.11

Table A1. Turkey Creek distances of attenuation (ft) (Ayres Associates 1993). The table shows the distance in feet between well pairs. A well pair consists of the groundwater source location and the downgradient monitoring location.

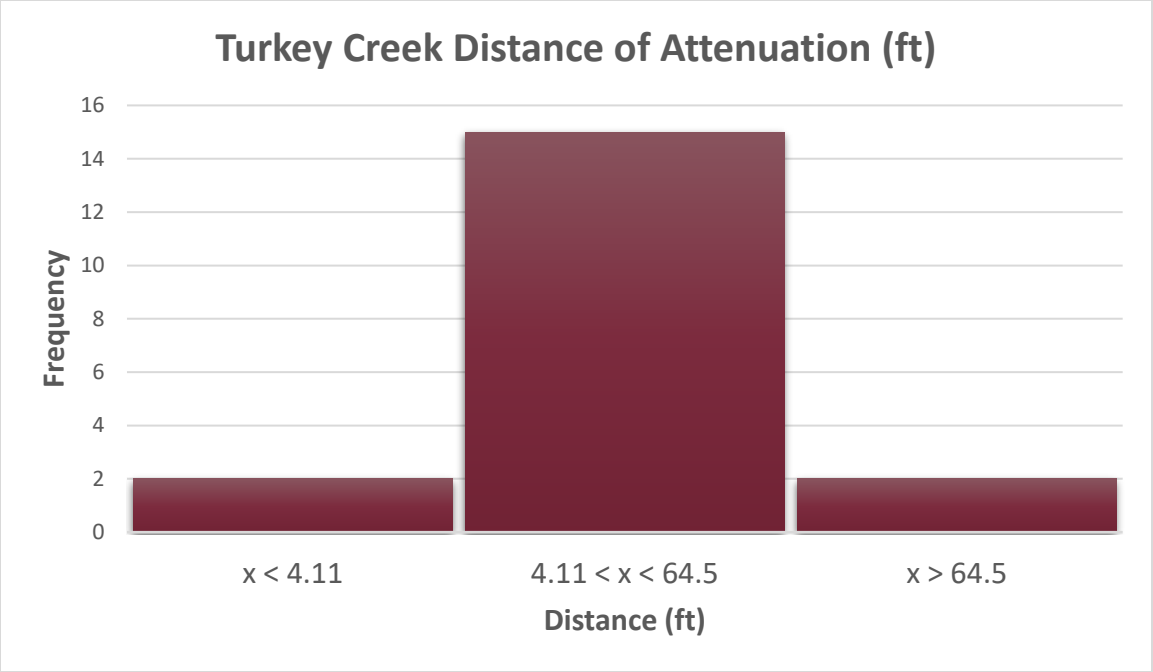

Figure A1. Turkey Creek distance of attenuation (ft) histogram (Ayres Associates 1993). The histogram shows the bin ranges for the distances between the groundwater source well and the downgradient monitoring location used in the Jones and Groseclose, Turkey Creek network.

Location	TP Attenuation Rate	Bin	Frequency
G5	0.00%	0% < x < 25%	4
J9	0.00%	25% < x < 50%	2
J7	0.00%	50% < x < 75%	4
J11	17.10%	75% < x < 95%	2
J5	44.33%	95% > x > 100%	7
G6	47.79%		
G8	56.64%		
G11	58.85%		
G7	66.37%		
G10	71.68%		
G9	79.65%		
J10	88.66%		
J8	95.29%		
J14	97.03%		
J12	97.21%	**Attenuation TP**	
G14	97.79%	mean	92.4%
G13	98.67%	STD	9.5%
J13	98.78%	mean + STD	101.9%
G15	99.12%	mean - STD	82.9%

Table A2. Turkey Creek total phosphorus (TP mg/L) attenuation rate (Ayres Associates 1993). The table shows the analyte attenuation rate between the groundwater source well and the downgradient monitoring location.

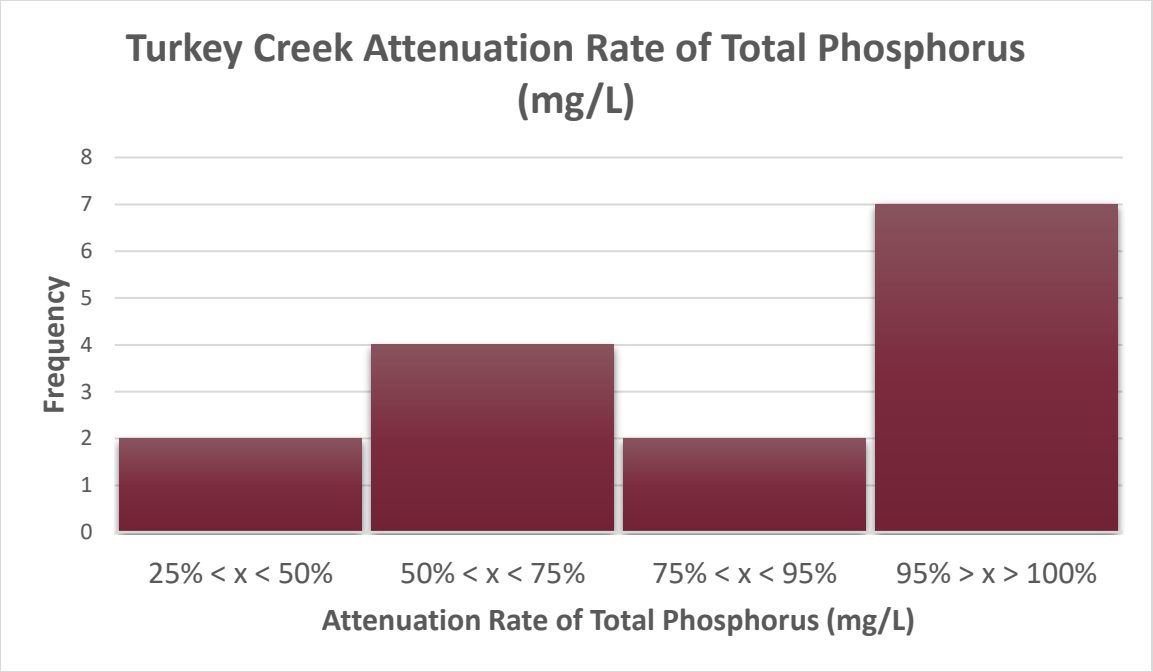

Figure A2. Turkey Creek total phosphorus (TP mg/L) attenuation rate histogram (Ayres Associates 1993). The histogram shows the bin ranges for the analyte attenuation between the groundwater source location and the downgradient well used in the Jones and Groseclose, Turkey Creek network.

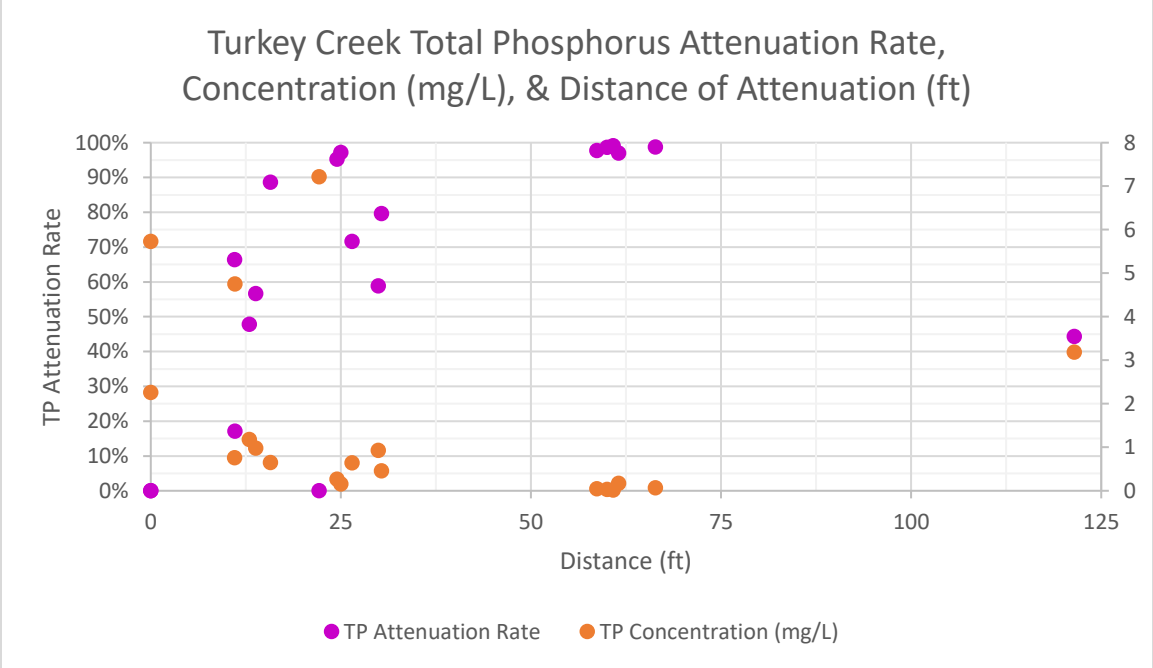

Figure A3. Turkey Creek total phosphorus (TP mg/L) attenuation rate, concentration (mg/L), and distance of attenuation (ft) plot. The plot shows the attenuation rate on the primary vertical axis, the analyte concentration on the secondary horizontal axis, and the distance of attenuation on the horizontal axis between the groundwater source well and the downgradient monitoring location. The majority of analyte attenuation occurs within 75 ft of the OSTDS.

Location	NO3-N Attenuation Rate	Bin	Frequency
G5	0.00%	0% < x < 25%	6
J9	0.00%	25% < x < 50%	2
J12	0.00%	50% < x < 75%	2
J11	3.43%	75% > x > 95%	1
J8	6.87%	95% > x > 100%	8
J7	9.23%		
G6	26.17%		
J10	44.92%		
G9	71.27%		
G7	72.61%		
J14	91.99%		
J5	96.36%		
G10	97.10%		
J13	98.59%		
G11	98.78%	**Attenuation NO3-N**	
G8	99.11%	mean	58.7%
G13	99.22%	STD	043.4%
G14	99.67%	mean + STD	102.1%
G15	99.89%	mean - STD	15.3%

Table A3. Turkey Creek nitrate nitrogen (NO3-N mg/L) attenuation rate (Ayres Associates 1993). The table shows the analyte attenuation rate between the groundwater source well and the downgradient monitoring location.

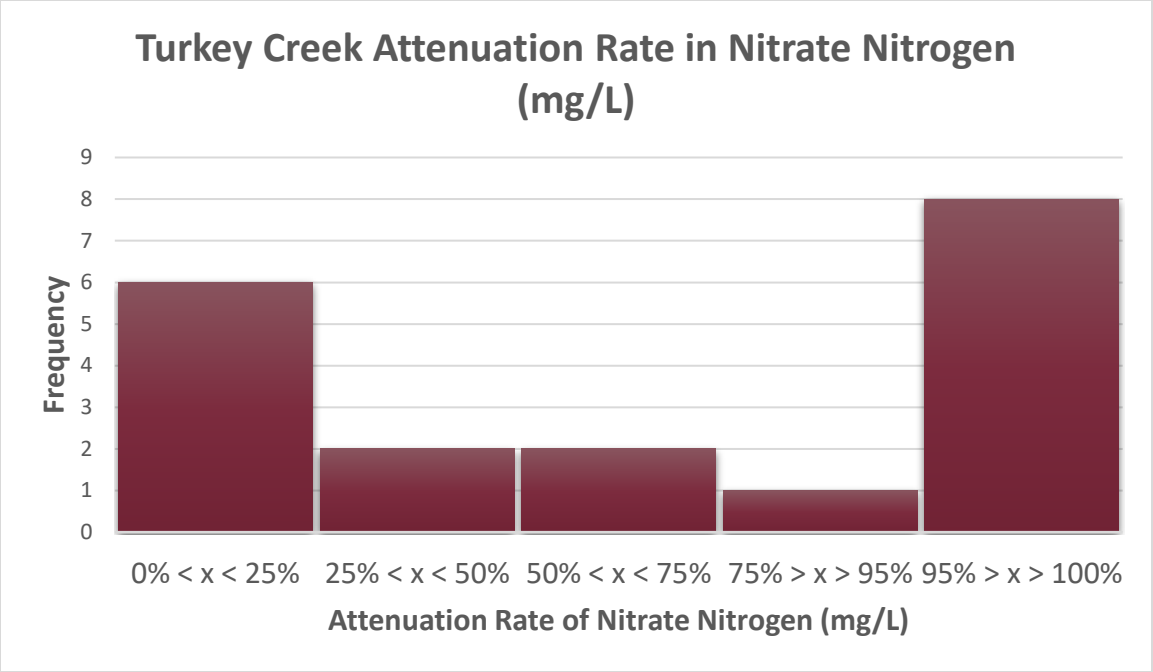

Figure A4. Turkey Creek nitrate nitrogen (NO3-N mg/L) attenuation rate histogram (Ayres Associates 1993). The histogram shows the bin ranges for the analyte attenuation between the groundwater source location and the downgradient well used in the Jones and Groseclose, Turkey Creek network.

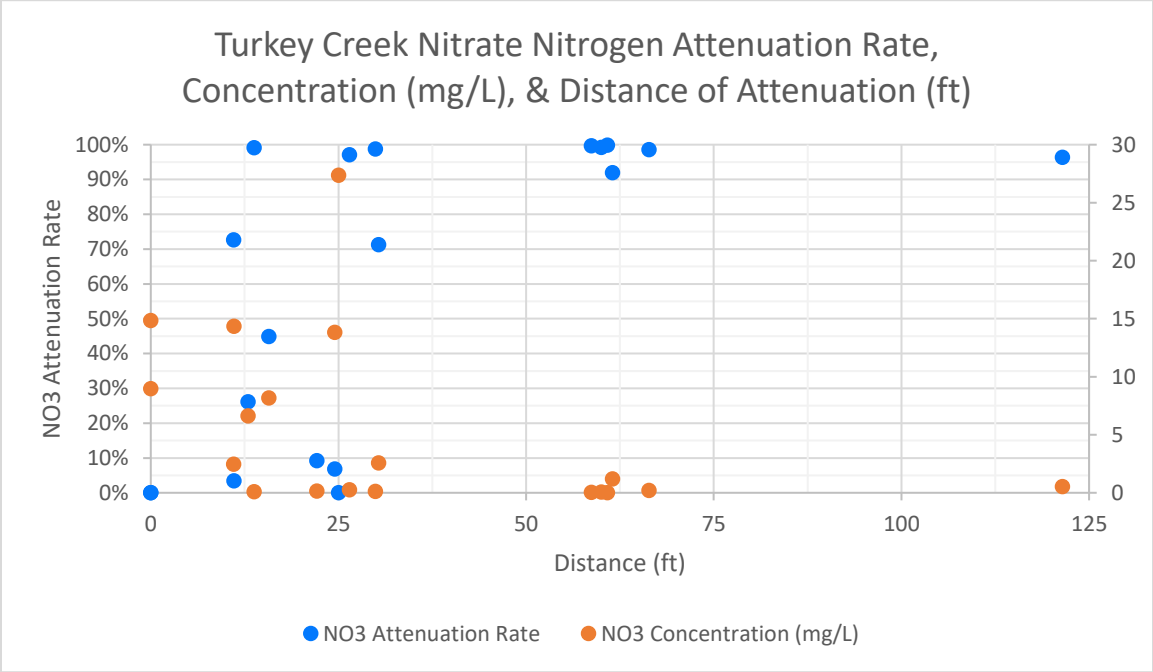

Figure A5. Turkey Creek nitrate nitrogen (NO3-N mg/L) attenuation rate, concentration (mg/L), and distance of attenuation (ft) plot. The plot shows the attenuation rate on the primary vertical axis, the analyte concentration on the secondary horizontal axis, and the distance of attenuation on the horizontal axis between the groundwater source well and the downgradient monitoring location. The majority of analyte attenuation occurs within 75 ft of the OSTDS.

Location	TKN Attenuation Rate	Bin	Frequency
G5	0.00%	0% < x < 25%	11
G6	0.00%	25% < x < 50%	4
G7	0.00%	50% < x < 75%	4
J9	0.00%	75% < x < 95%	0
J8	0.00%	95% < x < 100%	0
J7	0.00%		
J11	0.00%		
J12	0.00%		
J10	13.95%		
G10	15.14%		
G15	23.90%		
G8	25.50%		
G9	30.68%		
G11	41.04%		
J14	48.81%	**Attenuation TKN**	
G13	58.96%	mean	24%
G14	58.96%	STD	26%
J5	65.99%	mean - STD	50%
J13	71.26%	mean + STD	-2%

Table A4. Turkey Creek total Kjeldahl nitrogen (TKN mg/L) attenuation rate (Ayres Associates 1993). The table shows the analyte attenuation rate between the groundwater source well and the downgradient monitoring location.

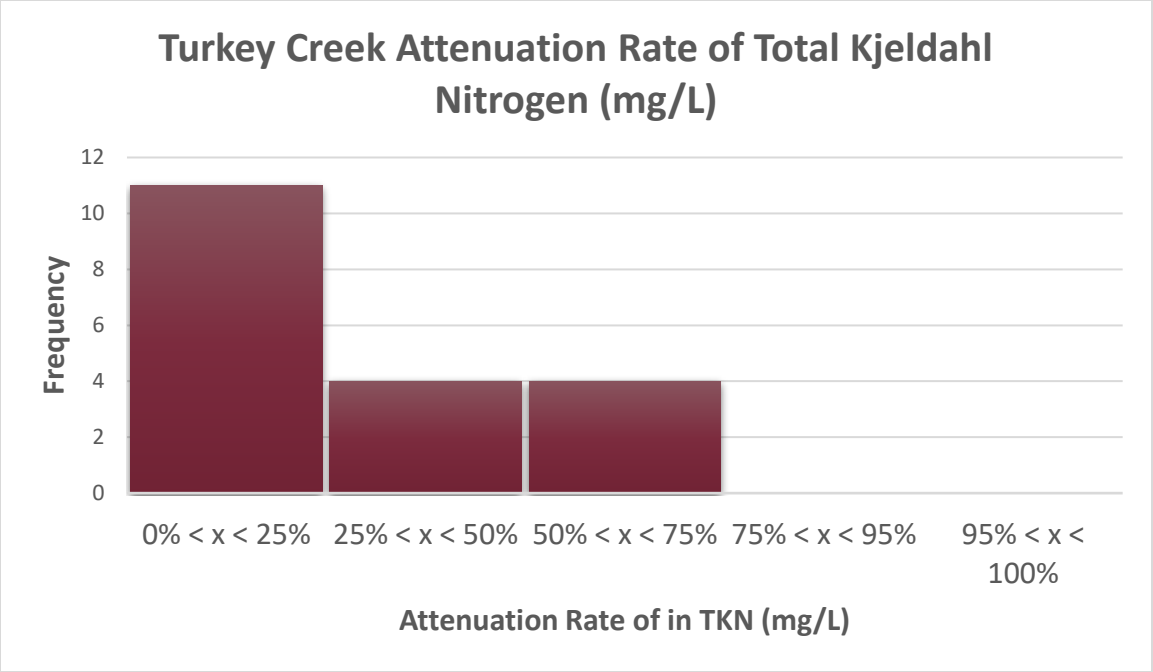

Figure A6. Turkey Creek total Kjeldahl nitrogen (TKN mg/L) attenuation rate histogram (Ayres Associates 1993). The histogram shows the bin ranges for the analyte attenuation between the groundwater source location and the downgradient well used in the Jones and Groseclose, Turkey Creek network.

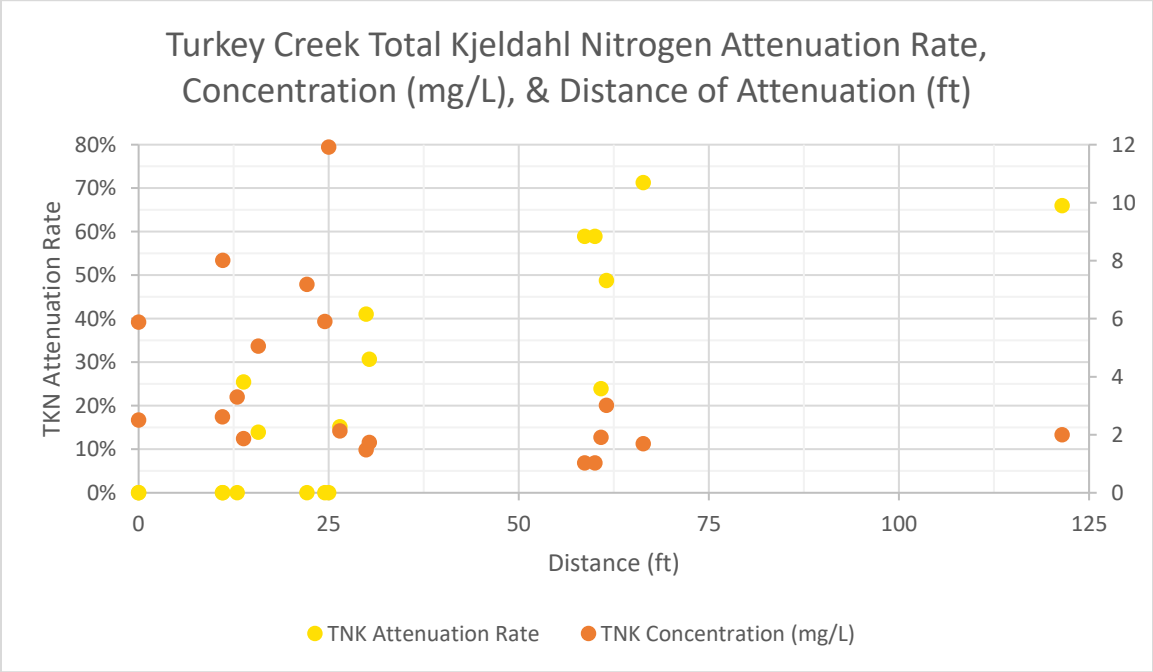

Figure A7. Turkey Creek total Kjeldahl nitrogen (TKN mg/L) attenuation rate, concentration (mg/L), and distance of attenuation (ft) plot. The plot shows the attenuation rate on the primary vertical axis, the analyte concentration on the secondary horizontal axis, and the distance of attenuation on the horizontal axis between the groundwater source well and the downgradient monitoring location. The majority of analyte attenuation occurs within 75 ft of the OSTDS.

Location	Distance (ft)	Well Pair	Bin	Frequency
RT22009-12-29NH3	9.14	1 & 2	x < 16.34	5
RT32010-06-02NH3	9.31	3B & 3	16.34 < x < 77.61	25
DH22010-09-27NH3	12.00	1A & 2	x > 77.61	7
DH12010-09-27NOx	13.20	1A & 1		
DH12010-09-27NH3	13.20	1A & 1		
CST82010-06-01NOx	21.62	2 & 8		
CST92009-12-31NH3	21.80	4 & 9		
CST92010-06-01NH3	21.80	4 & 9		
CST9A2010-09-27NH3	23.01	4 & 9A		
CST92010-06-01NOx	25.44	2 & 9		
CST82009-12-31NOx	27.58	4 & 8		
CST82009-12-31NH3	27.58	4 & 8		
CST82010-06-01NH3	27.58	4 & 8		
RTPZ22010-06-02NH3	32.96	3B & PZ2		
DH82010-06-01NOx	34.99	2 & 8		
DH72010-06-01NOx	38.92	2 & 7		
CST112010-06-01NH3	40.38	4 & 11		
CST112010-09-27NH3	40.38	4 & 11		
CST102010-06-01NOx	40.52	2 & 10		
CST112010-06-01NOx	42.53	2 & 11		
CST102010-06-01NH3	43.92	4 & 10		
DH82010-09-27NOx	44.72	1A & 8		
DH82010-09-27NH3	44.72	1A & 8		
DH72010-09-27NH3	44.81	1A & 7		
MM22010-09-27NH3	47.05	1A & 2		
DH92010-09-27NH3	47.22	1A & 9		
DH92010-09-27NOx	47.22	1A & 9		
MM12010-09-27NH3	47.67	1A & 1		
MM52010-09-27NH3	66.80	1A & 5		
MM42010-09-27NH3	67.65	1A & 4		
MM22010-06-02NOx	84.48	PZ1 & 2		
MM12010-06-02NOx	85.05	PZ1 & 1		
MM52010-06-02NOx	104.94	PZ1 & 5	**Distance**	
MM42010-06-02NOx	105.05	PZ1 & 4	mean	46.98
MM62010-06-02NOx	107.12	PZ1 & 6	STD	30.63
RTPZ42009-12-29NH3	107.70	1 & PZ4	mean + STD	77.61
MM72010-06-02NOx	118.11	PZ1 & 7	mean - STD	16.34

Table A5. Lakeshore and Julington Heights distances of attenuation (ft) (Belanger et al. 2011).

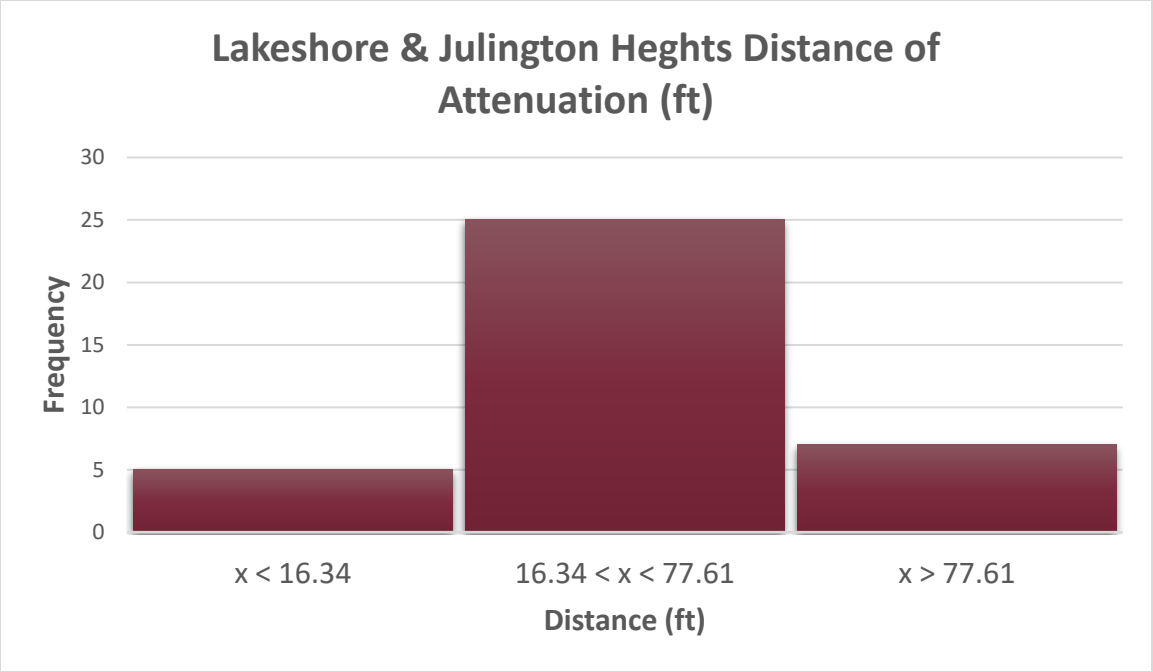

Figure A8. Lakeshore and Julington Heights distance of attenuation (ft) histogram (Belanger et al. 2011). The histogram shows the bin ranges for the distances between the groundwater source well and the downgradient monitoring location used in the CST, DH, MM, and RT, Lakeshore, and Julington Heights network.

Location	NOx Attenuation Rate	Bin	Frequency
DH12010-09-27NOx	37.27%	x < 25%	0
DH82010-09-27NOx	55.45%	25% < x < 50%	0
CST82009-12-31NOx	61.18%	50% < x < 75%	4
DH82010-06-01NOx	69.09%	75% < x < 95%	6
CST92010-06-01NOx	72.50%	x > 95%	5
MM42010-06-02NOx	85.78%		
MM62010-06-02NOx	86.56%		
CST102010-06-01NOx	87.22%		
DH72010-06-01NOx	90.45%		
MM22010-06-02NOx	93.28%		
CST112010-06-01NOx	94.72%		
DH92010-09-27NOx	95.27%	**NOx Attenuation**	
MM12010-06-02NOx	98.13%	mean	82.73%
MM72010-06-02NOx	98.44%	STD	18.45%
MM52010-06-02NOx	98.75%	mean + STD	101.19%
CST82010-06-01NOx	99.64%	mean - STD	64.28%

Table A6. Lakeshore and Julington Heights nitrate (NOx mg/L) attenuation rate (Belanger et al. 2011). The table shows the analyte attenuation rate between the groundwater source well and the downgradient monitoring location.

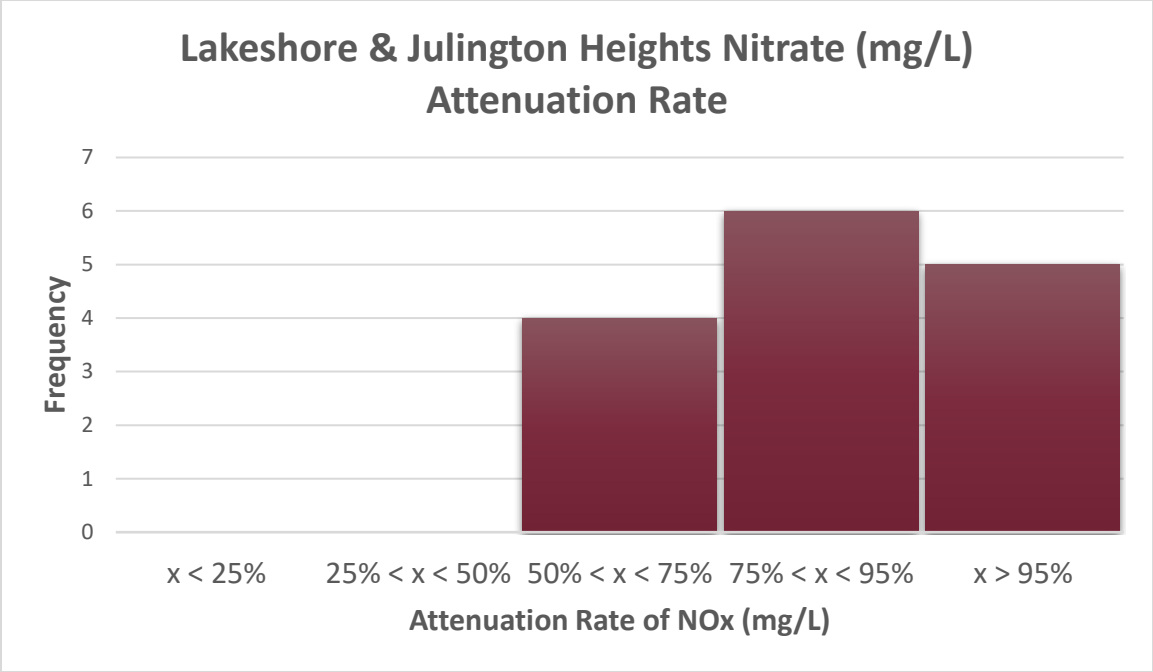

Figure A9. Lakeshore and Julington Heights nitrate (NOx mg/L) attenuation rate histogram (Belanger et al. 2011). The histogram shows the bin ranges for the analyte attenuation between the groundwater source location and the downgradient well used in the CST, DH, MM, and RT sites in the Lakeshore and Julington Heights study areas' networks.

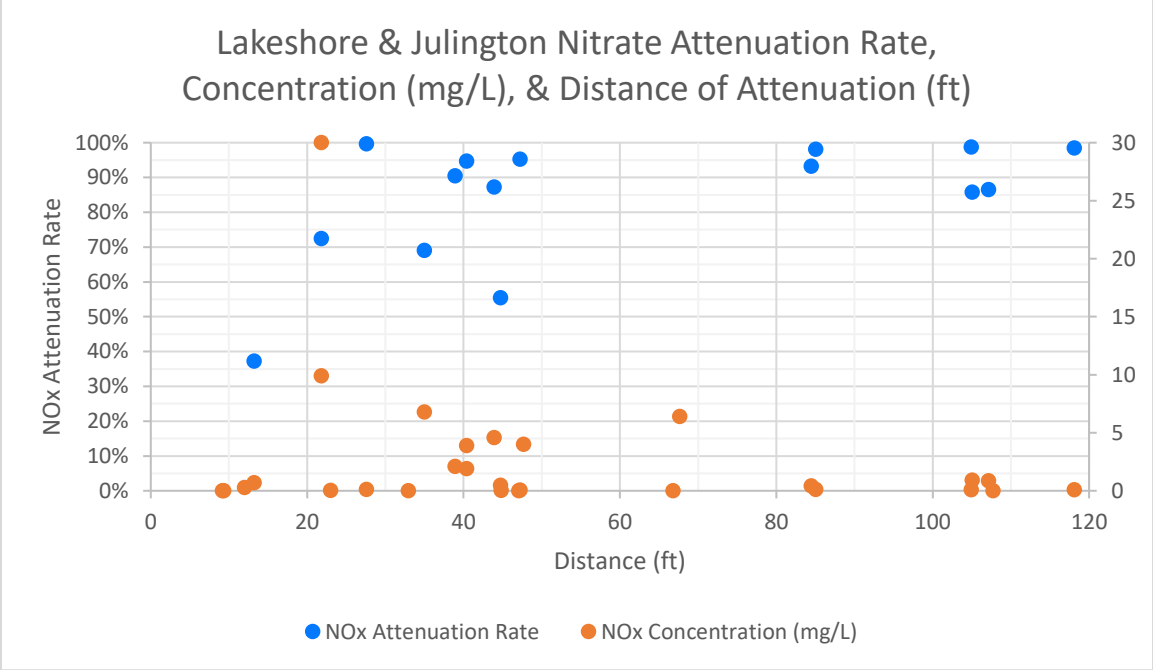

Figure A10. Lakeshore and Julington nitrate (NOx mg/L) attenuation rate, concentration (mg/L), and distance of attenuation (ft) plot. The plot shows the attenuation rate on the primary vertical axis, the analyte concentration on the secondary horizontal axis, and the distance of attenuation on the horizontal axis between the groundwater source well and the downgradient monitoring location. The majority of analyte attenuation occurs within 80 ft of the OSTDS.

Location	NH3-N Attenuation Rate	Bin	Frequency
CST9A2010-09-27NH3	25.00%	x < 25%	1
RT32010-06-02NH3	35.29%	25% < x < 50%	1
DH12010-09-27NH3	52.00%	50% < x < 75%	5
DH72010-09-27NH3	57.33%	75% > x > 95%	8
DH22010-09-27NH3	64.00%	95% > x > 100%	4
RT22009-12-29NH3	66.79%		
MM52010-09-27NH3	72.22%		
RTPZ42009-12-29NH3	75.71%		
DH92010-09-27NH3	77.33%		
MM22010-09-27NH3	77.78%		
DH82010-09-27NH3	81.33%		
CST112010-09-27NH3	81.67%		
RTPZ22010-06-02NH3	86.18%		
CST92010-06-01NH3	88.98%		
MM12010-09-27NH3	91.85%		
MM42010-09-27NH3	93.15%		
CST92009-12-31NH3	95.23%	**NH3-N Attenuation**	
CST102010-06-01NH3	99.94%	mean	77.23%
CST112010-06-01NH3	99.98%	STD	21.15%
CST82010-06-01NH3	99.98%	mean + STD	98.38%
CST82009-12-31NH3	99.98%	mean - STD	56.08%

Table A7. Lakeshore and Julington Heights ammonia nitrogen (NH3-N mg/L) attenuation rate (Belanger et al. 2011). The table shows the analyte attenuation rate between the groundwater source well and the downgradient monitoring location.

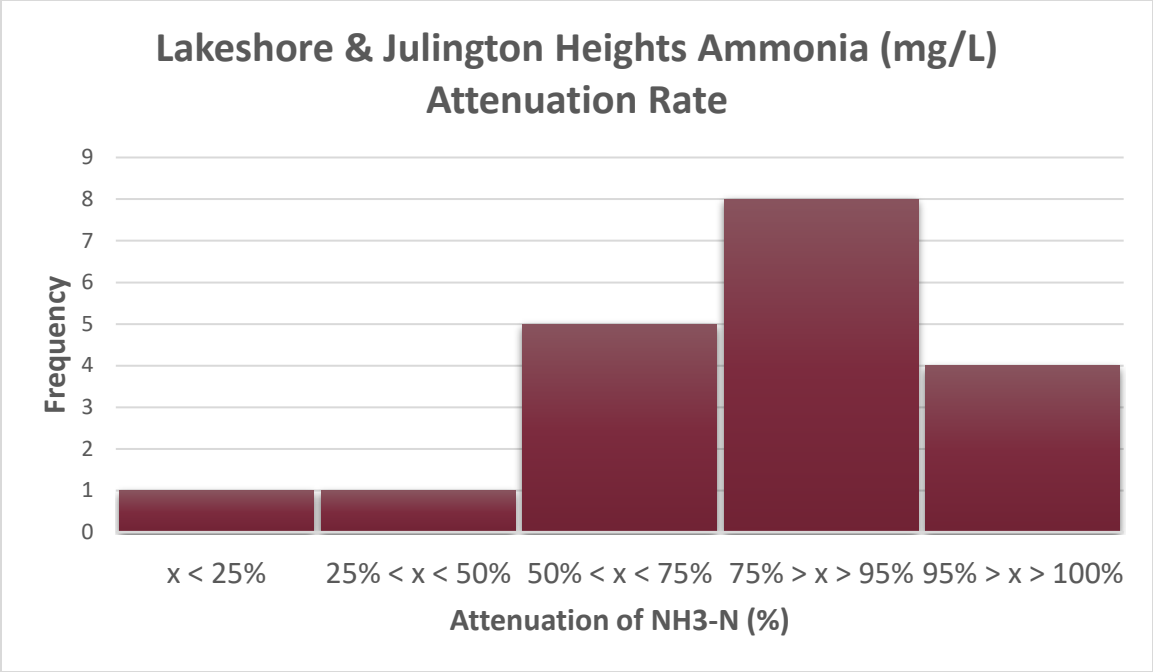

Figure A11. Lakeshore and Julington Heights ammonia nitrogen (NH3-N mg/L) attenuation rate histogram (Belanger et al. 2011). The histogram shows the bin ranges for the analyte attenuation between the groundwater source location and the downgradient well used in CST, DH, MM, and RT Lakeshore and Julington Heights network.

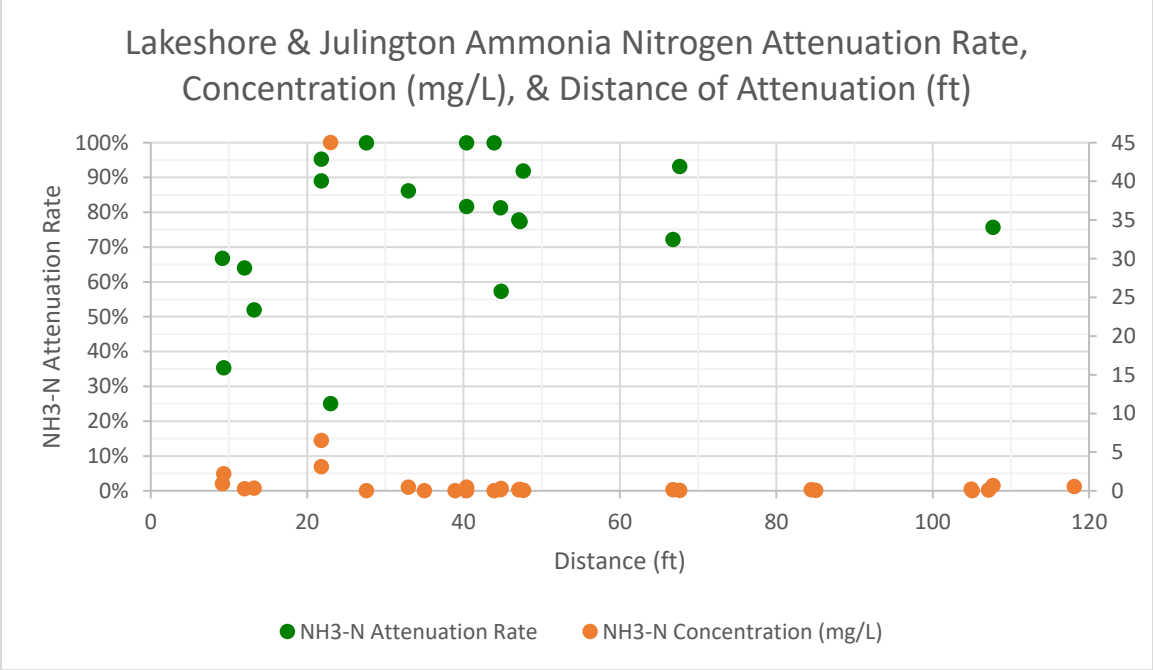

Figure A12. Lakeshore and Julington ammonia-nitrogen (NH3-N mg/L) attenuation rate, concentration (mg/L), and distance of attenuation (ft) plot. The majority of analyte attenuation occurs within 75 ft of the OSTDS.

Location	Distance (ft)	Bin	Frequency
JA4	0.00	x <= 0.0	2
SP14	0.00	0.0 < x < 150.6	6
JA7	25.94	x >= 150.6	2
SP15	33.84		
SP17	70.69		
JA8	43.31	**Distance**	
JA9	59.28	mean	75.00
SP7	125.66	STD	75.55
SP8	156.39	mean + STD	150.55
SP9	234.89	mean - STD	-0.55

Table A8. St. George Island distances of attenuation (ft) (Corbett and Iverson 1999; Corbet et al. 2002). The table shows the distance in feet between well pairs. A well pair consists of the groundwater source location and the downgradient monitoring location.

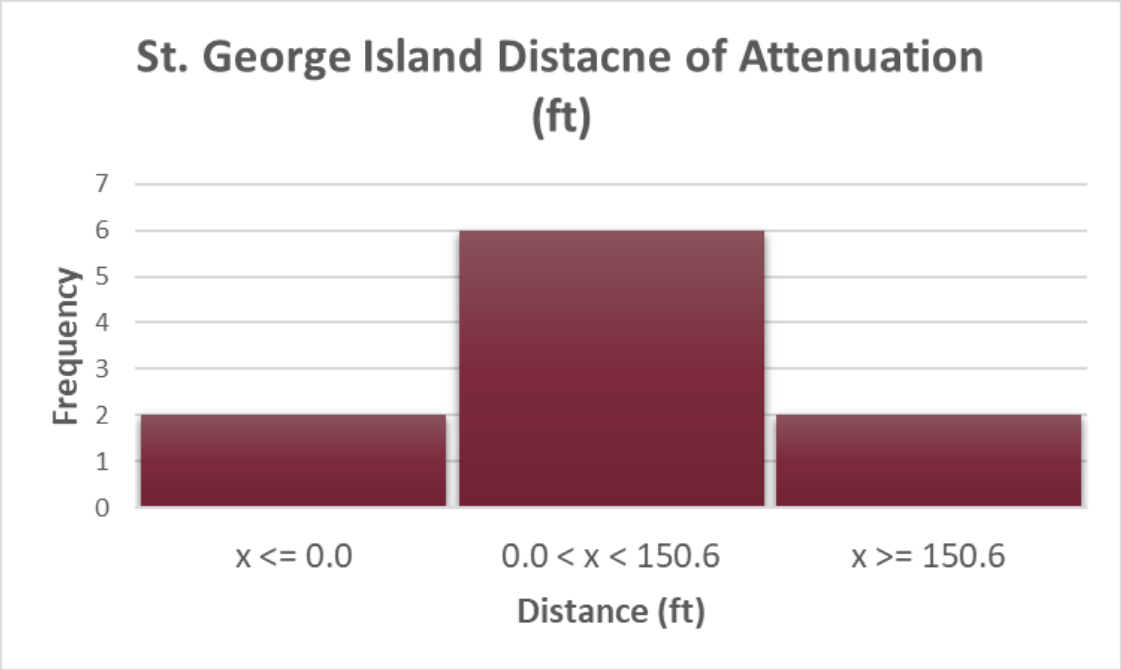

Figure A13. St. George Island distances of attenuation (ft) histogram (Corbett and Iverson 1999; Corbet et al. 2002). The histogram shows the bin ranges for the distances between the groundwater source well and the downgradient monitoring location used in the Jay Abott (JA) and State Park (SP), St. George Island, network.

Location	TN Attenuation Rate	Bin	Frequency
JA4	0.00%	0% to 25%	3
SP14	0.00%	25% to 50%	3
SP15	22.58%	50% to 75%	4
JA8	31.25%	75% to 95%	0
JA7	40.63%	95% to 100%	0
JA9	46.88%	**TN Attenuation**	
SP7	58.06%	mean	40.91%
SP17	67.74%	STD	27.19%
SP9	67.74%	mean + STD	68.10%
SP8	74.19%	mean - STD	13.72%

Table A9. St. George Island total nitrogen (TN mg/L) attenuation rate (Corbett and Iverson 1999; Corbet et al. 2002). The table shows the analyte attenuation rate between the groundwater source well and the downgradient monitoring location.

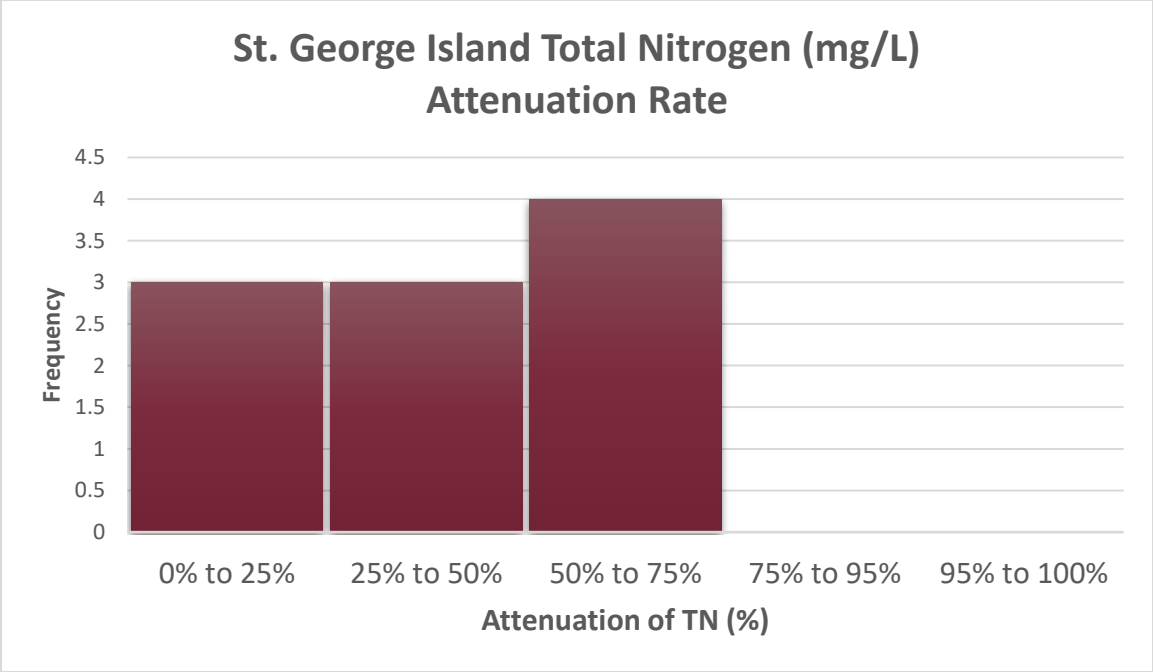

Figure A14. St. George Island total nitrogen (TN mg/L) attenuation rate histogram (Corbett and Iverson 1999; Corbet et al. 2002). The histogram shows the bin ranges for the analyte attenuation between the groundwater source location and the downgradient well used in the Jay Abott (JA) and State Park (SP), St. George Island network.

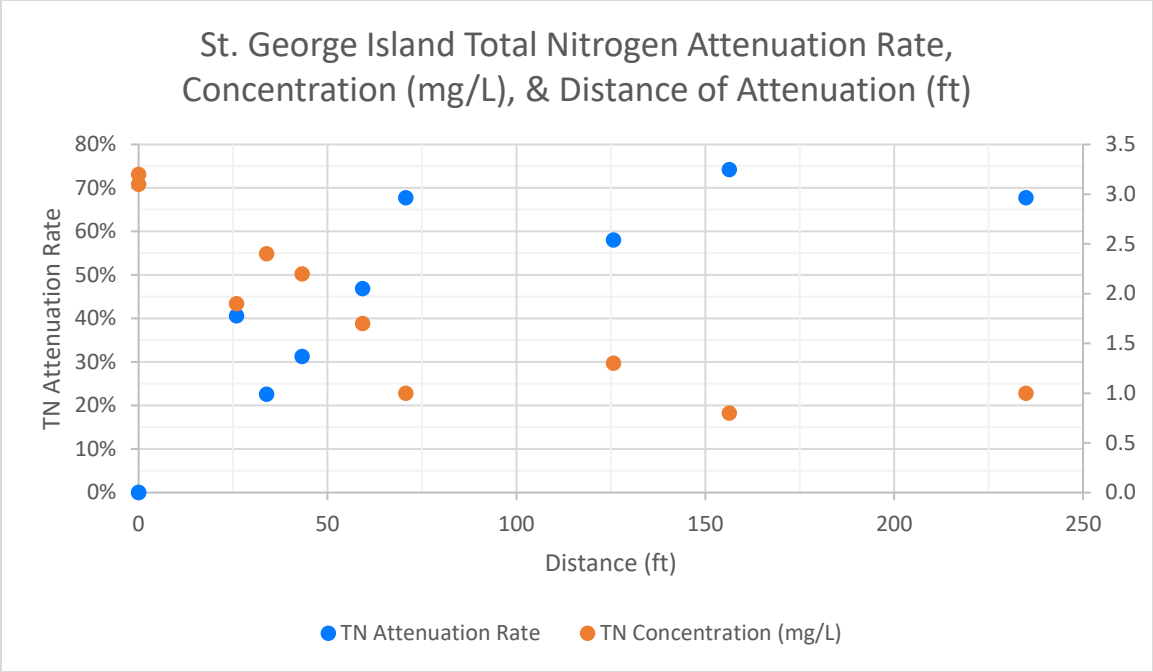

Figure A15. St. George Island total nitrogen (TN mg/L) attenuation rate, concentration (mg/L), and distance of attenuation (ft) plot. The plot shows the attenuation rate on the primary vertical axis, the analyte concentration on the secondary horizontal axis, and the distance of attenuation on the horizontal axis between the groundwater source well and the downgradient monitoring location. The majority of analyte attenuation occurs within 150 ft of the OSTDS.

Location	NH4 Attenuation Rate	Bin	Frequency
JA4	0.00%	0% to 25%	2
SP14	0.00%	25% to 50%	3
JA8	33.33%	50% to 75%	3
SP15	40.00%	75% to 95%	2
JA7	44.44%	95% to 100%	0
JA9	55.56%	**NH4 Attenuation**	
SP7	60.00%	mean	45.33%
SP9	60.00%	STD	28.33%
SP17	80.00%	mean + STD	73.66%
SP8	80.00%	mean - STD	17.01%

Table A10. St. George Island ammonium (NH4 mg/L) attenuation rate (Corbett and Iverson 1999; Corbet et al. 2002). The table shows the analyte attenuation rate between the groundwater source well and the downgradient monitoring location.

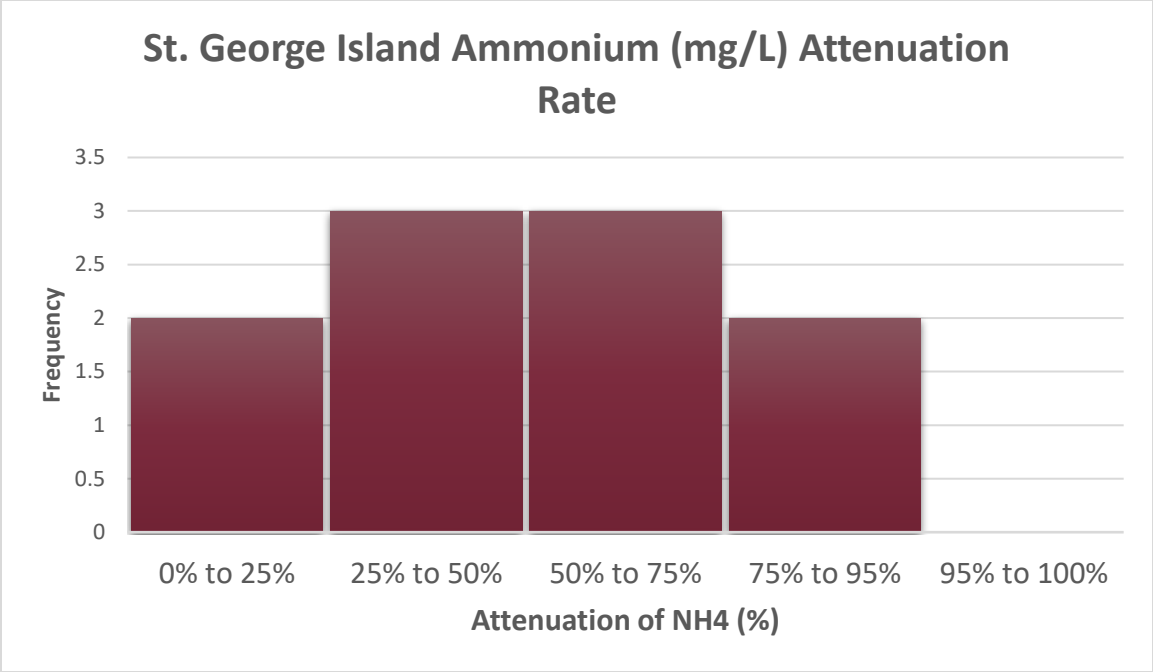

Figure A16. St. George Island ammonium (NH4 mg/L) attenuation rate histogram (Corbett and Iverson 1999; Corbet et al. 2002). The histogram shows the bin ranges for the analyte attenuation between the groundwater source location and the downgradient well used in the Jay Abott (JA) and State Park (SP), St. George Island network.

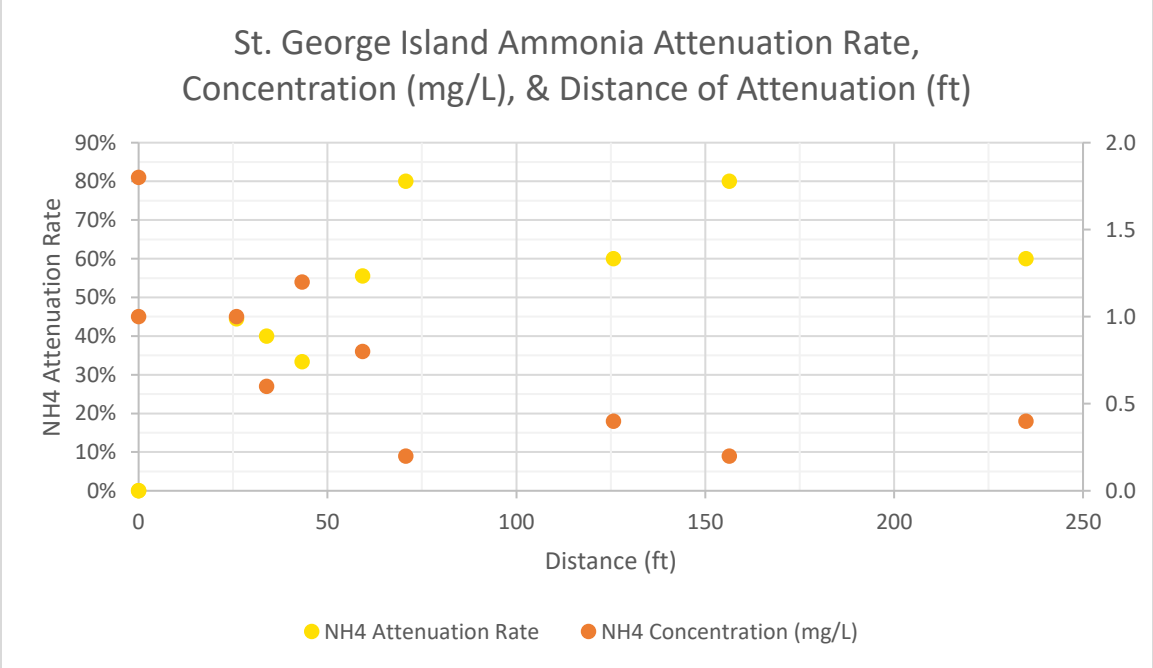

Figure A17. St. George Island ammonia (NH4 mg/L) attenuation rate, concentration (mg/L), and distance of attenuation (ft) plot. The plot shows the attenuation rate on the primary vertical axis, the analyte concentration on the secondary horizontal axis, and the distance of attenuation on the horizontal axis between the groundwater source well and the downgradient monitoring location. The majority of analyte attenuation occurs within 125 ft of the OSTDS.

Location	TP Attenuation Rate	Bin	Frequency
JA4	0.00%	0% to 25%	3
SP14	0.00%	25% to 50%	5
JA7	6.67%	50% to 75%	2
SP15	33.33%	75% to 95%	0
JA8	40.00%	95% to 100%	0
SP17	50.00%	**TP Attenuation**	
SP8	50.00%	mean	34.17%
SP9	50.00%	STD	23.16%
JA9	53.33%	mean + STD	57.33%
SP7	58.33%	mean - STD	11.00%

Table A11. St. George Island total phosphorus (TP mg/L) attenuation rate (Corbett and Iverson 1999; Corbet et al. 2002). The table shows the analyte attenuation rate between the groundwater source well and the downgradient monitoring location.

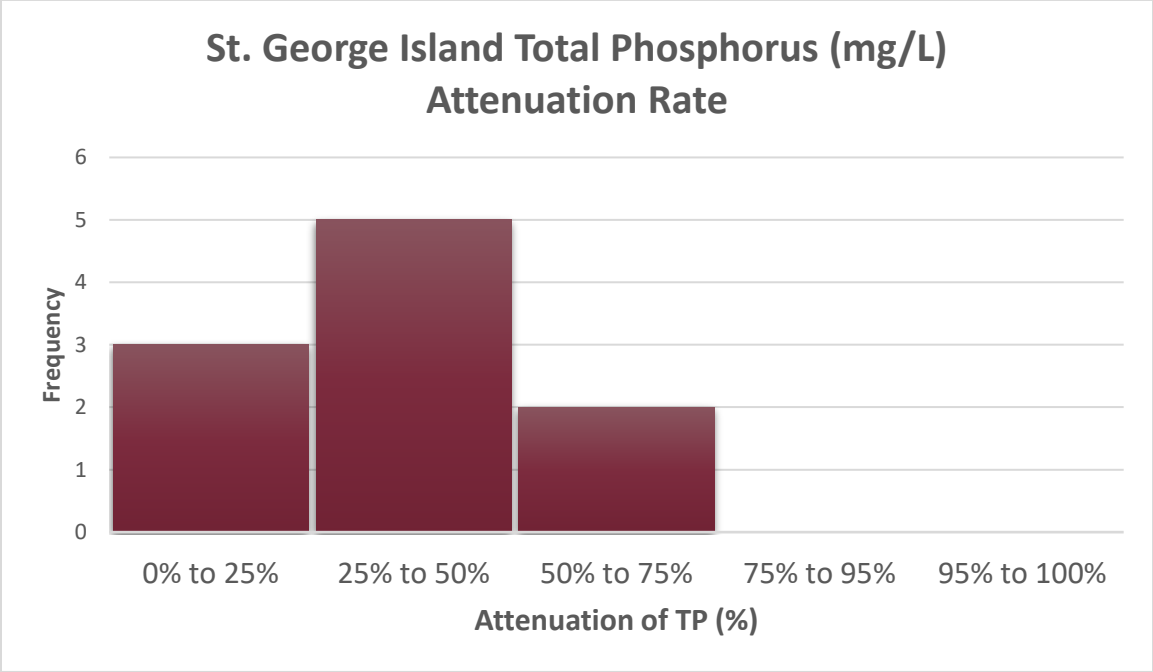

Figure A18. St. George Island total phosphorus (TP mg/L) attenuation rate histogram (Corbett and Iverson 1999; Corbet et al. 2002). The histogram shows the bin ranges for the analyte attenuation between the groundwater source location and the downgradient well used in the Jay Abott (JA) and State Park (SP), St. George Island network.

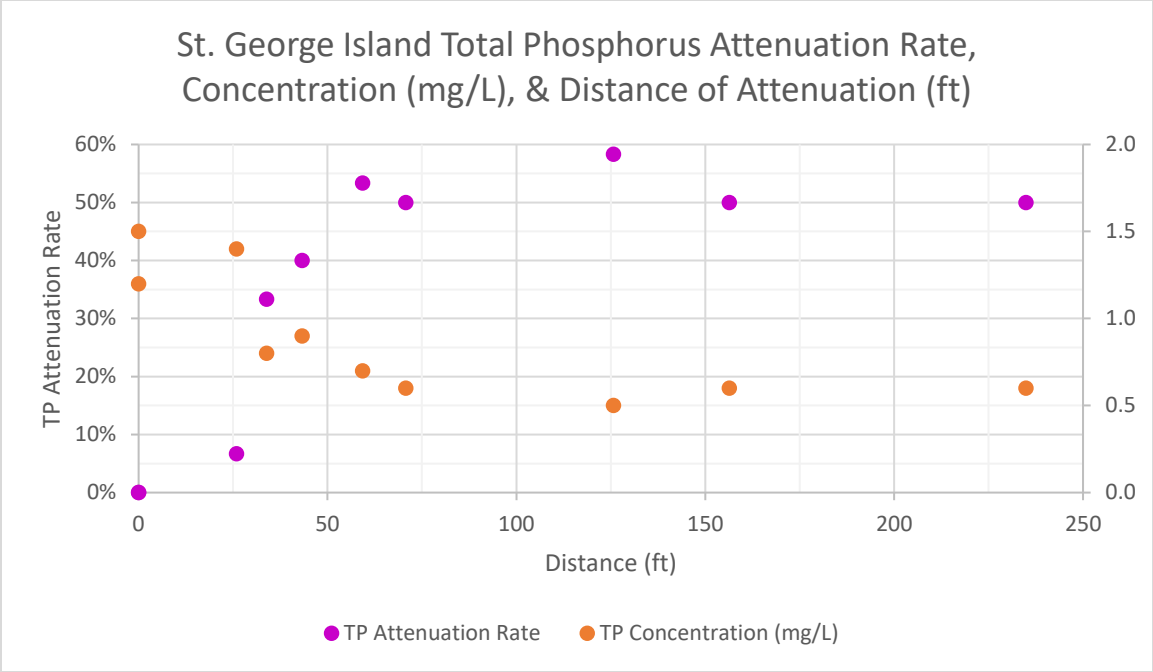

Figure A19. St. George Island total phosphorus (TP mg/L) attenuation rate, concentration (mg/L), and distance of attenuation (ft) plot. The plot shows the attenuation rate on the primary vertical axis, the analyte concentration on the secondary horizontal axis, and the distance of attenuation on the horizontal axis between the groundwater source well and the downgradient monitoring location. The majority of analyte attenuation occurs within 75 ft of the OSTDS.

Location	Distance (ft)	Bin	Frequency
SDATW16	0.00	x < 8.77	4
SDATW19	0.00	8.77 < x < 48	25
SDATW1	4.12	x > 48	3
SDATW3	8.55		
SDATW1	8.86		
SDATW10	12.05		
SDATW2	12.12		
SDATW10	12.85		
SDATW6	13.70		
SDATW5	15.72		
SDATW5	17.37		
SDATW6	18.90		
SDATW11	23.55		
SDATW11	24.17		
SDATW7	24.43		
SDATW9	27.09		
SDATW7	27.90		
SDATW8	28.45		
SDATW8	28.45		
SDATW9	29.28		
SDATW12	31.30		
SDATW12	32.25		
SDATW13	37.69		
SDATW25	37.77		
SDATW14	38.82		
SDATW15	40.98		
SDATW13	41.78		
SDATW14	42.16	**Distance**	
SDATW15	43.69	mean	28.38
SDATW28	71.64	STD	19.61
SDATW27	74.20	mean + STD	47.99
SDATW26	78.26	mean - STD	8.77

Table A12. St. Johns distances of attenuation (ft) (Ayres Associates 1996). The table shows the distance in feet between well pairs. A well pair consists of the groundwater source location and the downgradient monitoring location.

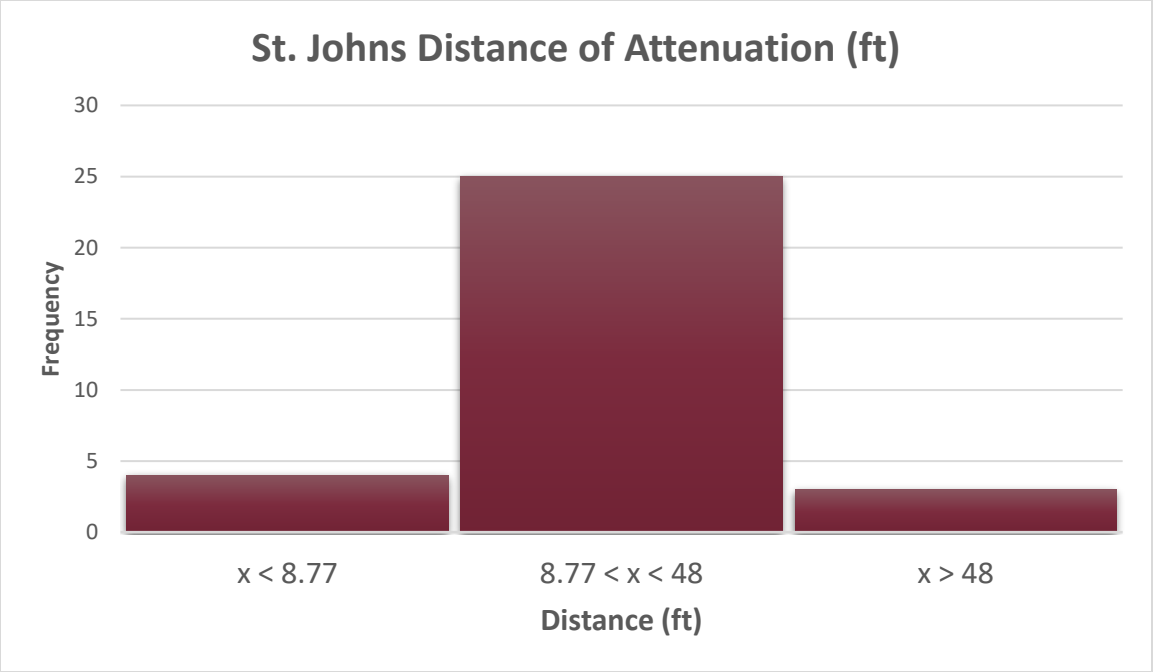

Figure A20. St. Johns distances of attenuation (ft) histogram (Ayres Associates 1996). The histogram shows the bin ranges for the distances between the groundwater source well and the downgradient monitoring location used in the St. Johns 1993 and 1995 network.

ocation	TKN Attenuation Rate	Bin	Frequency
SDATW19	0.00%	0% to 25%	2
SDATW1	24.19%	25% to 50%	0
SDATW11	51.61%	50% to 75%	1
SDATW10	83.87%	75% to 95%	4
SDATW6	85.48%	95% to 100%	10
SDATW5	92.42%		
SDATW12	94.35%		
SDATW9	95.32%		
SDATW7	96.13%		
SDATW8	99.00%		
SDATW14	99.34%		
SDATW15	99.35%		
SDATW28	99.60%	**TKN Attenuation**	
SDATW25	99.63%	mean	83.50%
SDATW26	99.69%	STD	29.64%
SDATW13	99.74%	mean + STD	113.15%
SDATW27	99.81%	mean - STD	53.86%

Table A13. St. Johns total Kjeldahl nitrogen (TKN mg/L) attenuation rate (Ayres Associates 1996). The table shows the analyte attenuation rate between the groundwater source well and the downgradient monitoring location.

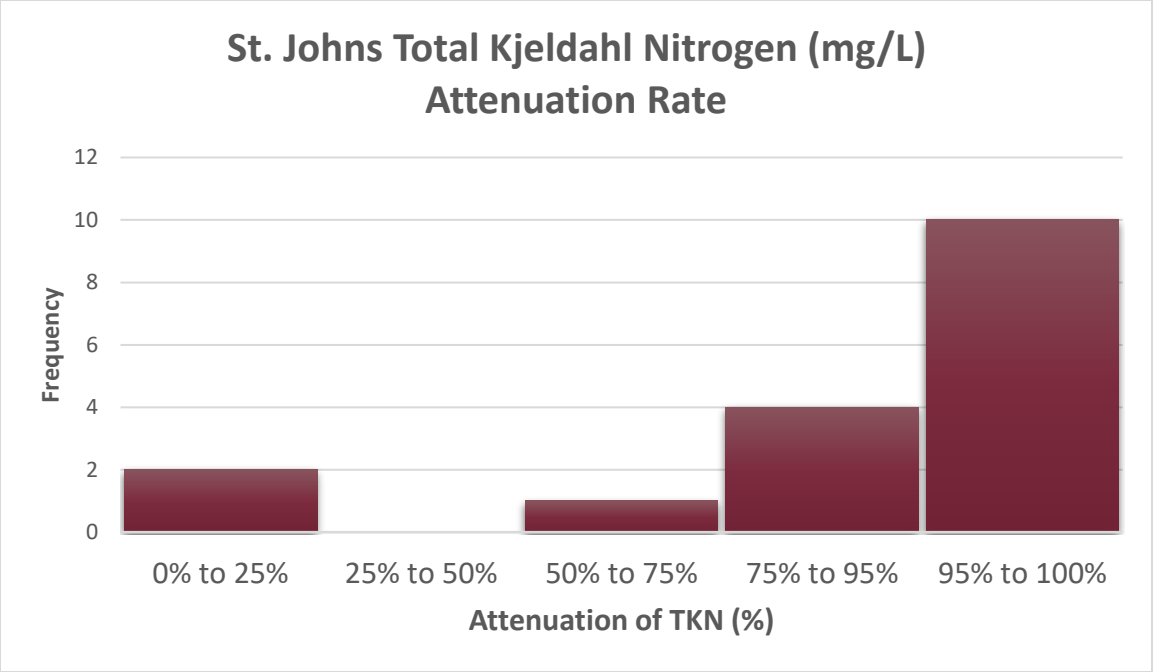

Figure A21. St. Johns total Kjeldahl nitrogen (TKN mg/L) attenuation rate histogram (Ayres Associates 1996). The histogram shows the bin ranges for the analyte attenuation between the groundwater source location and the downgradient well used in the St. Johns 1993 and 1995 network.

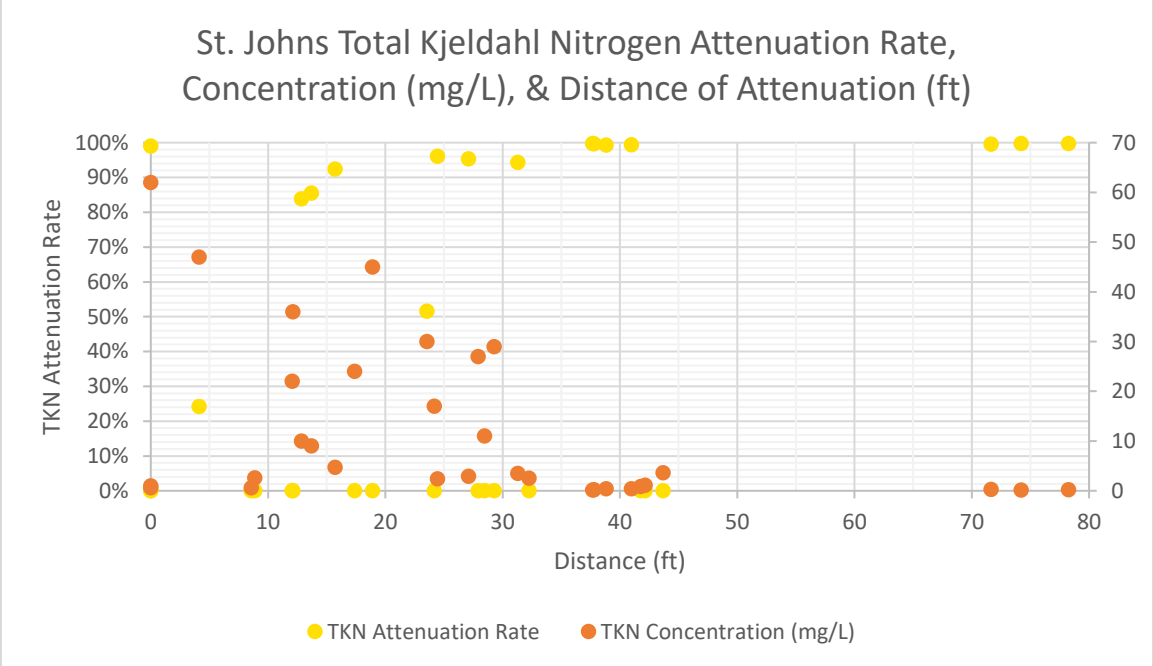

Figure A22. St. Johns total Kjeldahl nitrogen (TKN mg/L) attenuation rate, concentration (mg/L), and distance of attenuation (ft) plot. The plot shows the attenuation rate on the primary vertical axis, the analyte concentration on the secondary horizontal axis, and the distance of attenuation on the horizontal axis between the groundwater source well and the downgradient monitoring location. The majority of analyte attenuation occurs within 50 ft of the OSTDS.

Location	NH3-N Attenuation Rate	Bin	Frequency
SDATW19	0.0%	0% to 25%	2
SDATW1	24.59%	25% to 50%	0
SDATW11	52.46%	50% to 75%	1
SDATW10	83.77%	75% to 95%	4
SDATW6	86.07%	95% to 100%	10
SDATW5	93.28%		
SDATW12	94.92%		
SDATW9	95.90%		
SDATW7	96.56%		
SDATW8	99.39%		
SDATW14	99.75%		
SDATW15	99.85%		
SDATW28	99.87%	**NH3-N Attenuation**	
SDATW26	99.95%	mean	83.90%
SDATW13	99.97%	STD	29.68%
SDATW27	99.98%	mean + STD	113.58%
SDATW25	99.99%	mean - STD	54.22%

Table A14. St. Johns ammonia nitrogen (NH3-N mg/L) attenuation rate (Ayres Associates 1996). The table shows the analyte attenuation rate between the groundwater source well and the downgradient monitoring location.

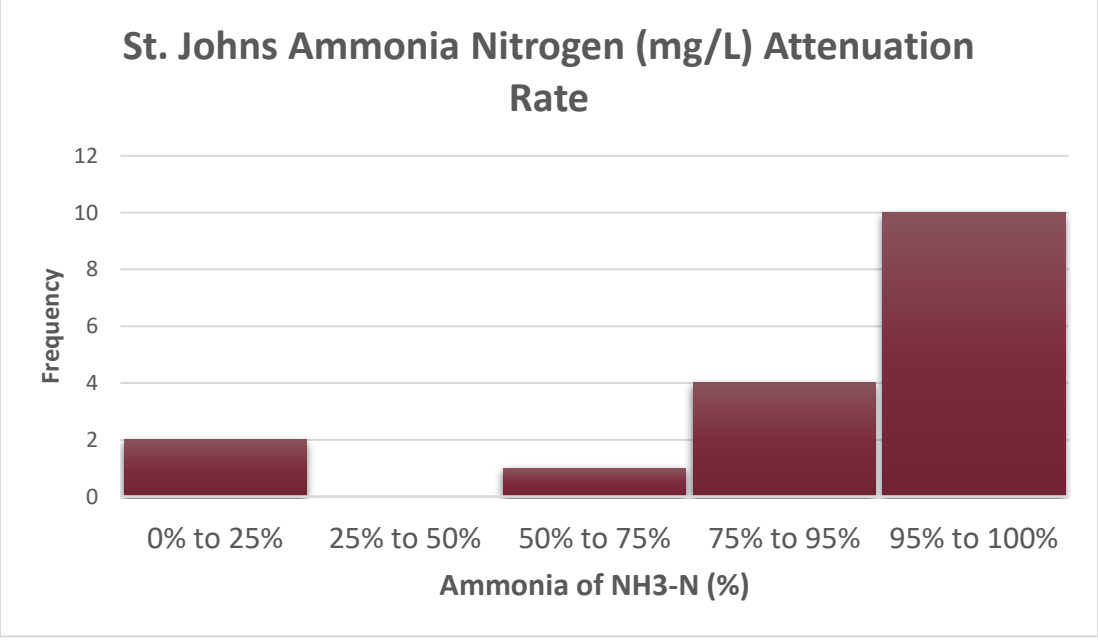

Figure A23. St. Johns ammonia nitrogen (NH3-N mg/L) attenuation rate histogram (Ayres Associates 1996). The histogram shows the bin ranges for the analyte attenuation between the groundwater source location and the downgradient well used in the St. Johns 1993 and 1995 network.

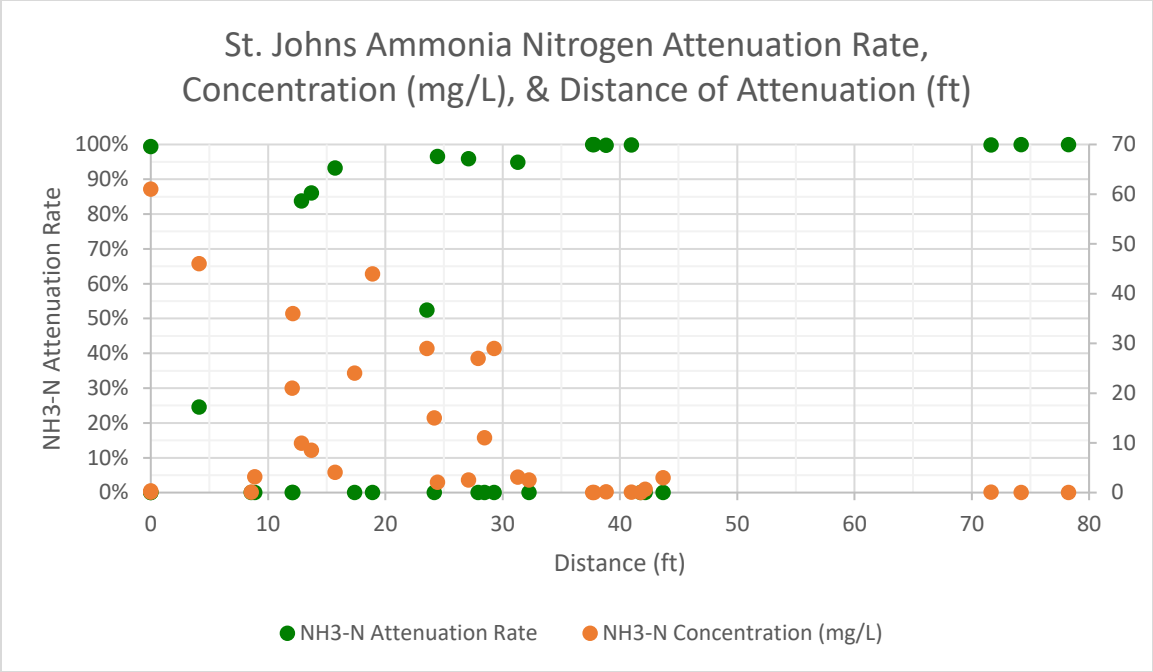

Figure A24. St. Johns ammonia-nitrogen (NH3-N mg/L) attenuation rate, concentration (mg/L), and distance of attenuation (ft) plot. The plot shows the attenuation rate on the primary vertical axis, the analyte concentration on the secondary horizontal axis, and the distance of attenuation on the horizontal axis between the groundwater source well and the downgradient monitoring location. The majority of analyte attenuation occurs within 50 ft of the OSTDS.

Location	NO3-N Attenuation Rate	Bin	Frequency
SDATW16	0.0%	0% to 25%	2
SDATW5	22.23%	25% to 50%	4
SDATW3	27.08%	50% to 75%	1
SDATW1	27.29%	75% to 95%	1
SDATW2	37.45%	95% to 100%	7
SDATW10	44.21%		
SDATW6	67.88%		
SDATW11	78.01%		
SDATW7	96.96%		
SDATW8	97.80%		
SDATW13	99.58%	**NO3-N Attenuation**	
SDATW12	99.99%	mean	66.56%
SDATW14	99.99%	STD	36.29%
SDATW15	99.99%	mean + STD	102.85%
SDATW9	99.99%	mean - STD	30.27%

Table A15. St. Johns nitrate nitrogen (NO3-N mg/L) attenuation rate (Ayres Associates 1996). The table shows the analyte attenuation rate between the groundwater source well and the downgradient monitoring location.

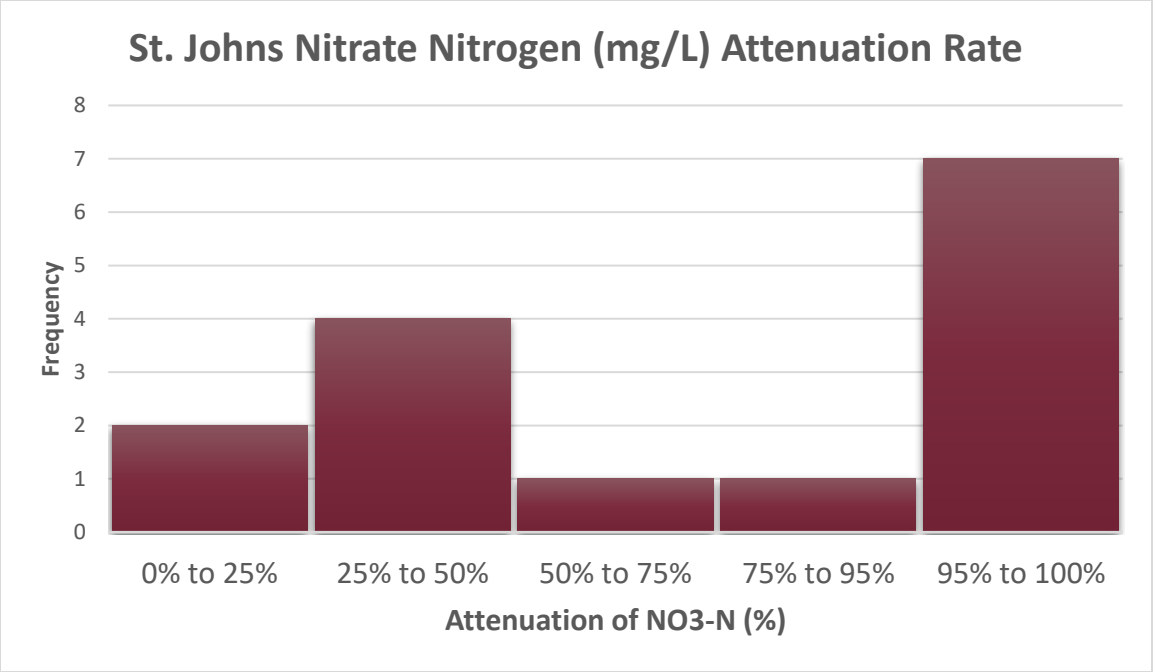

Figure A25. St. Johns nitrate nitrogen (NO3-N mg/L) attenuation rate histogram (Ayres Associates 1996). The histogram shows the bin ranges for the analyte attenuation between the groundwater source location and the downgradient well used in the St. Johns 1993 and 1995 network.

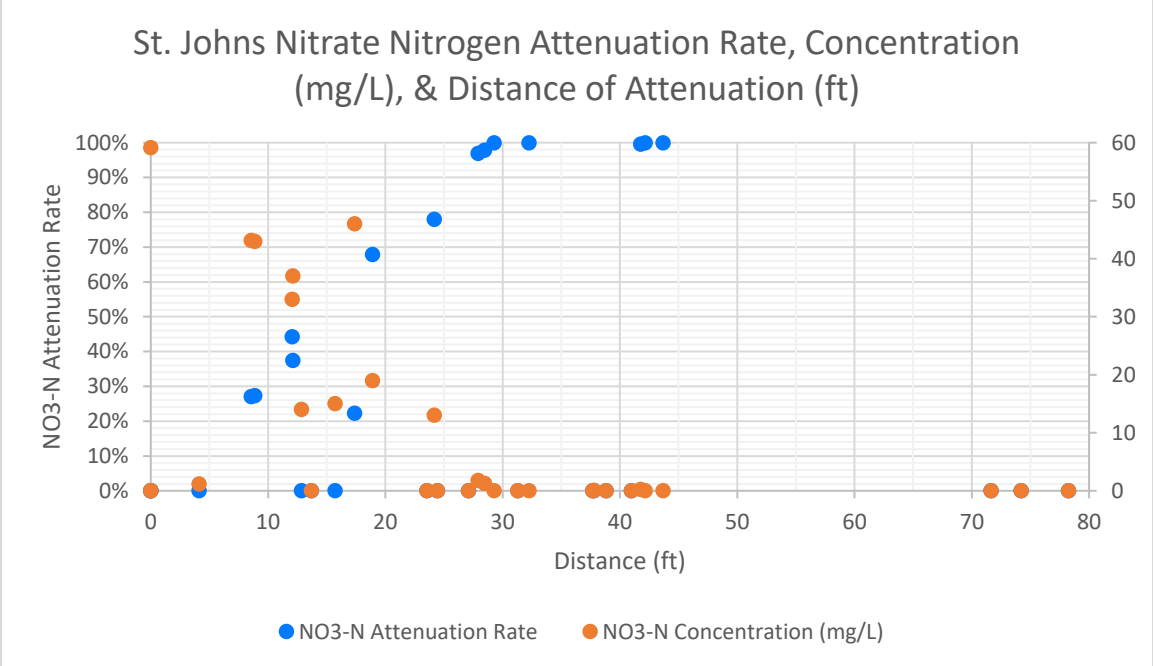

Figure A26. St. Johns nitrate-nitrogen (NO3-N mg/L) attenuation rate, concentration (mg/L), and distance of attenuation (ft) plot. The plot shows the attenuation rate on the primary vertical axis, the analyte concentration on the secondary horizontal axis, and the distance of attenuation on the horizontal axis between the groundwater source well and the downgradient monitoring location. The majority of analyte attenuation occurs within 50 ft of the OSTDS.

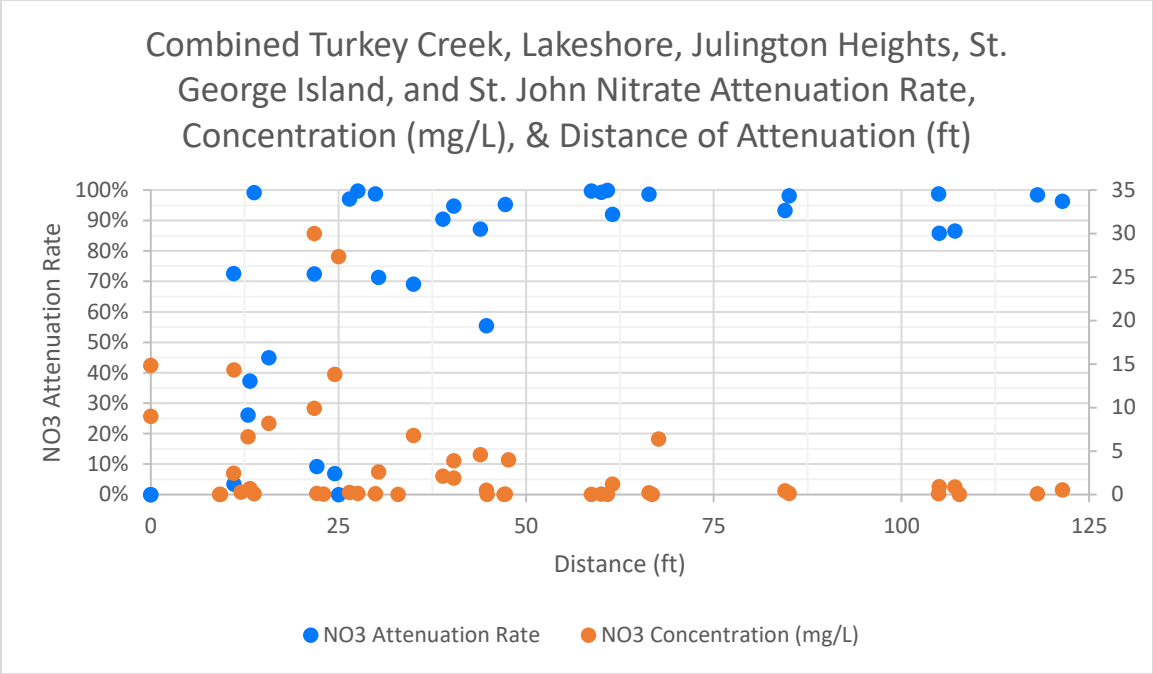

Figure A27. The combined Turkey Creek, Lakeshore, Julington Heights, St. George Island, & St. Johns nitrate (NO3 mg/L) attenuation rate, concentration (mg/L), and distance of attenuation (ft) plot. These data points were used on the combined Bayesian network. The majority of analyte attenuation occurs within 75 ft of the OSTDS.

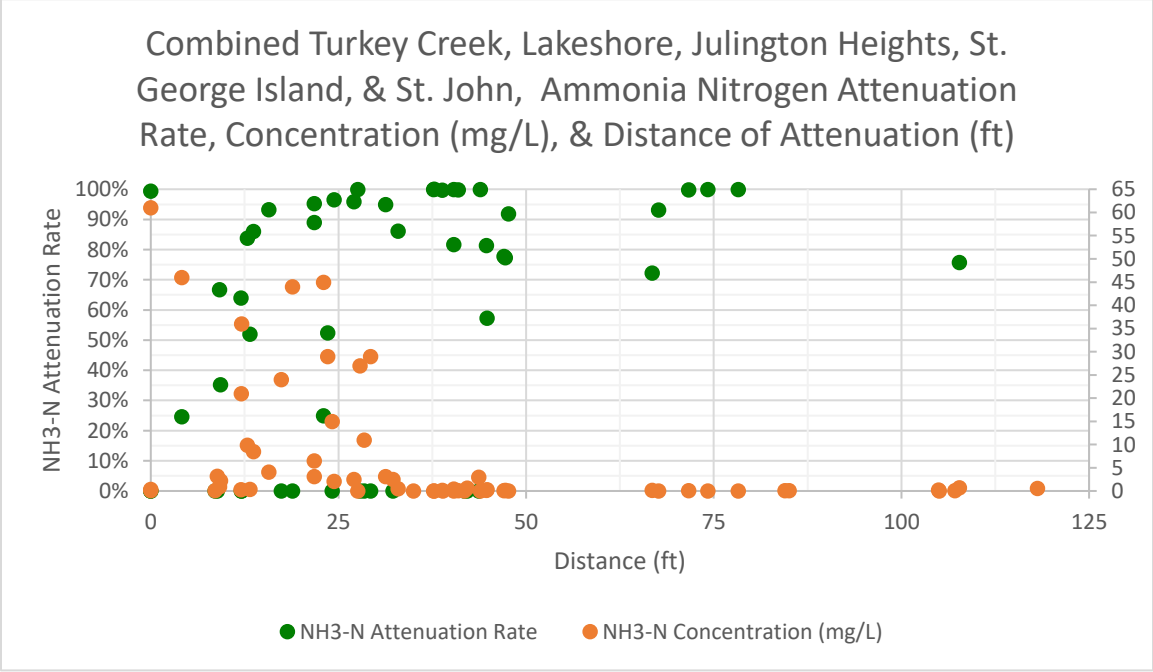

Figure A28. The combined Turkey Creek, Lakeshore, Julington Heights, St. George Island, & St. Johns ammonia-nitrogen (NH3-N mg/L) attenuation rate, concentration (mg/L), and distance of attenuation (ft) plot. These data points were used on the combined Bayesian network. The majority of analyte attenuation occurs within 75 ft of the OSTDS.

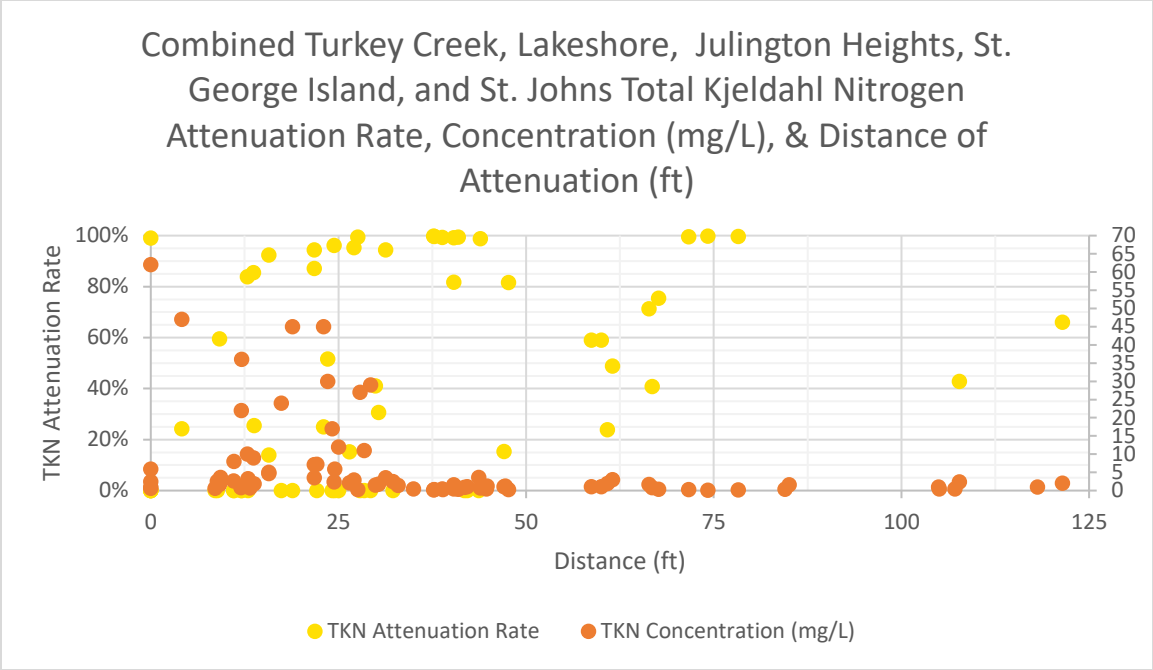

Figure A29. The combined Turkey Creek, Lakeshore, Julington Heights, St. George Island, & St. Johns total Kjeldahl nitrogen (TKN mg/L) attenuation rate, concentration (mg/L), and distance of attenuation (ft) plot. These data points were used on the combined Bayesian network. The majority of analyte attenuation occurs within 75 ft of the OSTDS.

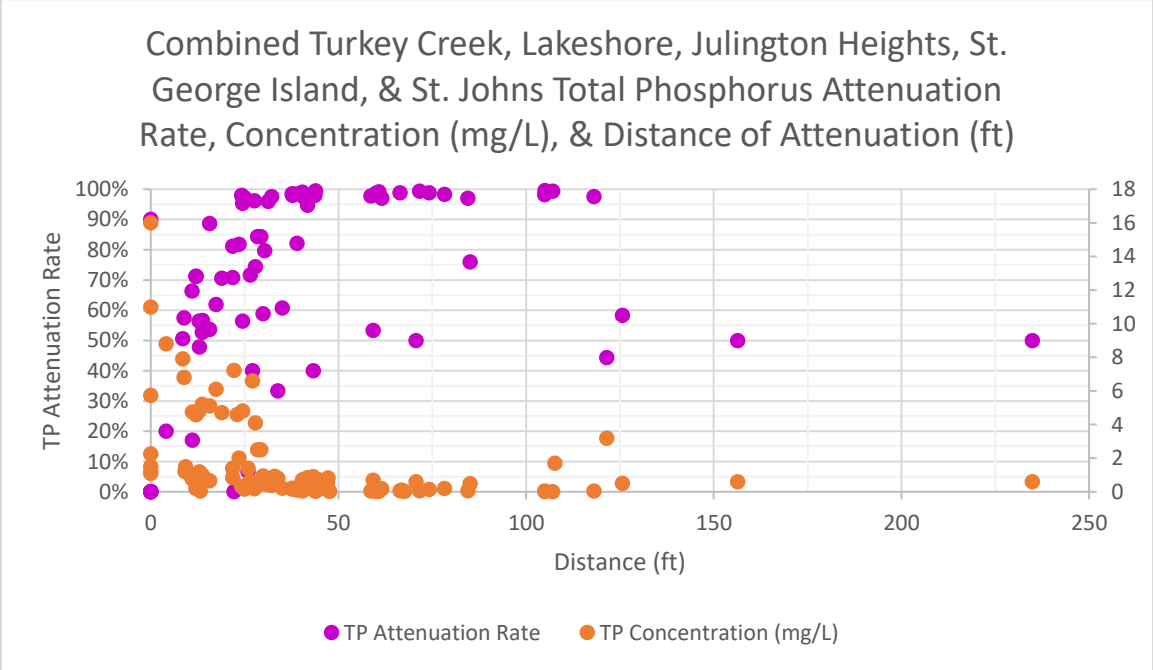

Figure A30. The combined Turkey Creek, Lakeshore, Julington Heights, St. George Island, & St. Johns total phosphorus (TP mg/L) attenuation rate, concentration (mg/L), and distance of attenuation (ft) plot. These data points were used on the combined Bayesian network. The majority of analyte attenuation occurs within 100 ft of the OSTDS.